University of Strathclyde

Department of Civil and Environmental Engineering

Design for Improved Seismic Performance of a Light Gauge Steel Portal Frame Structure

Alia Osman Mohamed Ahmed, B.Sc., M.Sc.

A Thesis Presented in Fulfilment of the Requirements for the Degree of

Doctor of Philosophy

December, 2013

Glasgow, United Kingdom

Copyright statement

Signed: Date:

Dedication

Dedicated to my parents,
for all the things that I have learned from them, and their
sacrifice of their life for their children.

Abstract

This research work develops a design methodology for improving the earthquake resistance of slender portal frame structures and evaluates the performance of this kind of light gauge steel portal frame structures in earthquake prone areas through the study of designed building using a finite element approach.

The design of the building was carried out for a site in Sudan for peak ground acceleration 0.23g according to the Eurocodes 3 and 8 for ductility class "Low".
Two analytical techniques (i.e. Static displacement pushover and dynamic time-history), were employed to assess the behaviour of the light gauge steel portal frame structure.

A new cyclic column link dissipation device is introduced to protect the structure under seismic loads and prevent buckling of frame rafter components. This link is made of back to back lipped channel cold formed steel section and dissipates energy in cyclic bending. It has a yield strength value less than the frame members, and moment resistance about 2/3 the buckling moment of resistance of the frame rafter members. The column link section is stockier than the rafters; the limiting slenderness of the columns was that for compact section.

To accomplish the main objective, the potential benefits (of lightness) of utilising light gauge, steel, slender steel for the construction of portal frame buildings in earthquake prone areas, preliminary analyses of the frame with different types of links were performed using the commercially available finite element software ANSYS. The frame was analysed by nonlinear static horizontal displacements. The inelastic behaviour of the steel elements was considered using the von Mises yielding criterion and the nonlinear geometry were considered as large displacement and P-δ effects in the analyses.

Abstract

Light gauge steel portal frame structure are inevitably prone to buckling, at their ultimate load and this characteristic is poor in earthquakes because it does not allow the structure to deform and absorb energy without failing. A light gauge portal frame was analysed under pushover displacement and a design earthquake level, corresponding to 0.23g. The preliminary static and dynamic analyses resulted in observations that were used to improve the energy absorbing capability, and therefore the earthquake resistance of the frame, by incorporating energy absorbing components described as links into the frame.

The optimised link was then subjected to an artificial earthquake corresponding to an increasing horizontal sine wave excitation at the first elastic sway natural frequency of the structure. This demonstrated an improvement of 217% in the resistance to ground acceleration in comparison with the initial fully slender design.

A light portal frame with slender rafters was improved for performance in earthquakes. The work used finite element analysis in which the earthquakes were represented by imposed horizontal displacement or increasing sinusoidal horizontal ground accelerations. Under the horizontal displacement:

- The original structure failed at a displacement of 34mm.
- The modified structure failed at a total displacement of 88mm.

Under the effect of ground acceleration:

- The modified structure failed at an applied acceleration of approximately 3 times that of the original structure.

The proposed design uses light gauge rafters with heaver steel columns, it has a better earthquake resistance than a fully light gauge structure and benefits from better economics, with lighter components to transport and erect than for a fully compact structure.

Acknowledgements

I am indebted to all the people who have assisted me in many ways towards my work in this research. To all those I send my faithful thanks and acknowledgements.

First and foremost, I am very glad to have this wonderful opportunity to work under the supervision of Professor Nigel Barltrop and I like to express my sincere appreciation and profound thanks to Professor Barltrop, for his active and consistent support, valuable guidance, wide knowledge and constructive advice throughout this research work. His valuable advice and guidance throughout my studies whenever and whatever I need have been fundamental to the completion of this work.

I gratefully acknowledge my sponsor: the Sudanese Government for supporting me financially towards my research work here in the United Kingdom.

Special gratitude must be sent to Dr. James Lim, the former lecturer in Civil Engineering Department, University of Strathclyde, for his kind help before I came to UK when I applied for the PhD program and after that for his assistance and advice during the first year meetings.

A vote of thank goes to Dr. Richard Martin the manager of the High Performance Computing (HPC) facilities who was of great help in fixing all the problems with the HPC machine that I encountered whilst using the high performance computer facility for my analyses work. My thanks also go to thesis committee, Dr. Adam Crewe and Dr. Shangtong for their suggestions and comments which have improved my thesis. Thank also goes to Prof. Robert Kalin, the head of the thesis committee for his help and arrangement for viva.

Greatest thanks and kind regards to the kind lady in Naval Architecture and Marine Engineering department: Mrs Thelma Will for her assistant and help. My thanks to my colleagues in the Naval Architecture and Marine Engineering research centre in University of Strathclyde for their help and the nice time that we had together.

Thanks are also extended to my friends in Glasgow for making life acceptable while I was away from home.

Special thanks to all my family members, including my brothers, my sister and my sisters in law for their encouragement and support during the time I was doing my PhD work.

Kind tribute and extreme gratitude to my brother Yassir Osman for his valuable assistance and help for me for all the things I needed in Sudan while I am here in UK provided me with a good environment for studying.

Finally, my great indebtedness to my parents Amna and Osman for what they had done for me throughout my life and that they brought me up. Their love, encouragement and that they believe in me all the time have stimulated me, supported me and motivated me to accomplish this work.

Alia O. M. Ahmed
April 2013, Glasgow, United Kingdom

Table of Contents

List of Symbols and Abbreviations

Fu Tensile strength

Fy Yield point

E Modulus of elasticity

σ Normal stress

ε Normal strain

$M_{j-\varphi}$ Moment–rotation

K_j Rotational stiffness

$M_{j,Rd}$ Design moment resistance

φ_{Cd} Rotational capacity

$M_{j,p}$ Plastic moment resistance

$K_{j,p}$ Plastic rotational stiffness

$F_{tr,RD}$ The effective design tension resistance of bolt row

$M_{j,Ed}$ Design bending moment

q Behaviour factor

EC3 EN 1993-1

EC8 EN 1998-1

IBC International Building Code

T The fundamental period of building

Fb Base shear

S Soil parameter

γ_G Partial factor for permanent loads

Gk Characteristic value of permanent loads (Dead load)

γ_Q Partial factor for variable loads

Q_k Characteristic value of variable loads (Imposed load)

DC Ductility class

$\bar{\lambda}$ Non dimensional slenderness

N_{Ed} Design value of the axial force

χ Reduction factor for the relevant buckling curve

$\alpha_{ult,k}$ Minimum load amplifier of the design loads to reach the characteristic resistance of the most critical cross section of the structural component considering

its in plane behaviour without taking lateral or lateral torsional buckling into account however accounting for all effects due to in plane geometrical deformation and imperfections, global and local, where relevant

α_{cr} Minimum force amplifier to reach the elastic critical buckling load

α Portion of a part of a cross section in compression

ψ Stress or strain ratio

l Length

γ_{M0} Partial factor for resistance of cross-sections whatever the class is

γ_{M1} Partial factor for resistance of members to instability assessed by member checks

γ_{M2} Partial factor for resistance of cross-sections in tension to fracture

$\sigma_{x,Ed}$ Design value of the local longitudinal stress

$\sigma_{z,Ed}$ Design value of the local transverse stress

τ_{Ed} Design value of the local shear stress

N_{Ed} Design normal force

$M_{y,Ed}$ Design bending moment, y-y axis

$M_{z,Ed}$ Design bending moment, z-z axis

N_{Rd} Design values of the resistance to normal forces

$M_{y,Rd}$ Design values of the resistance to bending moments, y-y axis

$M_{z,Rd}$ Design values of the resistance to bending moments, z-z axis

A_{eff} Effective area of a cross section

$N_{t,Rd}$ Design values of the resistance to tension forces

$N_{pl,Rd}$ Design plastic resistance to normal forces of the gross cross-section

$N_{u,Rd}$ Design ultimate resistance to normal forces of the net cross-section at holes for fasteners

A_{net} Net area of a cross section

$N_{net,Rd}$ Design plastic resistance to normal forces of the net cross-section

$N_{c,Rd}$ Design resistance to normal forces of the cross-section for uniform compression

List of Symbols and Abbreviations

$M_{c,Rd}$ Design resistance for bending about one principal axis of a cross-section

W_{pl} Plastic section modulus

$W_{el,min}$ Minimum elastic section modulus

$W_{eff,min}$ Minimum effective section modulus

A_f Area of the tension flange

$A_{f,net}$ Net area of the tension flange

V_{Ed} Design shear force

$V_{c,Rd}$ Design shear resistance

$V_{pl,Rd}$ Design plastic shear resistance

A_v Shear area

η Factor for shear area

S First moment of area

I Second moment of area

A_w Area of a web

A_f Area of one flange

α Parameter introducing the effect of biaxial bending

β Parameter introducing the effect of biaxial bending

$W_{eff,min}$ Minimum effective section modulus

$N_{b,Rd}$ Design buckling resistance of a compression member

χ Reduction factor for relevant buckling mode

Φ Value to determine the reduction factor χ

a0, a, b, c, d class indexes for buckling curves

N_{cr} Elastic critical force for the relevant buckling mode based on the gross cross sectional properties

i Radius of gyration about the relevant axis, determined using the properties of the gross cross-section

$\lambda 1$ Slenderness value to determine the relative slenderness

λT Relative slenderness for torsional or torsional-flexural buckling

$N_{cr,TF}$ Elastic torsional-flexural buckling force

$N_{cr,T}$ Elastic torsional buckling force

List of Symbols and Abbreviations

$M_{b,Rd}$ Design buckling resistance moment

χ_{LT} Reduction factor for lateral-torsional buckling

Φ_{LT} Value to determine the reduction factor χLT

α_{LT} Imperfection factor

λ_{LT} Non dimensional slenderness for lateral torsional buckling

M_{cr} Elastic critical moment for lateral-torsional buckling

$\lambda_{LT,0}$ Plateau length of the lateral torsional buckling curves for rolled and welded sections

β Correction factor for the lateral torsional buckling curves

$\chi_{LT,mod}$ Modified reduction factor for lateral-torsional buckling

f Modification factor for χLT

k_c Correction factor for moment distribution

ψ Ratio of moments in segment

L_c Length between lateral restraints

λ_f Equivalent compression flange slenderness

$i_{f,z}$ Radius of gyration of compression flange about the minor axis of the section

$I_{eff,f}$ Effective second moment of area of compression flange about the minor axis of the section

$A_{eff,f}$ Effective area of compression flange

$A_{eff,w,c}$ Effective area of compressed part of web

λ_{c0} Slenderness parameter

$f_{l\,k}$ Modification factor

$\Delta_{My,Ed}$ Moments due to the shift of the centroidal y-y axis

$\Delta_{Mz,Ed}$ Moments due to the shift of the centroidal z-z axis

X_y Reduction factor due to flexural buckling (y-y axis)

χ_z Reduction factor due to flexural buckling (z-z axis)

k_{yy} Interaction factor

k_{yz} Interaction factor

k_{zy} Interaction factor

k_{zz} Interaction factor

List of Symbols and Abbreviations

λ_{op} Global non dimensional slenderness of a structural component for out-of-plane buckling

$o_{p\,\chi}$ Reduction factor for the non-dimensional slenderness λop

$\alpha_{ult,k}$ Minimum load amplifier of the design loads to reach the characteristic resistance of the most critical cross section

$\alpha_{cr,op}$ Minimum amplifier for the in plane design loads to reach the elastic critical buckling load with regard d to lateral or lateral torsional buckling

N_{Rk} Characteristic value of resistance to compression

$M_{y,Rk}$ Characteristic value of resistance to bending moments about y-y axis

$M_{z,Rk}$ Characteristic value of resistance to bending moments about z-z axis

List of Tables

List of Plates

List of Figures

Chapter 1

1 Introduction

1.1 General Background

Earthquakes are one of the most powerful natural forces that can disrupt daily lives as they cause the destruction of cities and villages and their effects extend to pose a threat to human life by collapses of bridges, buildings, dams, and other works of man. They are the least understood of the natural hazards and an important distinction of the earthquake problem is that although tsunami and mud slides are a serious risk, the hazard to life is associated almost entirely with manmade structures.

Due to the extent and variety of structural damage in earthquakes a variety of research has been carried out to improve the state of knowledge, through fundamental and applied research. The aims of these researches are also to validate theoretical and experimental research on structural components and structural systems to provide protection against seismic hazards through earthquake resistant design.

In practice, this knowledge is translated into some well-established code provisions for earthquake resistant structure. Despite the fact that earthquakes are essentially random events, the level of knowledge acquired throughout the years and reflected in the current codes of practice can safeguard human lives, avoid structural collapse and consequently, ensure a post-seismic functional society.

Despite the establishment and development of codes for seismic design they still lack design guidance for some types of structure. Light gauge steel portal frame structure systems as shown in Plate 1.1, could be a popular and effective alternative to the traditional hot rolled structure and could be used in earthquake areas owing to its economy and ease of fabrication and transportation, but no recommendations for seismic design of these structures is provided in the design codes. Accordingly there is need for a lightweight design that is suitable for earthquake areas, which could be

transported using lighter vehicles and erected quickly using smaller plant than is required for conventional hot rolled sections following an earthquake. Thin gauge construction is light but is likely to buckle under large deflections. Such a characteristic is not desirable in earthquakes. This research proposes the use of light gauge steel sections, with compact columns which are weaker than the rafters, as a viable alternative and economical construction method for the framing of portal frame buildings and houses as earthquake resistant structures.

Plate 1.1 General view of a light gauge steel portal frame (IPL, 2011).

1.2 Scope and Motivation for Research

Portal frame structures are common structures used in single storey buildings which are widely used and have become the most often used structure within the industrial sector. It is estimated that 50% of single storey steel industrial buildings are constructed as steel portal frames owing to its economy, ease of fabrication and versatility for large spans; uses include warehouses, shopping centres and factories. However, there is a need for a lightweight design that is suitable for earthquake areas and that could also be used for shelter, schools, hospitals etc. It could become a permanent building but might be removed and reused. The frame ought to be capable of resisting large aftershocks or later earthquakes.

Thin-walled structural members have been increasingly used in construction during the last 100 years. They are advantageous in light-weight constructions, where they can carry tension, compression and bending forces.

The structural properties of thin-walled members cause the local or global loss of stability in form of different buckling imperfection as they are made of slender sections. Such a characteristic is not desirable in earthquakes. In addition to that no proper guidelines are available in seismic design codes, EN 1998-1 (2004) does not specifically mention the use of thin- walled steel sections for seismic resistant structures. However it classifies thin gauge structures as low dissipative structures (e.g. low ductility) structures. Previous research (Dubina, 2004b) showed the possibility of using light gauge steel as earthquake resistant structure but with recommendation to use shear walls as a lateral resisting system due to the problems of stability and imperfection of light gauge steel.

1.3 Research Objectives

This research aims to:

- Design a light, thin gauge, but earthquake tolerant structure.
- Design some component parts to yield and absorb the earthquake whilst protecting the slender components.

In more detail, the objectives are to develop a concept and design that:

1. Improve the seismic performance of lightweight steel portal frame structures;
2. Should be able to resist earthquakes and be repairable after a damaging earthquake event;
3. May be erected after an earthquake as a temporary structure (and re-used) or may be used as a permanent structure.
4. Include component parts made of cold–formed steel or thin walled steel materials with dissipative zones designed to yield and protect the whole structure from buckling.

5. Demonstrate a design analysis approach applying non-linear Finite Element analysis, which could be used for buildings with high safety requirements according to their function such as schools and hospitals.

1.4 Research Hypothesis

The design concepts followed for the structural design of the slender portal frame system in this work are:

1. Low dissipative structure for the whole of the frame as it is classified as low dissipative structure according to EN 1998-1 (2004) but having dissipative zones represented by the components parts which will play the role of seismic protection devices for the portal frame members. In this case the frame design will be on the basis of an elastic global analysis without taking into account a significant non-linear material behavior where there is a reduction factor used for estimating of the initial forces for earthquake design according to EN 1998-1 (2004).
2. Dissipative zone for the component parts as these parts of the structure (dissipative zones) have the capability to resist earthquake actions through inelastic behaviour. These zones would be predicted to yield before the frame member and protect the frame components from buckling and other imperfection of stability due to the use of light gauge steel material.

Where in this case:

- Yielding or local buckling should not affect the overall stability of the structure.
- The structure shall have adequate ductility and resistance.
- The whole structure shall have sufficient over strength to allow the development of cyclic yielding in the dissipative parts.

This could be achieved by using sections which are different from the main frame sections for the dissipative zone with different properties: greater buckling resistance but lower yield strength value in comparison with the frame main members to allow

for the yielding of the dissipative components in a cyclic bending and the same time act as buckling prevention for the frame components.

In this way the light gauge steel frame will respond as if it is dissipative structure in the presence of these components despite that it is classified in the EN 1998-1 (2004) as low dissipative structure and this achieves economical design by employing dissipative behaviour.

1.5 Research Methodology

In order to achieve the objectives of the research a design of a typical pitched roof steel portal frame building in Sudan has been carried out, as Sudan has seismic hazard in some regions such as the north east of Sudan close to the red sea. The building is 40 meters long by 20 metres wide as the research deals with the design for hospital or school. The frame model was designed for the following dimensions: span 20m; bay 5m; eaves height 6m and roof angle 5°. To estimate the initial forces this frame was analysed and designed according to EN 1993-1-1(2005) and EN 1993-1-3(2006) provisions.

The frame members are built up sections made of back-to-back lipped channel sections made of cold formed steel (The nominal yield strength and design strength of this steel is 355 MPa (N/mm^2).

The commercially available finite element software ANSYS used for the analyses of the frame structure model in this research project. Rafters, columns and brackets are modelled using the four-noded thin shell element SHELL181. SHELL181 is well-suited for linear, large rotation, and/or large strain nonlinear applications. The mesh size used in the finite element model for the shell elements was around 25x25mm.

The inelastic behaviour of the steel elements was considered using the von Mises yield criterion with isotropic yielding. Geometric nonlinearities: large displacement and P-δ effects were considered in the analyses. The stress- strain relationship is assumed to be elastic-perfectly plastic with a Young's modulus of 205E3 MPa up to the yield strength followed by strain hardening with value of 1% of the Young's modulus, i.e. the tangent modulus is 2.05E3 MPa.

The numerical investigation carried out first analysed the response of the frame for horizontal action by applying lateral displacements. This gave a general understanding of the behaviour of the frame structure under horizontal displacements and assistance with the design procedure of the structure by calculation based on the EN 1993-1-3(2006) loading code within the use of EN 1998-1 (2004) for the estimating the earthquake forces using reduction factor, since there are no specifications for the seismic design of this type of structure. The results of the numerical investigation combined with the code calculations checks resulted in an optimization of the model for the purpose of the study.

There are two types of linear-elastic analysis that could be used for the preliminary design of the structure for earthquake action: the "lateral force method of analysis" and the "modal response spectrum analysis".

The frame response was tested using the commercially available finite element software ANSYS using nonlinear static analysis by applying monotonic horizontal displacements until failure. The analysis resulted in the local buckling of the frame profiles. The frame sections have slender walls which are highly sensitive to imperfections and prone to complex instability problems, which is not desirable in earthquake resistant structures.

In order to improve the seismic performance for this frame structure, and achieve the objective of protecting the frame components a "link" has been designed to be included where the failure happened. This works as a dissipative zone with special specifications that allows for dissipating the energy by formation of plastic bending, so the inelastic action under strong earthquake motion is restricted primary to these links which will yield in flexural manner. The column link's yield strength was chosen as 190 MPa, while it is 355 MPa for the frame members, so as to have link's moment resistance equal to or less than 2/3 of the buckling moment resistance of the frame members. The link is shown in Figure 1.1 and is described in depth in sections 3.12 and 4.9.

Nonlinear static analyses were carried out for the preliminary assessment of the frame with different types of links and different arrangements in order to get the best results for the link. The preliminary assessment also included dynamic analysis for the frame with the best link using real earthquake records and artificial records.

Several link designs were investigated where stiffeners were used to attempt to control buckling of the column links. However even with large amounts of stiffening the stiffened designs investigated still buckled whereas unstiffened compact sections were found to perform well, so these were used in the selected design.

At the final stage of the research an assessment was carried out for the frame with link and without the link using nonlinear dynamic time history analyses, in an artificial earthquake (increasing harmonic excitation). This was tuned to the elastic natural period of each different structural concept and was considered a better basis for the comparison of different concepts than using specific earthquakes, where differences in the energy content at different frequencies may make a particular concept perform better, but only in that particular earthquake.

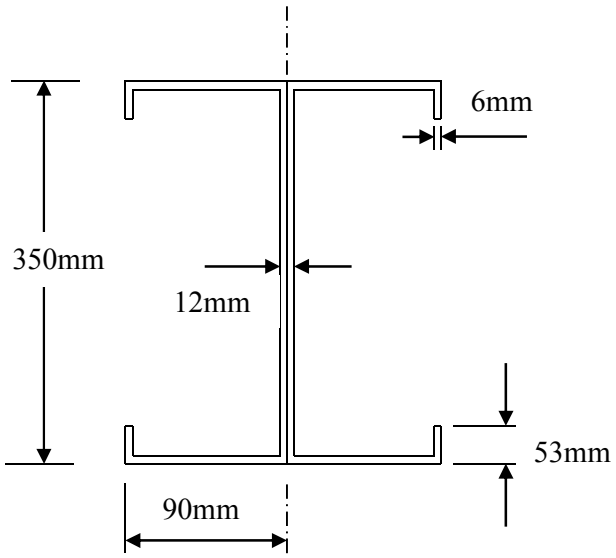

Figure 1.1 Details of proposed link

1.6 Research Output and Outcomes

The research outputs for this study are summarised as:

1. A design of light gauge steel portal frame structure was carried out.
2. The frame structure was designed using back to back lipped channel cold formed steel sections for the main frame members.
3. A link was used for the dissipative zone. It was designed to yield in cyclic bending and was made of cold formed steel section. The link covered the complete column length to allow plastic hinges to form at the upper and lower ends of the column.
4. The preliminary analysis of the frame with link resulted in the choice of the back to back lipped channel section to use for the design of the portal frame structure. The section was chosen to be a compact section for slenderness limitation, to avoid buckling.
5. The link chosen performed well, protected the structure from buckling and yielded before the frame members as no buckling was observed for the frame with link within the numerical analysis.
6. The overall earthquake resistance was improved with the column link resulting in a ductile and earthquake tolerant structure.
7. This design procedure could be applied generally to the design of this type of earthquake resistant structure and should be included in the design codes for seismic design.
8. However, more work will be required on:
    a. The effect of vertical ground accelerations.
    b. The selection of appropriate material strength for the columns: material availability will probably mean that a higher yield stress and lower breadth to thickness ratios in the link will be preferred.

1.7 Research plan and Thesis Structure

In order to address the objectives listed above; a comprehensive literature review was conducted, followed by a combined design and analytical study for the proposed structure and ended with a general assessment for the frame structure. The flow chart for the design sequences and assessment is shown in Figure 1.2.

This thesis consists of five chapters and three appendices beginning with this introductory chapter, stating the background, scope and motivation for research, research objectives, research hypothesis, research methodology and research output and outcomes as mentioned above.

Chapter 2 starts with a brief review of portal frame structures of light gauge steel and the properties of light gauge steel materials used for portal frame structures. This is followed by a review of connections and modelling of joints methods, previous relevant existing modelling methods and experimental and cyclic tests. It also covers previous relevant background for the seismic behaviour and seismic design philosophy of portal frame structures.

Chapter 3 presents the proposed design model for the analytical study of light gauge portal frame structures. It also presents detail of the specific geometry and member dimensions which were designed and detailed according to the recently revised European design codes of practise (EN 1998-1:2004, EN 1993-1-1:2005 and EN 1993-1-3:2006), governing the design of buildings in seismic regions. A model description and a detailed finite element idealisation of the frame and analysis are presented. The analysis was conducted using the commercially available finite element package, ANSYS. The finite element analysis considers the non-linear material and geometry of light gauge steel materials. The dynamic properties were obtained by numerical and hand calculations for the design of the structure. Three proposed seismic links are suggested for improving the seismic performance of the frame structure with different sections and dimensions.

Chapter 4 provides the results and discussion for the numerical analyses including a preliminary analysis of the frame with a link using the ANSYS software. The analyses are carried for the three types of link attached to the frame so as to find the link with best performance as a seismic protection device for the frame. The effect of

the link was tested with time history analyses under real earthquake records of Coalinga, Northridge and Duzce and finally, using an artificial earthquake corresponding to increasing harmonic excitation to determine the comparative failure acceleration of the structure. The results and effects of the link are discussed in detail. The final design of the link utilized compact section and the link covered the complete column (because localized links at each end caused the yielding of the middle part of the column).

Finally, in Chapter five, the last Chapter of this thesis, the conclusions with general discussion and review of the work in the present research is presented along with recommendations for further research.

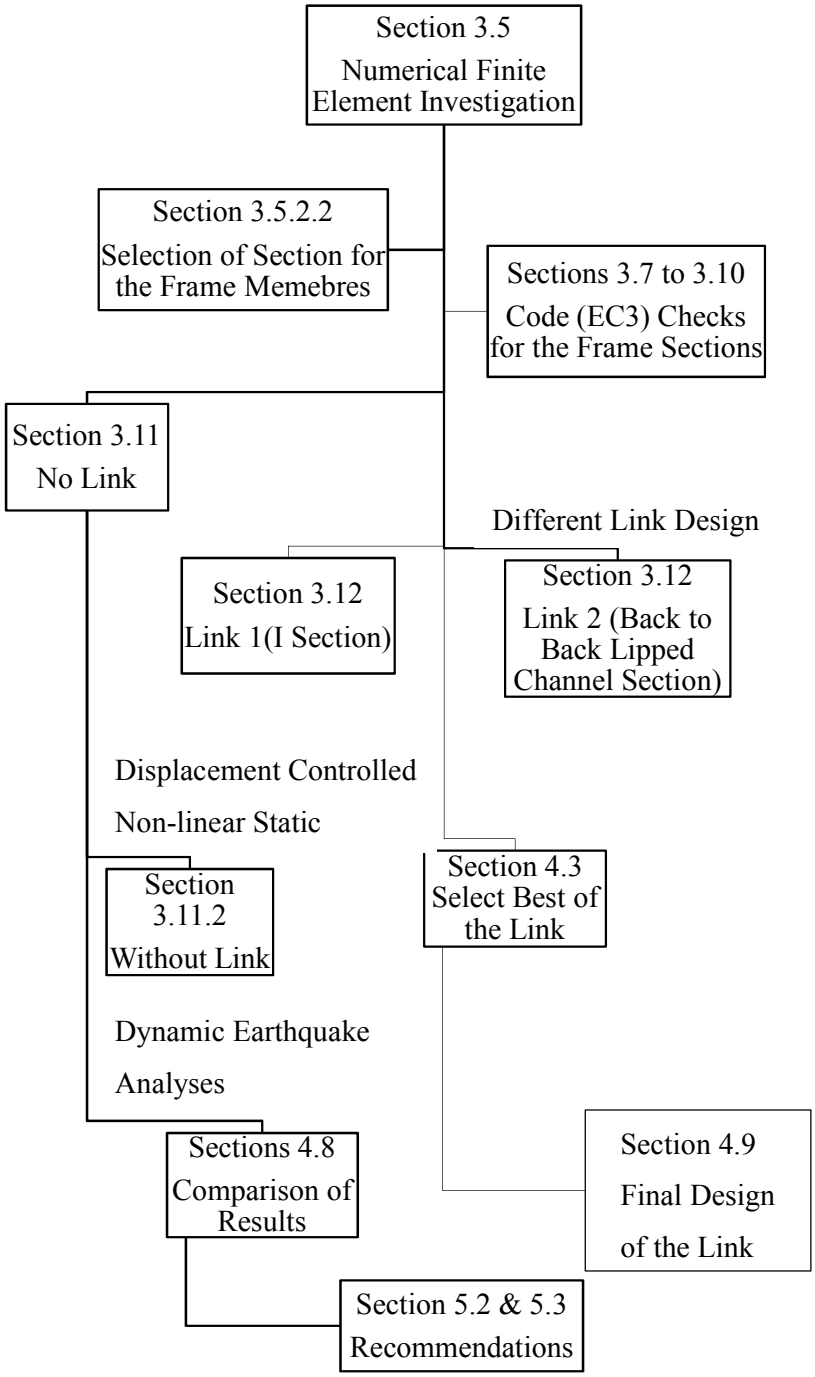

Figure 1.2 Flow chart shows design and assessment sequences.

Chapter 2

2 Literature Review

2.1 Introduction

Pitched-roof Steel Portal Frames are common structures used in single storey buildings which are widely used here in the UK and most of the countries including Sudan; and have become the most often used structure within this sector. It is estimated that 50% of the single storey steel work buildings are constructed by steel portal frames owing to its economy, ease of fabrication and versatility for large spans in the construction of pitched roofs portal frame such as warehouses, shopping centres, shops, factories etc. (Issa and Mohammad, 2009).

The basic structural form of this kind of structure was developed during the Second World War, as a result of the need to achieve the low rise- cost building envelope.

The portal frame structures are constructed mainly using hot-rolled sections, supporting the roofing and side cladding via cold-formed purlins and sheeting rails. However, in recent years, a significant growth in using cold-formed steel as an alternative of the traditional heavier hot-rolled steel structural members was driven by higher strength materials and a wider range of structural applications (Kumar and Kumar, 2012).

Because the sections are typically more slender than hot rolled sections their performance in earthquakes (or when subject to blast load) may be less good than hot rolled sections, this research proposes the use cold-formed steel or thin walled sections in a viable alternative and economical construction method for the framing of lightweight commercial, light industrial and agricultural buildings, community buildings and houses with modifications to improve the behaviour during earthquakes.

There are many advantages make using such lightweight materials is more economical compared with the conventional hot-rolled steel structural sections which include the following (Devos and Rensburgt, 1997):

l. Sections are marked and cut to the specifications in the factory and then bolted together on site with no need for specialist engineering services.

3. Lightweight Frames can often be erected manually without cranes leading to the reduction of the erection costs.

4. Often all the structural sections used for both the primary members and the secondary members can be purchased from the same supplier which may reduce acquisition costs.

2.2 Portal Frame Structures of Light Gauge Steel

This research work concentrates on portal frame structures made of lightweight materials which may be cold-formed steel or thin walled steel; and in this section we discuss the different lightweight materials and the uses and advantage of these materials.

2.2.1 Cold-formed steel and thin gauge steel

Thin-walled steel structures can be obtained either by cold-forming or thin plate welding. Cold-formed steel structures are thin gauge steel structural products that are made by bending flat sheets of steel at ambient temperature into shapes which will support more than the flat sheets themselves. They have been produced for more than a century since the first flat sheets of steel were produced by the steel mills (Hancock, 2003).

The important feature of cold-formed or thin-walled structures is formerly the lightness and therefore they are used mostly in products where the weight saving has a significant importance, this kind of lightweight products are naturally needed especially in transportation industries e.g. aircraft and motor industries.

However aluminium alloys rather than steel are generally used in the aircraft industry.

2.3 Advantage of Cold Formed Sections

Cold forming has the effect of increasing the yield strength of steel, the increase being the consequence of cold working well into the strain-hardening range. These

increases are predominant in zones where the metal is bent by folding. The effect of cold working is thus to enhance the mean yield stress by 15% - 30%.

Some of the main advantages of cold rolled sections, as compared with their hot-rolled counterparts are as follows (ISDG, 2011):

- Cross sectional shapes are formed to close tolerances and these can be consistently repeated for as long as required.
- Cold rolling can be employed to produce almost any desired shape to any desired length.
- Pre-galvanised or pre-coated metals can be formed, so that high resistance to corrosion, besides an attractive surface finish, can be achieved.
- All conventional jointing methods, (i.e. riveting, bolting, welding and adhesives) can be employed.
- High strength to weight ratio is achieved in cold-rolled products.
- They are usually light making it easy to transport and erect.

It is possible to displace the material far away from the neutral axis in order to enhance the load carrying capacity (particularly in beams). There is almost no limit to the type of cross section that can be formed (ISDG, 2011).

In Table 2.1 hot rolled and cold formed channel section properties having the same area of cross section are shown. From Table 2.1, it is obvious that thinner the section walls, the larger will be the corresponding moment of inertia values (Ixx and Iyy) and hence capable of resisting greater bending moments. The consequent reduction in the weight of steel in general applications produces economies both in steel costs as well as in the costs of handling transportation and erection. This, indeed, is one of the main reasons for the popularity and the consequent growth in the use of cold rolled steel. Also cold form steel is protected against corrosion by proper galvanising or powder coating in the factory itself. Usually a thickness limitation is also imposed, for components like lipped channels (ISDG, 2011).

While the strength to weight ratios obtained by using thinner material are significantly higher, particular care must be taken to make appropriate design provisions to account for the inevitable buckling problems (ISDG, 2011).

Table 2.1 Comparison of hot rolled and cold rolled sections (ISDG, 2011)

	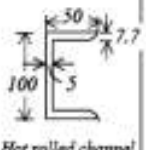 Hot rolled channel	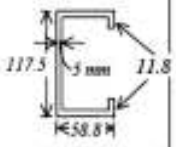 Cold rolled channel	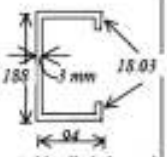 Cold rolled channel	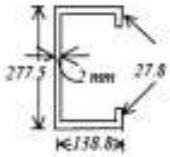 Cold rolled channel
A	$1193\ mm^2$	$1193\ mm^2$	$1193\ mm^2$	$1193\ mm^2$
I_{xx}	$1.9 \times 10^6\ mm^4$	$2.55 \times 10^6\ mm^4$	$6.99 \times 10^6\ mm^4$	$15.53 \times 10^6\ mm^4$
Z_{xx}	$38 \times 10^3\ mm^3$	$43.4 \times 10^3\ mm^3$	$74.3 \times 10^3\ mm^3$	$112 \times 10^3\ mm^3$
I_{yy}	$0.299 \times 10^6\ mm^4$	$0.47 \times 10^6\ mm^4$	$1.39 \times 10^6\ mm^4$	$3.16 \times 10^6\ mm^4$
Z_{yy}	$9.1 \times 10^3\ mm^3$	$11.9 \times 10^3\ mm^3$	$22 \times 10^3\ mm^3$	$33.4 \times 10^3\ mm^3$

2.4 Properties of Materials for Light Gauge Steel Structures

This section covers the properties of this structural material and as well as the approximate mechanical properties for this material used in commercial available software (ANSYS).

The stress-strain curve for cold formed steel can either be the sharp-yielding type (see Figure 2.1a) or the gradual-yielding type (see Figure 2.1b), (Yu, 1999). Design properties of materials that are essential for engineering design are determined using the stress –strain diagram which include the proportional limit, the elastic limit, the elastic modulus, the yield strength, the ultimate strength and the ductility (Philpot, 2011).

2.4.1 Properties of cold-formed steel

2.4.1.1 Yielding and ultimate strength

In strain controlled test cold formed steel when reaching the upper yield point the stress drops suddenly to a sustained lower yield stress. While there is an increasing strain without an increase in the stress the behaviour of the materials will be perfectly plastic (see Figure 2.1), and materials with this similar a stress- strain diagram are termed elasto-plastic (Philpot, 2011).

This section presents the different values of the yield stress and the ultimate stress in the different codes of design. These different values of stress in the three codes are driven out as result of the tensile test carried for different types of the cold rolled steel used, which are cold rolled steel sheet, cold reduced steel sheet of structural quality and cold-rolled flat products.

The value of yield strength (Fy) of cold rolled steel sheet based on minimum strength according to BS 5950-5(1998) is in the range of [200-350 MPa (N/mm^2)], in contrast the value is [220-320 MPa (N/mm^2)] for cold reduced steel sheet of structural quality and [240-400 MPa (N/mm^2)] for cold-rolled flat products made of high yield strength micro-alloyed steels for cold forming to EN 1993-1-3(2006).

The ultimate strength or high tensile strength (Fu) is the high stress value in the stress strain diagram. The value of the ultimate strength is 340 to 430 MPa (N/mm^2) for cold –formed steel sections and sheet to BS 5950-5 (1998), in the other hand in EN 1993-1-3(2006) it is 300 to 400 MPa (N/mm^2) for cold reduced steel sheet of structural quality and 340 to 460 MPa (N/mm^2) for cold-rolled flat products made of high yield strength micro-alloyed steels for cold forming.

In ASTM Standards the yield points or yield strengths of all 14 different steels range from 24 to 80 ksi (166 to 552 MPa). The tensile strengths of the same steels range from 42 to 100 ksi (290 to 690 MPa).The ratios of the tensile strength-to-yield point vary from 1.12 to 2.22 (Yu, 1999).

The mechanical properties (yield point, tensile strength, and ductility) of cold-formed steel sections, particularly at the corners (for bending), are sometimes substantially different from those of the flat steel sheet, strip, plate, or bar before forming. This is because the cold-forming operation increases the yield point and tensile strength and at the same time decreases the ductility. The effects of cold-work on the mechanical properties of corners usually depend on several parameters. The ratios of tensile strength-to-yield point, Fu/Fy, and inside bend radius-to-thickness, R/t, are considered to be the most important factors to affect the change in mechanical properties of cold-formed steel sections (Yu, 1999).

2.4.1.2 Modulus of elasticity, Tangent modulus, and Shear modulus

Modulus of elasticity (E) is a measure of the stiffness of a material and it is the ratio between the normal stress and normal strain in the elastic part of the stress – strain diagram (Philpot, 2011). And it can be stated mathematical as:

$$E = \frac{\sigma}{\varepsilon}$$

Equation 2.1

Where: σ the normal stress; ε the normal strain.

The modulus of elasticity adopted in BS 5950-5:1998 for cold-formed section and sheet is 205 KN/mm^2 (GPa), while it is 210E3 N/mm^2 (MPa) in EN 1993-1-1:2005.

The strength of cold-formed steel members that are governed by buckling depends not only on the yield point but also on the modulus of elasticity, E, and the tangent modulus, Et. A value of E equal to 29,500 ksi (203 GPa) is used in the AISI (2001) specification for the design of cold-formed steel structural members. This E value is slightly larger than the value of 29,000 ksi (200 GPa), which is being used in the AISC (1989) specification for the design of hot-rolled shapes (Yu, 1999).

The tangent modulus is defined by the slope of the stress-strain curve at any given stress level (Figure 2.1b). For sharp-yielding steels, Et equal to E up to the yield, but with gradual-yielding steels, Et equal to E only up to the proportional limit, f_{pr} (Figure 2.1b). Once the stress exceeds the proportional limit, the tangent modulus Et becomes progressively smaller than the initial modulus of elasticity (Yu, 1999). For cold-formed steel design to BS 5950-5(1998), the shear modulus G is taken as 79E3 MPa while it is 81E3 MPa in EN 1993-1-1(2005); and 11,300 ksi (77.9E3 MPa) according to the AISI (2001) specification.

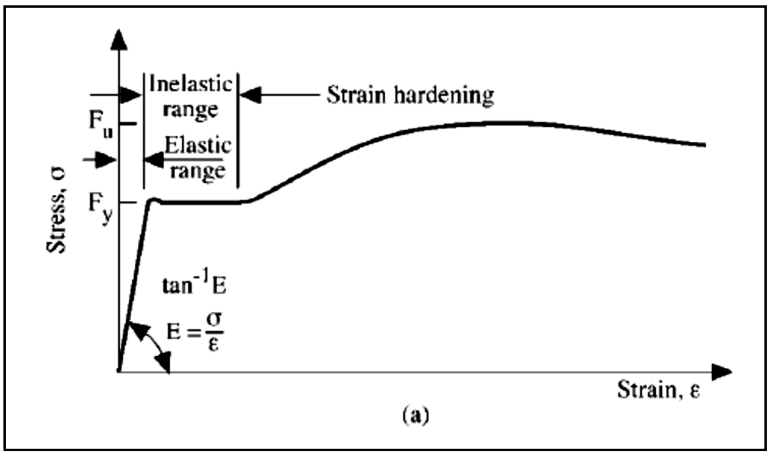

(a) Sharp- yielding

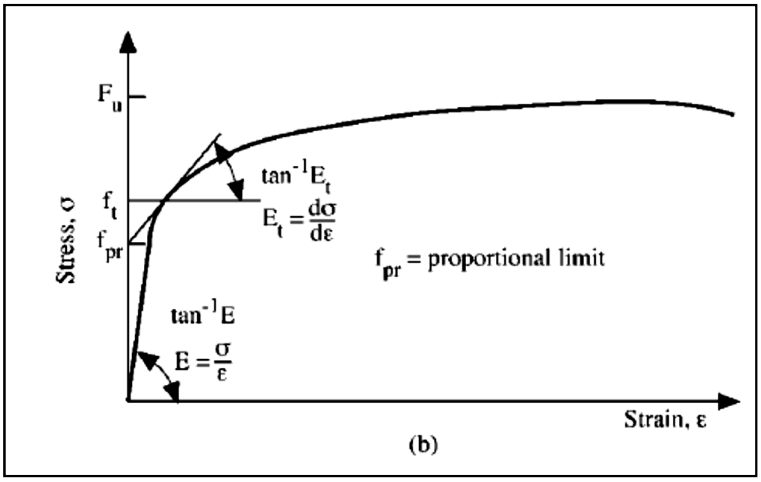

(b) Gradual- yielding

Figure 2.1 Stress strain curves of steel sheet or strip (Yu, 1999)

2.4.1.3 Poisson's ratio

This property is defined as the ratio of the lateral strain or transverse strain to the longitudinal or axial strain in which is denoted by ν (Philpot, 2011), and it is mathematically defined as:

$$\nu = \frac{\varepsilon_t}{\varepsilon_a} \qquad \text{Equation 2.2}$$

Where: ε_t the lateral strain; ε_a the axial strain.

The Poisson's ratio for cold-formed steel in the elastic range is adopted as 0.3 in both BS 5950-5:1998 and EN 1993-1-1:2005.

2.4.1.4 Ductility

Ductility describes the material's capacity for plastic deformation. A material that can withstand large strain before fracture is called a ductile material. According to the EN 1993-1-1:2005 , the ratio of Fu/Fy which represents the minimum ductility requirement for the steels used for structural framing members should not be less than 1.10, and the total elongation should not be less than 15% for gauge length of 5,65 $Ao^{1/2}$, where A0 is the original cross-sectional area (EN 1993-1-3:2006), while the minimum ductility should not be less than 1.08, and the total elongation should not be less than 10% for a 2-in. (50.8 mm) gage length according to the AISI specification (Yu, 1999).

2.5 Reviews of Connections (Joints) of the Frame

Methods for connecting thin walled materials members such as cold-formed are often quite different from those of the traditional hot-rolled members. For hot rolled sections the common connection methods are welding and bolting, however connection types as screws, riveting and clinching may be used for the lightweight members made of cold-formed or thin gauge members. Also the structural behaviour of cold-formed and thin gauge connections for bolted connections is often quite different from the conventional hot-rolled members due to the thin sheets and higher strength steels used (Hancock, 2003). Furthermore cold-formed steel portal frames joints are designed elastically with no need for rigid joints that are expensive to fabricate. Mainly due to the sectional buckling phenomena, cold formed sections are of class 4 or class 3, at the most, but also due to the effect of cold-forming by stress hardening; the cold formed steel sections possess a low ductility and are not generally allowed for plastic design (Bayan et al, 2011). In conventional hot-rolled steel portal frames, which are designed plastically, the rigidity of the joint is a key requirement in the design (Wrzesien, 2008).

2.5.1 Types of the connections

The classical and traditional analysis and design of portal frames structures, is often based on the assumption that beam-to-column connections are either as perfectly pinned or as fully rigid and other behaviour between those are semi-rigid. Pinned connections have no moment transfer between the beam and the column; this means that the connections have no rotational stiffness and cannot transmit moments although they do transmit axial and shear forces to the attached members (Figure 2.2a), while fixed connections have complete rotational continuity (Figure 2.2b) and therefore transmit all form of loads between beam and column (Díaz et al, 2011). Experimental work and research indicate that pinned connections often possess some rotational stiffness and exhibit some rigidity because of some ability to resist rotational deformations, whilst rigid connections (fully-welded connections) have finite flexibility (Ashtiani, 1996 & Feng, 1994), this affects the structural behaviour but it may be difficult to obtain a detailed understanding of the behaviour of the joint. With all these considerations it has been suggested that joints in steel portal frame structures in reality have finite stiffness and are therefore semi-rigid as shown in Figure 2.2c (Díaz et al, 2011).

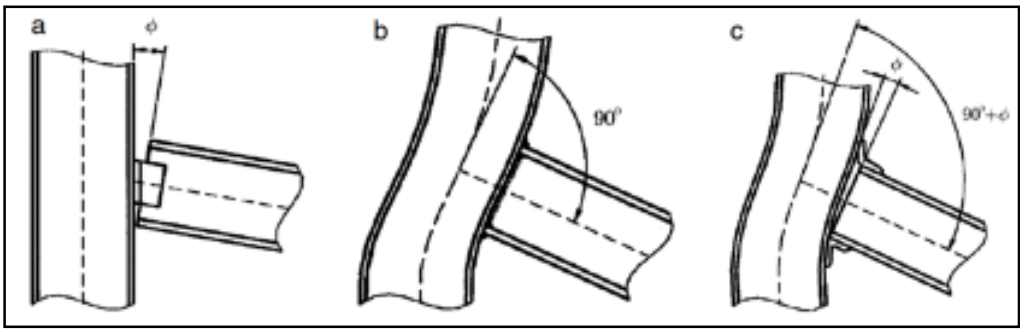

Figure 2.2 Joint types according to their behaviour, where φ is the angular rotation between the beam and the column: (a) pinned; (b) rigid; and (c) semi-rigid
(Díaz, 2011)

2.5.2 Modelling the rotational behaviour of the connections

Since the 1930s, there has been considerably evolution in the analysis methods of semi-rigid joints to obtain the true structural response. These analysis methods start with the traditional method such as slope-deflection equation and moment distribution methods, to the matrix stiffness methods in the 1960's and nowadays complex iterative analysis methods, coupling the global and joint structural analyses (Díaz et al, 2011).

Since the true behaviour of a joint can be incorporated within the global analysis of the structure by using the moment–rotation curve ($M_{j-\varphi}$), (Figure 2.3), which is used to model the beam-to-column joint behaviour, many methods for modelling moment-rotation curves of semi-rigid connections have been developed in conjunction with experimental studies. Modelling of the moment rotation curve could be achieved by determining the mechanical properties of the joint in terms of its rotational stiffness (K_j), moment resistance ($M_{j,Rd}$), and rotational capacity (φ_{Cd}), starting from their geometrical and mechanical properties (Díaz et al, 2011).

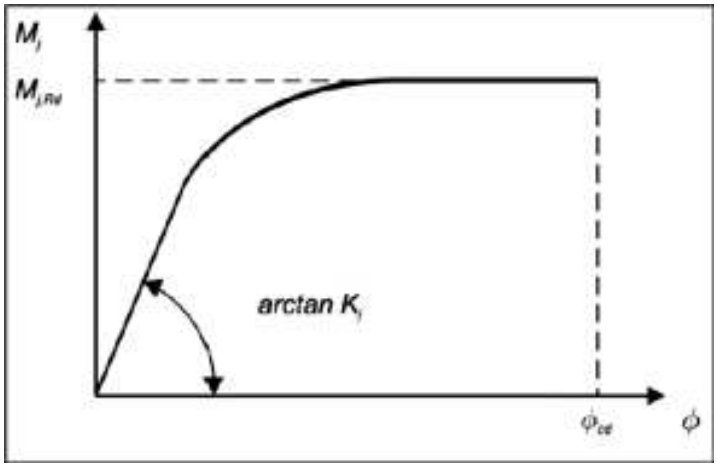

Figure 2.3 Moment-rotation ($M_{j-\varphi}$) curve. (Díaz et al, 2011)

2.5.3 Methods for modelling a joint, rotational behaviour

There are several models proposed in the literature to represent the moment-rotation behaviour of various types of connections in term of its mechanical behaviour, the most commonly used models are included, these are: analytical, experimental, mechanical and numerical. The most popular of these is the mechanical model,

which has several variances, the most popular being the Component Method, which is implemented in EN1993-1-8, (2005). This method considers a joint as a set of ‘‘individual basic components’’, which allows the determination of the moment resistance and stiffness characteristics of all the different components of the joint (Díaz et al, 2011). Modelling of joint behaviour in the global structural analysis of the frame is associated with mathematical representation of the moment–rotation curve which can be performed by means of different relationships and levels of precision and the selection for the representation which can be linear, bilinear, multilinear and nonlinear (Díaz et al, 2011). Details of these models as they had been used in the literature are presented here. This section covers only the modelling methods for the joint conducted in the past, the conclusions for these tests is discussed in section 2.5.6 and 2.6.

2.5.3.1 Experimental testing

The most accurate knowledge of the joint behaviour is obtained through experimental tests, but this method has its faults, like others methods of modelling, as there are errors accompany the experimental work. This technique is usually reserved for research purposes only, as it is too expensive for everyday design practice (Díaz et al, 2011).

The first experiment on cold-formed steel portal joints was performed by Baignent and Hancock (1982). It was the first test to assess the rigidity of steel portal frame connections as before that the joints were considered as rigid, due to the high-tensile grip bolts used to connect the parts of the joint (Wrzesien and Lim, 2008).

The next set of tests on joints of portal frame were reported by Kirk (1986) on the swagebeam portal framing system and undertaken by Professor Bryan at Salford University, the primary innovation was that the joints could formed through the swages rolled in the brackets which connected with matching swages in the webs of the channel-sections (Wrzesien and Lim, 2008). While Mäkeläinen and Kankaanpää (1996) used a portal framing system made of back-to-back sigma sections connected though the web via brackets in his tests (Wrzesien and Lim, 2008).

Chung and Lau (1999) and Lim and Nethercot (2003), reported tests on an arrangement of portal framing system constructed from back-to-back channel, with

the joints connected through brackets bolted between the webs of the channel-sections. Applications of such connections include the eaves and apex joints of portal frames, as illustrated in Figure 2.4 and Figure 2.5 also available in (Kirk, 1986) and (Lim and Nethercot, 2002). The particular problem of the moment-capacity of such joints being lower than that of the cold-formed steel sections being connected because of web buckling, caused by the concentration of load transfer from the bolts, is addressed. Lim and Nethercot (2003) performed a combination of laboratory tests and finite element analyses to investigate this mode of failure that is principally dependent on the length of its bolt-group. Their work was focused on the influence of the bolt-group size on the strength and stiffness of the channel-sections. It was demonstrated that there is good agreement between the measured ultimate moment-capacity and that predicted by using the finite element method (Lim and Nethercot, 2003). A full review of this and other related work is available in Lim (2001).

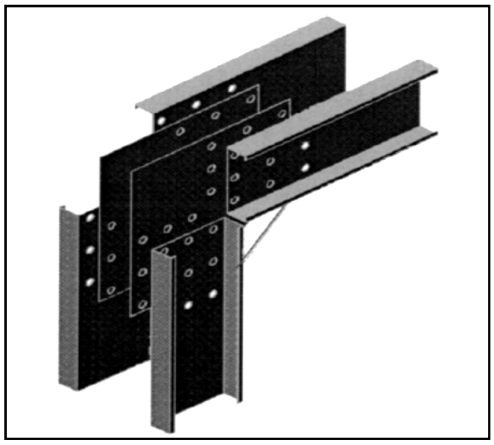

Figure 2.4 Details of arrangement for the knees joint by Lim (2003)

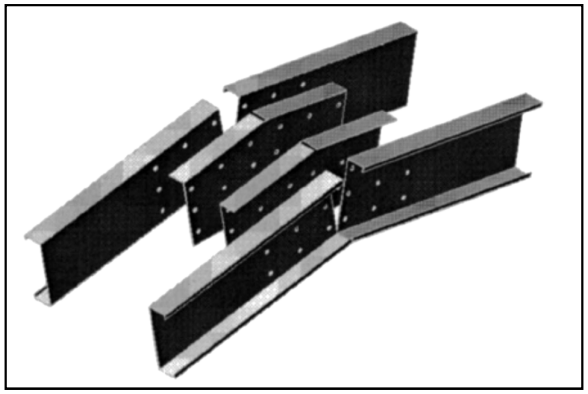

Figure 2.5 Details of arrangement for the ridge joint by Lim (2003)

Mills and LaBoube (2004) performed experimental tests on joints currently used in Australia, for cold-formed steel portal frame sheds, to study the feasibility and construction advantages of using self-drilling screws instead of conventional bolting as a connection alternative for the rigid knee joints in cold-formed channel portal frames. The joints were constructed from single channel-sections. Self-drilling screws were used. The apex joint was also studied with similar arrangement, but using double lipped channel-sections as the gusset plate, screwed back-to-back to the rafters.

Dubina et al (2004a) conducted experimental studies in order to evaluate the performance of eaves (knee) and ridge (apex) joints of pitched roof cold formed steel portal frames under monotonic and cyclic loading in terms of their rigidity, strength and ductility, in which the ductility was found low and the seismic force can be evaluated by using a reduction factor q of 1.5-2.0 corresponding to the Low "L" ductility class as specified in EN 1998-1 (2004). The back-to-back built up sections used for the elements of the frame were made by Lindab Ltd. C350/3.5 profiles (SUB350-fy = 350N/mm2). Three different types of joints using welded connecting gusset elements (S235-fy = 235N/mm^2) had been used (see Figure 2.6 and Figure 2.7). One group of specimens has the name (KSG and RSG) used spaced gussets, (Figure 2.8c). In this case, bolts were provided only on the web of the C350 profile. In the other cases, where two different details were used for the connecting bracket – i.e. welded I sections only has the name (KIS and RIS), and welded I section with plate bisector has the name (KIP and RIP), respectively - bolts were provided on the web only (Figure 2.8a), or both on the web and the flanges (Figure 2.8b). The case where bolts were also on the flanges had in their name the distinctive FB (Dubina et al, 2004a).

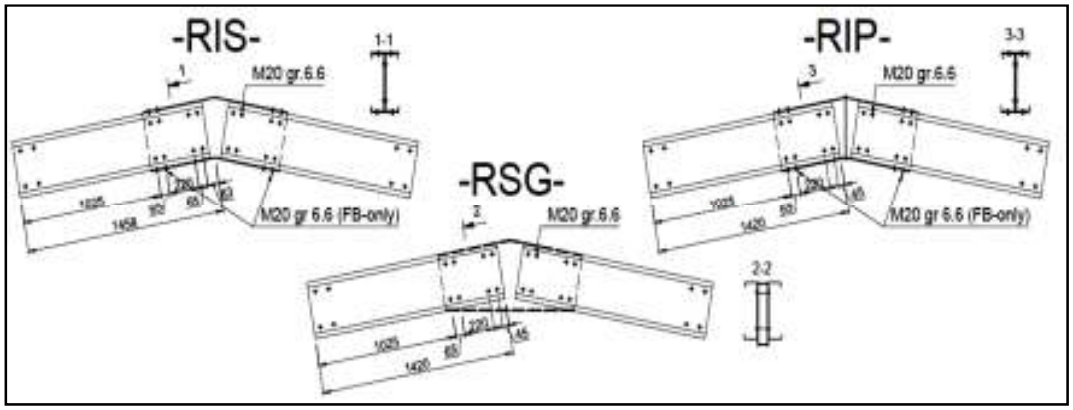

Figure 2.6 Main dimensions of ridge connections (Dubina et al, 2004a).

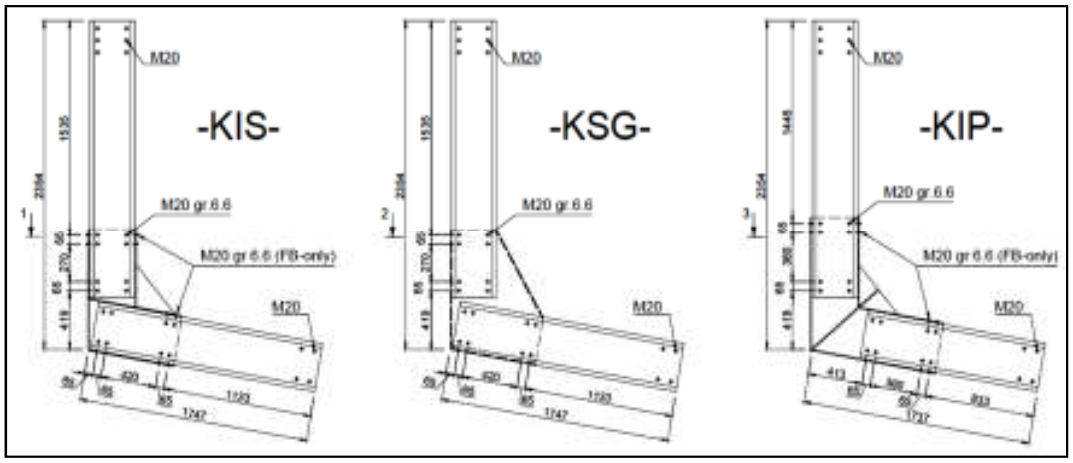

Figure 2.7 Main dimensions of knee connections (Dubina et al, 2004a).

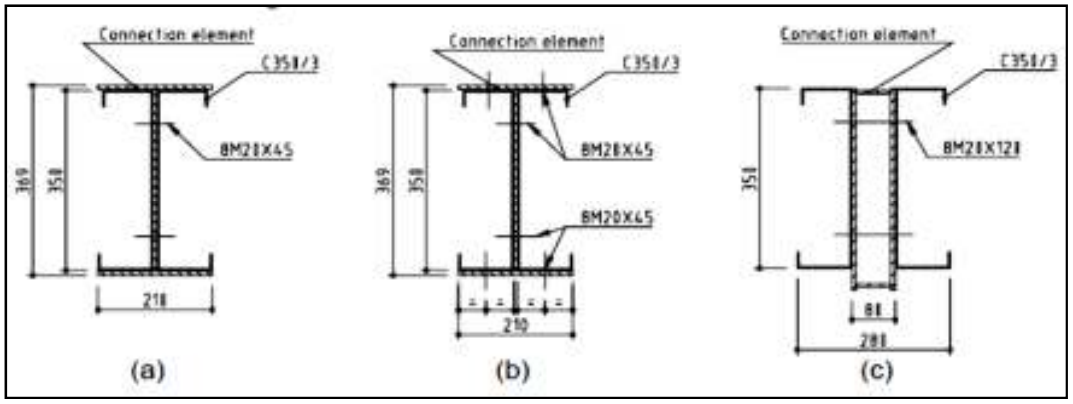

Figure 2.8 Bolt configuration in the cross section (Dubina et al, 2004a).

Dundu and Kemp (2006) described tests on a portal framing system constructed from single channels connected back-to-back as shown in Figure 2.9. This arrangement is similar to that of Mills and LaBoube (2004) when they developed and tested the self-drilling screw joints. Dundu and Kemp (2006) concentrated on the ductility of the joints as their tests were concerned with the development of a plastic hinge. In this test the primary innovation was providing lateral restraint for a cold formed portal frame which was introduced through an angle connection between the web of the rafter and purlin to provide effective lateral restraint to both the inside and outside flanges of the frame, which helped eliminated the lateral-torsional buckling failure mode (Dundu and Kemp, 2006).

Kwon et al (2006) conducted a research on applications of closed sections produced by a combination of cold-rolling and clinching techniques to construct portal frame (Wrzesien and Lim, 2008).

Rhodes and Burnsin (2006) reported extensive component tests on the eaves joint of a cold-formed steel portal framing system constructed from back-to-back channel-sections for the columns and rafters, the proposed eaves joint used knee-braces formed through back-to-back channel-sections bolted to the flanges of the column and rafter through a welded bracket. At the eaves, the joint was formed through a pair of angles sections; to avoid the failure of the flange under concentrated load a pair of angle stiffeners was introduced. The joint arrangement tested by Rhodes and Burnsin (2006) removed the necessity of constructing expensive rigid joints by introducing knee brace (Wrzesien and Lim, 2008).

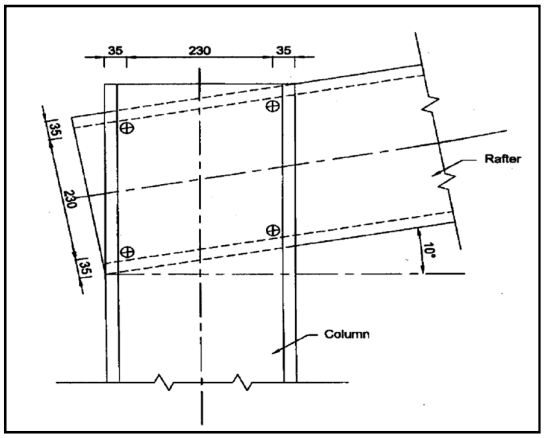

Figure 2.9 Bolted connection, arrangement of Dundu and Kemp (2006)

2.5.3.2 Mechanical models

This model is also known as a spring model. In this model the joint behaviour is represented by using a combination of rigid and flexible components, which are modelled by means of moment resistance and stiffness values obtained from empirical relationships. The nonlinear behaviour for this model is obtained by means of inelastic constitutive laws used for the spring elements.

To develop a mechanical model three steps are required:

(i) Identify the components of the joint that will have a significant influence on the behaviour of the joint according to the deformation and failure criteria.

(ii) Determine the constitutive laws for each component of the joint using analytical, experimental or numerical means.

(iii) Assemble all of the components together to produce the moment–rotation curve for a specific complete joint.

This procedure is very flexible as it can be applied to any type of joint: bolted or welded, and specific effects can be introduced, such as: plastic hardening or bolt pretensioning. This is because to represent the joint behaviour you need to have only the constitutive behaviour of the components which make up the joint.

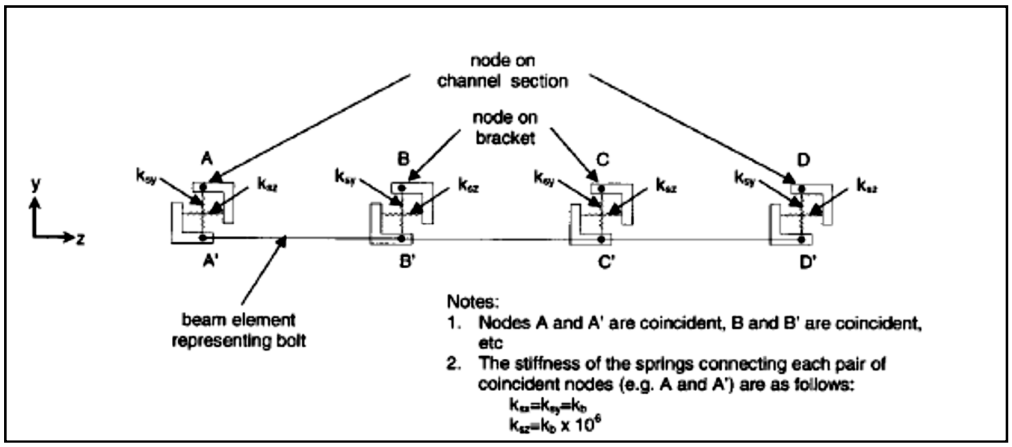

Figure 2.10 System of spring element in local y-z plane
(Lim and Nethercot, 2004b).

The historical records show that, this type of model was used first early in steel frames by Wales and Rossow (1983) and followed by Kennedy and Hafez (1984) and since then, significant research has been carried out using mechanical models to study the behaviour of joints until Lemonis and Gantes (2009) proposed a model based on the component method for bolted connections with end-plates and angles (Díaz et. al, 2011).

On the other hand Lim and Nethercot (2004b) used this type of model of a portal framing system to predict the deflection of the frame which divided into three components: Deflection due to flexure of the column and rafter members, deflection due to bolt-hole elongation and deflection due to in-plane bracket deformation. The bolt holes are represented by a system of spring elements to represent the effect that each bolt has on the behaviour of the joint. Figure 2.10 shows the details of the system of spring elements employed in this test. As can be seen, each bolt is modelled using three beam elements with nodes that are coincident with the centre of the bolt hole of each plate. Between coincident nodes, spring elements of zero size are defined in each of the *x*, *y*, and *z* directions.

Separation of the plates is prevented by the axial stiffness of the beam elements; the axial, flexural, and torsional stiffnesses of the beam elements are based on the properties of the bolt shank. The bolt-hole elongation caused by bearing of the bolt shank against the bolt hole is represented by the spring stiffnesses ksx and ksy, which Ksx=ksy=kb. The spring stiffness ksz is given a very high stiffness to prevent separation of the coincident nodes, Ksz= kb x 10^6 (Lim and Nethercot, 2004b). This test was performed to compare the apex deflections obtained using the beam idealization with those obtained using the shell idealization for two frames A and B. The total deflections obtained using both types of models were similar. There is excellent agreement between the two idealizations for the deflection due to bolt-hole elongation; representing the effects of bolt-hole elongation using rotational spring elements is therefore justified. More details for this work are available in Lim and Nethercot (2004b).

The component method is a hybrid analytical–mechanical method. The joint modelling consists of an assembly of extensional springs (components) and rigid links, where each spring represents a specific part of the joint with its own strength

and rigidity, dependent on the type of loading. The behaviour of the joint is obtained by knowing the mechanical and geometrical properties of each component of the joint. It gives good results for a joint which is acting primarily in bending with minimal axial loading.

Dubina (2008) implemented the component method for cold formed portal frames to evaluate their performance under horizontal (seismic) load, and to validate the joint model used in the global analysis. The results were compared with experimental test performed for groups of connections. The comparison between the experimental and analytical stiffness of the connection showed a fair agreement as detailed in 2.5.5.5 of this thesis. The detail of the frame members used is in section 2.5.3.1 of this thesis.

2.5.3.3 Numerical models

Numerical simulation started to be used for several reasons:

(i) As a means of overcoming the lack of experimental results; (ii) to understand important local effects which are difficult to measure with sufficient accuracy, e.g. prying and contact forces between the bolt and the connection components; (iii) to generate extensive parametric studies (Díaz et. al, 2011); and (iv) increased computer power made it practical.

Finite Element Analysis (FEA) is ideally suited to determine the rotation of a joint; however such analysis is still computationally expensive. The moment–rotation curve is the result of the complex interaction between the different elements of a joint. The analysis of steel joints requires the introduction of geometrical and material nonlinearities of the elementary parts of the connection; bolt preload and its response under a general stress distribution; interaction between bolts and plate components: i.e., shank and hole, head or nut contact; compressive interface stresses and friction resistance; slip due to bolt-to-hole clearance; variability of contact zones; welds; imperfections (Díaz et. al, 2011).

Currently the Finite Element Method (FEM) allows for the introduction into the model of: large deformations, plasticity, strain-hardening, instability effects, the representation of large strain and/or displacements, contacts between plates and pre-stressing of bolts (Díaz et. al, 2011).

The first FEM study was carried out on a steel frame with welded beam-to-column joints by Bose et al (1972). This included: plasticity, strain hardening and buckling. The results obtained compared favourably with available experimental results. Since then, several researchers have used the FEM to investigate joint behaviour. Krishnamurthy and Graddy (1976) were the first to model three-dimensional (3D) joints. They used an eight-node brick element to model the end-plate connection (Díaz et. al, 2011).

Lim (2001) investigated the behaviour of a overall cold formed steel portal frame with the effect of joints taken into consideration, and proposed design rules for this type of structure, based on finite element results and experimental tests, using different types of elements including beam, shell and solid elements. The study included the following aspects, behaviour of bolted moment connections, evaluation of bolt hole elongation stiffness and the effect of semi rigid joints and finite connection length on frame behaviour, (Lim, 2001).

Lim and Nethercot (2003) investigated the ultimate moment capacity of the apex joint for bolted moment-connections between cold-formed steel portal members, formed by using brackets bolted to the webs of the section, the ultimate moment capacity being lower because of web buckling. A combination of laboratory tests and finite element analyses was used to investigate this mode of failure which was always followed by the buckling of the compression flange, due to the reduction of the transverse bending stiffness of the section which caused by the premature buckling of the web (Plate 2.1 and Figure 2.11). The finite element program ABAQUS was used for the analysis. The channel-sections were modelled using the eight-noded thin shell element S8R5, with six layers through the thickness to allow for the effects of plastic yielding. Furthermore, as the bolts and bolt-holes were not modelled, at the location of each bolt-hole spring elements acting in the in-plane x- and y-directions were defined. These springs were modelled using SPRING2 elements.

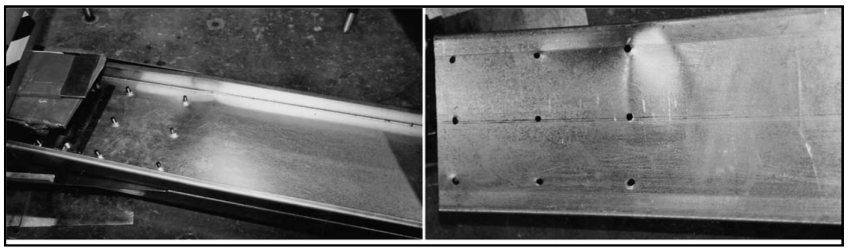

Plate 2.1 Failure of the joint after the experimental tests (Lim and Nethercot, 2003).

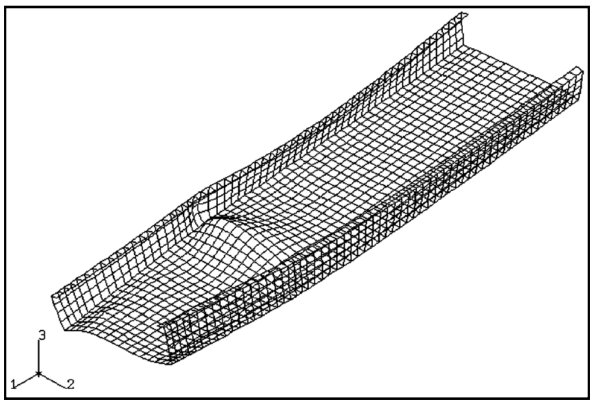

Figure 2.11 Deformed shape for channel section of joint A
(Lim and Nethercot, 2003).

Lim and Nethercot (2004a) also used FEA in simple bolted moment-connections, formed through brackets for both the eaves and apex joints to predict the initial stiffness. This stiffness was used to represent in-plane elongation of the bolt-holes caused by bearing against the bolt-shanks. The plate was modelled using solid element, only half the plate was modelled (Figure 2.12).The model was solved using non-linear large-displacement elasto-plastic analysis using the finite element program ABAQUS.

Further work was reported by Lim and Nethercot (2004b) with a cold –formed steel portal frame, where finite element modelling was used to study both the detailed joint behaviour and the overall frame response using beam element, shell element and experimental test. The main purpose of the study was to validate the use of beam elements for predicting frame deflections, comparison with shell elements and experimental tests. Beam elements were used to idealize the column and rafter

members and rotational spring elements were used to represent the rotational flexibility of the eaves and apex joints.

In addition, the beam idealization also took into account the connection length of the eaves and apex joints. Their study conclusion can be summarized as: beam idealization is suitable for the purposes of analysing a cold-formed steel portal frame to the ultimate and serviceability limit states, including making appropriate allowances for connection effects, without the need to resort to expensive finite element shell analysis.

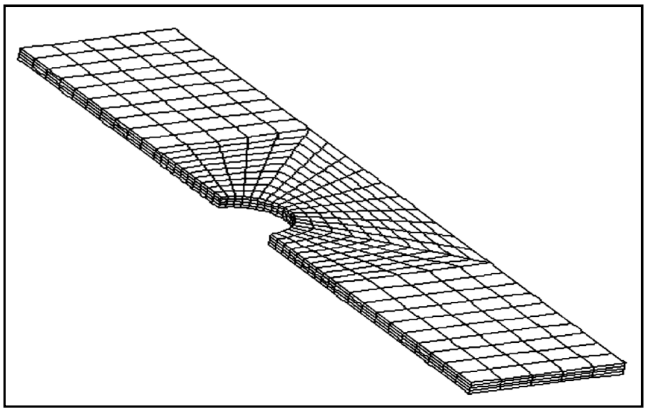

Figure 2.12 Details of finite element mesh of plate.
(Lim and Nethercot, 2004b)

Dubina et al (2010) performed experimental and numerical simulation programs carried out on full-scale pitched roof cold-formed steel portal frames of back-to-back lipped channel sections with bolted joints in order to evaluate the influence of different type of geometrical and structural imperfections on the structural stability performance of these structures. Two frames units have been tested under: (1) horizontal load, and (2) horizontal and gravity loadings. For numerical simulations the imperfections were taken according to the tolerances specified in EN 1090-2 and the provisions of EN 1993-1-1. The same sections and configuration used in this test for experimental work was as in section 2.5.3.1 of this thesis. Finite Element (FE) models have been prepared for each experimental test, e.g.: (1) one for the first experimental test (C1), where only lateral loading (seismic effect) was applied at left eaves up to failure and, (2) another one for the second experimental test (C2), where

constant gravity loading was applied, simulating the dead and snow loads corresponding to seismic load combination, followed by the lateral load up to failure. ABAQUS/CAE v.6.8 was used for these numerical simulations. For the FE model used in the study node shell element (S4R) used to model the cold-formed members. The mesh size for the shell elements was around 24x24mm. For the analyses the connections were assumed to be rigid. The material properties for thin-walled cold-formed elements, determined from coupon tests, are: yield strength of 486N/mm2, ultimate tensile strength 553N/mm2, Young's modulus E=210000N/mm2 and a measured thickness minus zinc coating of 2.93mm. Based on tests results, the material was modelled as bilinear, isotropic, elasto-plastic. The results of this test was in case of frame (C1) failure caused by local buckling in the beam near the right eaves; this local buckling in the beam near the right eaves was followed by a combined local buckling and lateral-torsional buckling of one of the columns at the mid-height in case of frame (C2). Finally, local buckling of the beam at the left eaves was observed. A good agreement was shown between the experimental and numerical results. Figure 2.13 shows the deformed shape of the nonlinear elastic-plastic model and local plastic mechanism formed at the edge of bracket-to-rafter lap for Frame C1, similar with the experimental one presented in Figure 2.14 (Dubina et al, 2010).

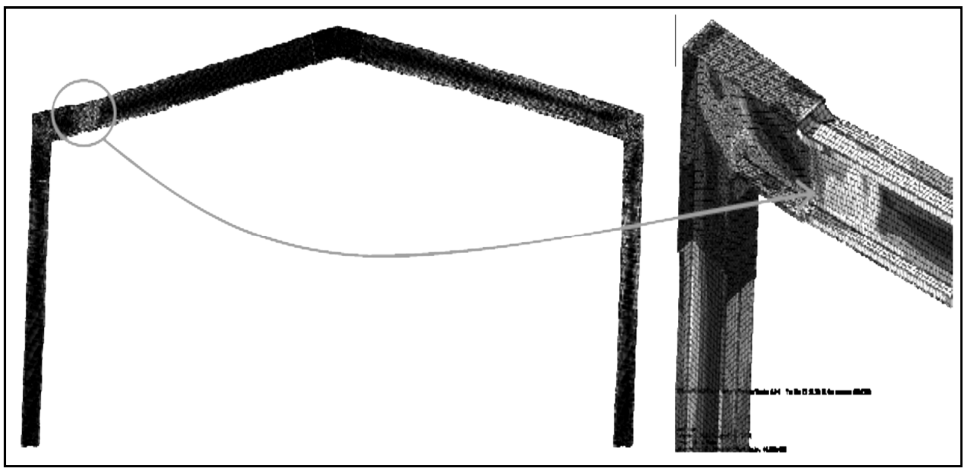

Figure 2.13 Frame C1: nonlinear elastic-plastic model and local plastic mechanism (Dubina et al, 2010)

Figure 2.14 C1 frame: local buckling of the left beam connection.
(Dubina et al, 2010)

2.5.3.4 Analytical models

Analytical models use the basic concepts of structural analysis: equilibrium, compatibility and material constitutive relations, to obtain the rotational stiffness (K_j) and moment resistance ($M_{j,Rd}$) of a joint due to its geometric and mechanical properties.

Dubina et al (2008) worked extensively to predict the influence of joint characteristics on global behaviour of cold-formed pitched-roof portal frames with bolted joints. Experimental tests were performed, with the primary objective to assess their performance under horizontal (seismic) loading and to validate the joint model used in the global analysis. Accordingly three frame models were analysed, with the same members properties and sections detailed in section 2.5.3.1 of this thesis, the first model (M1) the connections were considered rigid. Measured geometrical and mechanical characteristics were used to model members with analytically determined moment capacity (Mc), and effective cross-section modulus. The second model (M2) was obtained from model (M1) by adopting an elastic–perfectly plastic model of the connection moment–rotation response with rotational stiffness (K_j) and moment resistance ($M_{j,Rd}$) using the component method (Figure 2.15). While the third model (M3), the elasto-plastic model was enhanced with post elastic response in terms of rotation with applied moment (Figure 2.16),

Plastic rotation was determined assuming an ultimate rotation θ_{Cu} equal to 1.4 times yield rotation θ_{Cy}. The softening branch was determined by considering a drop of moment capacity to 50% from the maximum, at a rotation θ_{Cr} of 4.0 times the yield rotation. Model (M3) showed the best agreement between the numerical and experimental results.

2.5.4 Mathematical representation of moment–rotation curve

The behaviour of joints needs to be incorporated in the global analysis of a structure, to achieve this, the mathematical expression of the moment–rotation curve is considered in terms of rotational deformation, rotational stiffness and design moment resistance. This mathematical representation for the joint can be performed at different levels of precision: (a) linear; (b) bilinear; (c) multilinear (trilinear); (d) nonlinear as in (Figure 2.17), which shows the different mathematical representations of the moment–rotation curve (Díaz et. al, 2011).

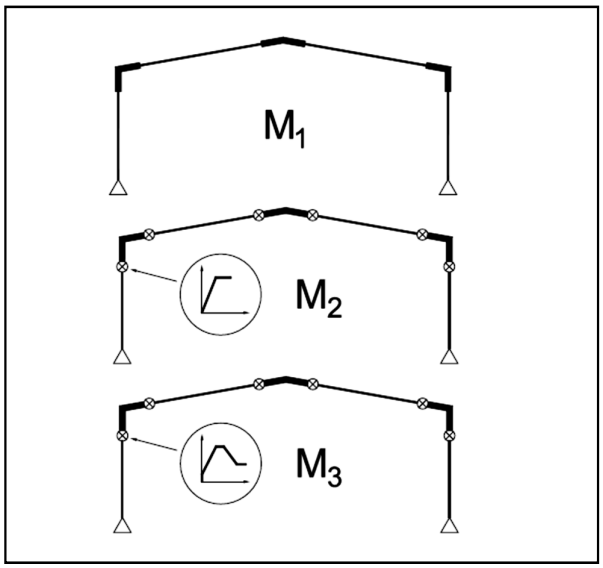

Figure 2.15 Structural models: (a) rigid connections M1 (b) elastic plastic connection M2(c) degrading connection M3. (Dubina et al, 2008).

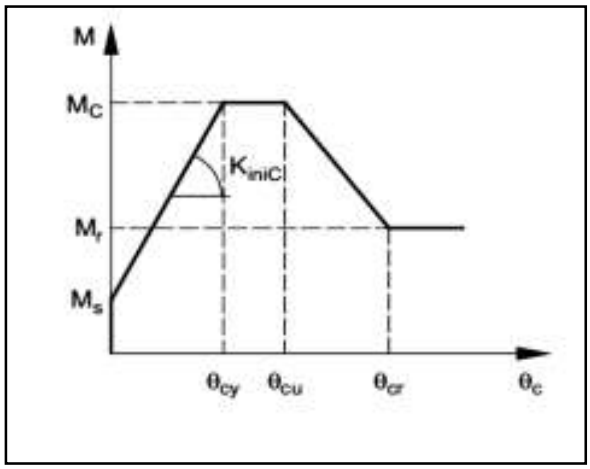

Figure 2.16 Parameters of the M3 connection model.
(Dubina et al, 2008).

i. Linear model

The linear model is the simplest to use but it is the least accurate. It usually overestimates the rigidity of the joint and is only dependent on the rotational stiffness (K_ϕ) of the joint (Equation 2.3). In the early of the twentieth century Bathoet al., Rathbun, Monforton and Wu, amongst others, used this model in steel frame (Díaz et. al, 2011).

$$M_j = K_\varphi \varphi$$

Equation 2.3

ii. Bilinear model

This model depends on three parameters, the: rotational stiffness (K_φ); plastic moment ($M_{j,p}$); and plastic rotational stiffness ($K_{\varphi,p}$) of the joint, (Equation 2.4), and as implemented in FEA programs, it has a sharp change in rigidity at the intersection of the two curves (Figure 2.17) (Díaz et. al, 2011).

This model has been used by many researchers in cold formed portal frames, Lim and Nethercot (2004b) used this model in experimental tests and numerical analysis to predict the deflection of a cold formed portal frame using beam finite elements in the program ABAQUS. This stiffness was used to represent in-plane elongation of

the bolt-holes caused by bearing against the bolt-shanks. More details about Lim's work could be found in Lim and Nethercot (2004a and 2004b). Dubina (2008) also implemented this model experimentally and numerically using the component method in Eurocode 3 (part1-8) to calculate the moment resistance and stiffness of the connection for one of the frame model (M2) as was explained in section 2.5.3.4 of this thesis. He also used experimental tests on the joints to find the moment resistance and stiffness of the connection. The main objective of this study was to assess performance of pitched-roof cold-formed portal frames with moment-resisting joints under lateral loading, with particular emphasis on earthquake loading by experimental test and numerical simulation. For the numerical work Dubina (2008) used a nonlinear static analysis under increasing lateral load. The SAP2000 computer code was applied using the values of the moment resistance and stiffness of the connection that already been calculated. The numerical and experimental results were compared and resulted in good agreement. More details for this work see Dubina (2008).

$$M_j = K_\varphi \varphi \quad \text{for} \quad M_j \le M_{jp}$$

Equation 2.4

$$K_{\phi,p}\varphi \quad \text{for} \quad M_j > M_{j,p} \qquad \text{Equation 2.5}$$

iii. Multilinear model

This model was proposed to remedy the problem of the bilinear model. Dubina et al (2008) used a trilinear representation with five parameters, (Equation 2.5), the: rotational stiffness (K_φ); first yielding moment ($M_{j,y}$); post-yielding rotational stiffness ($K_{\varphi,y}$); plastic moment ($M_{j,p}$); and plastic rotational stiffness ($K_{\varphi,p}$) of the joint when he conducted a full-scale tests and numerical simulation to assess performance of pitched-roof cold-formed portal frames with moment-resisting joints under lateral loading for the frame model (M3), as it had been explained in section 22.5.3.4 of this thesis.

$$M_j = K_\varphi \varphi \quad \text{for} \quad M_j \le M_{j,y} \qquad \text{Equation 2.6}$$

$$M_j = K_{\varphi,y} \varphi \quad \text{for} \quad M_{j,y} < M_j < M_{j,p} \qquad \text{Equation 2.7}$$

$$M_j = K_{\varphi,p} \varphi \quad \text{for} \quad M_{j,p} \le M_j$$

Equation 2.8

The representation proposed in Eurocode 3(2005) is divided into three segments as in Figure 2.18, although for elastic–plastic analysis, a simplified bilinear model is proposed. The first segment of the curve has the linear behaviour of Equation 2.3 up to the moment value of 2/3 $M_{j,Rd}$, where $M_{j,Rd}$ is the design value of the joint plastic moment $M_{j,p}$. The second segment is nonlinear in the range of $2/3M_{j,Rd} < M_j < M_{j,Rd}$ (Equation 2.6).

$$M_j = \frac{K_\emptyset}{\left(1.5 \frac{M_j}{M_{j,Rd}}\right)^\xi} \emptyset$$

Equation 2.9

Where ξ has different values:

2.7 for welded, bolted end-plate and base-plate connections.

3.1 for bolted angle flange cleats.

The last segment is a straight horizontal line representing plastic behaviour ($M_j = M_{j,Rd}$),

iv. Nonlinear model

This, the most accurate model so far, by Ramberg and Osgood (1943) as in Equation 2.7, depends on three parameters rotational stiffness (K_φ), rotation (φ) of the joint, and the shape factor (n) which characterizes the knee of the moment–rotation curve, as in Figure 2.19. The curve becomes bilinear with elastic–perfectly plastic behaviour as $n \rightarrow \infty$ at which point the plastic moment of the joint is equal to the reference moment M_0 (Díaz et. al, 2011).

$$\frac{\emptyset}{\emptyset_0} = \frac{M}{M_0}\left[1 + \left(\frac{M}{M_0}\right)^{n-1}\right] \qquad \text{Equation 2.10}$$

Where: $M_0 = K_\emptyset \emptyset_0$

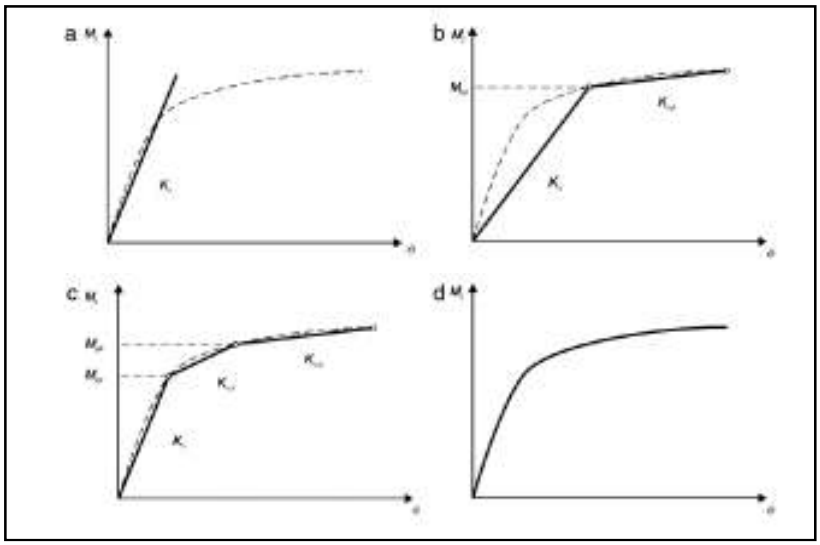

Figure 2.17 different mathematical representations of the ((M $_{j–\varphi}$) curve: (a) linear; (b) bilinear; (c) multilinear (trilinear); (d) nonlinear. (Díaz, 2011).

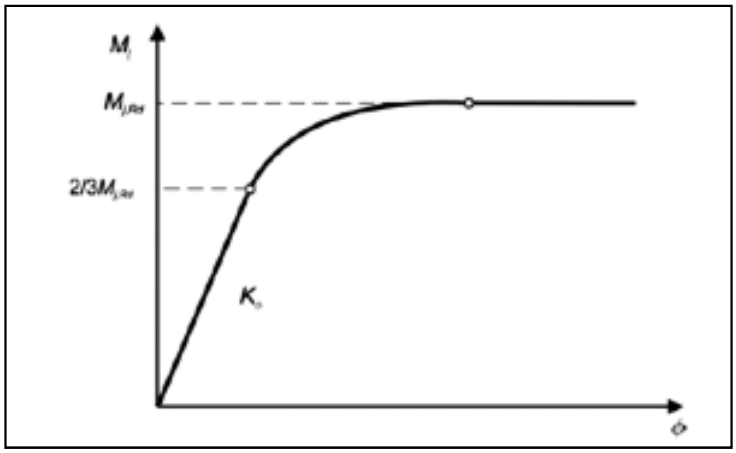

Figure 2.18 Three-segment approximation of the ($M_{j–\varphi}$) curve.

(EC3, 2005)

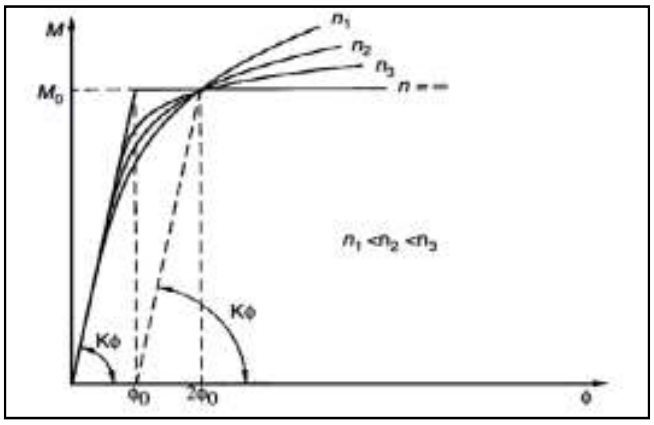

Figure 2.19 Ramberg–Osgood (1943) representation of the (M–φ) curve. (Díaz, 2011).

2.5.5 Structural joints connecting in Eurocode 3 (EC3 part1-8)

2.5.5.1 Design moment-rotation characteristics in EC3

As mentioned in section 2.5.3 of this thesis, on the basis of different joint models coupled with the use of experimental data, various theoretical relationships were proposed in order to represent the actual behaviour of semi-rigid connections. As a result of this experimental and analytical work, EC3 permits the use of semi-rigid connections subjected to static loading and gives in section 6.1.2.1 of EC3 the design moment-rotation curve for the connection. In this section, the methods of calculating the moment resistance, initial stiffness and rotation of the connection, given in 6.1.2.1 of EC3, are described and the proposed model for the moment-rotation curve for the connection is compared to experimental result.

(1) A joint may be represented by a rotational spring connecting the centre lines of the connected members at the point of intersection, as indicated in Figure 2.20 (a) and (b) for a single-sided beam-to column joint configuration. The properties of the spring can be expressed in the form of a design moment-rotation characteristic that describes the relationship between the bending moment $M_{j,Ed}$ applied to a joint and the corresponding rotation Φ_{Ed} between the connected members. Generally the design moment-rotation characteristic is non-linear as indicated in Figure 2.20 (c).

(2) A design moment-rotation characteristic, (Figure 2.20c) should define the following three main structural properties (i) moment resistance (ii) rotational stiffness (iii) rotation capacity.

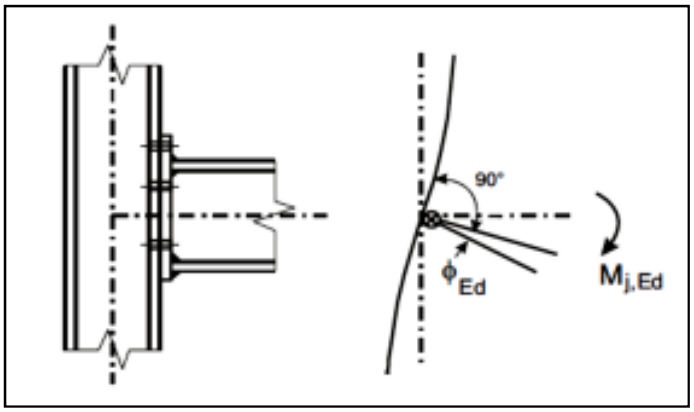

(a)Joint (b) Model

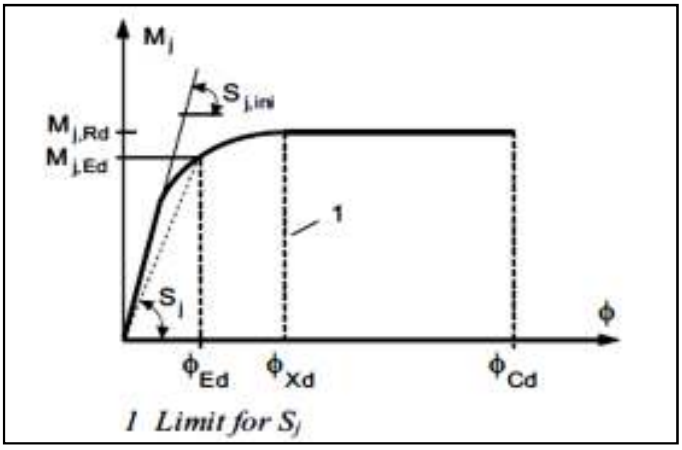

(c) Design moment-rotation characteristic

Figure 2.20 Design moment -rotation characteristic. (EC3, 2005)

2.5.5.2 Determination of the moment resistance of connections

The design moment resistance $M_{j,Rd}$, which is equal to the maximum moment of the design moment-rotation characteristic, (Figure 2.20c), is given by clause 6.1.3(4) in EC3 (part1-8).

The calculations of the moment of resistance of some types of connection are given in Eurocode 3 (part1-8) whilst other codes do not offer any guidance in this respect. Eurocode 3 makes a number of assumptions in calculating the moment of resistance of the connections. For example, in welded connections with end plates, the centre of compression is located at the mid-thickness of the beam flange in compression. In a bolted joint with more than one bolt-row in tension, the bolt-rows are numbered starting from the bolt-row farthest from the centre of compression.

By considering the above assumptions, the design moment of resistance of a beam-to-column joint with a bolted end-plate is determined from:

$$M_{RD} = \sum_{r} h_r F_{tr,RD} \qquad \text{Equation 2.11}$$

Where

$F_{tr,RD}$ is the effective design tension resistance of bolt row, h_r is the distance from bolt-row (r) to the centre of compression, r is the bolt-row number.

Full details for determining the design tension resistance of the bolts are given in clause 6.2.7.2 of EC3 (part1-8).

2.5.5.3 Calculation of the rotational stiffness

The rotational stiffness Sj, which is the secant stiffness as indicated in Figure 2.20c, is given by EC3 (part 1-8) clause 6.3.1(4). The rotational stiffness of a joint is determined from the flexibilities of its basic components, each represented by an elastic stiffness coefficient ki obtained from EC3 (part 1-8), 6.3.2. For a design moment-rotation characteristic the rotational stiffness S_j of a beam-to-column joint or beam splice, for a moment $M_{j,Ed}$ less than the design moment resistance $M_{j,Rd}$ of the joint (Figure 2.20c), may be obtained, according to EC3, with sufficient accuracy from:

$$S_j = \frac{\mathrm{E}z^2}{\mu \sum_i \frac{1}{k_i}}$$

Equation 2.12

Where:

k_i is the stiffness coefficient for basic joint component i.

z is the lever arm, as in 6.2.7 in EC3 (part 1-8).

μ is the stiffness ratio $S_{j,ini}$ / S_j , as in 6.3.1(6) in EC3(part 1-8).

The initial rotational stiffness $S_{j,ini}$, which is the slope of the elastic range of the design moment-rotation characteristic, is given by expression:

$$S_j = \frac{Ez^2}{\mu \sum_i \frac{1}{k_i}}$$

Equation 2.13

With μ = 1.0.

The stiffness ratio μ should be determined from the following:

if $M_{j,Ed} \leq 2/3\ M_{j,Rd}$:

μ = 1.0

if $2/3\ M_{j,Rd} < M_{j,Ed} \leq M_{j,Rd}$:

$$\mu = \left(\frac{1.5 M_{j,Ed}}{M_{j,Rd}}\right)^{\Psi}$$ Equation 2.14

In which

Ψ = 2.7 for bolted end-plate connections

Ψ = 3.1 for bolted angle flange cleats connections

2.5.5.4 Rotation capacity

The rotation capacity of a joint need not be checked provided that the design moment resistance $M_{j,Rd}$ of the joint is at least 1.2 times the design plastic moment resistance $M_{pl,Rd}$ of the cross section of the connected member. Full details are given in clause 6.4 of EC3 (part 1-8).

2.5.5.5 Comparison of moment-rotation curves with experimental data

As described in clause 6.3.1 of EC3 (part 1-8) for semi-rigid connections, if the design bending moment $M_{j,Ed}$ does not exceed 2/3 of the design moment resistance $M_{j,Rd}$ then the initial rotational stiffness $S_{j,ini}$ may be used for global analysis. However, if the design moment exceeds 2/3 $M_{j,Rd}$, the rotational stiffness should be taken as $S_{j,ini}/ \mu$, in which the stiffness coefficient μ is given in section 2.5.5.3 of this thesis. For further simplification, the value of rotational stiffness used for the elastic global analysis may be taken as $S_{j,ini}/ \mu$ for all values of the design bending moment.

For elastic-plastic global analysis, in the case of semi-rigid connections, a simplified bilinear model is given in a code in which the value of μ =2 is used in this bilinear model.

To validate this bilinear model with the test results, the moment-rotation curve for a cold formed portal frame with bolted joints by Dubina (2008) is compared with the bilinear model. The sections used in members of the frame structure for the test were described before in section 2.5.3.1 of this thesis, (Figure 2.6, Figure 2.9 and Figure 2.7).

Based on the conclusions of experimental programme, the study investigated only joints with both web and flange bolts (RIS-FB-M, KIS-FB-M, and KIP-FB-M).

The configuration of the outer group of bolts was the same in the case of all three specimens with web and flange bolts (RIS-FB-M, KIS-FB-M, KIP-FB-M), using the component method and implementing equations (2.8) and (2.10), a single set of analytical connection properties were determined includes initial stiffness, K_{iniC} and moment resistance, M_C. Qualitative FEM simulation (see Figure 2.21) showed that in the case of specimens with bolts on the web only there is a stress concentration in the web, which causes premature local buckling failure. The FEM simulation also demonstrated that load distribution in the bolts is not linear, and the centre of rotation of web bolts does not coincide with the centroid of web bolts. The centre of rotation of the connection is shifted towards the outer bolt rows (see Figure 2.22), whose corresponding force is an order of magnitude higher than the force in the inner bolts. Considering this observation, only the outer bolt group was considered for determination of connection characteristics using the component method. A

comparison of experimental vs. analytical characteristics of connections (stiffness and moment resistance as they perform the bilinear model described in EC3 part 1-8) is presented in Table 2.2 and Figure 2.23.The comparison between the experimental and analytical stiffness of the connection showed a fair agreement. Larger experimental values of stiffness can be explained by the fact that the contribution of the inner bolt group was ignored in the analytical model as explained above. For more details about this work see Dubina (2008).

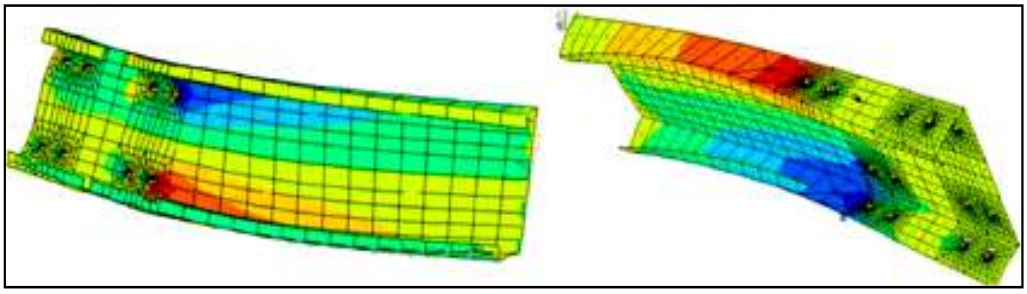

(a) (b)

Figure 2.21 Stress concentration in the case of specimens with (a) web bolts only, and (b) both web and flange bolts (Dubina, 2008).

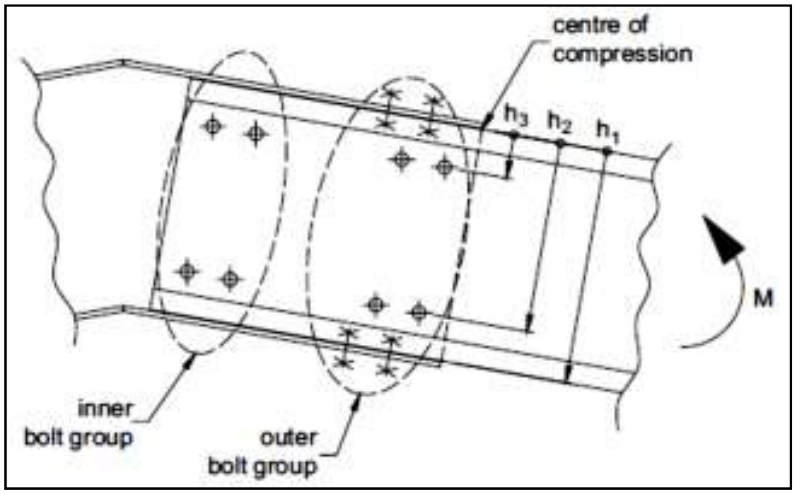

Figure 2.22 Bolt groups considered in analysis (Dubina, 2008).

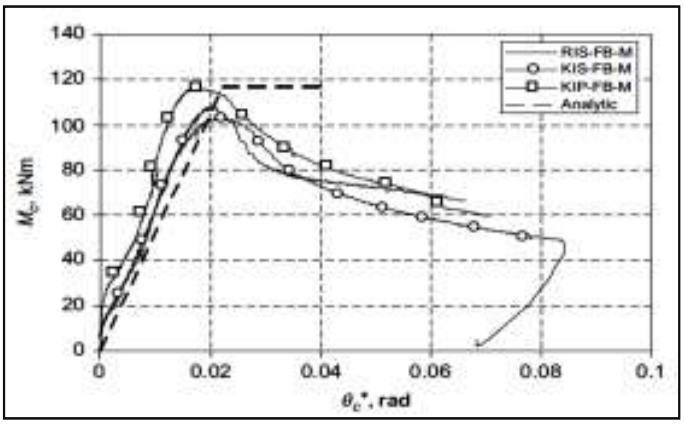

Figure 2.23 Experimental vs. analytical moment–rotation curves (Dubina, 2008).

Table 2.2 Experimental vs. analytical connection characteristics (Dubina, 2008).

Specimen	Initial stiffness, KiniC (kN m/rad)		Moment resistance, MC (kN m)	
	Experimental	Analytical	Experimental	Analytical
RIS-FB-M	6011	5224	108.0	117.8
KIS-FB-M	6432	5224	102.9	117.8
KIP-FB-M	6957	5224	116.7	117.8

2.5.6 Experimental and cyclic behaviour of connections on thin walled portal frames structures

The behaviour of connections of thin walled steel portal frames subjected to monotonic and cyclic loads have been an area of much experimental work in recent years, as mentioned in the previous sections. However, only a few cyclic and dynamic tests have been performed in order to obtain a better understanding, of their response to earthquake-type loading. In this section, some test and analytical results are presented and discussed.

Recently Dubina et al (2004) had performed an extensive experimental research at the "Politehnica" University of Timisoara, Romania, in order to characterize the behaviour of cold-formed steel bolted joints. Realistic specimens were designed, starting with a pitched-roof portal frame with the following configuration: span 12m,

bay 5m, height 5m and roof angle 10˚.The frame was analyzed and designed to EN 1993-1-3(2001). The size of the knee and ridge specimens, and testing setup, were chosen to obtain a similar bending moment in the connected members as observed in the structure. The sections used in members of the frame structures for the tests are described before in sections 2.5.5.5 and 2.5.3.1 of this thesis. Monotonic and cyclic experiments were made for each specimen type. For monotonically loaded specimens, the loading velocity was approximately 3.33mm/min, and the yield displacement was determined according to the ECCS (1985) procedure. Plate 2.2, Plate 2.3 and Plate 2.4 show the failure modes of some tested specimens (Dubina et al, 2004a). All specimens had a failure due to local buckling of the cold formed profiles, but the connection with bolts on the flanges showed good efficiency for web buckling reduction (Plate 2.4b) (Dubina, 2004b).

From this investigation for the connection behaviour, it was concluded that the ductility at the connections is limited under both monotonic and cyclic loads, and the design, including the design for earthquake loads, should take into account only the conventional elastic capacity corrected with safety factors. Because there is no significant post-elastic strength, there is no significant difference in ductility and capacity of cyclically tested specimens compared with the monotonic ones (Dubina, 2004b).

Plate 2.2 Failure of ridge specimens RIP-M (Dubina, 2004b).

Plate 2.3 Failure of ridge specimens RIS-FB-M (Dubina, 2004b).

(a) (b)

Plate 2.4 Failure of knee specimens KIS-M (without bolts on the flanges) (a) and KIS-FB-M (with bolts on the flanges (b) (Dubina, 2004b).

Also this study concluded that, if the joints are loaded under the limit of their maximum capacity, even cyclically, their strength is not too much affected. Consequently, if the joint detailing and connection component sizing may provide at least 20% overstrength, the cold-formed steel pitched-roof frames could be classified as class L of ductility (low) according to EN 1998-1 (2004), (Dubina et al, 2004a). Due to the semi-rigid and partially-resistant character of apex and eaves connections in steel cold-formed frames, moment-rotation characteristics have to be considered explicitly in design (Dubina, 2004b).

2.6 Seismic Behaviour of Thin Gauge or Cold–Formed Steel Portal Frames

This section presents some work of the researchers in the literature, was reported to examine the seismic behaviour of the thin gauge steel portal frame structures. From the previous work a comparison of the seismic behaviour of rigid and semi-rigid steel moment frames indicates that the seismic forces generated in semi-rigid frames are sometimes less than in comparable rigid frames.

The decrease in the forces and some increases in the displacements of semi-rigid frames are attributed to the elongation of the period of the structure, increase in damping and a decrease in the stiffness at an early stage of response. (Ashtiani, 1996).

Some experimental and analytical works were conducted by researchers to examine the seismic behaviour of semi-rigid frames. Research was started on this type of structure by Ono and Suzuki (1986), who proved significant post-elastic strength and ductility of some cold–formed steel frames through testing. Extended research on this subject was performed by Calderoni et al (1994). Figure 2.24 shows the frame tested by Japanese researchers, and the corresponding numerical model proposed and calibrated by Calderoni et al (1994) in order to study the behaviour of these structures. Using this cyclic load-displacement law, a lot of numerical step-by-step dynamic analyses were performed with reference to some built-up channel section portal frames. Geometrical and mechanical properties of frames were selected to provide monotonic F-D curves characterized by elastic stiffness, slope of the softening branch and residual strength. The results of this wide numerical investigation showed that the seismic behaviour of thin walled portal frames was not so different with respect to the corresponding ideal elastic-plastic structure (Dubina, 2004b).

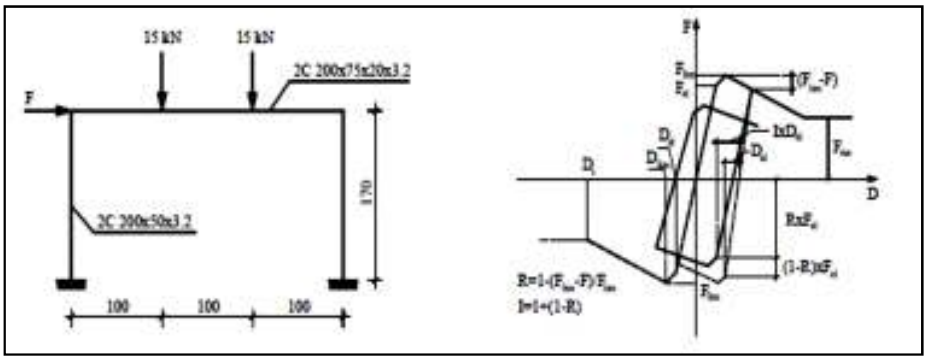

Figure 2.24 Analysed frame and analytical cyclic behaviour

Following experimental tests on cold-formed joints by Dubina (2004b), two full-scale tests on frames were performed. Frame dimensions were chosen identical to the ones in the initial design used to establish the dimensions of tested joints, as described in the previous sections (2.5.5.5 and 2.5.6). RIS-FB and KIS-FB joints and pinned column bases were used for frame construction. The objectives of the full-scale tests were to assess performance of pitched-roof cold-formed portal frames with moment-resisting joints under lateral loading, with particular emphasis on earthquake loading, (Plate 2.5).

The research included two tests. In the case of the first test (C1) only lateral loading was applied. For the second test (C2), gravity loading corresponding to a seismic design combination (permanent and a 0.3 fraction of the snow load) was applied, followed by increasing lateral load up to failure. Frame (C1) response during the test was characterized by an almost linear response up to the first local buckling of the beam at the connection 2 as shown in Plate 2.5 followed by a rapid loss of global frame resistance. The final collapse mechanism consisted in hinging of beam at connections 2 and 5 near the eaves. In the case of the C2 frame, response was very similar to the frame C1 up to 10–15kN lateral loading. Failure first included local buckling in the beam near the right eaves followed by a combined local buckling and lateral torsional buckling of one of the columns at the mid-height as shown in Plate 2.6. Finally, local buckling of the beam at the left eaves was observed at connection 2.

Plate 2.5 Local buckling of the left beam connection. (Dubina, 2004b)

Plate 2.6 Local buckling of the right beam connection. (Dubina, 2004b)

From this investigation and experimental work done by Dubina et al, The conclusion showed light gauge steel structures can be effectively used in seismic resistant structures, but seismic response of light-gauge steel framing can be significantly improved if shear walls are used to resist horizontal forces. Traditional capacity design based on equivalent elastic static analysis with reduction factors q of values $1< q \leq 2$ can be used for thin walled or cold formed steel structures provided the overstrength of joints and structural redundancy are available. In order to take benefit from some reduction q-factor, overstrength of joints is absolutely necessary because the ductility is insignificant. Both experimental and numerical results confirm the classification of light-gauge steel structures as low-dissipative which mean practically an elastic design has to be conducted and the seismic force can be evaluated by using a reduction factor q of 1.5-2.0 corresponding to the Low "L" ductility class as specified in EN1998-1 (Dubina, 2004b).

2.7 Seismic Design of Steel Portal Frame Structures

When moment resisting steel portal frame structures are subjected to earthquake ground motions, they are designed such that plastic hinges occur predominantly in beams rather than in columns (weak beam/strong column design) as shown in Figure 2.25. The plastic hinges are located in these elements to dissipate energy and permit the structure to survive earthquake forces through adequate ductility. This provides favourable performance, compared to strong beam/weak column behaviour through which significant deformation and second order effect may arise in addition to the likelihood of premature storey collapse mechanisms. The only exceptions to this requirement are, at the base of the ground floor columns, where plastic hinges may form and for single storey buildings. Designing to this procedure, the frame connections have to sustain forces developed in connected members by providing sufficient strength, (Elghazouli, 2009). This is described further in section 2.9.1 of this thesis.

It is observed that when a steel frame is prevented from premature local and overall buckling, as well as connection failure and shear failure in the panel zone, it is a very effective seismic resistance system. This is due to its favourable mass-to-stiffness ratio, inherent ductility and sustainable energy absorption capacity.

In the following sections, the material properties that influence ductility are presented.

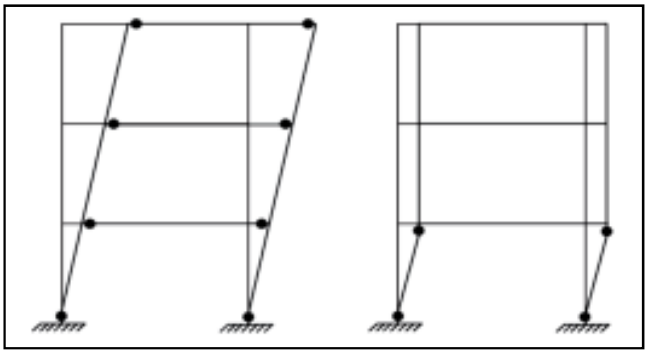

Figure 2.25 Weak beam/strong column and weak column/strong beam behaviour in moment –resisting frames. (Elghazouli, 2009)

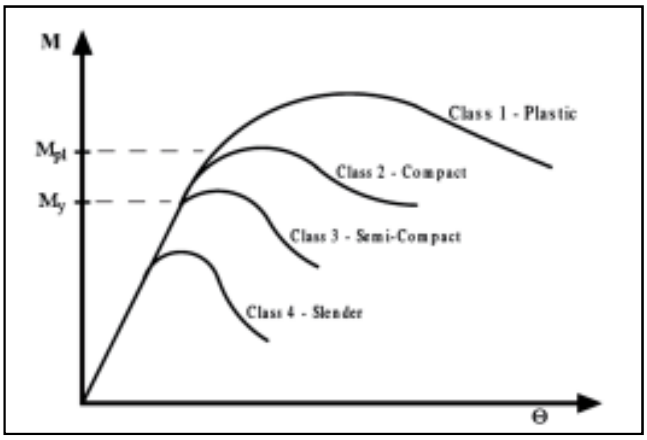

Figure 2.26 Cross-section behaviour classes. (Elghazouli, 2009)

2.7.1 Material of steel portal frames

According to EC3 and EC8 for plastic and seismic design it is recommended that the steel properties satisfy the following requirements:

1. The ratio between ultimate tensile strength Fu and the yield strength Fy has to satisfy the condition Fu/Fy >1.10;
2. Elongation at failure not less than 15%;
3. In order to guarantee an adequate deformation capacity, the ratio between the ultimate strain εu and the yield strain εy not to be less than 15.

2.7.2 Member of portal frames

In order to design cross-sections capable of providing sufficient rotational capacity, local buckling has to be controlled. In particular the occurrence of local buckling in the elastic range has to be avoided. Therefore, geometrical properties of the cross-sections have to guarantee the occurrence of buckling only well into the plastic range and after the realisation of the design ductility.

A very important concept in designing steel structures, which has been introduced in EC3, is represented by the sub-division of the structural sections into four different behavioural classes (Figure 2.26).

(1) Class 1: Sections belonging to the first class are characterised by the capability to develop a plastic hinge with high rotation capacity, hence they are defined as "plastic".

(2) Class 2: Sections are able to attain their maximum plastic flexural strength, but because they have limited deformation capacity due to local effects they are referred to as "compact".

(3) Class 3: Sections when the bending moment leading to first yielding can be attained but, due to local buckling, plastic redistribution is not possible. These are called "semi compact".

(4) Class 4: (slender sections) are not able to develop their total elastic flexural resistance due to the premature occurrence of local buckling of the parts of the sections under compression and failure occurs in the elastic range.

The parameter governing the above behaviour and defining the class of structural sections is the width- to-thickness ratio (b/t) of the compressed parts. The b/t limit values are given in EC3.

For the development of the full plastic moment capacity of the members such as columns, it is necessary to have a limitation on width-to- thickness ratios for the web and flanges. Also, the ratio of axial load to the yield capacity must be limited.

Members behaving mainly in flexure, such as beams, have a plastic moment capacity given by the product of the plastic section modulus Z_P and the material yield stress Fy.

In limit design of the structures, it is postulated that plastic hinges have a sufficient rotation capacity. Therefore, it is clear that the cross section of a member has to satisfy precise geometrical requirements in order to allow plastic deformations so as the collapse mechanism of the structure is reached, without losing its load carrying capacity, (Ashtiani, 1996).

2.7.3 Collapse mechanism

The collapse mechanism plays a very important role in the seismic design of structures because it influences the available global ductility and the energy dissipation capacity. The condition that the collapse mechanism should be of a global type is rather severe.

Sufficient local ductility of members which dissipate energy in compression or bending is ensured of by restricting the width-thickness ratio b/t according to the cross-sectional classes specified in EC3 (EN 1993-1-1:2005).

Depending on the ductility class and the behaviour factor q used in the design (Table 2.3), the requirements regarding the cross-sectional classes of the steel elements which dissipate energy are indicated in Table 2.4. Three ductility classes have been proposed, depending on the chosen values of the behaviour factor q:

***Class 1*:** $4 < q$; ***Class 2*:** $2 < q < 4$; ***Class 3*:** $q < 2$.

Sectional classes 1, 2 and 3 were explained before in section 2.7.2 of this thesis.

Table 2.3 Ductility classes and values of behaviour factors.

Design Concept	Structural ductility class	Range of behaviour factor (q)
Low dissipative structures	DCL (Low)	≤ 1.5-2.0
Dissipative structures	DCM (Medium)	≤ 4
	DCH (High)	> 4

Table 2.4 Cross-sectional class depending in behaviour factor

Ductility class	Value of behaviour factor	Required cross-sectional class
DCM	$1.5 < q \leq 2$	Class 1,2 or 3
	$2 < q \leq 4$	Class 1 or 2
DCH	$q > 4$	Class 1

2.8 Connections for Knees Joint and Ridge Joint

2.8.1 Introduction

In normal analysis and design of steel frames, beam-to-column connections are assumed to behave either as pinned or as fully rigid. Experimental work and research indicate that joint designed as pinned have some ability to resist rotational deformations and exhibit some rigidity. Also, it has been shown that fully-welded connections have finite flexibility.

The primary distortion of a steel beam-to-column connection is the rotational deformation ϕ caused by the in-plane bending moment M (Figure 2.27) (Ashtiani, 1996). This connection deformation has an effect on frame stability since additional drift will occur as a result of the decrease in stiffness of the members to which the connections are attached.

An increase in frame drift will intensify the P-δ effect and hence the overall stability of the frame will be affected. Thus, the non-linear characteristics of the beam-to-column connection play a very important role in frame stability.

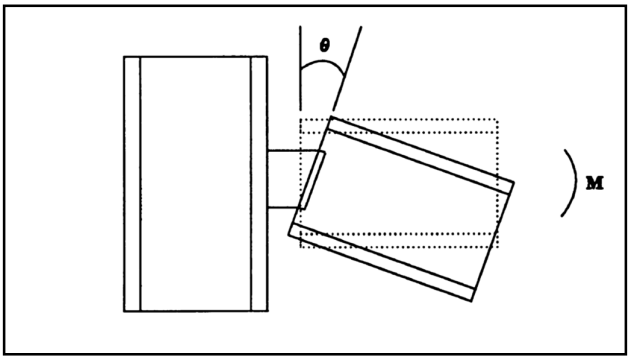

Figure 2.27 Rotational deformation of a connection. (Ashtiani, 1996)

2.8.2 Classifications of connections in design codes (B.S & EC3 part 1-8)

According to EC3 (part1-8), a connection is defined as a part of a building frame which transfers the internal forces, from one member to another in the form of bending moments, shear and normal forces. Always it is useful to think about the behaviour of the structure with the influence of the connections and estimate it in the preliminary design without having to perform a non-linear analysis. The main classification of connection of portal frames structures, in design codes is based in rigidity or stiffness while there is another classification in EC3 part (1-8) based on strength.

According to the rigidity of the joints the classification of the connection in the elastic design will be detailed in the three main categories as follow:

i. Nominally pinned connections, have no moment transfer, they should be capable of transmitting the internal forces which include the shear and eventually the normal force from the beam to the column, and should also be capable of accepting resulting rotation without developing significant moments which might adversely affect the members or the structure as a whole.

ii. Rigid connections have complete rotational continuity, their deformation is sufficiently small and justified by their sufficient rotational stiffness, and they should be capable of transmitting all end reaction forces including moments.

iii. Semi-rigid connections are designed to provide a predictable degree of interaction between members, based on the design moment-rotation characteristics of the connection. They should be capable of transmitting the internal forces and moments required by the design. It should be ensured that the connections are neither too rigid nor too flexible to fulfil accurately the assumptions that are made in the design.

The first two classifications, nominally pinned and rigid connections are traditional. Nominally pinned connections are widely used when the structure is provided by appropriate bracing systems for resisting lateral forces. While the rigid connections moment resisting frames often lead to excessive construction costs. The semi rigid connection has been introduced to fill the gap between pinned and rigid (fixed) connections and it is now accepted in modern codes (e. g. EC3) (Ashtiani, 1996).

The classification which based on strength according to EC3 (part1-8), in which the rule governs the classification, is based on comparing the design moment resistance of the connection with the design moment resistance of the members that it connects adopted in three main categories:

i. Nominally pinned connections, addition to the description above, this connection also may be defined as the connection that its moment design resistance is not greater than 0.25 times the design moment resistance required for a full strength connection.

ii. Full strength connections, the design resistance of this connection should be not less than that of the connected members.

iii. Partial strength connections, this is connection doesn't meet the criteria of a full strength connection or a nominally pinned connections.

2.9 Seismic Design Philosophy for Thin Walled Steel Portal Frame Structures

Thin-walled steel structures are usually made by thin-walled sections, of class 4 or, of class 3. Such types of structures are usually made by cold-formed or thin plate welded sections. Compared with hot-rolled sections (of class 1 or 2), they are characterised by a reduced post-elastic strength and, as a consequence, by a reduced ductility (e.g. they do not have sufficient plastic rotation capacity to form plastic hinges).

EN 1998-1 (2004) does not specifically mention the use of thin- walled steel sections for seismic resistant structures. However it provides low dissipative (e.g. low ductility) structures with a behaviour factor q of values from 1.5 to 2.0 (see Table 2.3). Assuming that such type of structures are made by "elastic" sections (e.g. class 3 or class 4), a behaviour factor q greater than 1.0 can be justified by overstrength and structural redundancy.

2.9.1 Seismic-resistant design

2.9.1.1 Fundamental requirement

Field evidence following destructive earthquakes has indicated, with few notable exceptions, that steel structures suffer less damage compared to structures built in other construction materials. This is due to their inherent ductility, relative uniformity of characteristics, flexibility and low weight. Eurocode 8 (EN 1998-1:2004) considered the fundamental requirements for seismic design of structures as:

(1) No collapse requirement

For which the structure shall be designed and constructed to withstand the design seismic action without local or global collapse.

(2) Damage limitation requirement

For which the structure shall be designed and constructed to withstand a seismic action having a larger probability of occurrence than the design seismic action, without the occurrence of damage and the associated limitations of use.

The above requirements (1) and (2) are naturally associated with the ultimate limit state and the serviceability limit state, respectively.

In order to satisfy the above two conditions, the steel frames should be capable of supplying the required stiffness strength and ductility. To satisfy the strength and stiffness requirements in the damage and ultimate limit states, beams should be verified as having sufficient resistance against lateral and lateral torsional buckling e.g. in accordance with EN 1993-1-3(2006). Columns should be verified in compression, considering the most unfavourable combination of the axial force and bending moments e.g. in accordance with EN 1993-1-3(2006).

2.9.1.2 Capacity design concept

The "capacity design" concept is an important design methodology for avoiding unexpected global collapse. In capacity design, certain members are expected to dissipate hysteretic energy during an earthquake event, and must therefore be designed to develop large inelastic deformation without fatal loss of strength. Those members should be used to ensure adequate seismic performance. All other members are then specified to behave within their elastic deformation range in the predetermined fashion.

Beams, columns, and their connections contribute to global plastic deformation of the assembly. The dissipating energy ratio of those components is dependent on the relative yield strength. In order to achieve a capacity design, many researchers worldwide have recommended a 'weak-beam strong-column' approach wherein the flexural strength of columns must be greater than that of the beams at the beam-column connections under consideration. At each connection, the following condition must be achieved

$$\sum M_{C,Rd} > \sum M_{B,Rd}$$

Where the left side is the summation of the moment capacities of the columns, and the right side is the summation of the moment capacities of the beams. This 'weak-beam strong-column' concept works very well in practice (Tsujii, 2001). This is because:

(a) Column failure tends to result in global collapse.

(b) By contrast, a strong-beam weak-column design induces large plastic deformation concentrated on only one storey.

(c) Columns should have sufficient resistance because axial forces decrease the deformation capacity of columns and shear forces are imposed individually.

2.9.2 Dissipative and non-dissipative structures

According to the new generation of seismic codes, such as Eurocode 8 (EN 1998-1:2004) a distinction is made between dissipative and non-dissipative structures.

(1) Non-dissipative structures: resist the most severe seismic event within the elastic range in which the action effects may be calculated on the basis of elastic global analysis without taking into account a significant non-linear material behaviour.

(2) Dissipative structures are designed by allowing yielding to occur in predefined zones where the capability of parts of the structure (dissipative zones) to resist earthquake actions through inelastic behaviour is taken into account.

During an earthquake these zones must dissipate energy by means of hysteretic ductile behaviour in the plastic range. The formation of appropriate dissipative mechanisms is related to the structural type.

Structures with dissipative zones should be designed such that yielding or local buckling or other phenomena due to hysteretic behaviour do not affect the overall stability of the structure. Dissipative zones should have adequate ductility and resistance and may be located in the structural members or in the connections. If dissipative zones are located in the structural members, the non-dissipative parts and the connections of the dissipative parts to the rest of the structure shall have sufficient overstrength to allow the development of cyclic yielding in the dissipative parts.

Sufficient local ductility of members which dissipate energy in compression or bending shall be ensured by restricting the width-thickness ratio *b*/*t* according to the cross-sectional classes specified in EN 1993-1-1(2005) as specified for dissipative structures in EN 1998-1(2004).

Connections in such dissipative zones must have sufficient over-strength to allow for yielding of the connected parts. For welded or bolted connections, the resistance R must be 1.2 times the resistance of the connected member, considering the upper value of its yield strength.

2.9.3 Behaviour factor

According to EC8 **(**EN 1998-1:2004), the ability of a structural system to resist seismic loads in the post-elastic range is allowed for by means of the behaviour factor (q-factor). The behaviour factor in Eurocode 8 is one of the structural response modification factors (or seismic force-reduction factors) that are applied in national codes to avoid explicit non-linear structural analysis in practical design. It is used in the evaluation of the normalised design spectrum given by the following expressions (see Figure 2.28):

$$0 \le T \le T_B : \mathrm{S_d(T)} = \mathrm{a_g}.\,\mathrm{S}.\left[\frac{2}{3} + \frac{\mathrm{T}}{\mathrm{T_B}}\left(\frac{2.5}{\mathrm{q}} - \frac{2}{3}\right)\right] \qquad \text{Equation 2.15}$$

$$T_B \le T \le T_C : \mathrm{S_d(T)} = \mathrm{a_g}.\,\mathrm{S}.\frac{2.5}{\mathrm{q}} \qquad \text{Equation 2.16}$$

$$T_C \le T \le T_D : \mathrm{S_d(T)} = \begin{Bmatrix} = \mathrm{a_g}\,\mathrm{S}\frac{2.5}{\mathrm{q}}\left[\frac{\mathrm{T_C}}{\mathrm{T}}\right] \\ \ge 0.2\,\mathrm{a_g} \end{Bmatrix} \qquad \text{Equation 2.17}$$

$$T_D \le T : \mathrm{S_d(T)} = \begin{Bmatrix} = \mathrm{a_g}\,\mathrm{S}\frac{2.5}{\mathrm{q}}\left[\frac{\mathrm{T_C T_D}}{\mathrm{T^2}}\right] \\ \ge 0.2\,\mathrm{a_g} \end{Bmatrix} \qquad \text{Equation 2.18}$$

Where:

*S*e (*T*) is the elastic response spectrum;

T is the vibration period of a linear single-degree-of-freedom system;

*a*g is the design ground acceleration on type A ground (*a*g = γI.*a*gR);

*T*B is the lower limit of the period of the constant spectral acceleration branch;

TC is the upper limit of the period of the constant spectral acceleration branch;

*T*D is the value defining the beginning of the constant displacement response range of the spectrum;

S is the soil factor;

η is the damping correction factor with a reference value of η = 1 for 5% viscous damping.

Sd (T) is the design spectrum;

q is the behaviour factor;

β is the lower bound factor for the horizontal design spectrum, the recommended value for β is 0.2.

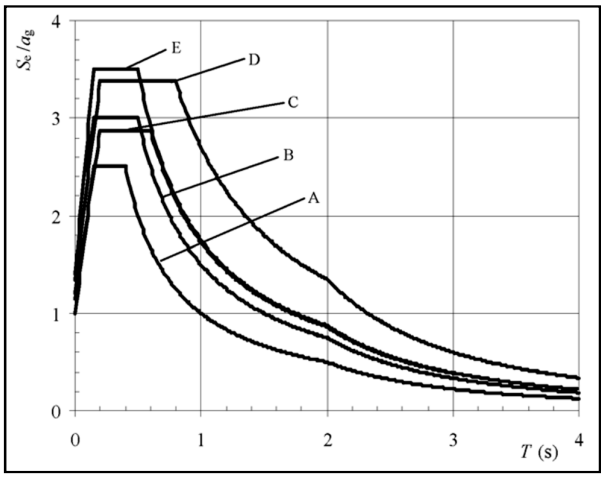

Figure 2.28 Eurocode reference shape of the elastic acceleration response spectrum S_e (T) for ground types A to E (5% damping)

Design forces are inversely proportional to the value of q. For example, q=1 implies that the structure must remain elastic even during a very strong earthquake. This condition is therefore necessary for non-dissipative structures. For dissipative structures, q is always greater than 1 depending to the ductility and over-strength of the structure.

Based on the bilinear idealisation of the real response, the ductility may be defined as:

$$\mu = \frac{\delta_u}{\delta_y} \qquad \text{Equation 2.19}$$

Where δu is the ultimate top displacement, δy is the top displacement at global yield (Figure 2.29).

It is well known that thin-walled steel sections do not possess a significant post-elastic strength. Therefore, assuming local plastic mechanisms instead of plastic hinges, the available redundancy of structures made by such a type of sections is based on their hyperstatic character only (Dubina, 2004b).

Behaviour factor is defined for a displacement design as displacement behaviour factor, qd. Ignoring such safety factors as the importance factor, the displacement behaviour factor, qd is expressed as follows:

$$qd = \frac{\delta_u}{\delta_y} \qquad \text{Equation 2.20}$$

Where: δ_u is the total displacement in elastic and inelastic regions corresponding to the ultimate limit state;

δ_y is the displacement determined by a linear analysis based on the design response spectrum.

According to this definition, the evaluation of the q-factor is performed by non-linear analysis. Many authors proposed approximate methods for determining the q-factor for design purposes but the corresponding results are often different and sometimes contradictory.

For slender structures, Dubina (2004) used an equivalent static elastic-plastic analysis, to evaluate the behaviour factor q with the following formula for the purpose of finding the ductility of the structure to confirm that the slender structures are low dissipative structures as in EC8 (2004):

$$q = \frac{\propto_u}{\propto_1} [(1 - \beta') \propto_{cr} + \beta'] \quad \text{Equation 2.21}$$

Where β' '=1-*T*; $\beta' \geq 0.5$; *T* is the fundamental period of structure; $\propto_{cr}$ is the critical load multiplier of gravitational loads, *V* (e.g. $\propto_{cr} = Vcr / V$) (Dubina, 2004b).

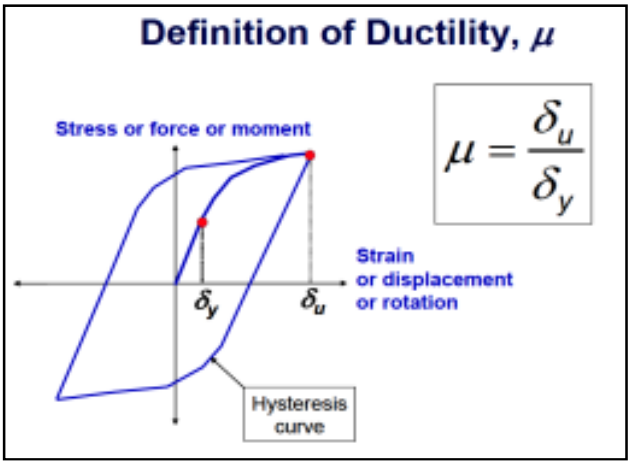

Figure 2.29 Ductility and behaviour factor (FEMA 2009).

2.9.4 Structural performance levels

The issue of building performance is currently a matter of discussion worldwide. Despite the fact that national, as well as international, codes of practice have attempted to increases the overall safety of structures they do not, as yet, reflect the latest concern that the damage sustained by structures is also a matter of economic, architectural and historical impact, particularly after the 1994 Northridge earthquake. It is obvious that the impact of the collapse of a landmark high rise building is more profound to society than that of other buildings. In a step towards relating the seismic risk to the damage control, (Konstantinidis, 2001), the FENIA 356 prestandard (FEMA 2000) suggested the following discrete structural performance levels:

Operational, when the structure substantially retains the original strength and stiffness and only minor cracking of facades, partitions and structural elements occurs.

Immediate Occupancy, when the structure after the earthquake event retains its design strength and stiffness and it is safe to be occupied immediately. In terms of element response, at this post seismic state, some minor hairline cracking and limited yielding might take place.

Life Safety, meaning that significant damage has occurred to the structure, but it still retains some margin against partial or total collapse. The damage is mainly located in the beams, while some spalling and shear cracking has occurred in ductile columns.

Collapse Prevention, defined as the post-earthquake damage state in which substantial damage to the structure has occurred, but although the structure continues to support gravity loads, it retains no margin against collapse. Extensive cracking and plastic hinges have formed in ductile elements

Not Considered, when the performance of the structure is not addressed enabling non-structural vulnerabilities like parapet bracing to be accounted for.

In order for a building to meet the first four of the above performance levels (the fifth one will not be considered as it refers to non-structural elements) it has to withstand the design seismic actions presented in the previous chapter. It is recalled that in Eurocode 8 the seismic actions are defined for the requirement of "no collapse" and of "damage limitation" in terms of the probability of exceedance of 10% in 50 years and 10% in 10 years respectively, which correspond to mean return periods of 475 years and 95 years, (Konstantinidis, 2001).

2.10 Performance of Steel Structures during the Past Earthquakes

Experience shows that steel structures subjected to earthquakes behave well. Global failures and huge numbers of casualties are mostly associated with structures made from other materials (ArcelorMittal, 1996). The earthquake resistance of steel frames has been known to be very reliable overall, with steel building collapse so far being a rare occurrence worldwide (Yanev et al, 1991). This may be explained by some of the specific features of steel structures like ductility, flexibility and low weight. In this section the performance and observed damage to steel structures from past earthquakes is presented. All the structures or the buildings are heavy steel structures as the use of light gauge steel in earthquake prone areas was a rare. These

observations were taken from the most major earthquakes all over the world include Northridge, Christchurch and Tohoku Japan.

2.10.1 Northridge earthquake (USA)

During Northridge earthquake, in 1994, steel frames sustained well the ground shaking, as no fatalities were attributed to unsatisfactory performance of steel structures and no collapses of steel buildings were reported (AISC, 1994). However, evidences of significant inelastic response and several structural deficiencies were observed on steel-framed structures after the event. Most of these observations corroborate the current state-of-the-art in seismic design in USA and Canada. Nevertheless, some cases need to be brought to the attention of the design engineer as these cases led to modifications to the provision in the design codes after Northridge in order to ensure that safer steel structures be built in the future. A total of 14 cases are presented, among which 12 are building structures. The structures were either concentrically braced frames, moment resisting frames, or a combination of the two (Tremblay et al, 1995). A summary of the observed structural damage is presented in Table 2.5.

2.10.2 Christchurch earthquakes (New Zealand)

This section presents field observations on the performance of selected steel structures in Christchurch during the earthquake series of 2010 to 2011. This comprises 6 damaging earthquakes, on 4 September and 26 December 2010, February 22, June 6 and two on June 13, 2011. Most notable of these was the 4 September event, at Ms7.1 and MM7, and most intense was the 22 February event at Ms 6.3 and MM9-10 (Clifton, 2011). Focus is on performance of concentrically braced frames, eccentrically braced frames, moment resisting frames and industrial storage racks. With a few notable exceptions, steel structures performed well during this earthquake series, to the extent that inelastic deformations were less than what would have been expected given the severity of the recorded strong motions (Bruneau et al, 2011).

Table 2.5 Summary of observed structural damage after the Northridge earthquake (Tremblay et al, 1995).

Structure	Type*	Structure damage
Kaiser Permanente Hospital penthouse	CBF	Buckling of bracing members; excessive sway
First Interstate Bank Building at Northridge	CBF	Buckling of brace connecting plates; possible yielding of anchor bolts
Student Union Building, California State University at Northridge	CBF	No structural damage observed
Roof structure for the bleachers of the football field	CBF	Failure of anchor bolts (uplift)
Oviatt Library, California State University at Northridge	CBF	Failure of brace connecting plates; cracking of base plates; yielding of anchor bolts
Three-storey building under construction in Van Nuys	CBF, MRF	Buckling of bracing members
NO. 2 Brewhouse, Anheuser-Busch Inc.	CBF	Buckling of bracing members
Asphalt and rock plant	CBF	Yielding and failure of anchor bolts
Department of Water and Power San Fernando Generating Station	CBF	No structural damage observed
Four-storey commercial office structure	CBF	Buckling and failure of bracing members; failures of brace welded connections; failure of a beam-column moment connection
Two-storey fashion plaza	CBF, MRF	Cracking in floor slab; buckling of bracing members
Holy Cross Hospital administration building	?	Excessive sway; failure of anchor bolts
Van Nuys office building	MRF	No structural damage observed
MRF under construction	MRF	Failure of beam-column moment connections

***CBF:** concentrically braced frame; MRF: moment resisting frame.

However, a few eccentrically braced frames developed link fractures, CBF brace fractures were observed in connections unable to develop the brace gross-section

yield strength, and multiple industrial steel storage racks collapsed (Clifton, 2011). A summary of the observed structural damage is listed in Table 2.6.

Table 2.6 Summary of observed structural damage after Christchurch earthquakes

Structure	Type*	Structure damage
22-storey Pacific Residential Tower in Christchurch's CBD	EBF	Paint flaking and residual link shear deformations ; fracture of EBF active link (see Plate 2.7)
Three level parking garage of a shopping mall west of the CBD	EBF	Very minor movement of the bolted splice connections in the braces
Hospital parking garage closer to the epicentre	EBF	Link yielding and fractures in two braced bays (see Plate 2.8 and Plate 2.9)
Modern steel frames	MRF	Out-of-plane yielding of the gusset plate of the connection
Portal frame building	MRF	Tensile failure of a row of bolts in the moment end-plate connection
A single suspended level parking garage	CBF	Buckling of bracing members; non-ductile fracture of brace-to-column connection (see Plate 2.10)
A low rise MRF building in the CBD	MRF	No structural damage observed
A 7 storey building located in the region of the CBD	MRF	No structural damage observed
Warehouses have light roofs with light rod braces	CBF	Buckling of bracing members
A long span steel portal frame building	MRF	Brittle failures of the cast-steel connectors (see Plate 2.11)
Steel storage racks	MRF	Extensive failure due to a combination of overloaded and fractured beam to column connections, and column local buckling. (see Plate 2.12)

***EBF:** eccentrically braced frames; CBF: concentrically braced frame; MRF: moment resisting frame.

Plate 2.7 Fractured EBF active link in top level of EBF system (Clifton, 2011)

Plate 2.8 EBF link yielding (Bruneau et al, 2011)

Plate 2.9 Fractured link at lower level EBF (Bruneau et al, 2011)

Plate 2.10 Fractured non-ductile brace-to-column connection (Clifton, 2011)

Plate 2.11 Brittle failures of the cast-steel connectors (Clifton, 2011)

Plate 2.12 Collapse of industrial storage racks (Clifton, 2011)

2.10.3 Tohoku earthquake (Japan)

The 2011 Tohoku Japan earthquake and tsunami caused extensive damage to steel building structures. The observed damages to steel buildings are classified into those caused by ground motions and those caused by tsunami. Severe ground motion caused damage to beam-to-column connections, buckling of diagonal braces, cracking and fracture of concrete overlaying the column base, yielding and fracture of anchor bolts, which are the similar damage aspects observed from past earthquakes. The ground motion caused damage to many low-to mid-rise buildings. Judging from the types of members and framing system, the majority of damaged buildings were constructed in older years preceding the major change in the seismic provisions of the Building Standard Law in 1981 (Midorikawa et al, 2012). A summary of the observed structural damage is presented in Table 2.7.

Table 2.7 Summary of damage caused by Tohoku earthquake

Structure	Structural members	Structure damage
An older structure with built-up HSS (hollow structural steel) columns made up of a light W-shape	Beam-to-column connections	Brittle fracture of beam-to-column connections (see Plate 2.13)
Many brace framed structures	Braces and bracing connections	Brace buckling, net-section fracture; distortion and fracture of the gusset plates; Failure of angle-section braces; out-of-plane bending of the gusset plates (see Plate 2.14 to Plate 2.17)
Buildings low- to mid-rise, with exposed base plate connections	Column bases	Fracture of anchor bolts led to dislocation of the column and severe residual story drift (see Plate 2.18 to Plate 2.20)

Plate 2.13 Yielding of an older built-up column (Midorikawa et al, 2012)

Plate 2.14 Local buckling in square-HSS brace (Midorikawa et al, 2012)

Plate 2.15 Out-of-plane deformation of gusset plate (Midorikawa et al, 2012)

Plate 2.16 Yielding of column web near bracing connection
(Midorikawa et al, 2012)

Plate 2.17 Out-of-plane deformation of gusset plate caused by compression
(Midorikawa et al, 2012)

Plate 2.18 Elongation of anchor bolts in an exposed base plate
(Midorikawa et al, 2012)

Plate 2.19 Spalling of reinforced concrete foundation supporting a column base (Midorikawa et al, 2012)

Plate 2.20 Fracture of anchor bolts, out-of-plane deformation of base plate (Midorikawa et al, 2012)

From these observations it should be noticed that the ground motion caused limited structural damage to steel buildings constructed after major revision in the seismic provisions of the Building Standard Law was implemented in 1981. However, older buildings constructed prior to 1981 saw notable damage caused by ground motion.

2.11 Summary of the Literature Review

Dubina et al (2004 and 2008) showed that the light gauge steel structures can be effectively used in seismic resistant structures mainly due to their reduced weight/strength ratios and proved with experimental and numerical tests on thin walled steel frame that they are low dissipative as in EN 1998-1(2004). The frame that was used in the study was analysed and designed to EN 1993-1-3 (2001). However he included in his investigation that the cold formed structure or these type

of light gauge steel structure their seismic performance can be significantly improved if shear walls are used to resist horizontal forces. Dubina also confirmed that the seismic force can be evaluated by applying a reduction factor q of 1.5-2.0 applying elastic design only as in EN 1998-1(2004), as this is, in fact pseudo ductility because it is mostly based on overstrength and structural redundancy rather than on the post-elastic strength reserve of members and connections.

This review leads to the idea that local ductile weaker area or members but part of the frame in the portal frame could allow local yielding, protect other parts from exceeding their buckling strength, allow them of a larger behaviour factor (q) and, overall result in a more cost effective structure than one designed with a behaviour factor (q) of 1.5-2.0.

Chapter 3

3 Seismic Design Model of Light Gauge Steel Portal Frame Structures

3.1 Introduction

In order to investigate the benefits of utilising lightweight materials for the construction of steel portal frame structures in earthquake prone areas, the design of a typical steel portal frame building in Sudan has been carried out and is presented in this chapter. In order to analyse the building under earthquake motion, the types of elements of the structure must first be determined. EC3 Loading Codes (EN 1993-1-1:2005 and EN 1993-1-3:2006) are used to estimate the loads on the structure. This building will be analysed using commercially available finite element software ANSYS and the modelling of parts of the structural elements are described as well in this chapter.

Despite the ever-increasing need for the portal frame structures, Eurocode 8 which governs the earthquake resistant design of buildings does not explicitly cover thin walled portal frame structures.

Since the structural systems formed by built-up cold-formed sections are not entirely covered by design code specifications, the design procedures are based on numerical investigation using numerical analysis tools and package such as ANSYS. Numerical investigation can be used to calibrate and/or validate calculation models and methods which are proposed as an alternative to those from design codes or existing in technical literature. Numerical finite element investigation can also be used either to replace design by calculations or combined with calculations. In this work models were designed for numerical investigation to find the best one that had a good response to horizontal displacements. Then the proposed section obtained from the numerical investigation was checked by calculations to code procedure. The performance was then assessed when subject to earthquake motion by nonlinear dynamic analysis (see Figure 1.1).

3.2 Structural Configuration of the Models Employed

The three pitched roof single storey frame building models considered in this study have the same overall structural configuration of nine identical, equally spaced, moment resistant frames. The building is 40 meters long by 20 metres wide for all the models. The steel frames are fixed at their columns bases and have a span of 20 metres and are spaced at 5 metres which leads to 8 bays or 9 frames (Figure 3.1). The purlins are spaced equally at about 1.5 metres and span between the steel frames. The columns are 6 metres high and the distance from ground level to the apex of the frame is approximately 10 metres for the first two models (Figure 3.2), while it is 6.875 metres for the last model (Figure 3.4).

The key features of this structural system were the use of creative built up cold-formed steel sections made from largest back-to-back lipped channel that can currently be rolled for the column and rafter members.

The rafters in each frame for the first two models have 570 mm total depth, the upper and lower flange width is 300mm, the thickness is 3mm and there is a lip of 43 mm. The columns of the frames have the same dimension of the rafters for the first two models (see Figure 3.3).

The rafters in each frame for the last modified model have 750 mm total depth, the upper and lower flange width is 500mm with thickness 3mm and lip of 53mm (see Figure 3.5).

The columns of the frames have 850 mm total depth and 6 mm web thickness, the upper and lower flange width is 650mm with 3mm thickness and 63 mm lip.

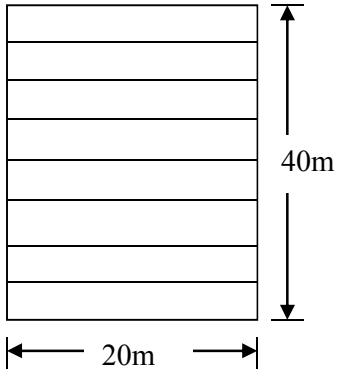

Figure 3.1 Plan of the building

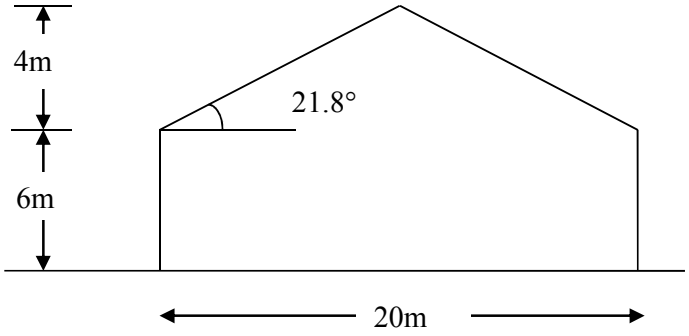

Figure 3.2 Portal frame for models 1 &2

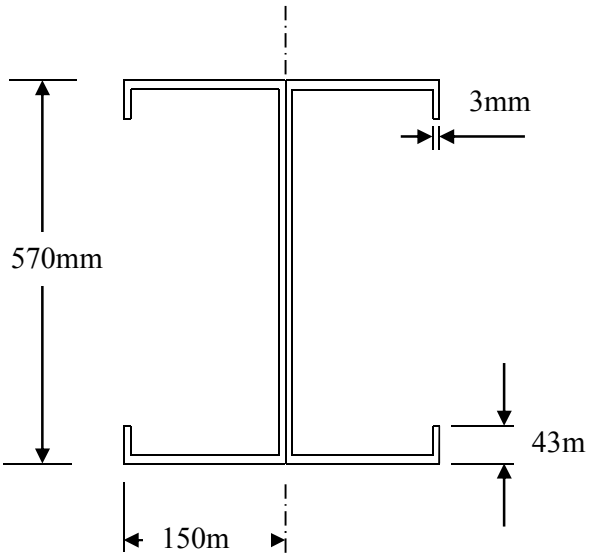

Figure 3.3 Dimensions of back- to back lip channel section used for column and rafter member for model 1 & 2

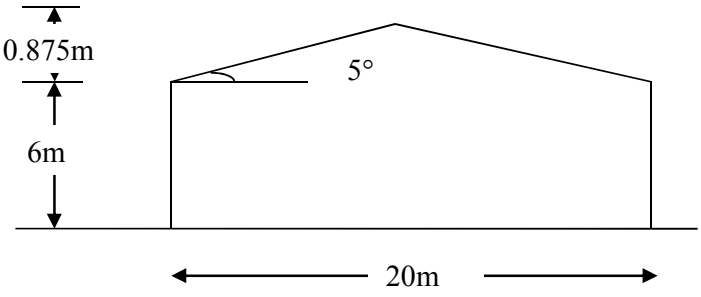

Figure 3.4 Portal frame for model 3

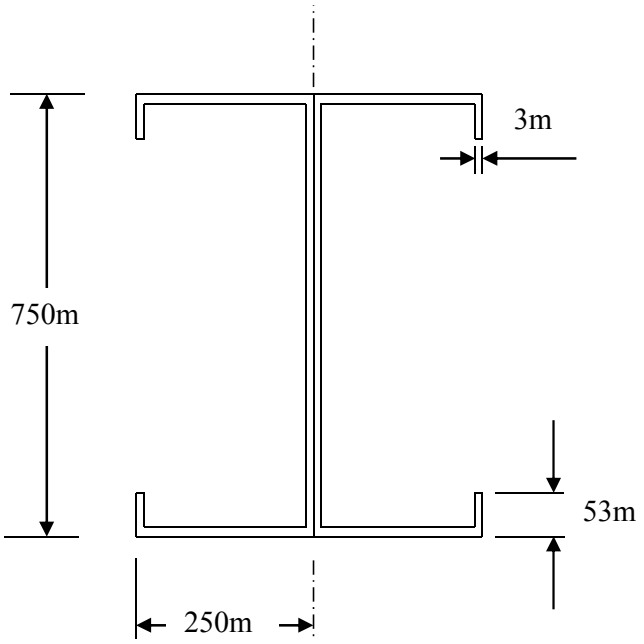

Figure 3.5 Dimensions of back to back lip channel section for rafter member for model 3

3.3 Benefit of Utilizing Cold Formed Sections Compared with Hot Rolled Sections

In this section universal beam hot rolled section as alternative section to the back to back channel cold formed section used here for framing the portal frame structure is compared. Table 3.1 presents the section properties for the proposed cold formed section, and universal beam hot rolled section from BS 4-1 (2005) having the same elastic modulus. From Table 3.1, it is obvious that thinner the section walls, the larger will be the corresponding moment of inertia values (Ixx and Iyy) and elastic modulus values (Zxx and Zyy). This produces cold formed section or thin section with section area less than the area of the hot rolled section with the same section modulus, and results in a lighter section. This reduction in the weight of the steel makes the use of cold formed steel sections more economical in terms of transportation and erection cost compared with the heavy hot rolled steel sections.

Table 3.1 Comparison of a hot rolled section and the proposed cold formed section

	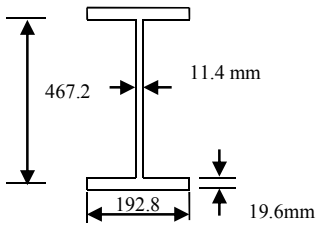 Hot rolled section	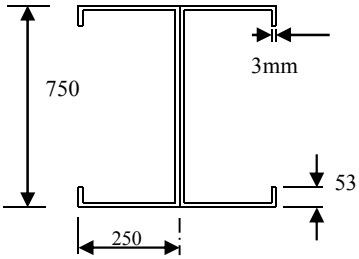 Cold formed section
A	125 cm^2	81 cm^2
I_{xx}	45700 cm^4	71020 cm^4
Z_{xx}	1960 cm^3	1894 cm^3
I_{yy}	2350 cm^4	7100 cm^4
Z_{yy}	243 cm^3	284 cm^3

3.4 Structural System Considered and Properties of Cold Formed Steel

The portal frame buildings that were designed and detailed have the same structural configuration, and differ from one another in terms of the sections dimensions, but have the same properties of the materials used. The first two models for investigation were modelled with steel with yield strength 400 MPa, while for the last model the grade of the steel was considered as steel grade S355 which is known as normalized and normalized rolled steels in both British Standard BS 5950-5(1998) for cold formed steel and Eurocode EN 1993-1-3(2006) for design of cold formed steel as tabulated in (Table 3.2). The nominal yield strength and design strength of this steel is 355 MPa while the nominal ultimate tensile strength is 470 MPa as shown in table (Table 3.2). The same grade of steel was used for the rafters, columns and the plates for joints as well.

The material properties used in the design are shown in (Table 3.3) in accordance with BS 5950-5(1998) compared with EN version for design of steel structures of Eurocode 3 (May 2005), for the modulus of elasticity, shear modulus, Poisson's ratio and density.

Table 3.2 Steel grade and values of yield and ultimate strength

Type of steel	Standard	Grade	Fyb (MPa)	Fu (MPa)
Normalized and normalized rolled steels (BS 5950-5:1998).	EN 149-3	S355NC	355	470
Normalized/normalized rolled weldable fine grain structural steels (EN 1993-1-3:2006).	EN10025: Part 3	S355 NL	355	470

Table 3.3 Physical properties of cold formed steel

Material Property	Value (BS 5950-5:1998)	Value (EN 1993-1-:2006)
Modulus of Elasticity	205E03 MPa	210E03 MPa
Poisson's Ratio	0.3	0.3
Density	7.850E-09 Kg/mm^3	7.850E-09 Kg/mm^3
Shear Modulus	79E03 MPa	81E03 MPa

3.5 Numerical Investigation Models

This section presents the first part of the numerical studies that have been carried out. The section presents computational simulation techniques using the commercially available finite element software ANSYS. The main objective of this study is to investigate the response of a frame model to horizontal displacements which will be used for the seismic design of the frame combined with code calculations check. The first part of the section describes the model. This followed by general modelling technique for the frame, including the choice of a suitable shell element, material behaviour, boundary conditions and load application.

3.5.1 Model description and finite element idealisation of the frame

The first model used for the numerical investigation and will be used for the calibration of the seismic design is frame of span 20 m with rigid joints and fixed at column bases, pitch 21.8˚ as was explained in section 3.2 of this thesis (see

Figure 3.2). The brackets for the joints for ridge and knees are 5 mm thickness from cold formed steel. The joints connected through brackets bolted between the webs of the channel-sections (see Figure 3.6 and Figure 3.7). This arrangement of cold formed members' connections was used in the literature by Lim and Nethercot (2003) and others as detailed in section 2.5.3.1 of this thesis and as shown in Figure 2.4 Figure 2.5. This arrangement of joints used for the first model is the first proposal for joints for seismic area, which could be effective or not to be used in cold formed portal frame structure in earthquakes area. This decision will be a fact results from the finite element analysis in this study.

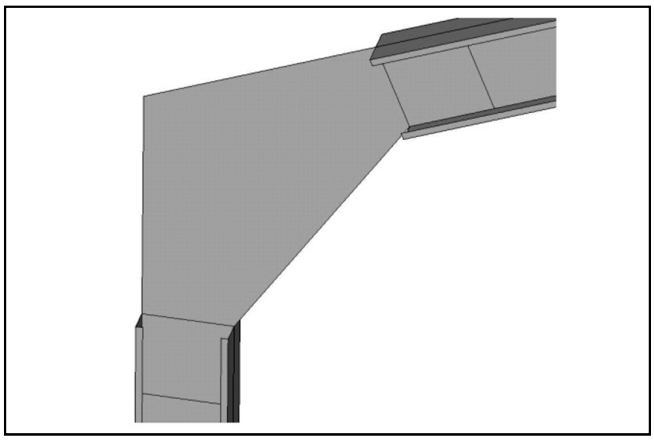

Figure 3.6 Knee connection of model frame1

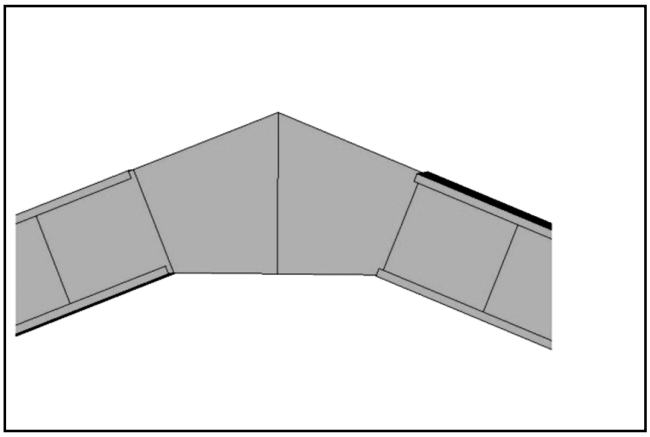

Figure 3.7 Ridge connection of model frame1

3.5.1.1 Element choice

Two different types of elements are considered to model the cold formed steel frame members, namely shell and beam elements as the effect of loading for the frame structure is bending of the structural member. A shell model is required to predict the buckling behaviour, which is of high importance for the light gauge materials that the frame is made of. ANSYS offers several different shell elements, and runs were carried out using 4-node 3D structural quadrilateral SHELL181. The element has six degrees of freedom at each node, translations in the x, y and z directions and rotations about the x, y and z axes. The element z axis is always perpendicular to shell surface. Required element constants include the thickness at each node (TK (I,), TK (J), etc.) and material properties include Young's modulus, Poisson's ratio and density (EX, NUXY and DENS). Other constants and material properties can also be input depending on the applications. It is suitable for analysing thin to moderately-thick shell structures; SHELL181 is well-suited for linear, large rotation, and/or large strain nonlinear applications (ANSYS Inc. 2009a). Two sets of material constants were used in the model, for shell elements. The number of material constant sets mainly reflects the number of element thickness in the model.

The use was made for shell elements when compared with solid elements (both type solid and plane), as solid elements have only translations in x, y and z as degrees of freedom and plane elements have only translations in x, y, while shell elements have both degrees of freedom-displacements and rotations (ANSYS Inc. 2009a). Another advantage for using shell elements according to (ANSYS Inc. 2009a) and (Nelson and Wang, 2004) is that, shell elements are typically taken to model a structure subjected to a bending load that is thin in two dimensions relative to a third. When a thin structure is idealized using shell elements one should know the following: by means of shell elements one actually predicts the structural behaviour of the mid surface of the thin structure. All these features made shell elements suitable for the analysis of the portal frame model in this study. Table 3.4 lists the element constant sets for shell element (SHELL181). More details of the elements can be found in ANSYS users' guide (ANSYS Inc. 2009a).

Table 3.4 Element constants for the shell elements

Set No.	TK (mm.)
1(Columns and Rafters)	3
2(Connections brackets)	5

3.5.1.2 Finite elements modelling of the frame

In this section a finite element idealisation is used for the cold formed steel frame using the finite element software ANSYS. The finite element idealisation uses shell elements for the Valley beams and the brackets. The finite element mesh used for the frame is shown in Figure 3.8. Some difficulties were encountered when generating the finite element mesh. The difficulties were caused by the irregular locations and varying dimensions of the structural components and by the fact that elements must be connected properly. For example, a spring element cannot pierce a shell element in the middle, it must meet a shell element at a node, and also it was difficult to find the size of the mesh that makes all the elements connect properly. The problems were ultimately solved by manual meshing. The mesh size for the shell elements was around 25x25mm.

This mesh size was chosen based on model validation (see appendix A) and according to Dubina et al (2010) when they performed experimental and numerical simulation programs on full-scale pitched roof cold-formed steel portal frames of back-to-back lipped channel sections with bolted joints in order to evaluate the influence of different type of geometrical and structural imperfections on the structural stability performance of these structures. As they used shell elements with mesh size around 24x24mm which resulted in a good agreement between the numerical and experimental results in their study. This made the start point of selecting the mesh size to be 25x25mm, which gave good results for this study when compared with higher size of mesh such as 35x35mm, 50x50mm and 100x100mm, as in using higher mesh size leads the convergence of the solution to be poor for steps after yielding. For the analyses the connections are assumed to be rigid for all configurations as a full strength connection is required so as to achieve sufficient

rigidity in beam-column connections until the energy dissipation capacity of the frame members is fully exhausted.

A nonlinear static analysis under increasing lateral displacements is applied to the model. Only lateral loading was applied here without gravity load (roof services) as a first stage to assess performance of pitched-roof cold-formed portal frames under lateral loading, with particular emphasis on earthquake loading. The model will be solved using non-linear large–displacement elasto-plastic analysis. The material is introduced by means of bilinear isotropic model. The inelastic behaviour of the steel elements was considered using the von Mises yield criterion as von Mises yield surface allows isotropic yielding. To include the geometric nonlinearities, large displacement and P-δ effects were considered in the analyses. The stress-strain relationship is assumed with a young's modulus of 205E3 MPa and a yield strength of 400 MPa and by considering the strain hardening with value of 1%, the tangent modulus is 2.05E3 (Figure 3.9). The full frame is analysed, where the gravity load and the horizontal load due to earthquake could have been applied at the apex and the knees. A validation for the finite element model has been carried out and available in appendix A of this thesis.

Extra triangular brackets were added at the eaves to allow application of the prescribed displacement loading conditions as shown in Figure 3.8 to prevent concentration of the stresses when applying the load in one node.

3.5.1.3 Finite elements analysis results

Figure 3.10 shows force displacement diagram for the analysis of the frame up to the failure (failure is defined as the analysis failing to continue, which can be indicative of overall or localized exceedence of strength, often involving buckling, of the frame structure, web panels, stiffeners or flanges). The analysis involves subjecting the frame to monotonically increasing static lateral displacements as it is an efficient tool to describe the behaviour of the frame beyond the plastic zone or within the strain hardening region. The lateral displacements were used first to test the response of the frame to lateral displacement until failure as the earthquake effect on the structure is assumed to be horizontal without considering the gravity load. The displacements were applied in the structure on both the knee joints in order avoid the failure of the

node where the displacement was applied. Also the displacements applied at five nodes in the triangular area (to represent the jack used to apply the load in an experimental test) as the concentration of the stress when the displacement is applied at a single node leads to premature failure. For this model the failure occurred at the node knee connections of the frame which means the connections are not strong enough (see Figure 3.11 and Figure 3.12). The frame behaved elastically as we have linear force displacement relationship (see Figure 3.10) and the failure happened before achievement of any nonlinear behaviour or ductility because of the failure of the connection. The displacement after failure was 40 mm. Figure 3.11 shows the stresses concentration in the connections with values between 436 to 498 MPa, more than 400 MPa the yield strength used for the frame members; this shows the failure of the connection with yielding of the connected members. This result made the use of this arrangement of connections used in the literature by Lim and Nethercot (2003) and others is not possible in framing portal frame system in earthquake prone areas. The next section presents the improvement of the connections in the second model.

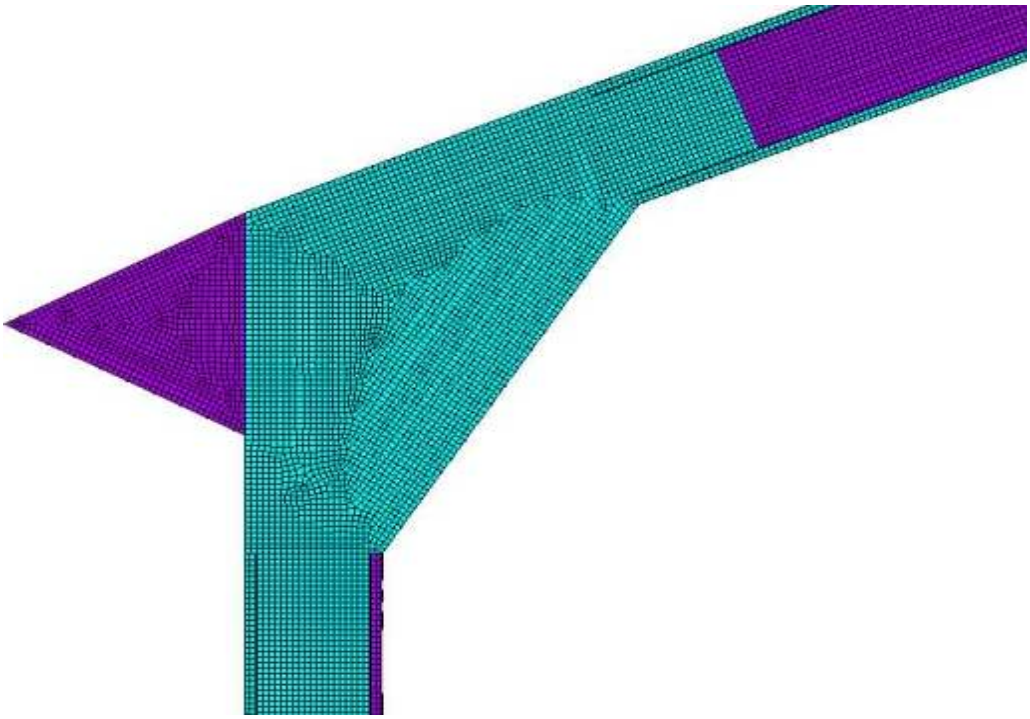

Figure 3.8 Finite element abstract of the structure

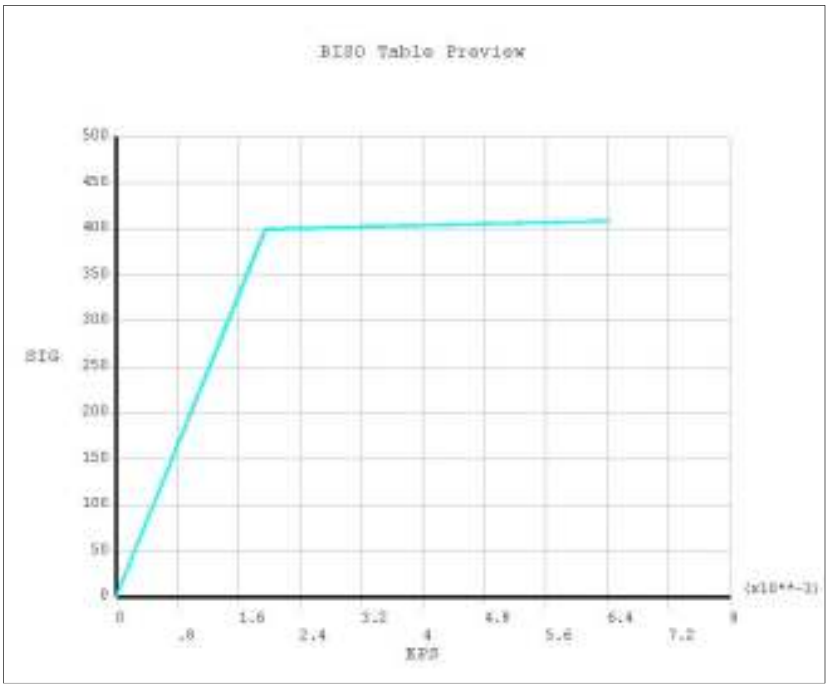

Figure 3.9 Stress strain assumption

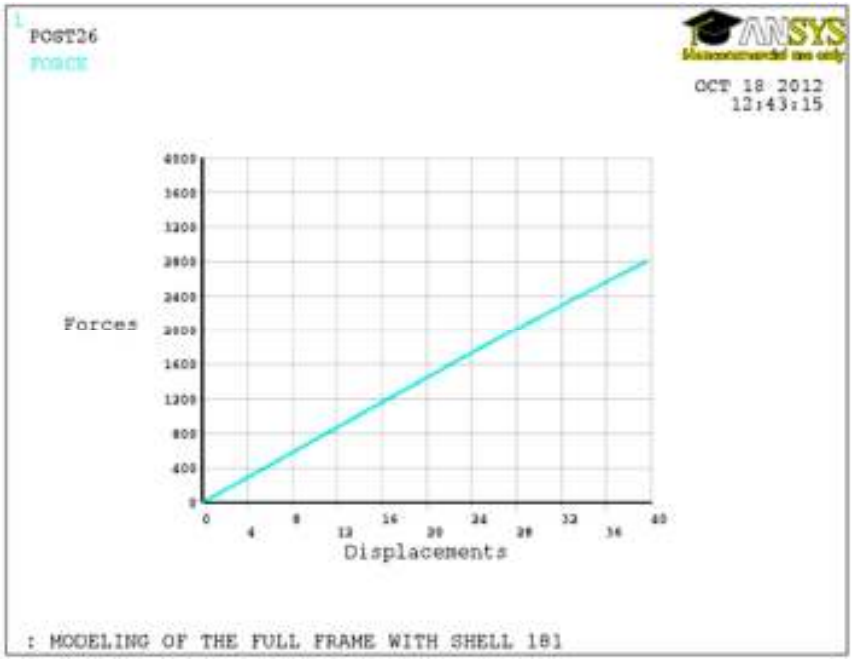

Figure 3.10 Force (N) vs. displacement (mm)

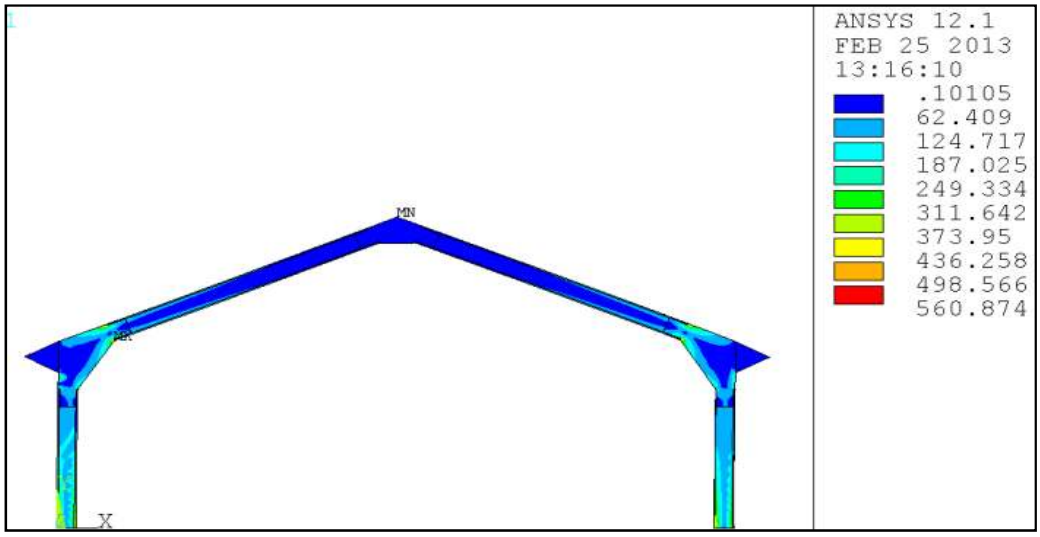

Figure 3.11 Von Mises stress of the frame (MPa)

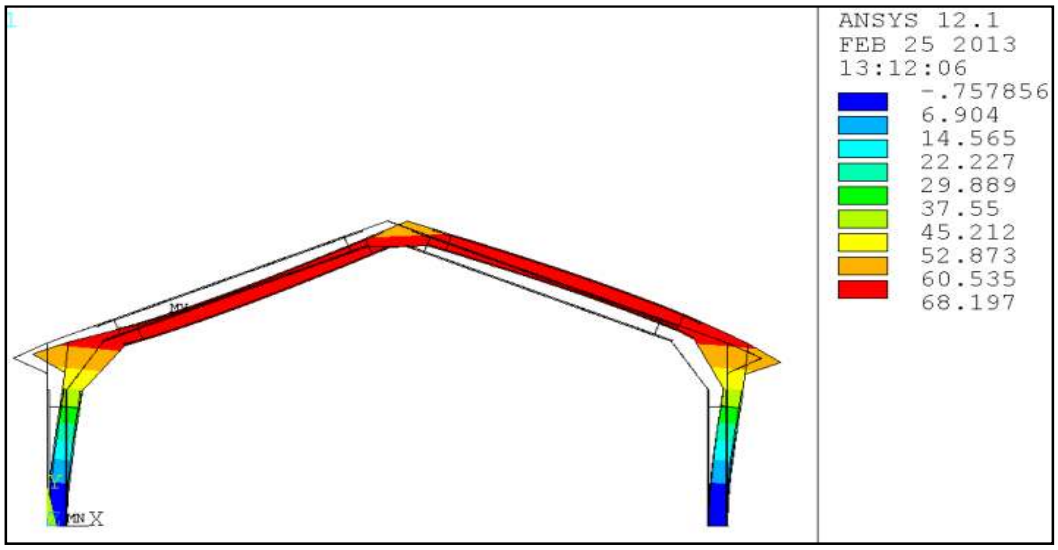

Figure 3.12 X displacement (mm)

3.5.2 Model modification

Since the frame structure model has failed with the failure of the connections, the model needed to be modified: the connections were improved while the structural configuration and dimensions of the structure are the same as the previous model. New details of the connection for ridge and knees are shown in (Figure 3.13 and Figure 3.14); the proposed connections are bolted connections. The connected

members are connected together through cold formed steel plate using welded bracket elements (S355: Fy = 355 N/mm2) and M20 grade 8.8 bolts. To achieve a good performance of the connections the plate was enhanced with folding stiffeners. A gap in the lower part of the plate was applied to avoid the interaction between the folding stiffeners and the frame members for the finite element model. For simplicity the connections for knees and ridge were modelled in the finite elements model as rigid. The same materials properties, type of element, material modelling and finite element idealisation are used in ANSYS analysis as in the last model to check the frame structure model for the nonlinear static analysis under increasing lateral displacements. The analysis was carried out for the new modified model of the frame structure by applying horizontal displacement until the failure of the frame structure model.

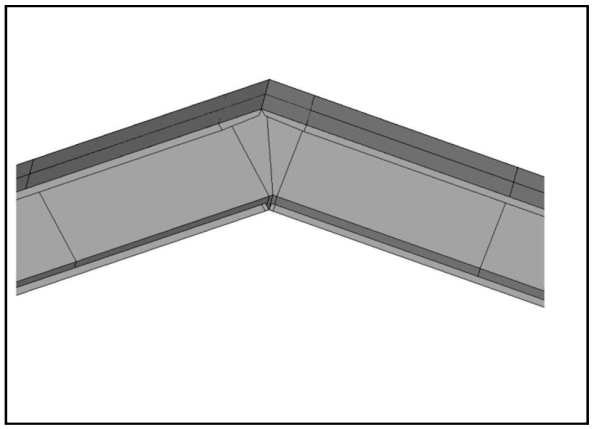

Figure 3.13 New ridge arrangement

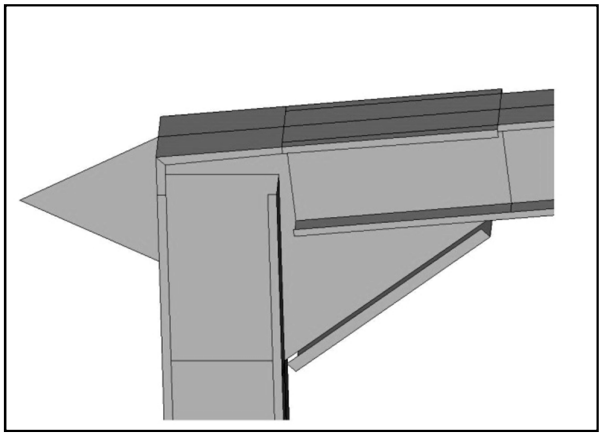

Figure 3.14 New knee arrangement

3.5.2.1 Finite elements frame analysis results

The force displacement diagram is shown in Figure 3.17 with the displacement in the horizontal direction in Figure 3.18, the structure had a considerable nonlinearity as the displacement after yielding was value about 33 mm 47 mm with yielding value about 33 mm. As shown in (Figure 3.15 and Figure 3.16) the structure appears to be buckling, in a lateral-torsional mode, at the right hand knee and failed due to the lateral-torsional buckling of the rafter and columns. The right side of the frame suffered worse torsional buckling than the left side because of the effect of the loading directions. The horizontal displacement in Figure 3.18 shows the maximum value of 62 mm caused by the lateral tensional buckling of the right side of the frame. Since such type of failure is not desirable in earthquake resistant structures, the frame structure needs to be modified for better behavior and good resistance under large deflection and earthquake motion. The torsional buckling of structural members should be prevented to have a good seismic design. The improvement of the frame could be only in terms of frame members sections without considering the connections as the connections performance was noticed very well and the failure caused by the lateral-torsional of the frame members. This observation leads to make this arrangement of connections recommended for portal frame in earthquakes and would be applied for the third model in this study.

3.5.2.2 Some design considerations

The torsional buckling of structural members and structures could be prevented and controlled by many types of structural solutions such as, increased inner flange width or by providing the frame with some type of restraint for the rafter and columns which could be achieved by a light bracing of the inner flanges back to the roof purlins or along the structure to the next frame. These results gave a general understanding for the behavior of the frame structure under horizontal displacements which should reflect the frame structure response and resistant to earthquake motion. The frame design in this study for the earthquake resistance will be the result of combining evaluation of structural performances by these numerical finite element investigations with check calculations based on EN 1993-1-3 loading code. The section used for the last model is built up cold-formed steel sections made from

largest back-to-back lipped channel as detailed in the last paragraph of section 3.2 of this thesis. The sections for column and rafter are chosen as result of the numerical finite element investigation, and then are checked by code calculation for different requirements to Eurocodes 3 and Eurocode 8. Use is made of EN 1993-1-3 (2006) for cold formed steel members and EN 1993-1-1(2005) for design of steel structures to estimate the loads on the frame structure within the use of EN 1998-1(2004) for the ductility class and behavior factor for the proposed last model. In the next section a brief discussion about earthquake analysis and dynamics is presented first and then the design procedure was used to Eurocodes 3 and Eurocode 8 are presented in section 3.7 and to IBC in section 3.8.

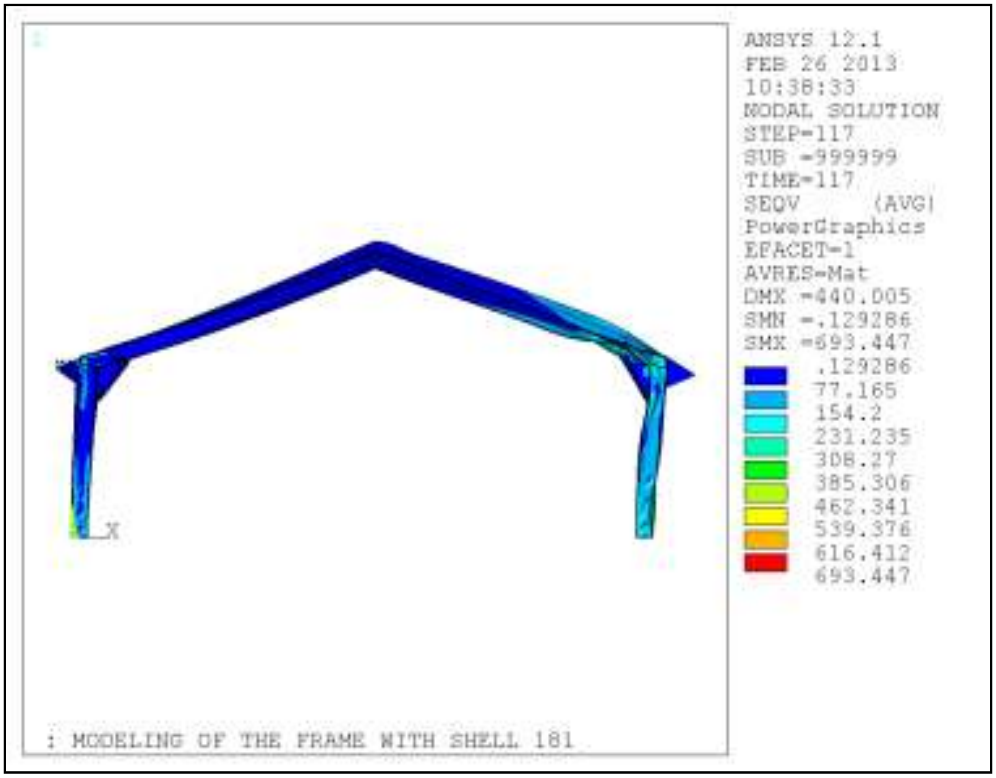

Figure 3.15 Von Mises stress (MPa)

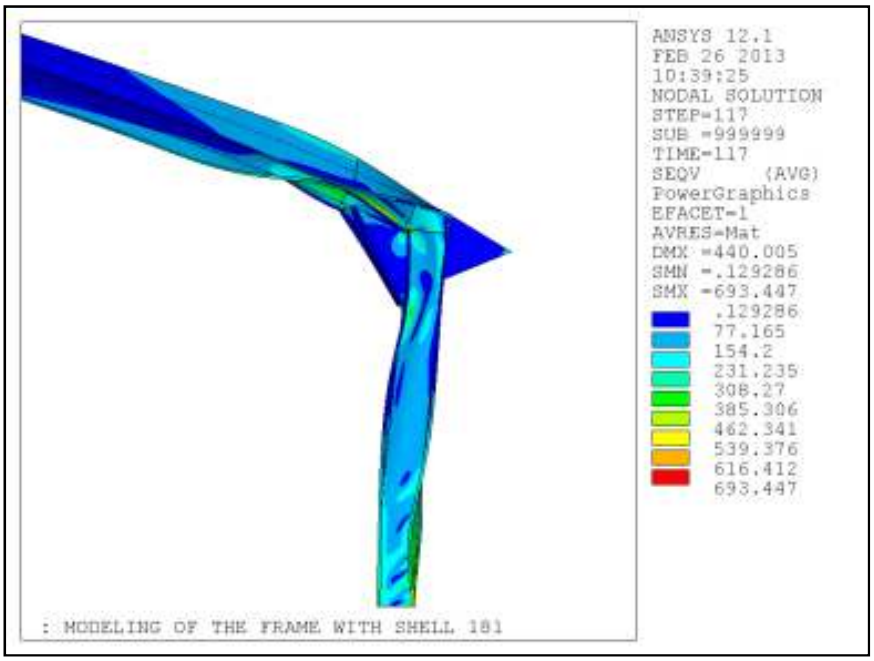

Figure 3.16 Von Mises stress (MPa) shows the torsional buckling mode

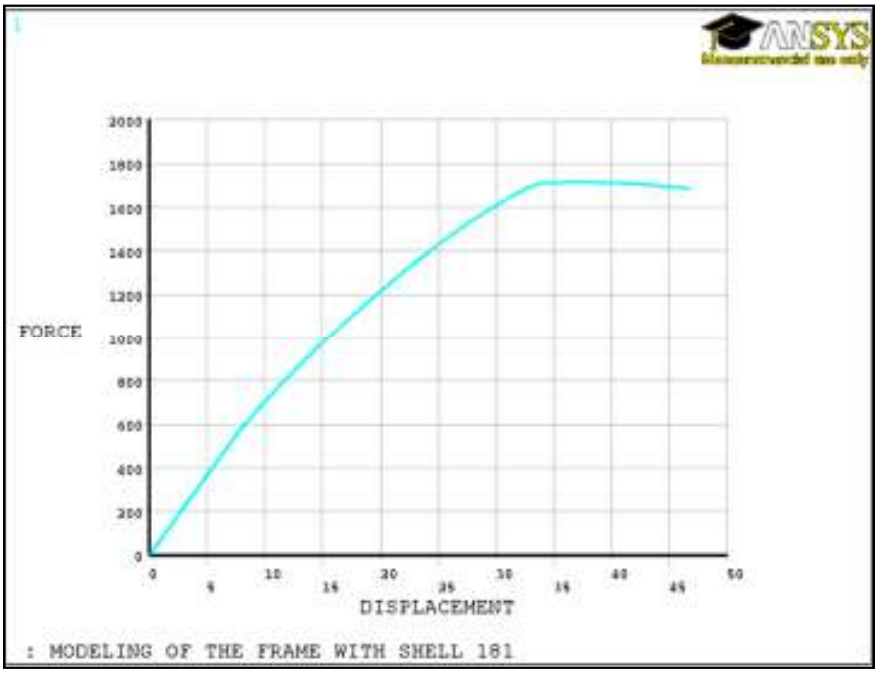

Figure 3.17 Force (N) vs. displacement (mm)

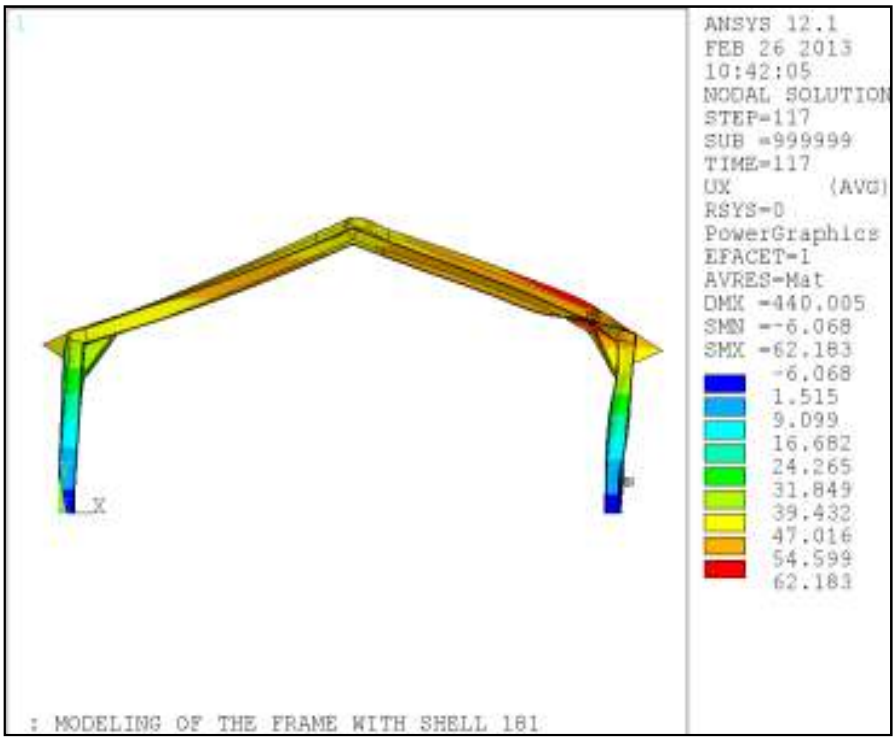

Figure 3.18 X displacement (mm)

3.6 Earthquake Analysis and Dynamic Behaviour of the Frame Structure

3.6.1 Introduction

The seismic effects and the effects of the other actions included in the seismic design situation are determined on the basis of the linear-elastic behavior of the structure. Large earthquakes will induce non-linear response in the structure and the inelastic behaviour is considered in the design, through the use of a behavior factor.

Two types of linear-elastic analysis may be used for the preliminary design of the structure, the "lateral force method of analysis" and the "modal response spectrum analysis", choice of method depends on the structure and on the objectives of the analysis. More details of the two analysis types could be found in EN 1998-1(2004) and Elghazouli (2009).

The modal analysis procedure, also known as the dynamic analysis procedure is specified to be generally applicable to all types of buildings, be they regular or irregular in plan and/or elevation. For irregularly asymmetric buildings, the use of the modal analysis rather than the equivalent static force procedure is required by the

codes. Dynamic analysis takes place always in two stages: first to estimate the dynamic properties of the structures in terms of natural frequencies and mode shapes without applied forces and then use these properties for analyzing the structure response to earthquake motion.

3.6.2 Dynamics of multi degree of freedom system (MDOF)

The frame structure in this study is analyzed for dynamic behaviour as multi degree of freedom (MDOF) system which if only in-plane behavior is considered has three degrees of freedom in every node, translation, axial and rotation. For the simplest analysis with 5 nodes there are nine degrees of freedom for the global matrix of the structure, after applying the fixed boundary conditions. The mass of the structure is simply derived by dividing the mass of each element between its nodes. This results in a lumped mass matrix. The equation of motion of the system or the equation of dynamic equilibrium is as (Chopra, 2001):

$$M\ddot{u} + C\dot{u} + Ku = f(t) \qquad \text{Equation 3.1}$$

Where $\ddot{u}, \dot{u}$ and u are the acceleration, velocity and displacement respectively, f (t) is the load vector; and M, C and K are the mass, damping and stiffness matrices respectively (dimensions 9x9). The mass matrix for a lumped system is diagonal.

3.6.3 Vibration modes shape and frequencies

In order to find the dynamic properties of the structure we need to solve equation 3.1. Before attempting to solve equation.3.1 it is helpful to consider the free vibration of the structure, corresponds to no damping (C = 0) and no applied loads (f = 0), so that equation 3.1 becomes (Chopra, 2001):

$$M\ddot{u} + Ku = 0 \qquad \text{Equation 3.2}$$

For a linear system, the solution to this equation has the form of (Chopra, 2001):

$$u = \varphi_i \sin\omega_i \qquad \text{Equation 3.3}$$

φ_i: is the eigenvector that defines the modes shape of the system; ω_i is the circular frequency of the structure for mode i.

Introducing equation 3.3 and its second derivative into equation 3.2 gives (Chopra, 2001):

$$K\varphi = \omega_i^2 M\varphi_i \text{ or}$$

$$\left[K - \omega_i^2 M\right]\varphi_i = 0$$

Equation 3.4

This is solved to give nine eigenvalues, ω_i^2 (i = 1, 2,..., 9), which in turn gives the circular natural frequencies, ω_i. For each natural frequency, an eigenvector is found that define the modes shape of the system, each having a distinct deformed shape and each occurring at particular natural frequency (or period). The modes shapes of vibration are dynamic system properties which are independent of the external loading.

For the frame structure in this study a hand calculation using finite element method was done to find the dynamic properties of the frame structure, include the actual vibration periods and the mode shapes of the frame structure by solving the eigenvalue problem. These values of the mode shapes with the corresponding vibration periods were used for determination of the modal base shear. This modal base shear was used in the preliminary design of the structure to estimate the forces in the structure as linear dynamic procedure according to design code procedure as explained in sections 3.6.5 and 3.7.5 . The details of these hand calculations are given in appendix B of this thesis.

Also the finite element software ANSYS has been used to find the dynamic properties of the frame structure as well, using beam element (BEAM4) for a beam analysis and shell element (SHELL181) for a shell analysis. The results were compared with each other and with the hand calculations. The modal analysis in ANSYS is a mode-frequency analysis and it assumes constant stiffness and mass, no

damping and free vibration governed by the equation of motion (equation 3.2), the analysis procedure for the modal analysis is described in Sections 3.4 through 3.8 of the ANSYS Structural Analysis Guide(ANSYS, Inc. 2009b). BEAM4 is a 2-node, 3-D, elastic, uniaxial element with tension, compression, torsion and bending capabilities. The element has six degrees of freedom at each node, translations in the x, y and z directions and rotations about the x, y and z axes. The element x axis is always along the axis of the beam with element y and z axes forming the cross-section plane. Required element constants include cross-section area, thickness in the y and z directions (TKZ and TKY) and moments of inertia (IZZ and IYY which are IYY and IXX respectively for this structure axes). The material properties were used for this beam element are the Young' modulus or modulus of elasticity (EX) and density (DENS). The shell element used in the model for modal analysis is SHELL181 which has been identified already in previous section (see 3.5.1.1). More details of the elements can be found in ANSYS users' guide (ANSYS Inc. 2009). Two sets of material constants were used in every model, for each type of elements. Table 3.4 and Table 3.5 list the element constant sets for the shell and beam elements, respectively.

Table 3.5 Element constant for beam elements

Set #	Area ($m.^2$)	IZZ ($m.^4$)	IYY ($m.^4$)	TKZ (m.)	TKY (m.)
1(Columns)	0.009756	0.000148508750	0.001128810788	0.850	0.650
2(Rafters)	0.008136	0.000071000000	0.000710205008	0.750	0.500

The sets of material properties (The Young's modulus, Poisson's ratio and density) used in the model are the same as in the first model, as in Table 3.3 for both beam and shell elements. It must be pointed out that in ANSYS, the density must be entered as mass per unit volume, not weight per unit volume for modal analysis. Also of paramount importance the units used in a dynamic analysis must belong to a coherent system of physical units to avoid errors that can easily be by using system not coherent. For this research work use is made of the International System of units (SI), masses are defined in kg, forces in N, lengths in m, Young's modulus in N/m^2 and time in s.

The boundary conditions for the analysis are, all the nodes of the models for both shell elements and beam elements at the foundation level are fixed, i.e., the displacements, translational and rotational, were set to zero. Nine circular natural frequencies and nine modal shapes were obtained from the modal analysis by hand calculations using the stiffness matrix method are shown in Table 3.6.

For the modal analysis by ANSYS; thirteen circular natural frequencies and nine mode shapes were obtained from the modal analysis by beam element. Three of the lowest natural frequencies are shown in Table 3.7 with the first three mode shapes are shown in Figure 3.19 through Figure 3.21. While nine circular natural frequencies with their 9 mode shapes were obtained from the modal analysis by shell element. Four of them are shown in Table 3.8. The first four mode shapes of these 9 mode shapes are shown in Figure 3.22 through Figure 3.25. We will use only first 3 mode shapes and natural frequencies for the calculation.

The fundamental period of the building is 0.243 sec, 0.238 sec and 0.237sec is obtained by hand calculations, ANSYS with beam element and ANSYS with shell element respectively. The results of other higher modes vibration periods in each type of calculation (hand calculation, beam element and shell element) are different from each other although the models for the same structure. This could be explained as they are different type of calculations and analysis procedures in which the representation of the mass and stiffness for every method may be varies and results in these different values for vibration periods. For that the value which controls the comparison between each method will be the fundamental vibration period of the structure. This value was found 0.36 sec from the following empirical formula (3.5) developed by EN 1998-1(2004) based on actual ground shaking. The value 0.085 in the equation is the constant value used for steel moment frame.

$$T_1 = 0.085 H^{3/4} \qquad \text{Equation 3.5}$$

Here T_1 and H are the fundamental period and building height, respectively. This shows that the hand calculations and the model developed in this project is a realistic one. It could be noticed from Table 3.8 that the analysis with shell element derived an odd value for the first vibration period of the structure compared with hand calculation and beam element. This odd value of vibration period caused by the fact that the structure has not been restrained for this analysis from lateral and torsional movement or rotation about the out-of-plane axis (z) which resulted in an extra mode shape of lateral movement of the rafters at the middle span of the frame as shown in Figure 3.22. This why the first mode shape for the beam calculation in Figure 3.19 is equivalent to the second mode shape not the first one for shell calculation in Figure 3.23.

Table 3.6 Frequencies and periods of the structure (hand calculations)

Mode	Frequency F_i (cycles/sec)	Natural Frequency ω_i (rad/sec)	T(sec)
1	4.111796747	25.82208357	0.243
2	8.4978752	53.4	0.118
3	15.45980722	9.71E+01	0.064684
4	87.30414116	5.48E+02	0.011454
5	121.7398084	7.65E+02	8.21E-03
6	140.8853271	8.85E+02	7.10E-03
7	214.4662695	1.35E+03	4.66E-03
8	316.3544293	1.99E+03	3.16E-03
9	326.5690256	2.05E+03	3.06E-03

Table 3.7 Frequencies and periods of structure (ANSYS- beam element)

Mode	Frequency(F_i) cycles/sec	Natural Frequency (ω_i) rad/sec	T sec	Mode Shape
1	4.1978	26.362184	0.23822	Vertical Bound
2	4.375	27.475	0.228571	Sway
3	10.914	68.53992	0.091625	Vertical Bound with Sway

Table 3.8 Frequencies and periods of the structure (ANSYS shell element)

Mode	Frequency(Fi) cycles/sec	Frequency ω rad/sec	T sec	Mode Shape
1	0.68211	4.2836508	1.466039	Lateral Movement
2	4.2154	26.472712	0.237225	Vertical Bound
3	5.7385	36.03778	0.174262	Vertical Bound with Sway
4	7.1008	44.593024	0.140829	Torsional

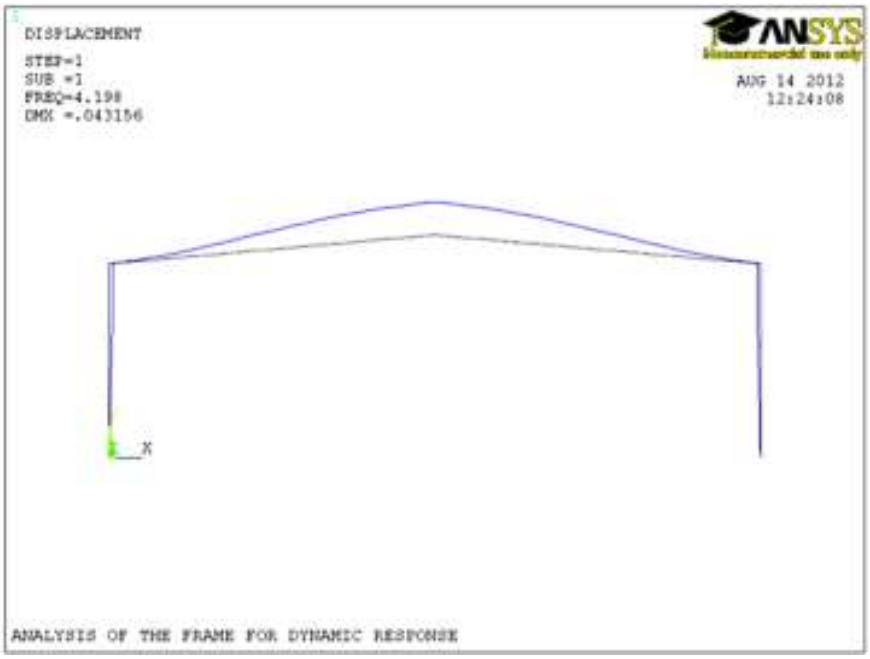

Figure 3.19 Beam mode shape 1 (Vertical bound)

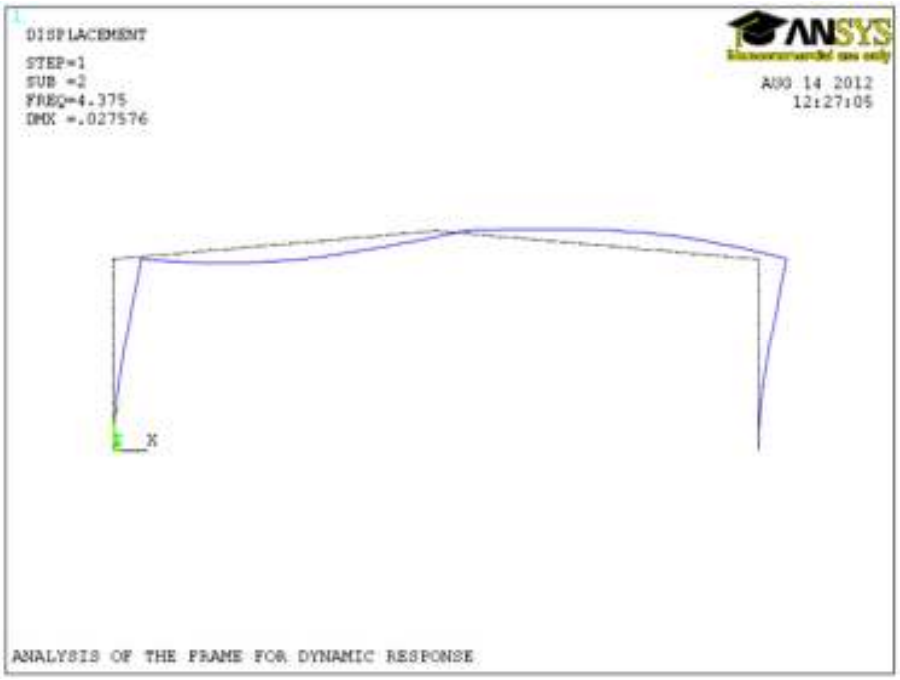

Figure 3.20 Beam mode shape 2 (Sway)

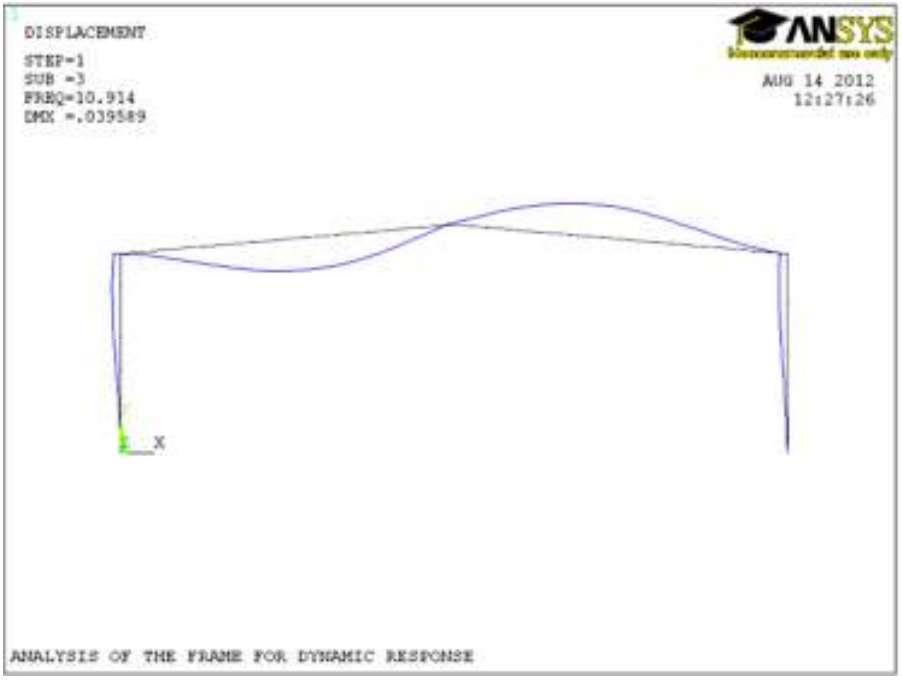

Figure 3.21 Beam mode shape 3 (Vertical bound with sway)

Figure 3.22 Shell mode 1 (Lateral movement)

Figure 3.23 Shell mode 2 (Vertical bound)

Figure 3.24 Shell mode 3 (Vertical bound and sway)

Figure 3.25 Shell mode 4 (Torsional)

3.6.4 Modal equations of motion

To determine the earthquake response we need to solve the equation of motion of the multi degree of freedom structure with earthquake as an applied force. Equation 3.1 the equation of motion for a multi degree of freedom system can be simplified, because of the orthogonality properties of the modes for a multi degrees of freedom system which makes modes independent of one another. The natural frequencies can be shown to satisfy the following orthogonality conditions. When $\omega_i \neq \omega_n$ (Ghosh, 2003):

$$\varphi_i^T M \varphi_n = \varphi_i^T C \varphi_n = \varphi_i^T K \varphi_n = 0 \qquad \text{Equation 3.6}$$

Using the principal of modal superposition which states that any set of displacements can be expressed as linear combination of the mode shapes (Ghosh, 2003):

$$u = U_1\varphi_1 + U_2\varphi_2 + U_3\varphi_3 + \ldots\ldots + U_n\varphi_n = U_i\varphi_i \qquad \text{Equation 3.7}$$

In which U_i is a modal displacement. Equation 3.7 allows transforming the equation of motion into a set of equations in terms of modal displacement rather than the original degrees of freedom. Substituting equation 3.7 and its derivatives into equation 3.1 and multiplying the resultant equation by the transposition of any mode shape vector yields (Ghosh, 2003):

$$\varphi_i^T M \varphi_i \ddot{U} + \varphi_i^T C \varphi_i \dot{U} + \varphi_i^T K \varphi_i U = \varphi_i^T f(t) \qquad \text{Equation 3.8}$$

By virtue of the orthogonality properties of equation 3.6 introducing:

Generalized mass $M_i = \varphi_i^T M \varphi_i$

Generalized damping $C_i = \varphi_i^T C \varphi_i$

Generalized stiffness $K_i = \varphi_i^T K \varphi_i$ Equation 3.9

Generalized force $f_i(t) = \varphi_i^T f(t)$

Using the relationship between ω_i, ξ, M, C and K as:

$C_i = 2\xi_i \omega_i M_i$ and $K_i = \omega_i^2 M_i$

Where ξ_i is the fraction of critical damping in mode i, equation 3.8 becomes (Ghosh, 2003):

$$\ddot{U}_i + 2\xi_i \omega_i \dot{U}_i + \omega_i^2 U_i = \frac{f_i(t)}{M_i}$$

Equation 3.10

The dynamic analysis of a multi degree system by modal superposition requires the solution of equation 3.10 for each mode to obtain its contribution to response. In case of earthquake the external force is equal to mass times ground acceleration and the load f (t) will be as (Ghosh, 2003):

$$f_{eff}(t) = M1\ddot{x}g(t) \qquad \text{Equation 3.11}$$

Where 1 represents a unit vector of dimension n (numbers of degrees of freedom) and $\ddot{x}g(t)$ is ground acceleration then equation 3.9 becomes (Ghosh, 2003):

$$f_{i\,eff}(t) = \varphi_i^T M1\ddot{x}g(t) = -L_i \ddot{x}g(t) \qquad \text{Equation 3.12}$$

Where: $L_i = \varphi^T M1$ represents the earthquake participation factor for mode i.

Substituting equation 3.12 into equation 3.10, the equation of motion for mode i of a multi degree system subject to earthquake excitation becomes (Chopra, 2001):

$$\ddot{U}_i + 2\xi_i \omega_i \dot{U}_i + \omega_i^2 U_i = -\frac{L_i}{M_i} \ddot{x}g(t)$$

Equation 3.13

Where:

$$L_i = \sum_n m_n \varphi_{in}$$

Equation 3.14

$$M_i = \sum_n m_n \varphi_{in}{}^2 \qquad \text{Equation 3.15}$$

L_i is an earthquake modal excitation factor or earthquake modal participation factor, M_i is the modal mass.

The total horizontal force in the structure (base shear) (Elghazouli, 2009):

$$F_b = \frac{L_i{}^2}{M_i} S_i \qquad \text{Equation 3.16}$$

Where $\frac{L_i{}^2}{M_i}$ is the effective weight, S_i is the spectral acceleration corresponding to that mode's natural period and damping.

3.6.5 Response spectrum analysis

Having determined the dynamic properties of the system, the natural frequencies and the mode shapes, we can go on to analyse the response of the structure to an applied load. To analyse the response spectrum first we need to determine the earthquake participation factor from equation 3.14.

The normal modes and the natural periods of the system are determined before we used them to find the maximum accelerations from the design spectrum for each mode. Five percent damped design spectral response acceleration obtained according to the code provision as the formula used is being prepared for 5% damping value. The earthquake participation factors and the effective modal masses are determined using equations 3.14 and 3.15 respectively. Then the effective weight is obtained by dividing the earthquake participation factor over the effective modal masses for every mode. While the participating mass for every mode is calculated by dividing the effective weight by the total weight of the structure. Then the maximum spectra acceleration and seismic design coefficient are determined. At the end the modal base shear Fb_i and total dynamic base shear Fb_d are determined using equation 3.16.

In order to obtain an approximate value of total response the modal responses are combined using simple combination rules. EN 1998-1(2004) permitted employing either the Square Root of the Sum of Squares (SRSS) procedure or the Complete Quadratic Combination (CQC) procedure. The SRSS method is based on the concept that all modes do not reach their maximum value simultaneously and that the response of both translational and torsional modes may be considered as independent from each other. Thus, the peak overall response is taken as the Square Root of the Sum of Squares (SRSS) of the peak modal responses. When the concept of the mode independence is not fulfilled, and which according to the EN 1998-1(2004) code is that for any two successive modes of vibration the shorter period is smaller than the 90% of the longer period, the CQC method must be adopted.

The total lateral force, or strength, at the building's base obtained from the modal analysis is usually lower than the base shear determined from the static force method. Hence, some codes require that the strength of all structural elements to be scaled up such that the total strength at the building's base is equal to or at least 90% (IBC, 2000) of the base shear determined by the static force procedure. However, EN 1998-1 (2004) code does not require such a scaling procedure. The detail of the hand calculation procedure for the earthquake analysis is given in appendix B of this thesis. For more about earthquake analysis procedure see Barltrop and Adam (1991).

3.7 Design Criteria for Proposed Model with Eurocode

3.7.1 Design for gravity loads

The frame structure was designed to carry, in addition to self-weight, all superimposed dead loads, live loads and seismic load. For simplicity as this a PhD work and the research focus in the performance of the structure during earthquakes it was assumed that wind load will not govern the design and would be unlikely to be large at the structure of a large earthquake and therefore was not considered.

The permanent gravity loads ("dead loads") per frame consisted of the roof, purlins, cladding, sheeting, insulation and rafters self-weight and the architectural finishes. Gravity loads on the roof are transferred from the purlins to the horizontal and vertical members, as shown in Figure 3.26. The load transferred from the beams

(rafters) spanning in the transverse direction to the columns of the frame. The value of the load, due to purlins, cladding, sheeting and insulation was taken equal to 1.826 KN/m at all spans. The specific weight of structural cold formed steel was taken as 7850 kg/m^3. Given the assumed load values it was found that the "dead load" is equal to 2.48 kN/m; on each frame, for all the spans in the building according to EN 1991-1-1(2002).

A uniformly distributed value of 0.6 kN/m^2 was assumed to act as "imposed load on roof" at every frame, leading to a distributed beam (rafter) load equal to 3 kN/m according to UK National Annex (NA) to EN 1991-1-1(2002). The value of imposed load here is the value used in the design procedure for estimating the forces according to Eurocode3 while the value in the IBC 2000 presented in section 3.8.1 is only for comparison between Eurocode and IBC. No snow load was considered in the design as the structure was designed for Sudan where the snow is not applicable in the design procedure.

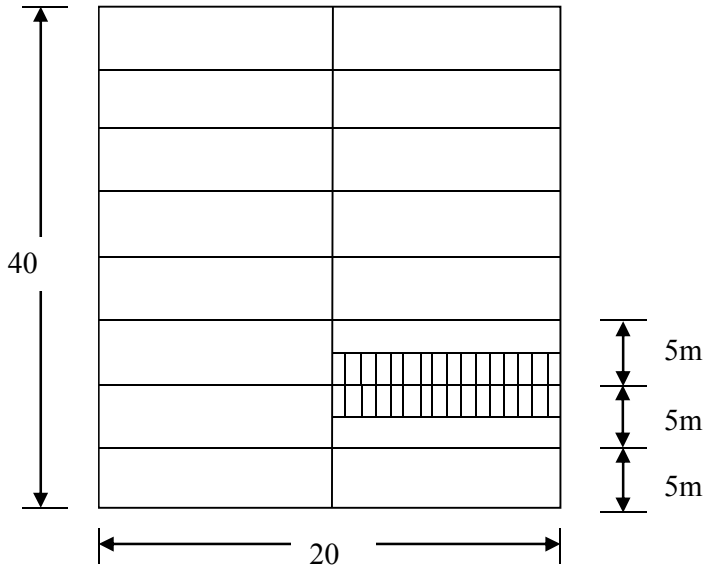

Figure 3.26 Distribution of load in plan

3.7.2 Design of seismic actions

The design spectrum proposed for the elastic analysis for this frame structure by Eurocode 8 is shown in Figure 3.27 and is defined by equations 2.12 to 2.15.

The following site and building data values have been adopted for the various parameters:

- Importance category IV: γ_I=1.4 (buildings whose integrity during earthquakes is of vital importance for civil protection)
- Effective peak ground acceleration normalised by the acceleration of gravity: a_{gR}=0.163 g, the design ground acceleration on type A ground a_g is equal to a_{gR} times the importance factor γ_I, $a_g = \gamma_1 a_{gR}$=0.23(medium-to-high seismicity)
- Subsoil class: C (referring to Deep deposits of dense or medium dense sand, gravel or stiff clay with thickness from several tens to many hundreds of metres).
- Type 1 response spectrum (for earthquake magnitude greater than 5.5)
- Break points periods : $\begin{Bmatrix} T_B = 0.20 \\ T_C = 0.60 \\ T_D = 2.0 \end{Bmatrix}$
- Soil parameter: S=1.15
- Behaviour factor: q={1.5 for Ductility Class Low (DCL)}

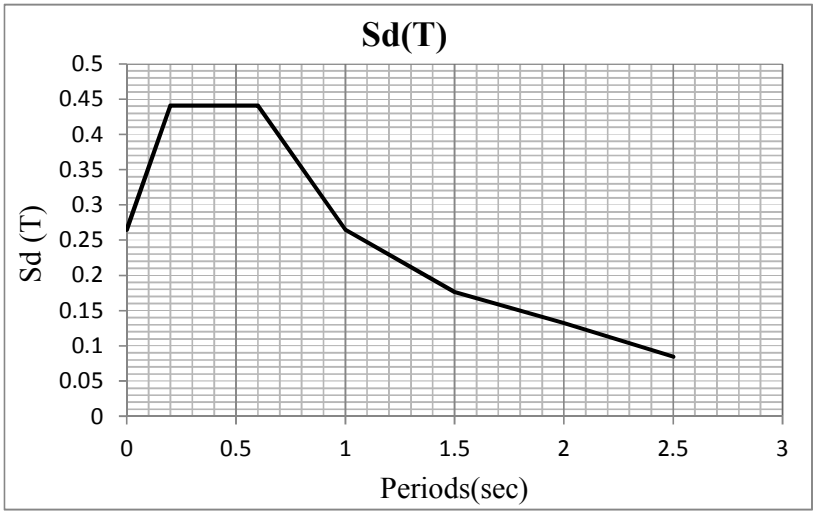

Figure 3.27 Design spectrum for elastic analysis to EN 1998-1(2004).

3.7.3 Static analysis by lateral force method

The design seismic actions used in the analysis of the buildings were determined from the elastic response spectrum given the fundamental period of vibration T of the building. For buildings with heights of up to 40 m the value of the fundamental period of the building T (in s) may be approximated by the following expression recommended in EN 1998-1(2004).

$$T = 0.085\,H^{3/4} = 0.36 \text{ sec} \qquad \text{Equation 3.17}$$

Then the corresponding design pseudo acceleration (seismic coefficient) was calculated with T equal 0.36 sec for $S_d(T)$: $T_B < T < T_C$, using equation 2.13, which resulting in the value equal to 0.441 for the building designed for the Ductility Class Low (DCL). For the given total weight of the building this yields a value of seismic design base shear Fb of 3.621 KN for DCL. Seismic mass equals 9.66 tonne and λ is equal to 0.85 according to EN 1998-1(2004) provision which expresses the fact that part of the mass does not contribute to the mass involved in global modes.

Fb = m Sd (T) λ = 9.66 x 0.441 x 0.85 = 3.621 KN

The inertia forces contributing to the structure's weight masses present in the structure at the time of the earthquake were evaluated from the following combination,

$$G_{k,j} + \sum \varphi_{E,i} Q_{k,i} \qquad \text{Equation 3.18}$$

$$\varphi_{E,i} = \phi \varphi_{2,i} \qquad \text{Equation 3.19}$$

$G_{k,j}$ is equal 58.658 KN for dead load, $Q_{k,i}$ is equal 60.24 KN for imposed load and $\varphi_{E,i}$ is equal 0.6. $\varphi_{E,i}$ is the combination coefficient according to EN 1998-1(2004) provision for variable action i used to estimate a likely value of service loads not being present over the entire structure during the earthquake and to take into account that some masses do not contribute to the vibration of the structure.

Where,

$\phi = 1$ for the rafters in EN 1998-1(2004).

$\varphi_{2,i} = 0.6$ in EN 1990 (2002).

More detail for loads for this section and further associated with earthquake design is given in appendix B of this thesis.

3.7.4 Torsional effects

Torsional effects have to be added to the translational effects in the seismic design. In the structure analysed, due to double symmetry in the x and y directions, the centre of mass CM and the centre of rigidity CR are both, at the geometrical centre of the building. This means that only accidental eccentricity results in torsional forces. In this case, torsion is taken into account by amplifying Fb by $\delta = 1 + 0.6x/L$. In this expression, L is the horizontal dimension of the building perpendicular to the earthquake in direction x (40m), while 'x' is the distance from the centre of rigidity to the frame in which the effects of torsion are to be evaluated. The greatest effect is obtained for the greatest x, which is x = 0.5 L (20m), so that:

$\delta = 1 + 0.6 \times 0.5 = 1.3$

The design shear Fb including torsional effects is therefore:

Fb = 1.3 x 3.62= 4.71 KN

This value used for the preliminary design of the frame.

3.7.5 Dynamic analysis by modal response spectrum method

The design seismic actions used in the analysis of the buildings were determined from the elastic response spectrum. The response of all modes of vibration contributing significantly to the global response was taken into account with effective modal masses amounting to the total mass of the structure given the period of vibration T_k corresponding to a mode k of vibration of the building.

Then the corresponding design pseudo acceleration (seismic coefficient) was calculated for S_d (T): $0 < T < T_D$, for the different range of periods of vibration associated with different modes. The seismic coefficient obtained had values in the range from 0.441 to 2.226 E12 for the design for the low ductility class. More details of the calculations are available in appendix B of this thesis.

3.7.6 Design load combinations

Two basic load combinations were considered, one with the live load as the main variable action given in equation 3.20 and one with the seismic action as the main action as per equation 3.21

$$Ed=(1.35G+1.5Q)$$

Equation 3.20

$$Ed=\left(G+\sum\varphi_{2,i}+E_i\right) \qquad \text{Equation 3.21}$$

3.8 Design Criteria for Proposed Model from International Building Code (IBC)

3.8.1 Design for gravity loads

The frame structure was designed to carry, in addition to self-weight, all superimposed dead loads, live loads and seismic load. For simplicity as this a PhD work and the research focus in the performance of the structure during earthquakes it was assumed that wind load will not govern the design and would be unlikely to be large at the structure of a large earthquake, and therefore was not considered.

The permanent gravity loads ("dead loads") per frame consisted of the roof, purlins, cladding, sheeting, insulation and rafters self-weight and the architectural finishes. Gravity loads on the roof are transferred to the horizontal and vertical members, as shown in Figure 3.26. The load transferred from the beams (rafters) spanning in the transverse direction to the columns of the frame. The value of the load, due to roofing services and purlins was taken equal to 1.826 kN/m at all spans. The specific weight of structural cold formed steel was taken as 7850 kg/m^3. Given the assumed load values it was found that the "dead load" is equal to 2.48 kN/m; in each frame, for all the spans in the building according to 1606 IBC 2000.

A uniformly distributed value of 0.75 kN/m^2 was assumed to act as "imposed load on roof" at every frame, leading to a distributed beam (rafter) load equal to 3.75 kN/m

according to section 1607.11 IBC 2000. The value of imposed load approved for the design procedure is the one was estimated according to Eurocode requirements in section 3.7.1.

3.8.2 Design of seismic actions

The design spectral acceleration for the elastic analysis of this frame structure by IBC is shown in Figure 3.28 and is defined by equations 3.22 to 3.25.

$$S_{DS} = \frac{2}{3} S_{MS} \qquad \text{Equation 3.22}$$

$$S_{D1} = \frac{2}{3} S_{M1} \qquad \text{Equation 3.23}$$

$$S_{MS} = F_a S_S \qquad \text{Equation 3.24}$$

$$S_{M1} = F_v S_1$$

Equation 3.25

The seismic design coefficient, Cs for calculating the base shear is defined by equations 3.26 to 3.29.

$$C_s = \frac{S_{DS}\, I_E}{R} \qquad \text{Equation 3.26}$$

$$< C_s = \frac{S_{DI}\, I_E}{R\, T} \qquad \text{Equation 3.27}$$

$$> C_s = 0.044\, S_{DS} I_E \qquad \text{Equation 3.28}$$

$$> C_s = \frac{0.5 S_1 I_E}{R} \qquad \text{Equation 3.29}$$

The fundamental period of the building above has been calculated as Ta = 1.2 T.
The following site and building data values have been adopted for the various parameters:

- Importance category III: I_E=1.5 (buildings and others structures designated as essential facilities)
- The maximum considered earthquake spectral response acceleration for short periods: S_{MS}= 1.5 g for $S_{MS} = F_a S_s$ for the site coefficient F_a = 1.0 with mapped spectral acceleration for short periods S_s equal to 1.5g, the design spectral response acceleration S_{DS} which is the product of 2/3 and the maximum spectral response acceleration for short periods S_{MS}, S_{DS} =2/3 S_{MS}=1.0 g.
- The maximum considered earthquake spectral response acceleration for 1 second period: S_{M1}= 0.9 g for $S_{M1} = F_v S_1$ for the site coefficient F_v = 1.5 with mapped spectral acceleration for 1 second period S_1 equal to 0.6g, the design spectral response acceleration S_{D1} which is the product of 2/3 and the maximum spectral response acceleration for 1 second period S_{M1}, S_{D1} =2/3 S_{M1}=0.6 g.
- T_O=0.2S_{D1}/S_{DS}, T_S=S_{D1}/S_{DS}.
- Subsoil class: D (referring stiff soil profile).
- Force reduction factor: R={4 for Ordinary steel moment frames}
- Seismic Design Category: The SDC for this structure is D.

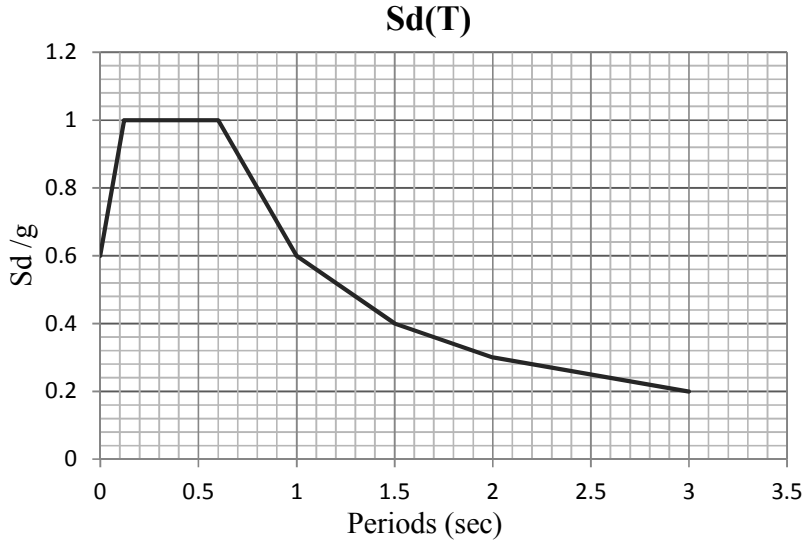

Figure 3.28 Design response spectrum for elastic analysis to IBC (2000)

3.8.3 Static analysis by equivalent lateral force procedure

The design seismic actions used in the analysis of the buildings were determined from the elastic spectral acceleration, given the fundamental period of vibration T of

the building. T (in s) may be approximated by the following expression 3.30 in IBC 2000.

$$T = 0.085\,H^{3/4} = 0.36 \text{ sec} \qquad \text{Equation 3.30}$$

Then the corresponding design spectral acceleration and seismic design coefficient, Cs was calculated for $Cs=S_{DS}\ I_E/R$, which had the value equal to 0.375g for the building designed as Ordinary Steel Moment Frames (OSMF). For the given total weight of the building equal to 29000 N, this yields a value of seismic design base shear Vs of 10.87 KN for OSMF.

Vs = Cs Wt = 0.375x29000 = 10.87 KN

3.8.4 Dynamic analysis by modal method

The design seismic actions used in the analysis of the buildings were determined from the elastic response spectrum. The response of all modes of vibration contributing significantly to the global response was taken into account with effective modal masses amounting to the total mass of the structure given the period of vibration T_k corresponding to a mode k of vibration of the building.

Then corresponding design spectral acceleration and seismic design coefficient, C_{sm} was calculated as $S_{am}\ I_E/R$, for which S_{am} is the design spectral response acceleration has values of SDS and SD1 above, and has been calculated for the different range of periods of vibration associated with different modes which had the value equal to 0.15g for the building designed as OSMF. For the given total weight of the building this yields a value of seismic design base shear V_m of 4.508 kN for OSMF from the summation of the products of equation $V_m = C_{sm}xW_m$, for three modes participated in the vibration of the structure as we used three modes from the result since the higher modes above three have very small vibration periods in this structure (see Table 3.6) and will not contribute significantly to the global response of the structure. Since the base shear from static method is greater than the base shear from dynamic method, the last one had been scaled to have value equal to 6.54 KN according to IBC (2000).

3.8.5 Design load combinations

Two basic load combinations were considered, one with the live load with earthquake and snow if it is applicable given in equation 3.31 and one with the seismic action as the main action as per equation 3.32.

$$C1 = (I.\ 2D + 1.0E + f_1L + f_2S) \quad \text{Equation 3.31}$$

$$C2 = (0.9D + 1.0\ E) \quad \text{Equation 3.32}$$

3.9 Structural Analysis of the Frame

The elastic analysis of the buildings involved the analytical cold formed light gauge steel model with respect to the steel strength and ductility class as it is steel grade S355 with ductility class low. The ductility class used to estimate the behaviour factor, as it reduction factor used for estimation the seismic forces. The joints were assumed to be; fixed for column bases and rigid for beam to column. This model was analysed and the action effects for each individual member of the building were obtained for the two aforementioned load combinations mentioned before in equations 3.20 and 3.21 according to Eurocode, using the commercially available structural analysis software (ANSYS). The analysis for earthquake and the estimation for the forces for the initial design were carried out according to IBC2000 code within EC8. Both of the equivalent lateral force procedure and the modal spectrum procedure were used for determination of base shear according to Eurocode 8 as in section 3.6.2, 3.6.3 and 3.6.5 and according to IBC 2000 as in sections 3.7.2, 3.7.3 and 3.7.4. The values obtained by the Eurocode 8 compared with the values obtained by IBC 2000 and was found little different in values which is reasonable for two different codes. Likewise there is different in the shape of design spectrum obtained by Eurocode 8 in Figure 3.27 and the shape of design spectrum obtained by IBC 2000 in Figure 3.28. As in this research we deal with Eurocode for the design procedures, the value used was the value obtained by Eurocode in 3.7.4 resulted from the static procedure after considering the torsional effects specially it is quite typical to the value obtained by the modal spectrum method by IBC.

The imposed loads on the buildings were considered as a uniform load on the spans. Upon determination of the action effects per each element, the design of beam (rafter) or column section was carried out "manually". The second order effects (P-δ effects) were ignored according to EN 1993-1-1(2005) as the condition of equation 3.33 was found. It has been found that the resulting value of α_{crest} is greater than 10, for that first order analysis used for the structure. Below are the formulas used to find value of α_{crest} and φ, more detail for the calculation is given in appendix B of this thesis.

$$\alpha_{crest} = 0.8\left\{1 - \left(\frac{N_{Ed}}{N_{cr}}\right)_{max}\right\}\left(\frac{1}{200}\frac{h}{\delta_{NHF}}\right) \geq 10 \quad \text{for linear elastic analysis}$$

Equation 3.33

Where:

α_{crest} is the factor by which the design loading would have to be increased to cause elastic instability in a global mode.

N_{Ed} is the design axial load in rafter at ULS.

N_{cr} is the elastic critical buckling load for the complete span of the rafter or the Euler load of the rafter for the full span of the rafter pair (assumed pinned).

δ_{NHF} is the horizontal displacement at the top of the storey obtained by linear elastic analysis, relative to the bottom of the storey, when the frame is loaded with a notional horizontal force H_{NHF}, $H_{NHF} = \frac{1}{200} V_{Ed}$, V_{Ed} is the vertical reaction at each base.

h is the storey height.

α_{crest} is used with this formula above when the axial compression in the rafter is significant when $N_{Ed} \geq 0.09\, N_{cr}$.

Since the frame sensitive to buckling in a sway mode, the global initial sway imperfection was allowed and determined from equation 3.34 below to EN 1993-1-1(2005):

$$\boldsymbol{\varphi = \varphi_0 \alpha_h \alpha_m}$$ Equation 3.34

Where:
φ_0 is the basic value: $\varphi_0 = 1/200$.

α_h is the reduction factor for height h applicable to columns:

$\alpha_h = \frac{2}{\sqrt{h}}$, but $\frac{2}{3} \leq \alpha_h \leq 1.0$.

h is the height of the structure in meters.

α_m is the reduction factor for the number of columns in a row: $\alpha_m = \sqrt{0.5}\left(1 + \frac{1}{m}\right)$

m is the number of columns in a row including only those columns which carry a vertical load N_{Ed} of not less than 50% of the average value of the column in the vertical plane considered.

The initial sway imperfection should be considered by applying Equivalent Horizontal Forces (EHF) which is calculated as: φV_{Ed}, where φ calculated as above and V_{Ed} is the vertical reaction at the base of the frame. As we mentioned before we have two load combinations which are in equations 3.20 and 3.21 according to Eurocode. In combination two a horizontal load was included as earthquake load, resulting that the sway imperfection has only to be into account for combination one. As EHF should be applied when the horizontal loading is not considered for the frame loading, but for the case where the frame is designed for wind load or earthquake there is no need to apply the EHF. For more details about the procedure used for the sway imperfection according to EN 1993-1-1–see the hand calculation for the design of portal frame in appendix C of this thesis and EN 1993-1-1.

3.10 Design of Frame Members

In EN 1998-1(2004), light gauge steel or the thin walled steel are classified as low dissipative structure, the ductility class, is recognised for low dissipative structural behaviour as low (DCL). According to EN (European Standard) Eurocode 8, for low dissipative structures, the design forces may be calculated on the basis of an elastic global analysis without taking into account any significant non-linear material behaviour.

The frame structure, which is proposed to be a hospital building, studied herein is a regular structural system which meets the criteria for regularity in plan and in elevation and satisfies the geometrical constraints of EN 1998-1(2004). The concept of design for the frame structure in this project will be as elastic structure with ability of some parts of the structure to dissipate energy in plastic mechanisms in dissipative zones which will be where the structure develop plastic hinge or plastic mechanism as it is light gauge steel, enabling the structure to develop stable mechanisms associated with large dissipation of hysteretic energy under repeated reversed loading, without suffering fracture.

For dissipative zones in the case of columns, the normalised design axial force N_{Ed} for this frame structure is conformed to $\frac{N_{Ed}}{N_{pl,Rd}} < 0.3$ is well below the limiting values for the low DC building, as it is found 0.02 for the elastic design. Hand calculations for the design procedures of the frame structure according to EN 1993-1-3(2006) and EN 1993-1-1(2005) are given in appendix C in this thesis.

3.10.1 Column design & verification

The section 850x650x63x3-back to back lip channel section-cold formed steel grade S355 was selected for the column member and the verification of the member was carried out for the critical load combination. Since for design use of the critical load combination is made, the design actions for columns were those resulting from the seismic combination and, as pointed out earlier, the normalised design axial force N_{Ed} was found to be well below the limiting values specified in Eurocode 8 for the low ductility class. Many checks for the section of column were carried out to verify the ability of the column to carry the service load during the service life of the building such as resistance of the cross section for shear, compression and bending moment in accordance with EN 1993-1-3:2006 for cold formed steel and EN 1993-1-1:2005 for steel. Columns also have been verified as having sufficient resistance against lateral and lateral torsional buckling in accordance with EN 1993.

3.10.2 Rafter design & verification

The section 750x500x53x3 – back to back lip channel section – cold formed steel grade S355 was selected for the rafter member and the verification of the member

was carried out for the critical load combinations same as for the column member. The design of the rafters was performed for the gravity load combination Ed = (35G + 1.5Q), for low ductility class examined, which yielded larger bending moments than the seismic load combination. Many checks for the section of rafter were carried out to verify the ability to carry the service load such as resistance of the cross section for shear, compression and bending moment in accordance with EN 1993-1-3(2006) for cold formed steel and EN 1993-1-1(2005) for steel. Rafters also have been verified as having sufficient resistance against lateral and lateral torsional buckling in accordance with EN 1993 (These are of paramount importance for earthquake resistance).

3.11 The Proposed Designed Model of Portal Frame Structure

3.11.1 Model description

The model used herein is a result of calibration of the seismic design using numerical investigation and calculations. The frame building model is frame of span 20 m with rigid joints and fixed at column bases, pitch 5˚.The columns are 6 metres high and the distance from ground level to the apex of the frame is approximately 6.875 metres (see Figure 3.4).The brackets for the joints for ridge and knees are 5 mm thickness from cold formed steel (see Figure 3.29 and Figure 3.30). The connection used here as same as the connections used in model two in Figure 3.13 and Figure 3.14 for both ridge and knees as this arrangement of connections showed good performance when the frame model was tested to lateral displacements loading. The model was defined with the same materials properties, type of element, material modelling and finite element idealisation like last models using ANSYS software; to check response of the new proposed designed modified model of the frame structure for the nonlinear static analysis under increasing lateral displacements until the failure of the frame structure.

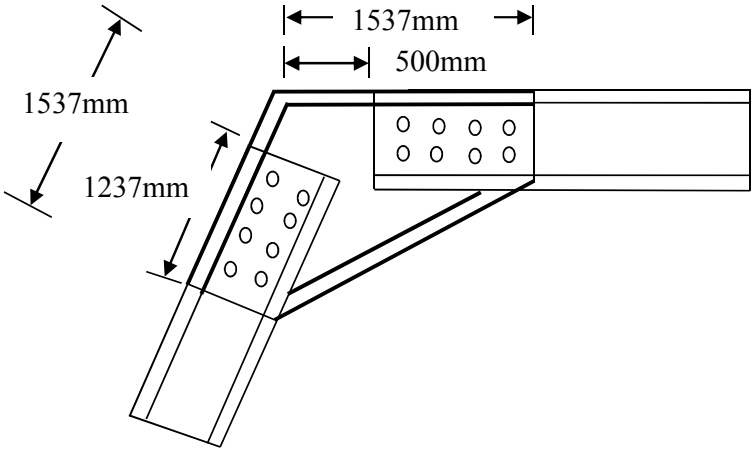

Figure 3.29 Knee arrangement for the new model

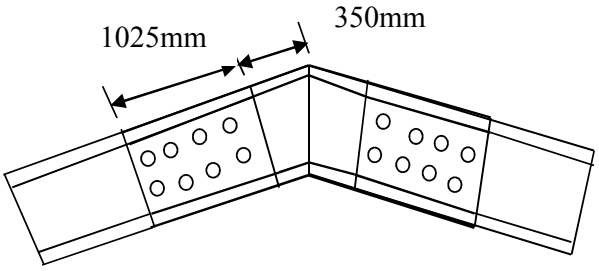

Figure 3.30 Ridge arrangement for the new model

3.11.2 Finite elements results of the proposed designed model

Since the frame members are sensitive to buckling, the frame needed to be restrained to prevent lateral and lateral torsional buckling by providing the frame members with restraint members in areas sensitive to buckling. These restraints include purlins as beam (rafter) restraints and rails as column restraints as detailed later in section 3.11.2.2. The frame was tested first without the effect of lateral restraint and later with the lateral restraint provided where in this case with lateral restraint the study was carried for web thickness 3mm and 6mm, as we use back to back channel section with channel having 3 mm thickness for flanges and web, which combine together to make built up section with overall web thickness 6mm. The results for both cases are presented in Table 3.9 below, while the discussions for the results are presented later in section 3.11.2.1 and section 3.11.2.2.

Table 3.9 Results of frame finite element analyses

Frame section	Restrained condition	Comments
Channel web thickness 3mm	Without lateral restraint	The frame failed due to the **lateral-torsional buckling** of the right column. (Figure 3.31 and Figure 3.34)
Channel web thickness 3mm	Lateral restraint provided	The frame failed by the **local buckling of the web** of the right column. (Figure 3.35 to Figure 3.37)
Channel web thickness 6mm	Lateral restraint provided	The frame failed by the **local buckling of the flange** of the right column. (Figure 3.38 to Figure 3.40)

3.11.2.1The frame structure without lateral restraints (purlins and rails)

First the structure was tested without the effect of lateral restraints to report the response for the frame as general. As shown in (Figure 3.31 and Figure 3.33) the structure appears to be buckling, in a lateral-torsional mode, at the right hand knee and failed due to the lateral-torsional buckling of the rafter and columns. The right side of the frame suffered worse torsional buckling than the left side which is same as for the previous model (see Figure 3.31, Figure 3.33 and Figure 3.34).

The lateral-torsional buckling caused the failure of the frame by the yielding of the frame members. Figure 3.31 shows values of stresses between 402 to 453 MPa when the frame failed more than 355 MPa the yield strength of the frame members. This is explained with the failure of the frame by yielding of the cold formed profiles.

However the ductility has considerably improved, when the frame failed the total displacement after the elastic zone was about 35 mm with displacement at global yield equal to about 8 mm (Figure 3.33). For determination of the frame ductility or the behaviour factor according to equation 2.16 and Figure 2.29 the total displacement of the frame after failure (35mm) divides by the top displacement with first yield of the frame members (8mm) to give value equal to 4.375 as the ductility of the frame. This value of ductility or behaviour factor indicates that the frame has a

good ductility response when subjected to lateral loading or earthquake motion. From these results the application of the effects of restraints when studying the response of light gauge steel is important to prevent lateral torsional buckling of the frame members' profiles.

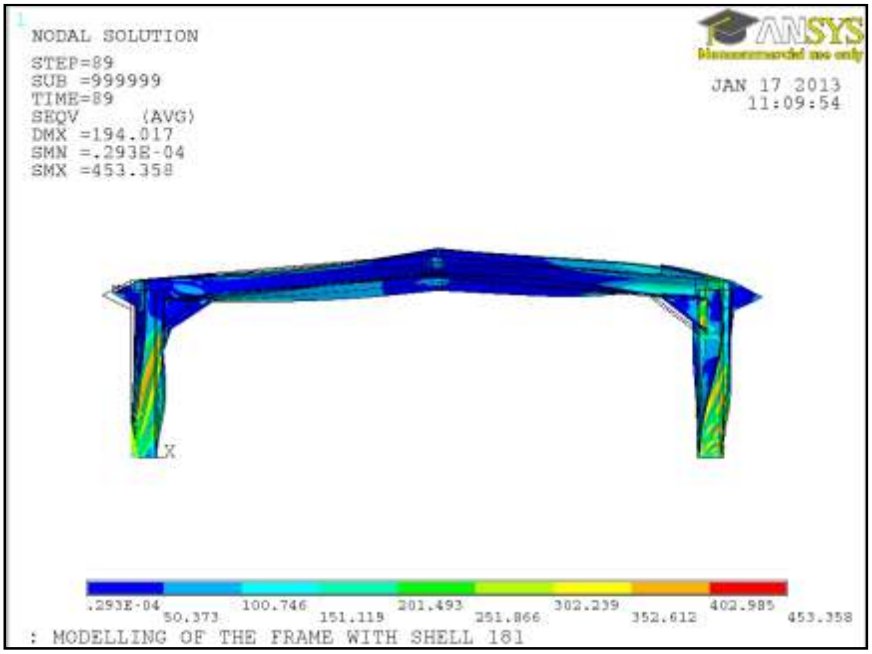

Figure 3.31 Von Mises stress (MPa)

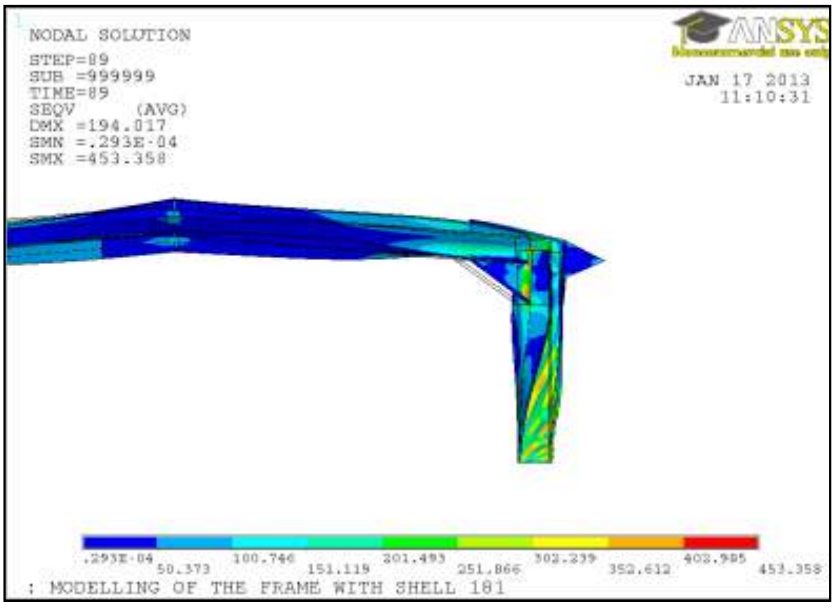

Figure 3.32 The torsional buckling mode

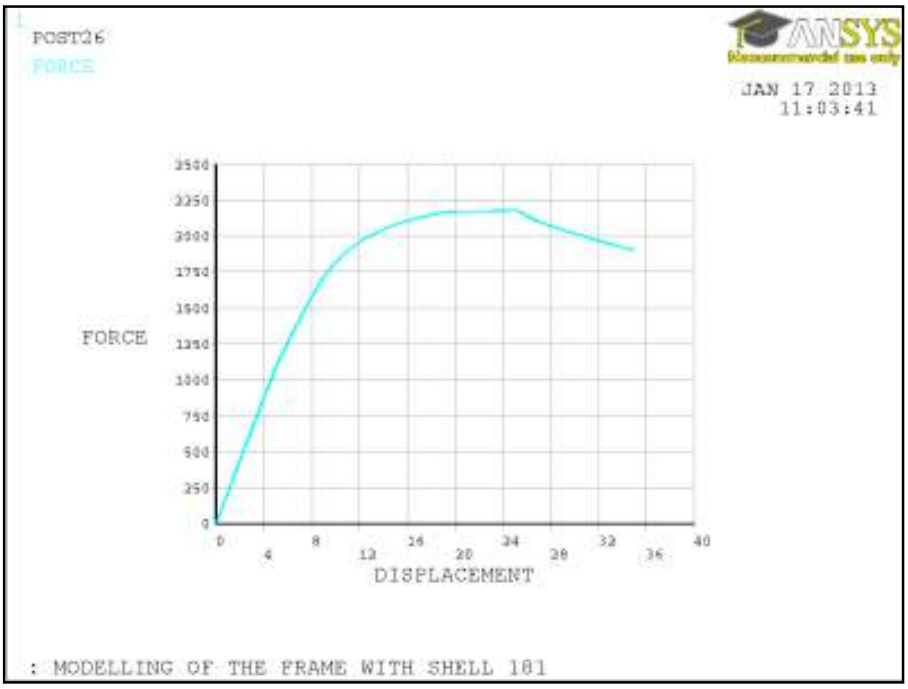

Figure 3.33 Force (N) vs. displacement (mm)

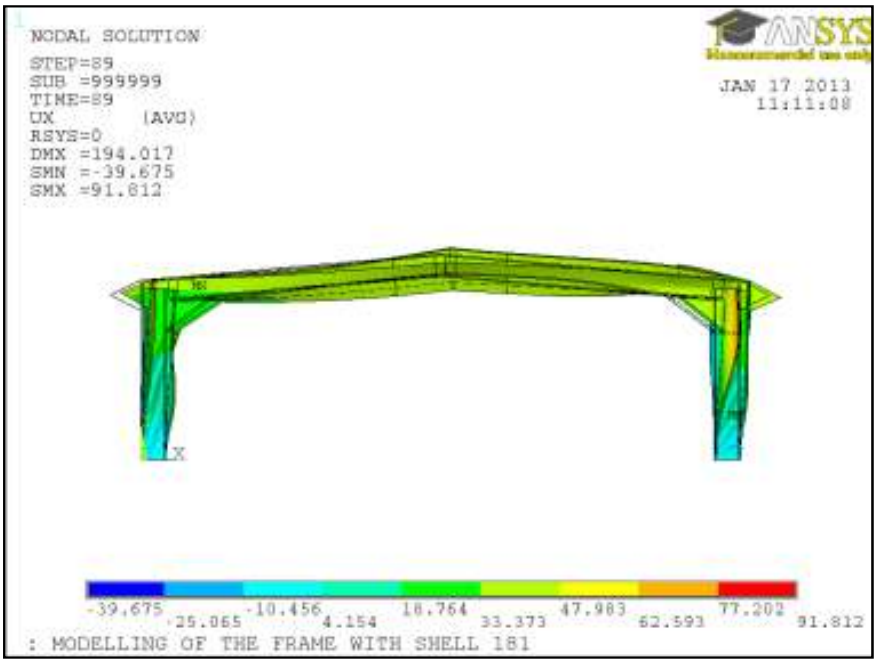

Figure 3.34 X displacement (mm)

3.11.2.2 The frame structure restrained (by purlins and rails).

The effects of restraints (purlins and side rails) were applied to the proposed model to obtain the response of the frame to lateral displacement with lateral and torsional prevention, the restraint include lateral restraint to prevent lateral movement of the compression flange, torsional restrains to prevent rotation of a member about its longitudinal axis (x axis here), and intermediate restraints to the tension flange. These effects have been applied in the finite element model for the light gauge steel portal frame in ANSYS as spring element known in ANSYS as COMBIN40. This spring element has one degree of freedom at each node, either a nodal translation, rotation, pressure, or temperature.

The element is defined by two real constants, spring constant to represent the stiffness of the purlin or rail attached to the rafter or column, and the moment resistance of the purlin or rail. The stiffness value (K) used was about 2.6E10 N/mm which was assumed as maximum as to give enough stiffness to the frame members, just to prevent the lateral torsional buckling mode, as it is not scope of the research to study the behaviour of the purlins and rails which are another area of research. The value for the moment resistance (Mc) was used in combin40 was the moment resistance of the frame sections to avoid the failure due to the reducing of the moment resistance of the purlins, as it is less than the moment resistance of the frame sections. The moment resistance value was used for spring element is 100E7 N mm which is the moment resistance of the column as it is bigger than the rafter's.

Every restraint was modelled with two spring elements (combin40), every spring continuing to distance out of the frame section to represent the extension of the purlins through the span of the structure. This distance was fixed at each end for translations in x, y and z while the rotation is allowed in all directions.

The analysis resulted in the absence of the torsional buckling of the frame sections and the failure was seen to be by the local buckling of the right column which was caused by the web buckling of the section, resulting in the reduction of the bending stiffness of the section that led to flange buckling. This buckling of the web followed by the flange which has a higher value of buckling than the web changed into a local plastic mechanism for the right column under the connection. This caused the failure of the frame structure. The von Mises stress after failure is shown in Figure 3.35 and

Figure 3.36. The force displacement relationship showed a good ductility of the frame as shown in Figure 3.37, where the horizontal displacement after yielding or in the plastic zone is equal 24 mm and at the yielded point is 8 mm. Due to the column buckling a premature failure happened to the structure before yielding into plastic mechanism. According to this result the frame structure needs to be improved to be protected against this kind of premature failure which is not desirable in earthquake resistant structures. The previous results for the frame section with thickness 3mm, there are also other results when considering the web with a double thickness of 6mm for the back to back channel section. The results for the frame with web thickness 6mm, a double of the thickness showed ductility with value of 34 mm beyond the plastic zone and at the yielded point is 8 mm displacement as shown Figure 3.40. Also the failure mode is different in case of using web thickness 6 mm as there is buckling in the flange upper part of the right column with yielding of the column base due to buckling of the flange and the web of the column as shown in Figure 3.38 and Figure 3.39. This result is better when compared with frame results using web thickness 3 mm, where the buckling is much greater in the flange and the web of the right column together with less ductility value in case of using web thickness 3mm as shown in Figure 3.36 and Figure 3.37.

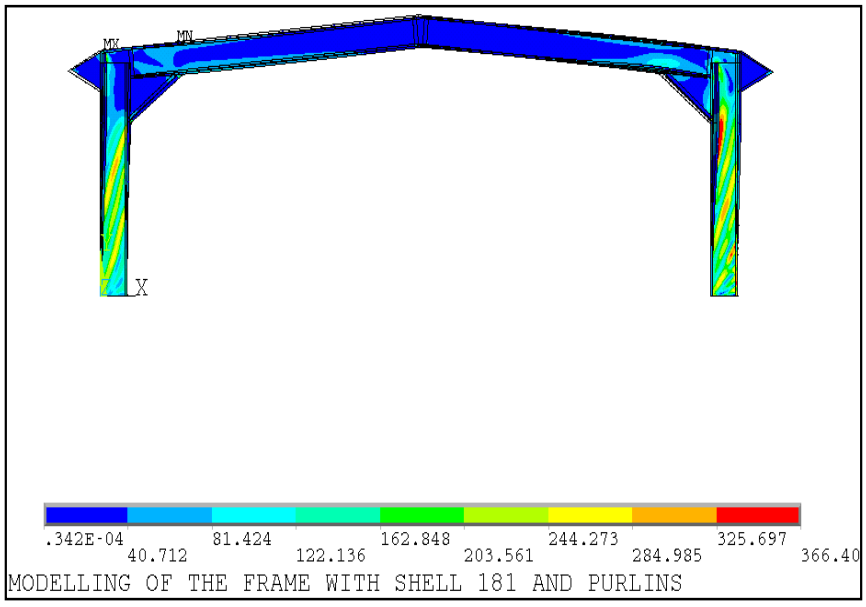

Figure 3.35 Von Mises stress (MPa)

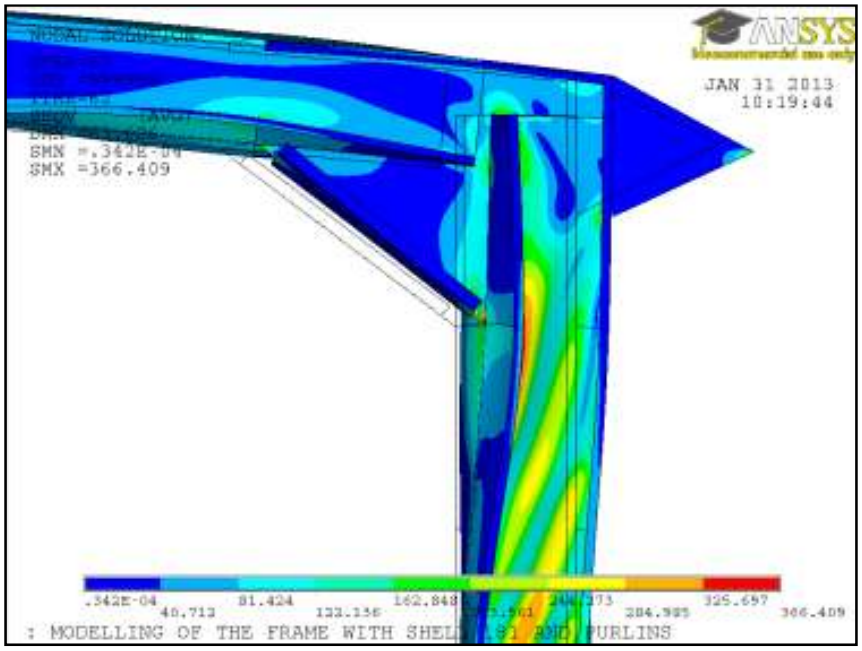

Figure 3.36 Von Mises stress (MPa)

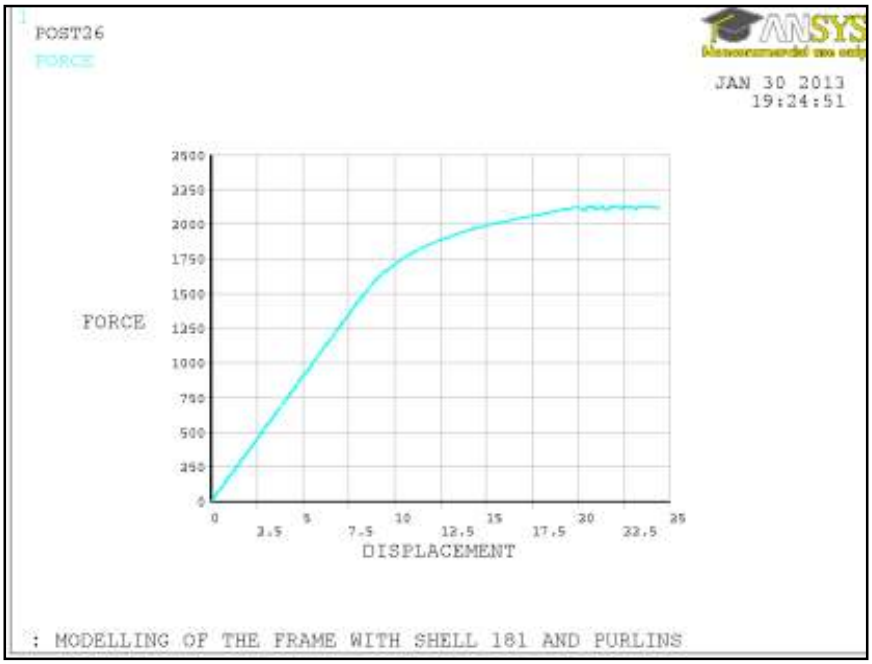

Figure 3.37 Force (N) vs. displacement (mm)

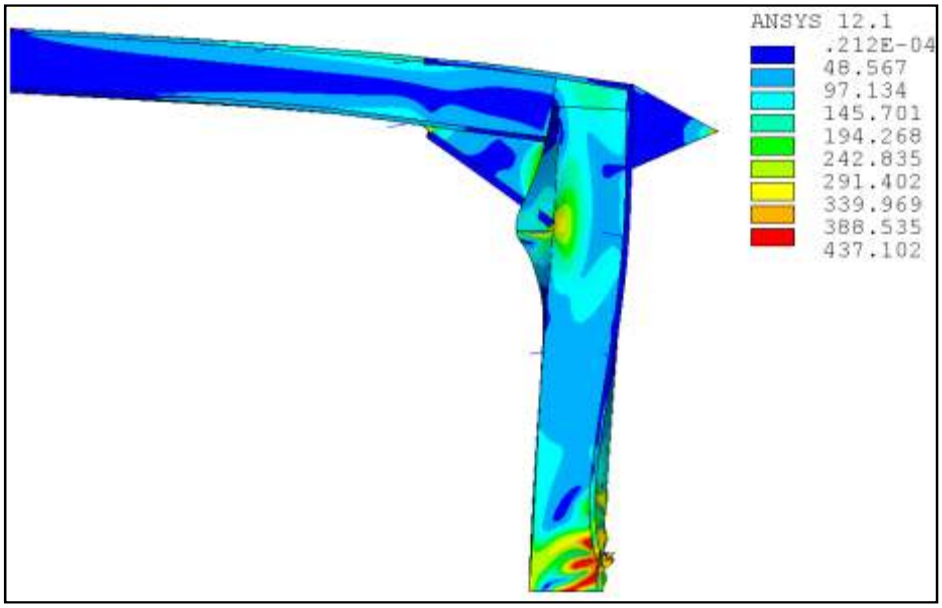

Figure 3.38 Von Mises stress (MPa) right

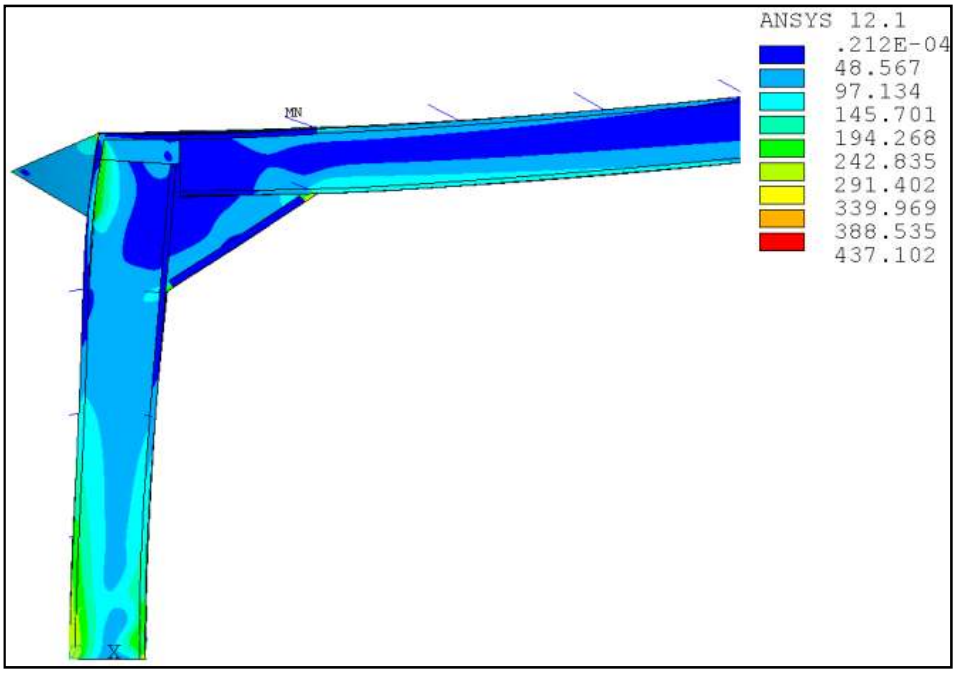

Figure 3.39 Von Mises stress (MPa) left

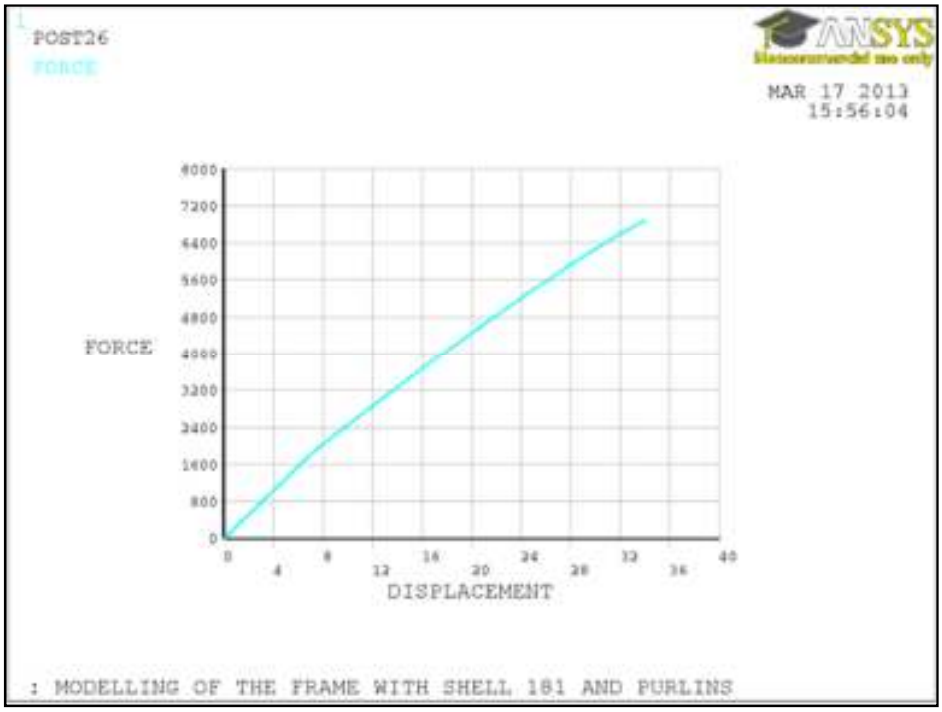

Figure 3.40 Force (N) vs. displacement (mm) diagram

3.12 Proposed Link to Improve Seismic Performance of the Frame

3.12.1 Introduction

In order to improve the seismic resistance for this frame structure, a link is proposed in this section. The link will be attached where the failure happened with special specifications that allow for dissipating the energy by formation of plastic bending as mentioned below. The inelastic action under strong earthquake motion is restricted primarily to these links which will yield in flexural manner.

3.12.2 Design for ductile behaviour

To survive strong earthquake without collapse, the structure should be designed as ductile structure (Utexas, 2013a). Ductility is the ability of a structure to sustain its load and dissipate energy for several load cycles after initial yield, i.e. it can carry the gravity loads without collapse (Szakats, 2006). A ductile behaviour, which provides extended deformation capacity, is generally the better way to resist earthquakes

(ArcelorMittal, 1996), (see Figure 3.41 and Figure 3.42). One reason for this is that because of the many uncertainties which characterise our knowledge of real seismic actions and of the analyses we make, it may be that the earthquake action and/or its effects are greater than expected. By ensuring ductile behaviour, any such excesses are easily absorbed simply by greater energy dissipation due to plastic deformations of structural components (ArcelorMittal, 1996), (see Figure 3.43). In this research the portal frame structure will be designed to have ductile structure. Since this frame structure is made of thin gauge steel which classified as low dissipative structure with low ductility class, having ductile structure could be achieved by design some component parts (links) of the structure to yield and behave plastically to absorb earthquake.

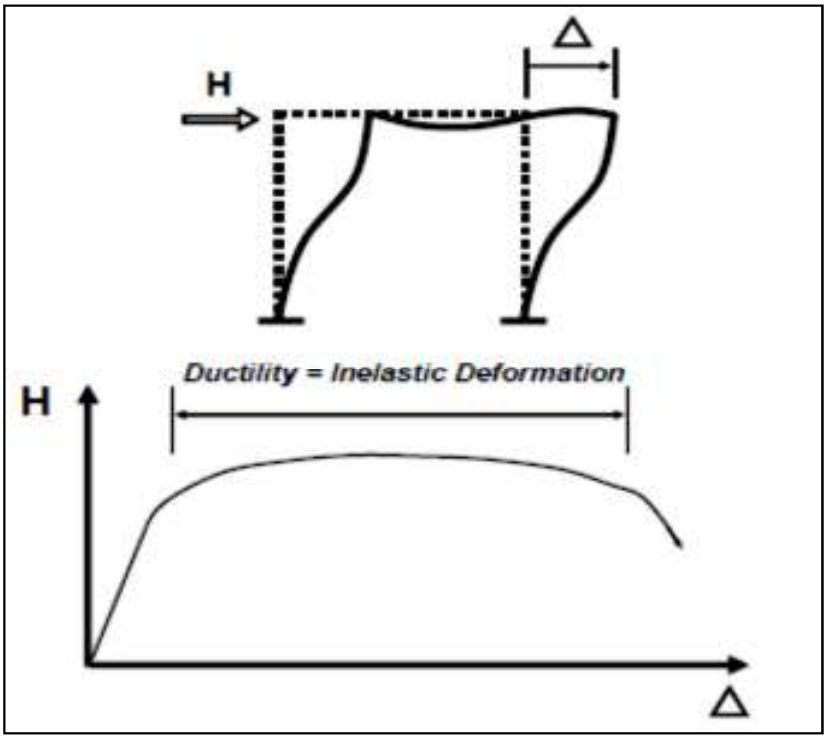

Figure 3.41 Ductility of the structure (Utexas, 2013a).

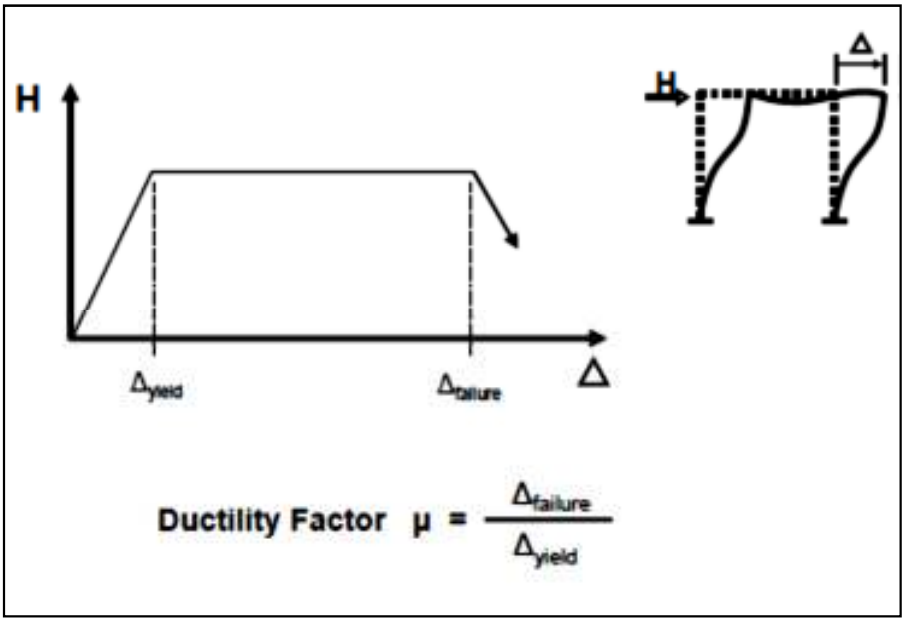

Figure 3.42 Ductility factor (Utexas, 2013a).

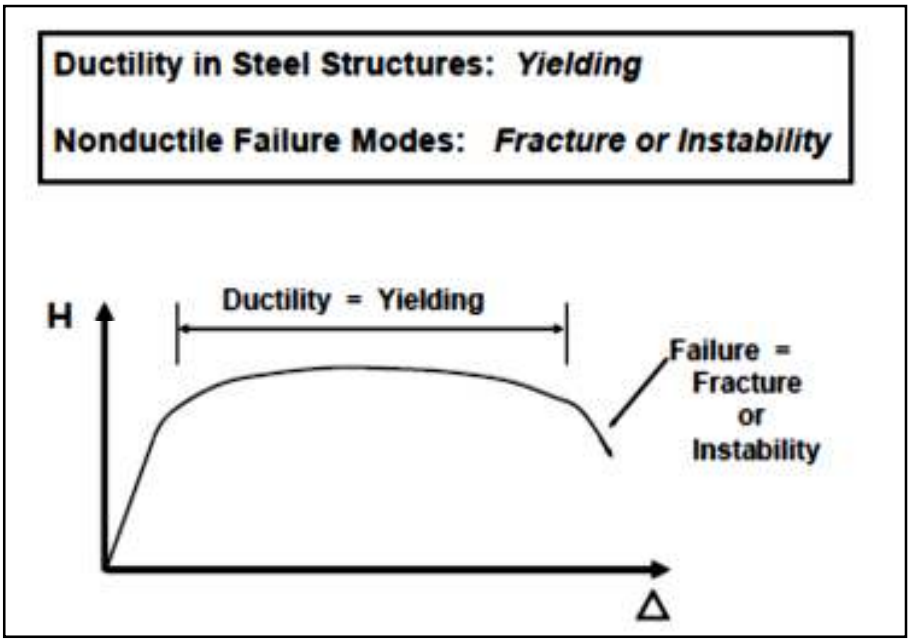

Figure 3.43 Ductility in steel structures (Utexas, 2013a).

3.12.3 Developing ductile behaviour

The concept of having structure with dissipative zones to dissipate the energy by nonlinear behaviour and develop ductility could be achieved following these steps (Utexas, 2013a):

- Choose frame elements ("fuses") that will yield in an earthquake; e.g. beams in moment resisting frames (see Figure 3.44), braces in concentrically braced frames (see Figure 3.45), links in eccentrically braced frames (see Figure 3.46), and the proposed column links for the frame in this study.
- Detail "fuses" to sustain large inelastic deformations prior to the onset of fracture or instability.
- Design all other frame elements to be stronger than the fuses, i.e., design all other frame elements to develop the plastic capacity of the fuses.

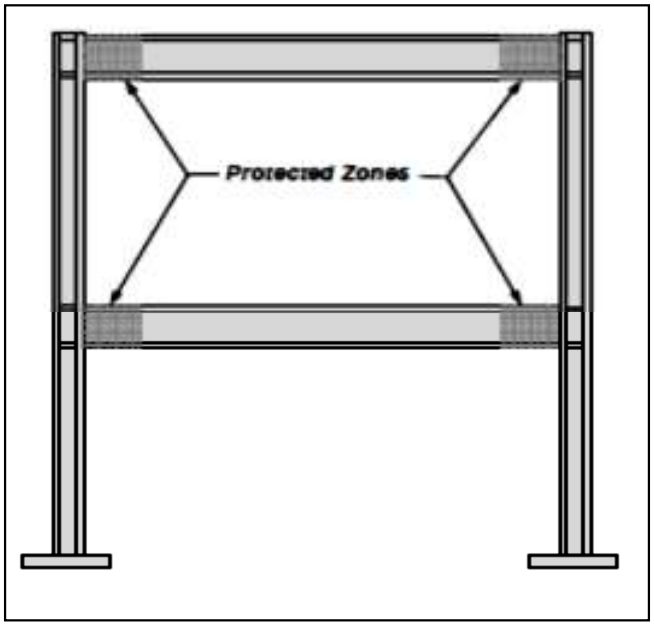

Figure 3.44 Dissipative zones in moment resisting frame (Utexas, 2013a).

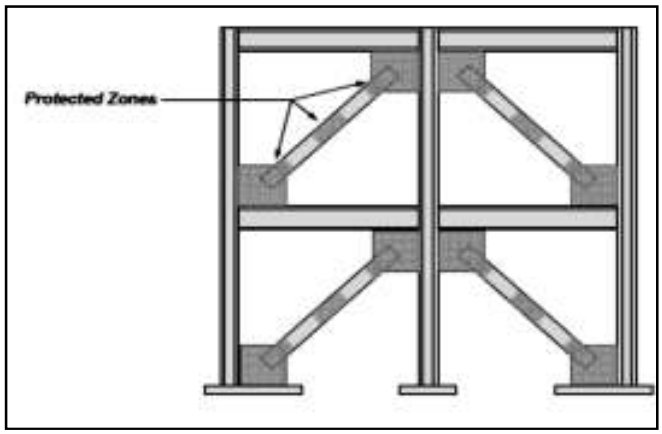

Figure 3.45 Dissipative zones in concentrically braced frames (Utexas, 2013a).

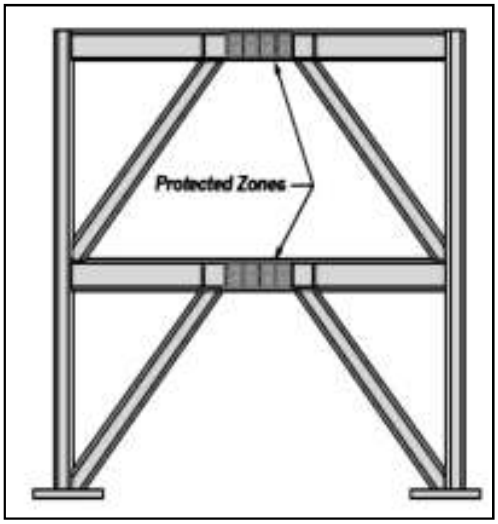

Figure 3.46 Dissipative zones in eccentrically braced frames (Utexas, 2013a).

3.12.4 Classification of sections for local buckling

Local buckling of members can significantly affect both strength and ductility of the member. Members of the seismic load resisting system (SLRS) that are expected to experience significant inelastic action (e.g. beams in steel moment frames (SMF), braces in steel concentrically braced frames (SCBF), links in eccentrically braced frames (EBF), etc), must satisfy strict width-thickness limits to assure adequate ductility can be developed prior to local buckling. Such members must be seismically compact according to AISC (2005). For seismically compact sections, the width-thickness ratios of the elements of the cross-section cannot exceed the limiting

width- thickness ratio λ_{ps}, as specified in Table I-8-1 of AISC (2005) (Utexas, 2013a). These rules could not be applied in thin gauge structure or section class 3 and 4 (slender section) as the thickness is very thin for light gouge steel section. However they could be replaced by the buckling slenderness limit rules used by Wilkinson and Hancock (1997) for compact and non compact cold formed sections. These slenderness limits has been used by Wilkinson and Hancock (1997) when they made experimental tests to investigate the web slenderness limit for cold formed sections in bending. Table 3.10 shows the b/t limits in AS 4100 (Standard Australia, 1990) for cold formed RHS and hot rolled I section bending about major principal axis were used by Wilkinson and Hancock (1997). Their study had showed that there is a considerable interaction between flange and web has been observed. For that they concluded, to not to continue in the current design philosophy in which the web and the flange slenderness limits are prescribed separately. They recommended the use of a simple straight line interaction formula could be useful for classification of sections in bending. Resulting from this a slight change may be appropriate in slenderness ratio for the cold formed section buckling limits.

Table 3.10 Plate element slenderness limits in AS 4100 (Standard Australia, 1990) for bending about major principal axis.

Element	Slenderness definition		Compact		Non- compact	
	RHS	I-Section	RHS	I- Section	RHS	I-Section
Web	$\lambda_w = \frac{d-2t}{t}\sqrt{\frac{fy}{250}}$	$\lambda_w = \frac{d-2t_f}{t_w}\sqrt{\frac{fy}{250}}$	82	82	115	115
Flange	$\lambda_f = \frac{b-2t}{t}\sqrt{\frac{fy}{250}}$	$\lambda_f = \frac{b_f - t_w}{2t_f}\sqrt{\frac{fy}{250}}$	30	9	40	16

3.12.5 Energy dissipation through flexural strains

3.12.5.1 Introduction

In most applications of energy dissipation in structure, like base isolators and viscoelastic dampers, the energy is dissipated through shear strains. Some steel structures dissipate energy through flexural strains such as moment resisting frames, and eccentrically braced frames when using flexural link. In case of eccentrically braced frames the inelastic behaviour of link is controlled by: Flexural yielding, shear yielding or a combination of flexural and shear yielding. In this research the inelastic behaviour of the link for the portal frame of this study will be controlled by flexural yielding as the link in the column and will dissipate energy in cyclic bending manner.

This section presents the design of link and how shear or flexure controls the behaviour of the link. The length of the link (*e*) serves as a key design parameter to have shear link or flexure link. Shorter links expected to yield in shear and longer links are expected to yield in flexure. In the following procedures the basis of how the link could be long link and yield in flexural or could be short and yield in shear.

3.12.5.2 Shear vs. flexural yielding links (Utexas, 2013b):

Static equilibrium of link: Ve = 2M or e=2M/V Equation 3.35

Shear yielding occurs when: $V = V_p = 0.6Fy\ (d- 2tf)\ tw$ = fully plastic shear

Equation 3.36

Flexural yielding occurs when: $M = M_p = Z\ Fey$ = fully plastic moment

Equation 3.37

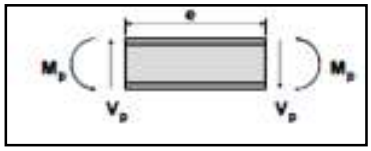

Shear and flexural yielding occur simultaneously when $V=V_p$ and $M=M_p$ or, when: $e=2M_p/V_p$

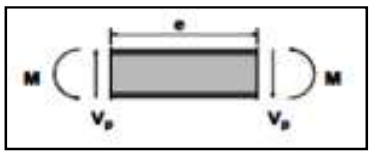

Shear yielding only will occur when $V=V_p$ and $M < M_p$ or, when: $e \leq 2M_p/V_p$

Equation 3.38

Simple Plastic Theory (assume no strain hardening and no shear-flexure interaction):

Shear yielding link: $e \leq 2M_p/V_p$ Equation 3.39

Flexural yielding link: $e \geq 2M_p/V_p$ Equation 3.40

Real behaviour-accounting for strain hardening:

Predominantly shear yielding link: $e \leq 1.6M_p/V_p$ Equation 3.41

Predominantly flexural yielding link: $e \geq 2.6\ M_p/V_p$ Equation 3.42

Combined shear and flexural yielding: $1.6Mp/V_p \leq e \leq 2.6\ M_p/V_p$ Equation 3.43

The equation used in this research to find the length of the link is equation (3.42).

3.12.6 Detailed description of the proposed link

There are three proposed links for this study, I section and back to back lip channel sections with span 2500 mm for every one (see Figure 3.47, Figure 3.48 and Figure 3.49). This span was calculated according to equation (3.42) above as the link will yield in flexure manner. The dimension and specification for the links as presented in Table 3.11. The sections properties and the yield strength for the three links were chosen as to give moment resistance to the link equal to or less than 2/3 of the weaker section of the frame members (the rafter), to allow the inelastic bending of the link while the other components of the frame remain essentially elastic.

The preliminary design of the link is made according to the concept of design of dissipative zone in EN 1998-1(2004) on the basis of the nominal value of the yield strength Fy of the steel specified for the component of the frame (non dissipative zones) exceeds the upper value of the yield strength Fy, max of the link (dissipative zone). This leads to the use of steels of grade S355 for frame members and steel of

grade S235 for the link where the minimum yield strength is 235 MPa and the upper yield strength is limited to 355 MPa.

There are number of parameters that may be manipulated to control the behaviour of the link. These parameters include:

- Thickness of the flange and the web of the link
- Length of the link and position
- Size and shape of steel section
- Number of stiffeners and placing of the stiffeners
- Type of steel (yield strength value)

The link is constructed from cold formed steel, the same steel type of the frame members sections and can be assembled in the same structural steel fabrication plants; this is projected to have a relatively low cost. Also it is easy to replace the link after earthquake event with another one as it is made of light gauge steel.

In the next chapter, a preliminary analysis of the frame structure with the link is described, using finite element software ANSYS. In this analysis, the effect of different parameters on the link response was investigated. The link modelling will be solved using non-linear large–displacement elasto-plastic analysis. The material model introduced by means of bilinear isotropic model. As there is no material test data available for the cold formed section in this model, and according to Elnashai and Izzuddin (1993) study, use was made for bilinear model. Elnashai and Izzuddin (1993) study titled modelling of material nonlinearities in steel subjected to transient dynamic loading, demonstrated that in the absence of material test data under cyclic loading the bilinear model provides acceptably accurate response predictions. The stress- strain relationship is assumed to be elastic perfectly plastic with a young's modulus of 205E3 MPa and a yield strength of 235 MPa. The strain hardening was considered for the plastic behaviour so to allow the link to undergo plastic deformation while protecting the frame from buckling.

The analysis included different links with different dimensions and properties to find the best link for frame response improvement. After that, the link was attached to portal frame structure and the effectiveness of the link was determined by analyzing

the portal frame structure with the link and without the link under different ground excitations using real and generated records. This will be discussed in the next chapter with the frame performance assessment.

Table 3.11 Dimensions and properties of the proposed links.

Link type	**Dimensions (mm)**				**Yield strength**
	b	**d**	**tf**	**tw**	235 MPa
Link 1(I section)	650	850	3 to 5	3	
	B1	**B2**	**B3**	**T**	190-235 MPa
Link 2 (Back to back	650	200	48	3 to 6	
lipped channel section)	850	325	63	3 to 6	

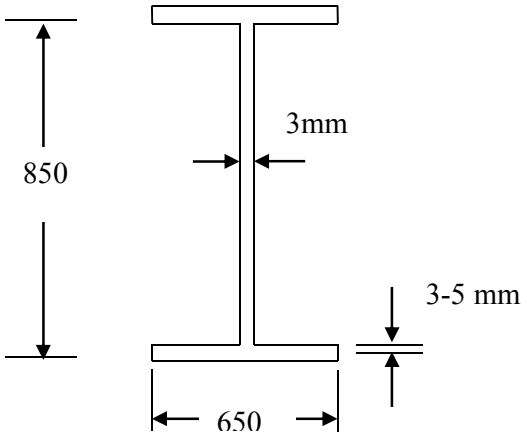

Figure 3.47 Link type 1

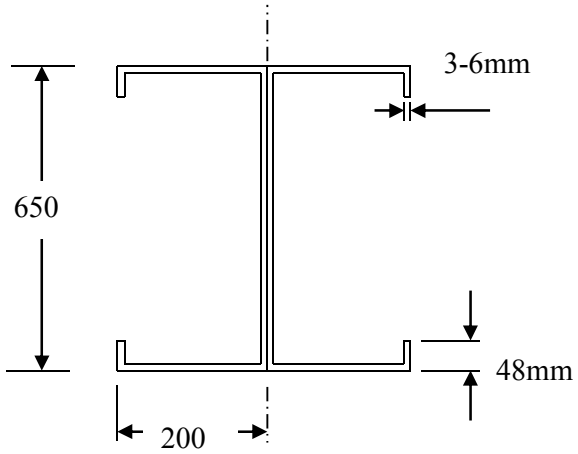

Figure 3.48 Link type 2 section1

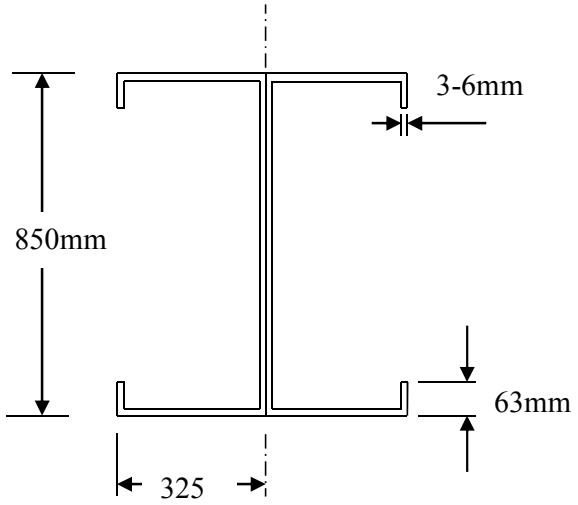

Figure 3.49 Link type 2 section 2

3.13 Summary of the seismic design

In this chapter the design of thin gauge steel frame structure was carried out using cold formed steel. The response of the designed structure was checked for horizontal displacements to find the failure mode of the structure when subject to earthquake motion. The analysis for the preliminary assessment of the frame showed that the

thin walled steel could be used for earthquake resistance but there is need to protect the structure from buckling which effects on the resistant capacity of the frame. A flexural link is proposed for the frame to work as a dissipative component to yield and absorb the earthquake whilst protecting the slender components. The assessment of the frame structure as earthquake resistant will take place in the next chapter to examine the frame using different types of analyses, such as non-linear static push over analysis and time history analysis with the link and without link. The explanation of the two types of the analysis methods (push over and dynamic) are detailed in the next chapter.

Chapter 4

4 Results & Discussions: Analytical Assessment of Seismic Performance of Designed Light Gauge Steel Structure

4.1 Introduction

In the previous chapter, the design of a thin gauge cold formed steel portal frame structure according to Eurocode 3 (2006) and Eurocode 8 (2004) was carried out. The analysis was performed to the portal frame model. The analysis for the preliminary assessment of the thin gauge steel frame showed that the thin walled steel could be used for earthquake resistance but there is need to protect the structure from buckling. In the previous chapter a flexural link was chosen preliminarily for the frame to work as a dissipative component to yield and absorb the earthquake whilst protecting the slender components. In this chapter the inelastic response of these structural systems will be evaluated in a quantitative and systematic way at discrete performance levels and for several performance criteria to examine the frame with and without the link.

The analysis procedure used plays an important role with regard to assessing the seismic response of structures. In day to day practice, the majority of analyses are based on linear-elastic analysis, either because of the limited time or the cumbersome nature and the high degree of expertise required for carrying out a nonlinear analysis. Understandably, the use of nonlinear methodologies for many years was limited to academic research studies. The recently published, Federal Emergency Management Agency (FENIA) Report 356 includes a prestandard and commentary for the seismic rehabilitation of buildings, (FEMA 2000) (Konstantinidis, 2001).

In the FEMA prestandard four analysis procedures are presented. The first two recommended procedures refer to the linear elastic static and the linear elastic dynamic procedures, which are appropriate when the expected level of nonlinearity is low. The third one refers to the nonlinear static (also called pushover analysis), which is acceptable for most buildings. Finally, the fourth procedure is the most

demanding in terms of time and modelling effort and refers to the nonlinear dynamic procedure (also known as nonlinear time history analysis). The choice between the application of a static or dynamic procedure mainly depends on the effect that higher modes of vibration have on the overall structure's behaviour. The linear methods (static and dynamic) have been applied as assessment tools for the preliminary design of the structure as detailed in chapter three of this thesis. In addition some non-linear static analysis was performed.

4.2 Non- linear Seismic Analyses

The two types of non-linear analyses are used to assess the seismic performance of the portal frame structure are nonlinear static analysis or push over analysis and non-linear dynamic analysis or time history analysis.

4.2.1 Non-linear static analysis

In recent years there has been a substantial growth of interest of the use of non-linear static, or pushover, analysis as an alternative to the lateral linear static approach. In this approach appropriate lateral load patterns are applied to the numerical model of the structure and their amplitude is increased in stepwise fashion. A non-linear static analysis is performed at each step, until the building forms a collapse mechanism. A pushover curve (base shear against top displacement) can then plotted. This often referred to as capacity curve since it describes the deformation capacity of the structure. The generation of pushover curve also provides the engineer with a good feel for the non-linear behaviour of the structure under lateral loading (Elghazouli, 2009). More details about this method are available in Elghazouli (2009) and Eurocode 8.

4.2.2 Non-linear dynamic analysis

A final alternative, which remain comparatively rare, is the use of full non-linear dynamic analysis. In this approach a non-linear model of the structure is analysed under a ground acceleration time history whose frequency content matches the design spectrum. The time history is specified as a series of data points at a time intervals of the order of 0.01 s, and the analysis is performed using stepwise procedure usually referred to as direct integration (Elghazouli, 2009). This is a highly

specialised topic that will not be covered in details here-see Clough and Penzien (1993) for presentation of several popular time integration methods.

4.3 Preliminary Analysis of the Frame Structure with Link

This section explains the analyses were carried out to study the effect of the proposed link on the response of the structure. As first stage a nonlinear static analysis was carried out, applying monotonic lateral displacements until failure which is equivalent to the nonlinear static (push over) analysis approved in the seismic design codes but instead of applying horizontal forces use was made of applying horizontal displacements as in this way the nonlinear behaviour especially any unloading characteristic at large deflection should be demonstrated. After that, a dynamic analysis was carried out using real ground motions records and artificial generated records.

In the previous chapter the frame structure response has been studied without the link. Due to the nature of the slender sections which are prone to complex instability problems, the frame suffered local buckling. There are many parameters that control the behaviour of the link. Hence, it is important to investigate how these parameters affect the behaviour of the link and its effect on the response of portal frame structure under different static and dynamic loads. A finite element model was developed to be used in analysis of structures using ANSYS. Frame models were prepared with the link attached for the three different sections of the link in chapter three, a detailed investigation was carried out with different dimensions and arrangement of the link using nonlinear static analyses by applying horizontal displacements (pushover analysis), in order to get the best improvement of the seismic performance of the structure. After that, a detailed investigation was carried out on the portal frame structure with the best link attached. The response of the frame structure was studied without and with the link. The analyses were carried out under real earthquake excitation and artificial harmonic excitation to help for optimizing the link in order to get the best results out of using it.

4.4 The frame with the link for the static analysis

The three-dimensional finite element model has the same structural configuration as the model in section 3.11.1. The finite element assemblies for frame members are fundamentally the same as the frame modelling explained in section 3.5.1.2 of this thesis. With the exception for the link materials properties, the model was defined with the same materials properties, type of element, material modelling and finite element idealisation as the last models. The link was modelled with the same element type (SHELL 181) but with different material properties to enhance the development of yielding in the link to absorb the earthquake and protect the slender components of the frame structure. The material properties considered for the link were given in the previous chapter (section 3.12) and tabulated in Table 3.11. The model of the steel frame with the link is shown in Figure 4.1.

In all the aforementioned analyses, the large displacement and P-δ effects were included in the nonlinear analyses. The two section types I and channel sections have been tested for the parameters effect on the link response and performance and the results are presented in the next two sections in the thesis.

4.4.1 Presentation of first link results (I section link)

A nonlinear static analysis was performed on the steel frame with an I section link (see Figure 3.47) attached in both columns under the connection. The frame with the link was analysed by changing the parameters were explained in 3.12.6 which affect in the link response to find the best link result. The results are tabulated in Table 4.1 below and presented in Figure 4.2 to Figure 4.25. For each analysis the curve of the nonlinear result, defined as the horizontal force at the bottom nodes (base shear) in N unit, versus the top drift (the roof displacement at the top node of the frame) in mm unit, is plotted for all the link results. The change in slope of this curve indicates yielding of the structural elements.

4.4.1.1 Effect of thickness

(1) The first link has dimensions as in Table 3.11was attached and the frame was analyzed, stiffeners attached to the link at middle and ends in one side of the link (see Figure 4.1). The results show that the failure happened with yielding

of the part of the rafter and the bottom of the right column as well (see Figure 4.4 and Figure 4.5). Also the buckling of the frame member for the column section was observed. The displacement after yielding was 28 mm which is less than the value without link (34mm) as shown in Figure 4.2 and Figure 4.3. The results include the force displacement diagram, the horizontal displacement and the von Mises stress of the frame when failed as shown in Figure 4.2 to Figure 4.5 respectively.

Table 4.1 I section link results

Link result No.	Yield strength (MPa)	Link's stiffeners	Comments
Result (1) for link's web thickness 3mm and flange thickness 3mm	235	At the middle and ends (one side)	Failure of frames profiles (Figure 4.2 to Figure 4.5)
Result (2) for link's web thickness 2.5 mm and flange thickness 3mm	235	At the middle and ends (one side)	Failure of link (Figure 4.6 to Figure 4.9)
Result (3) for link's web thickness 3mm and flange thickness 3mm	235	At one end only (one side)	Yielding of the rafter and buckling of the frame sections and link (Figure 4.10 to Figure 4.13)
Result (4) for link's web thickness 3mm and flange thickness 3mm	235	No stiffeners	Buckling of the frame sections and link (Figure 4.14 to Figure 4.18)

Result (5) for link's web thickness 3mm and flange thickness 3mm	235	No stiffeners but applying reduced beam section	Severe buckling of the frame sections and link (Figure 4.18 to Figure 4.21)
Result (6) for link's web thickness 3mm and flange thickness 5mm	235	No stiffeners	Buckling of the frame sections and link (Figure 4.22 to Figure 4.25)

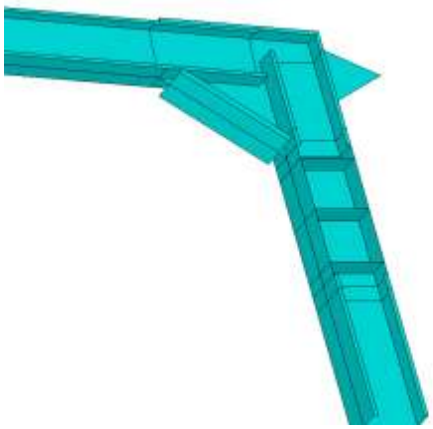

Figure 4.1 Frame with link

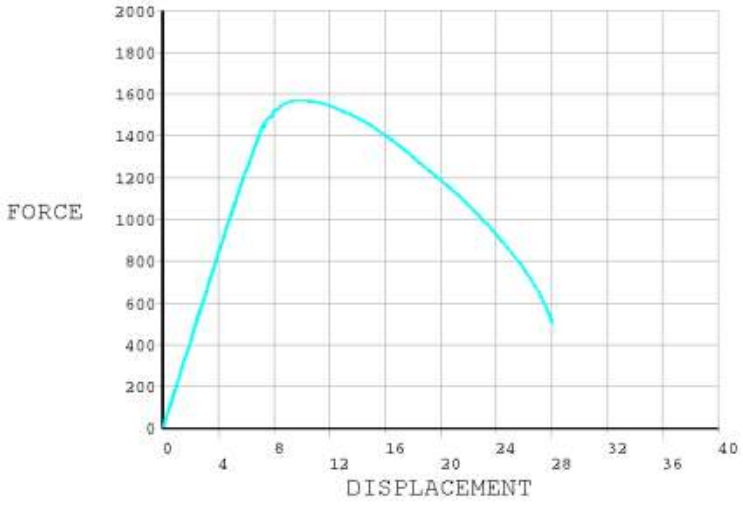

Figure 4.2 Force (N) vs. displacement (mm) diagram

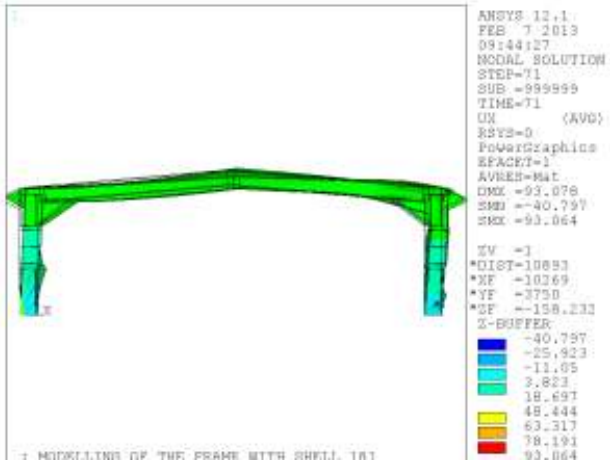

Figure 4.3 Horizontal displacement (mm)

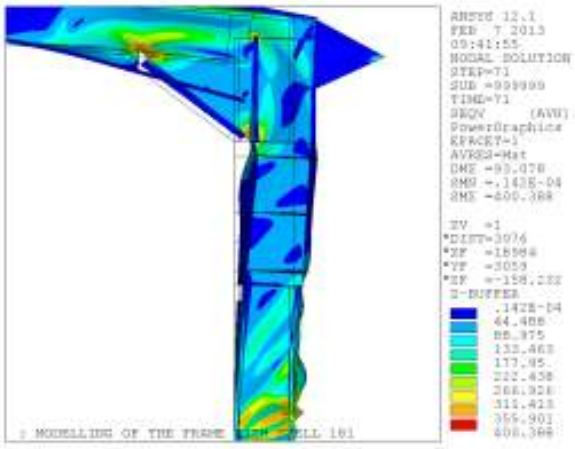

Figure 4.4 Von Mises stress (MPa) (right)

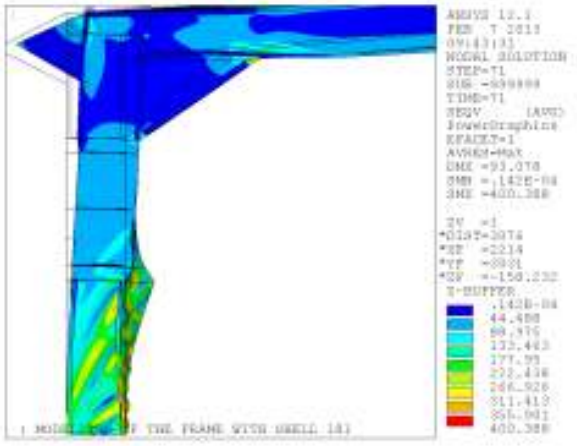

Figure 4.5 Von Mises stress (MPa) (left)

(2) Result (1) showed that the link has more resistance than the frame member, so there was a need to reduce the strength of the link. This could be by changing the web thickness for the link from 3mm to 2.5mm. The results for this new link web thickness are shown in Figure 4.6 to Figure 4.9 for the force displacement diagram, the horizontal displacement and the von Mises stress respectively. From Figure 4.6 for the force displacement diagram the capacity reduced with failure of the link which was totally destroyed (see Figure 4.7). Also the result shows the buckling of the thin walled frame sections (see Figure 4.8 and Figure 4.9).

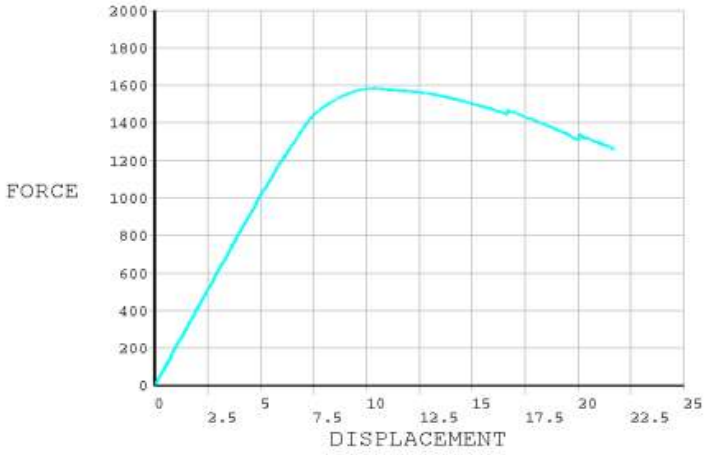

Figure 4.6 Force (N) vs. displacement (mm) diagram

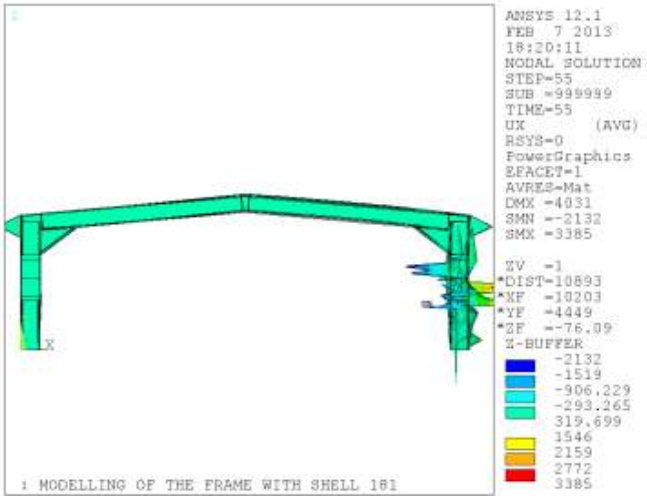

Figure 4.7 Horizontal displacement (mm)

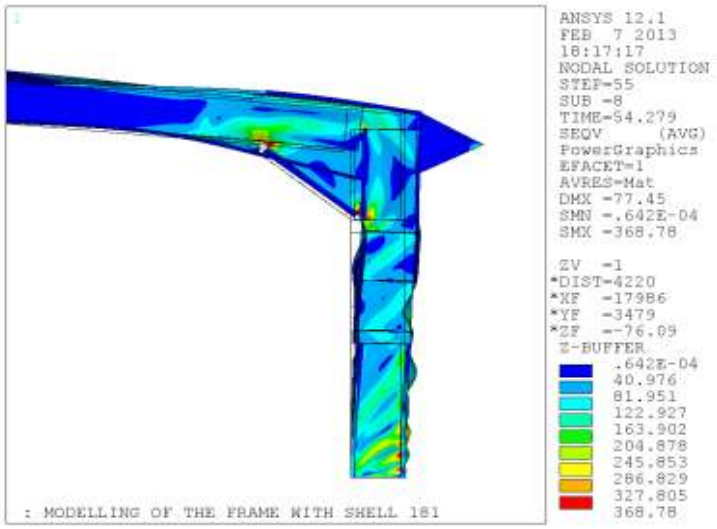

Figure 4.8 Von Mises stress (MPa) (right)

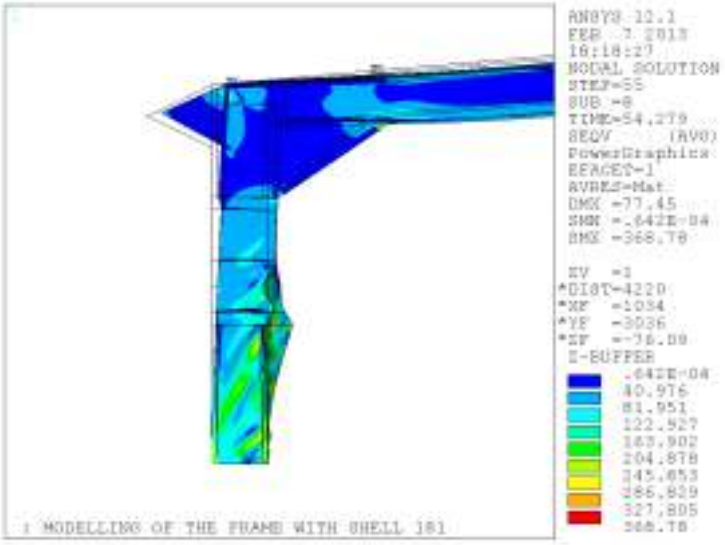

Figure 4.9 Von Mises stress (MPa) (left)

4.4.1.2 Effect of stiffeners

(3) Previous results supported more change to reduce the capacity of the link in comparison with the frame components. Some of the stiffeners in the link were removed, leaving only one stiffeners where the link is connected to the frame while

the dimension for the link is like the first test as in Table 3.11. The results after this modification are shown in

Figure 4.10 to Figure 4.13 for the force displacement diagram, the horizontal displacement and the von Mises stress respectively. From

Figure 4.10 and Figure 4.11 the displacement after yeilding is about 12 mm which is less than the displacement for the frame without the link (34mm). The failure was caused by the yield of the rafter near the connection with a little sign of buckling for the frame section (rafter). Figure 4.12 and Figure 4.13 show value of stresses about 396.33 MPa when the frame failed, more than the 355 MPa yield strength of the frame members. This is a case where the true strength of the structure may be greater than the finite element analysis suggests, because the finite element analysis may have been halted by a localized area of zero stiffness which may or may not have immediately spread and caused an overall structural failure. Note however, the occurrence of very high cyclic stresses is not ideal in an earthquake as it could cause a failure by cracking.

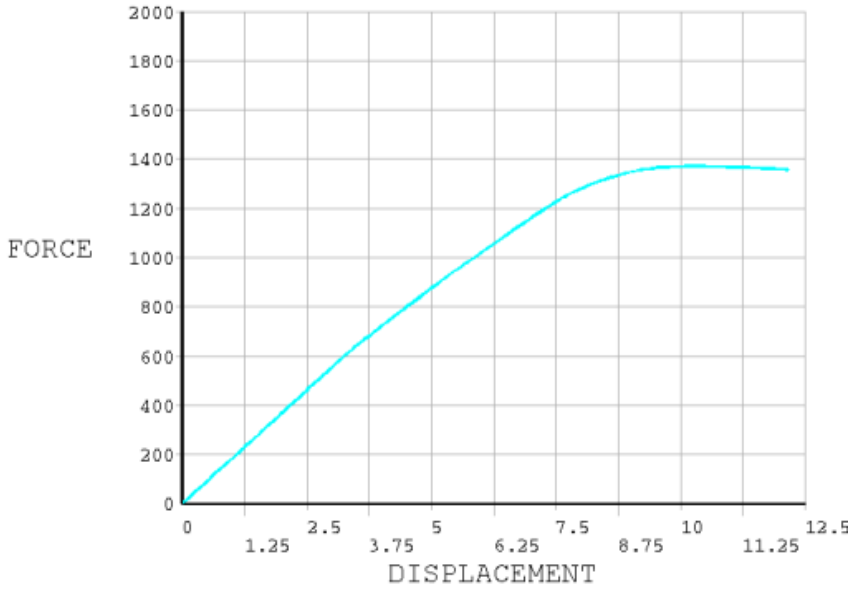

Figure 4.10 Force (N) vs. displacement (mm) diagram

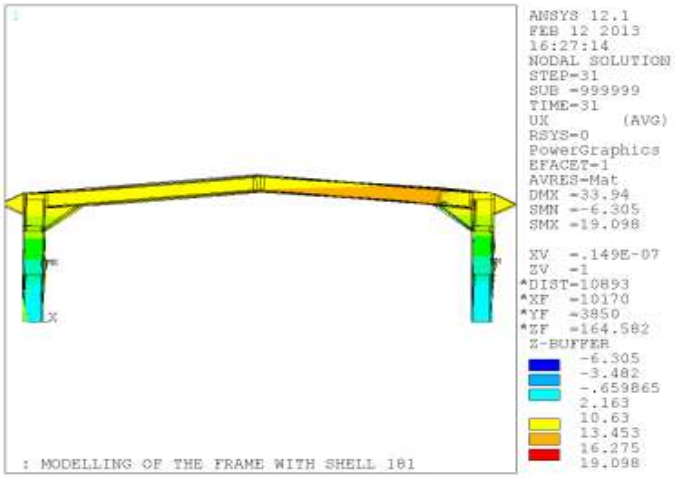

Figure 4.11 Horizontal displacement (mm)

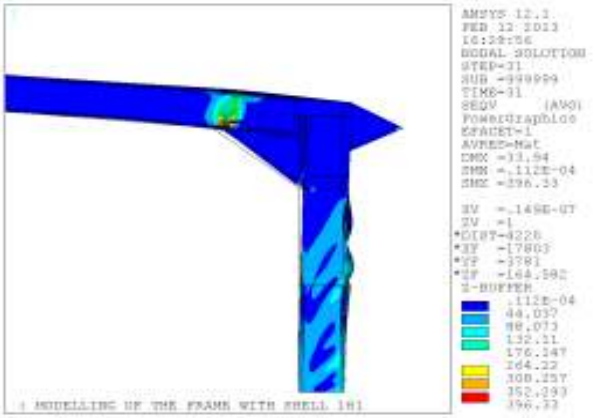

Figure 4.12 Von Mises stress (MPa) (right)

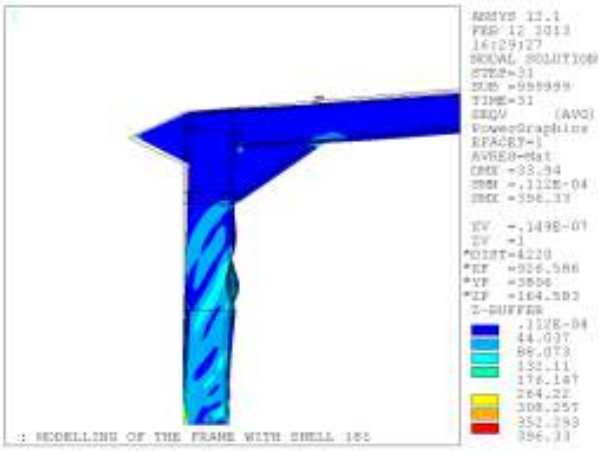

Figure 4.13 Von Mises stress (MPa) (left)

(4) Result (3) motivated to leave the link without stiffeners to make the frame sections having better resistance than the link section.The result for this change are shown in Figure 4.14 to Figure 4.18 for the force displacement diagram, the von Mises stress for the right and left sides with the value of frame's yield strength, the von Mises stress for the right side with the value of link's yield strength and the horizontal displacement respectively. From these results we can observe that the frame members and link still having buckling in both sides of the frame (see Figure 4.15, Figure 4.16 and Figure 4.17). Additionally the capacity of the frame, referring to the force displacement diagram, is worse than for the frame without the link as shown in Figure 3.40. However the displacement at failure has improved from 25 mm in the previous results to 32 mm (see Figure 4.14 and Figure 4.18).

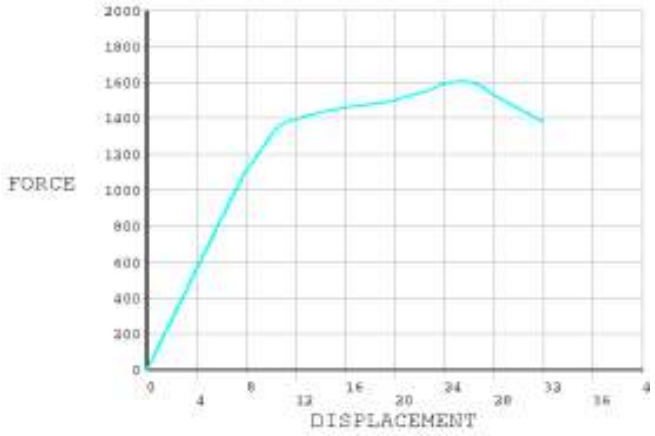

Figure 4.14 Force (N) vs. displacement (mm) diagram

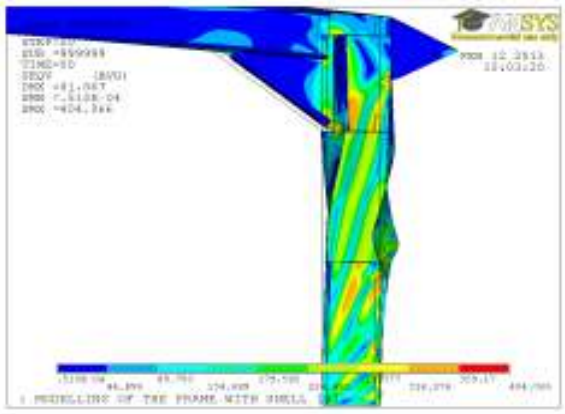

Figure 4.15 Von Mises stress (MPa) with frame value (right)

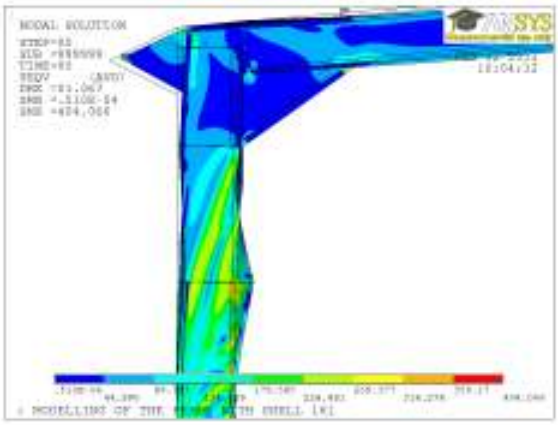

Figure 4.16 Von Mises stress (MPa) with frame value (left)

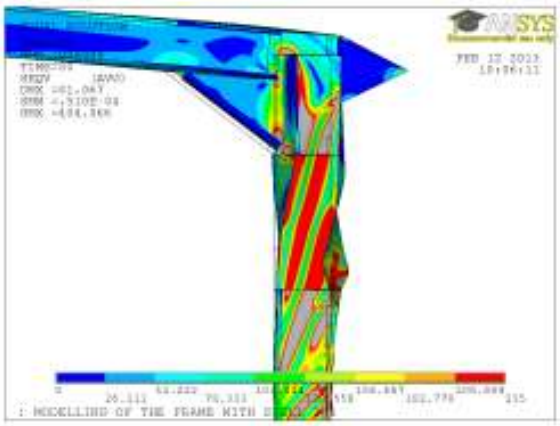

Figure 4.17 Von Mises stress (MPa) with link value (right)

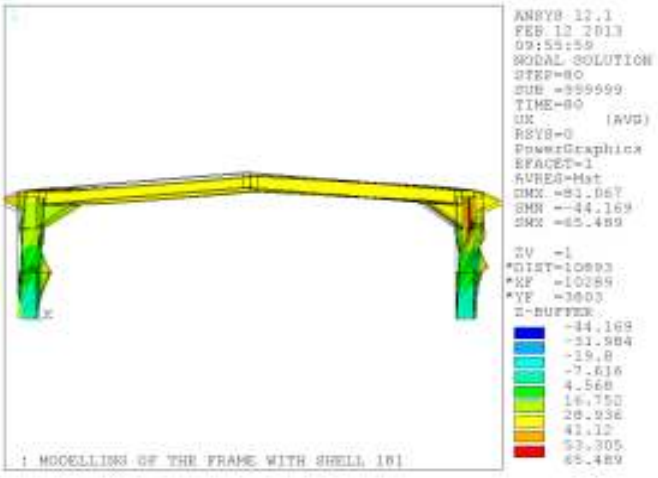

Figure 4.18 Horizontal displacement (mm)

(5) After results (4) the improvement was made to the connection of the link with the frame memeber (without stiffeners) so as to apply the well known rule of the reduce beam section (RBS) to make the part of the connection of the link stronger to have better resistance than the link. The results for this updating are shown in Figure 4.19 to Figure 4.21 for the force displacement diagram, the von Mises stress for frame with the value of frame's yield strength and the von Mises stress for the right and the left sides of the frame with the value of link's yield strength respectively. The results show that the link had buckled and there is also severe buckling in the columns of the frame which is not desirable (see Figure 4.20 and Figure 4.21). Also the displacement at failure it is about 26 mm (see Figure 4.19), which is less than in case without the link (34mm).

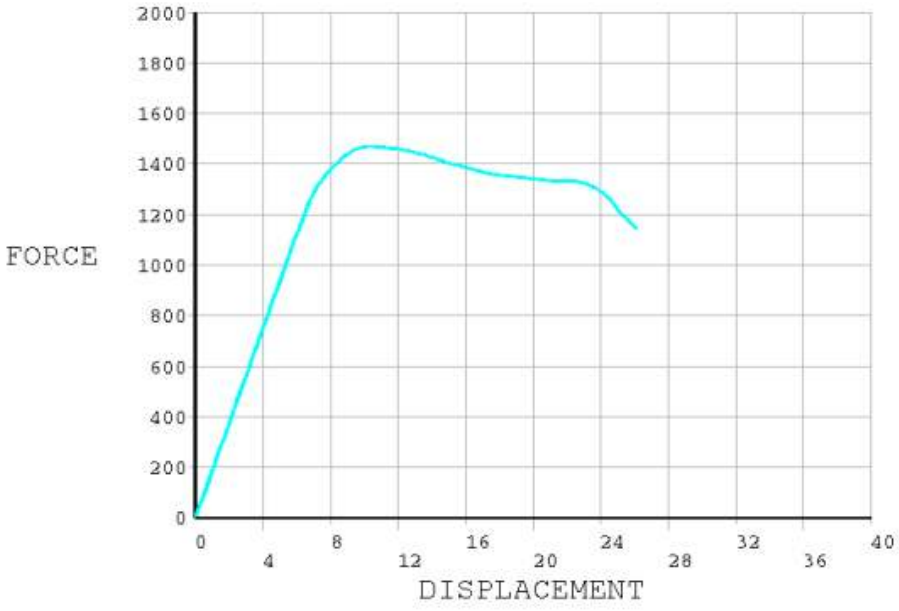

Figure 4.19 Force (N) vs. displacement (mm) diagram

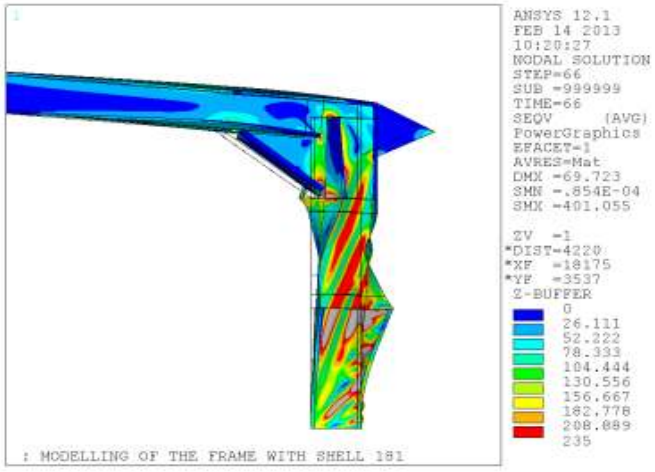

Figure 4.20 Von Mises stress (MPa) with link value (right)

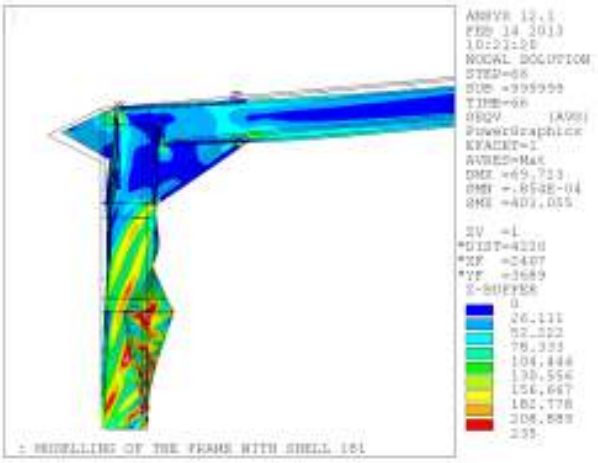

Figure 4.21 Von Mises stress (MPa) with link value (left)

(6) After results (5) the thickness of the link flange was increased from 3mm to 5mm for the same link section. The results are shown in Figure 4.22 to Figure 4.25 for the force displacement diagram, the horizontal displacement of the frame, the von Mises stress for the right side of the frame with the value of frame's yield strength and link's yield strength respectively. The results show that the column and the link buckled (see Figure 4.24 and Figure 4.25). Also no improvement was observed for the horizontal displacement as was found 27mm less than the frame without the link (see Figure 4.22 and Figure 4.23).

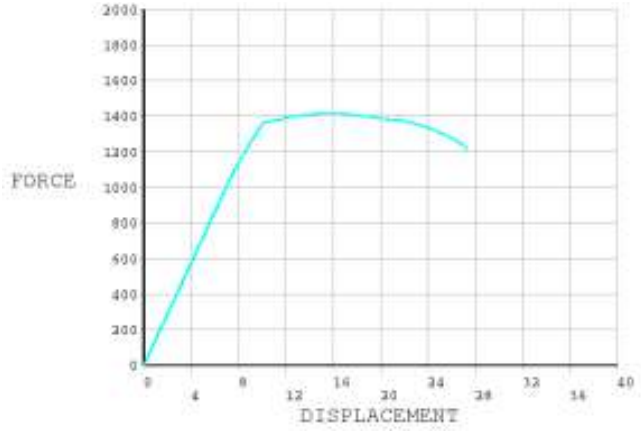

Figure 4.22 Force (N) vs. displacement (mm) diagram

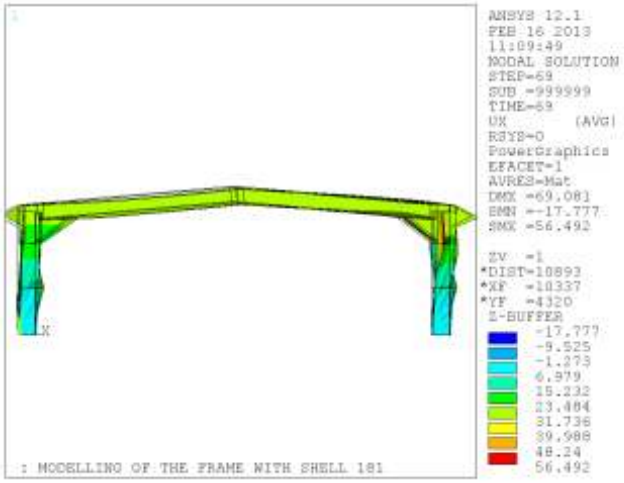

Figure 4.23 Horizontal displacement (mm)

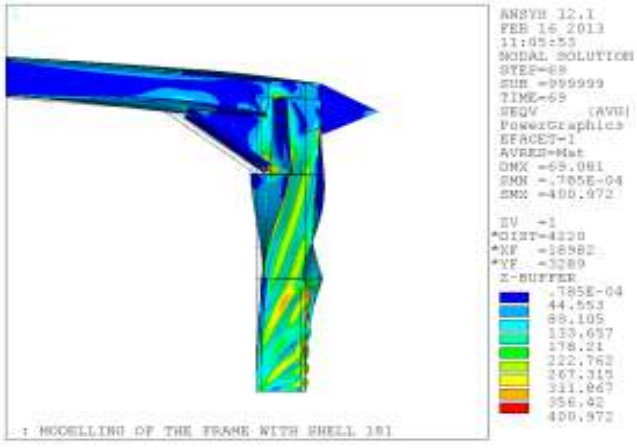

Figure 4.24 Von Mises stress (MPa) with frame value (right)

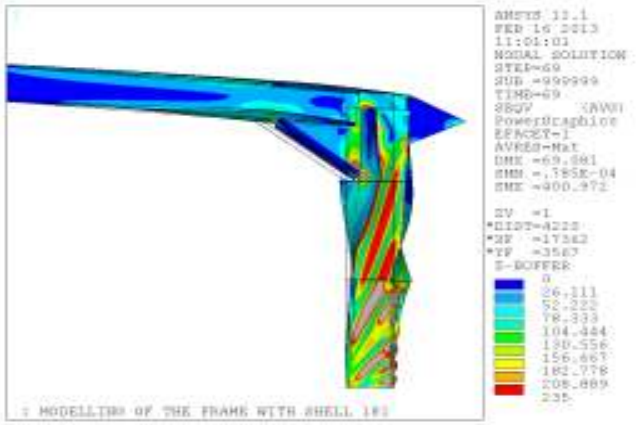

Figure 4.25 Von Mises stress (MPa) with link value (right)

4.4.2 Presentation of second link results (channel section link)

In the previous section the study of the frame with an I section link with a nonlinear static analysis was carried out. In this section the link is 650x400 back to back lipped channel section (see Figure 3.48) as in Table 3.11. The links were attached in both columns under connection. The analyses were performed by changing the parameters were explained in 3.12.6 which affect in the link response to find the best link result. The effective link is expected to protect the thin walled members of the frame from buckling and to yield whilst keeping the whole frame undamaged.

4.4.2.1 Effect of thickness

(1) The first result for the frame with channel link without stiffeners and 3mm thickness for the link web and flange are shown in Figure 4.26 to Figure 4.29, for the force displacement diagram, the horizontal displacement of the frame, the von Mises stress for the right side of the frame with the value of link's yield strength and frame's yield strength respectively. The frame failed with yielding in the link where the frame members connected with the link as there is high stress concentrated in this area (see Figure 4.28 and Figure 4.29). Another observation is that the capacity of the frame referring to the force displacement diagram is not showing better behaviour when compared with that one for the frame without the link in Figure 3.40. The horizontal displacement when the frame failed is 13 mm only as shown in Figure 4.26 and Figure 4.27.

Table 4.2 Channel section link results

Link result No.	Yield strength (MPa)	Link's stiffeners	Comments
Result (1) for link's web thickness 3mm and flange thickness 3mm	235	No stiffeners	Yeilding of frame members where connnected with the link (Figure 4.26 to Figure 4.29).
Result (2) for link's web thickness 3mm and flange thickness 3mm	235	No stiffeners but improving connection area with link	Yielding of the frame members with buckling of the frame columns (Figure 4.30 to Figure 4.32).
Result (3) for link's and frame's web thickness 6mm and flange thickness 3mm	235	No stiffeners but improving connection area with link	Frame sections buckling (Figure 4.33 to Figure 4.35).
Result (4) for link's web thickness 3mm and flange thickness 6mm	235	No stiffeners But improving connection area with link	Buckling of web of the link (Figure 4.36 to Figure 4.39).
Result (5) for link's web thickness 3mm and flange thickness 6mm	235	At the middle and ends (one side) with improving connection area with link	Good ductility but severe buckling of the frame sections (Figure 4.40 to Figure 4.43).
Result (6) for link's web thickness 3mm and flange thickness 6mm	235	At the middle and ends (one side)	Good resistance for buckling for both link and frame members and good ductility behaviour (Figure 4.44 to Figure 4.49).
Result (7) for same link with plates 3mm in the column's flange section under link	190-235	At the middle and ends (one side)	Good resistance for buckling for and frame members but buckling of the link and weaker structure. (Figure 4.50 to Figure 4.53).

Continued Table 4.2 channel section link results

Link result No.	Yield strength (MPa)	Link's stiffeners	Comments
Result (8) for link's web thickness 3mm and flange thickness 6mm	235	At the middle and ends (both side)	Good resistance for buckling of both link and frame members but poor failure forces (Figure 4.54 to Figure 4.57).
Result (9) for link's web thickness 3mm and flange thickness 6mm	235	At the middle and ends (one side) with improving connection area with link	Good resistance for buckling for both link and frame members but poor ductility (Figure 4.58 to Figure 4.61).
Result (10) for link's web thickness 3mm and flange thickness 6mm	235	At the middle and ends (both side)	Good ductility but buckling of some parts of the frame members (Figure 4.62 to Figure 4.65).
Result (11) for link's web thickness 3mm and flange thickness 6mm	190	At the middle and ends (one side)	Same as result (6) Good resistance for buckling for both link and frame members and good ductility behaviour (Figure 4.66 to Figure 4.68).
Result (12) for link's web thickness 3mm and flange thickness 6mm attached to each ends of the columns	235	At the middle and ends (one side)	Buckling of the the web of the links and yeidling of the columns at the middle where there is no links (Figure 4.69 to Figure 4.73)
Result (12) for link's web thickness 3mm and flange thickness 6mm attached cover the whole column length	235	Along all the length of the column link	Buckling of the web of the link and buckling of the rafter (Figure 4.74 to Figure 4.76)

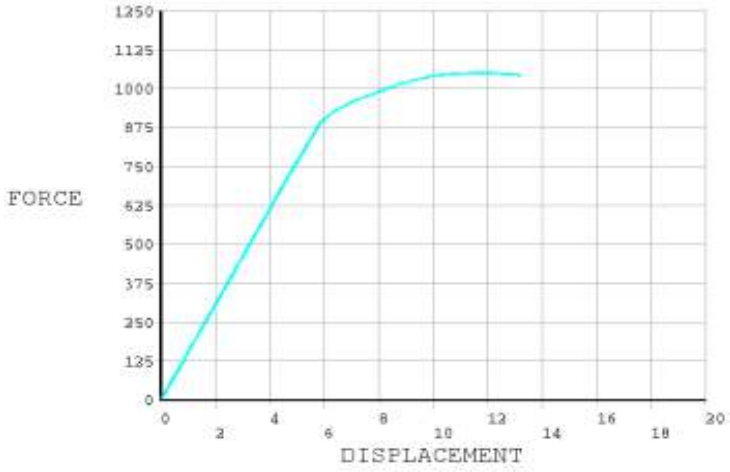

Figure 4.26 Force (N) vs. displacement (mm) diagram

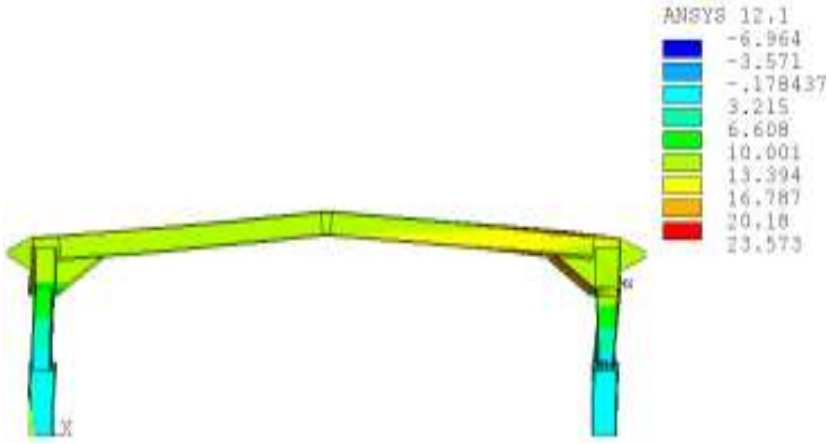

Figure 4.27 Horizontal displacement (mm)

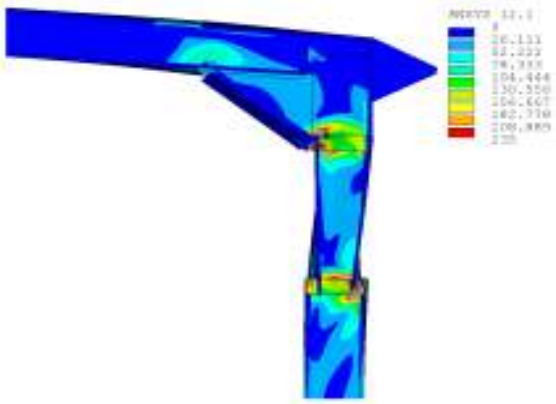

Figure 4.28 Von Mises stress (MPa) with link value (right)

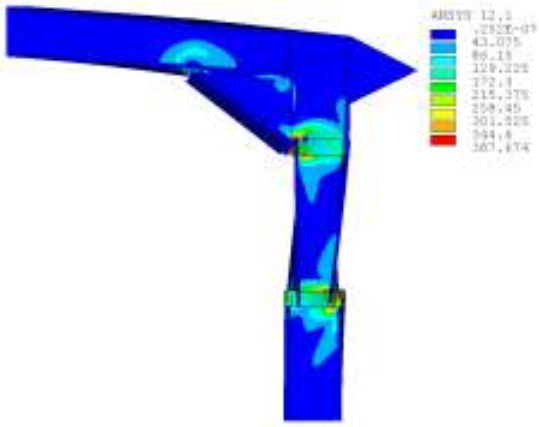

Figure 4.29 Von Mises stress (MPa) with frame value (right)

(2) After result (1) the link connection with the frame section improved by changing the thickness of the web and the flange in this area about 250mm distance from the frame connection in each side. The thickness was changed to 8mm for web and 4mm for flange. The results are shown in Figure 4.30 to Figure 4.32, for the force displacement diagram, the von Mises stress for the right side of the frame with the value of link's yield strength and frame's yield strength respectively. The results showed yielding of the frame members with buckling of the frame columns (see Figure 4.31 and Figure 4.32). From the force displacement diagram in Figure 4.30 the frame failed with horizontal displacement 20 mm which is less than the one for the frame without link (34mm).

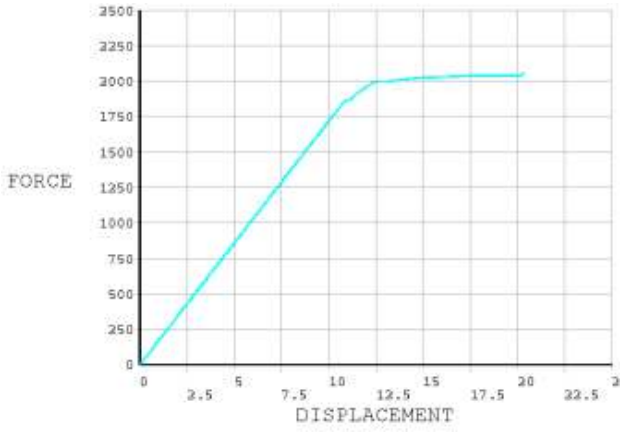

Figure 4.30 Force (N) vs. displacement (mm) diagram

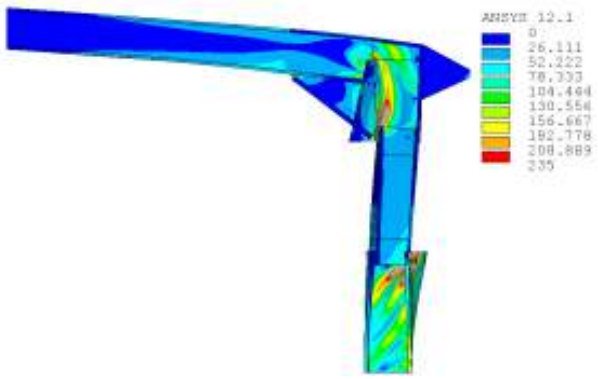

Figure 4.31 Von Mises stress (MPa) with link value (right)

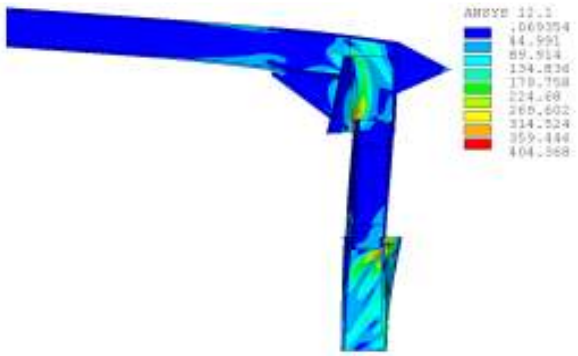

Figure 4.32 Von Mises stress (MPa) with frame value (right)

(3) After result (2) the change included the frame members, as the thickness last time for the frame members channel section was dealing the channel section having single thickness for the web ,the change now will be to using the channel with double thickness for the web as it is back to back channel section (see Figure 3.5). This is the original design of the frame, with web thickness 6 mm. Now the flange and web thickness for the link are 3mm and 6mm respectively and the connection area are 4mm for flange and 8mm for the web. The result after this improvement for the column and rafter are shown in Figure 4.33 to Figure 4.35, for the force displacement diagram, the von Mises stress for the right side of the frame with the value of link's yield strength and frame's yield strength respectively. The results show the buckling of frame sections at the upper and lower parts of the column (see Figure 4.34 and Figure 4.35). However there is improvement in the ductility

of the frame compared with the previous result as the horizontal displacement when the frame failed is 32 mm (see Figure 4.33).

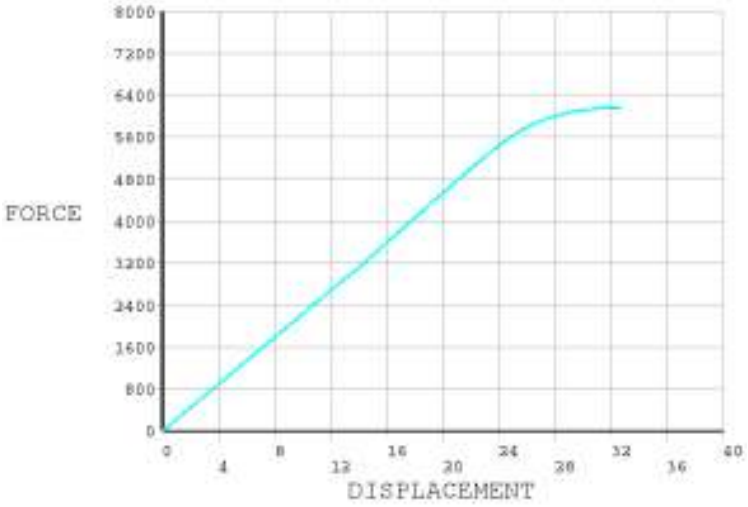

Figure 4.33 Force (N) vs. displacement (mm) diagram

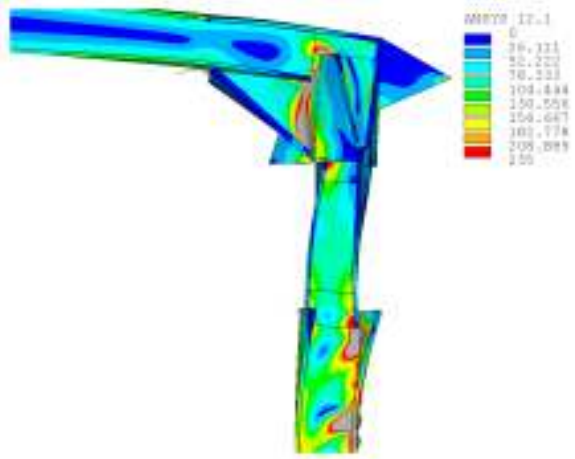

Figure 4.34 Von Mises (MPa) with link value (right)

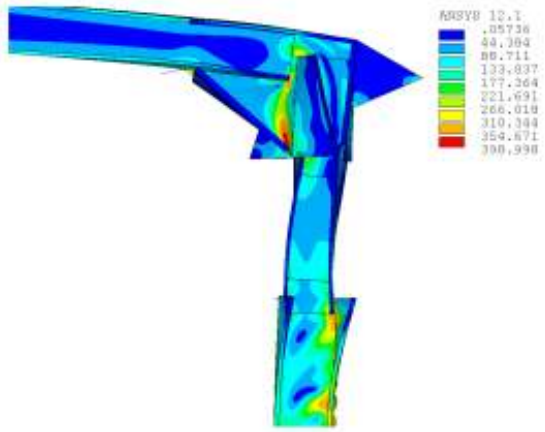

Figure 4.35 Von Mises stress (MPa) with frame value (left)

(4) Results (3) put an attention to the link flange thickness, as the effective solution to the buckling is inceasing the thickness for the flange and web. The limitation for the ratio of flang e thickness to width of flange as 1:10 and on the other hand for the web thickness to the depth of the web and 1:35 to prevent buckling. In our case we can't follow this rule as the frame made of thin guage steel but we can try to improve the buckling resistance of the flange link by increasing the flange width while keeping the web thickness less than the flange thickness. By this arragament we can prevent buckling of the link flange which affects in overall buckling and at the same time allow for link yielding before the frame members. The thickness used for the link flange is 6mm with web thickness 3mm . The thicknes was madefor the connection area with the frame as 8mm for the flange and 4mm for the web.

The results after this new arrangement are shown in Figure 4.36 to Figure 4.39, for the force displacement diagram, the horizontal displacement, the von Mises stress for the right side of the frame with the value of link's yield strength and frame's yield strength respectively. These results show better resistance for buckling comparing with the previous ones but the web of the link buckled and this led to premature failure due to the web buckling as show in Figure 4.37 and Figure 4.38. From Figure 4.36 and Figure 4.39 no improvement in the ductility compared with the frame without link in

Figure 3.40 as the horizontalm displacement when the frame failed is only 26mm.

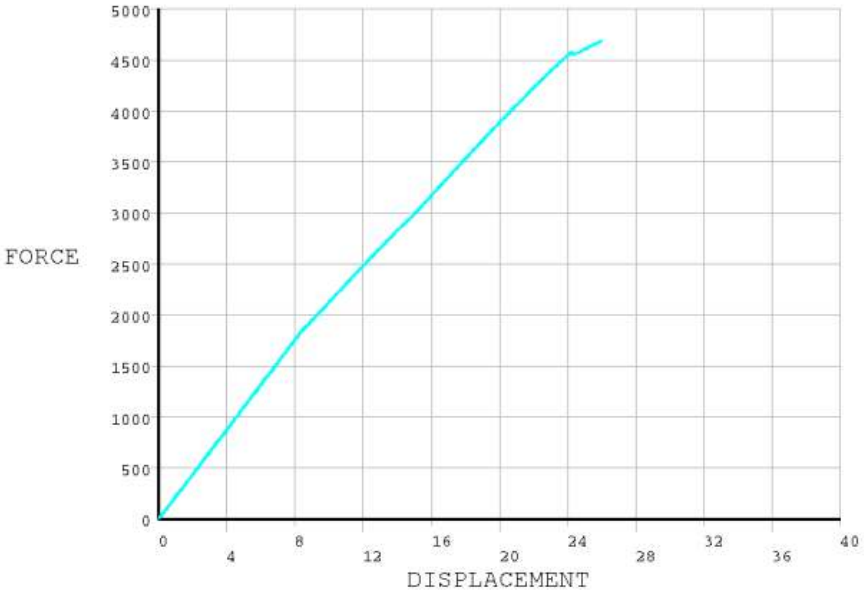

Figure 4.36 Force (N) vs. displacement (mm) diagram

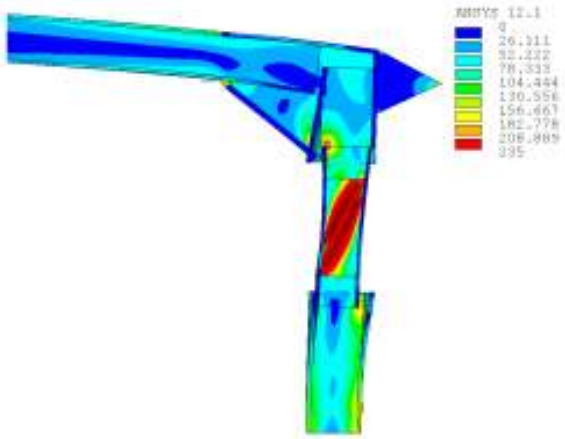

Figure 4.37 Von Mises stress (MPa) with link value (right)

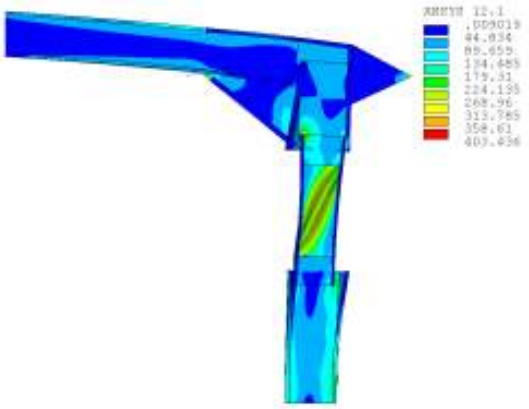

Figure 4.38 Von Mises stress (MPa) with frame value (right)

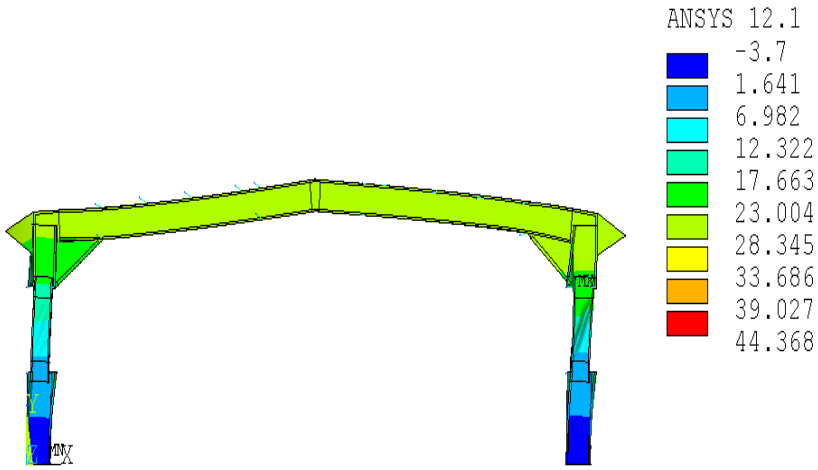

Figure 4.39 Horizontal displacement (mm)

4.4.2.2 Effect of stiffeners

(5) To pevent web buckling while keeping the link weaker than the frame memebrs, the link web was enhaced with stiffeners at the middle and ends on one side of the link section with the same dimensions and thickness for web and flange of the link. The result after link provided with stiffeners are shown in Figure 4.40 to Figure 4.43, for the force displacement diagram, the horizontal displacement, the von Mises stress for the right side of the frame with the value of link's yield strength and frame's yield strength respectively. The results show good capacity for the ductility of the frame when compared with the last one with value of 35mm for the horizontal displacement when

the frame failed (see Figure 4.40 and Figure 4.41), but there is still severe buckling in the frame members (see Figure 4.42 and Figure 4.43).

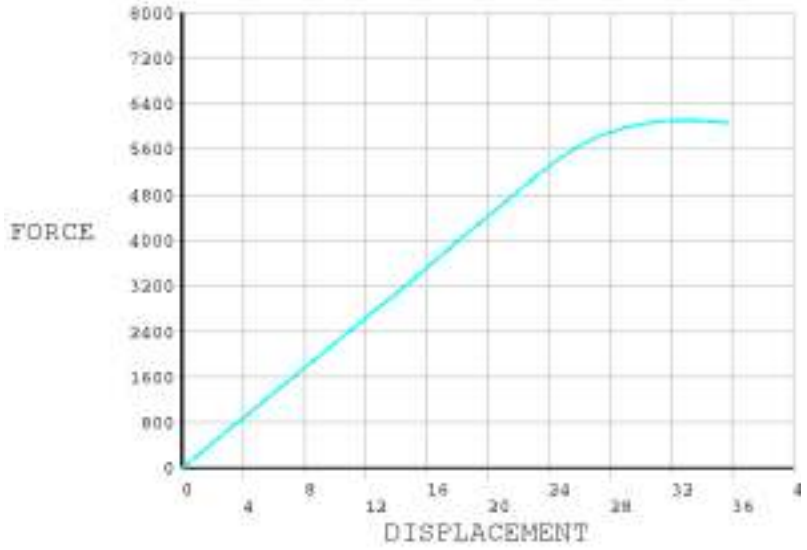

Figure 4.40 force (N) displacement (mm) diagram

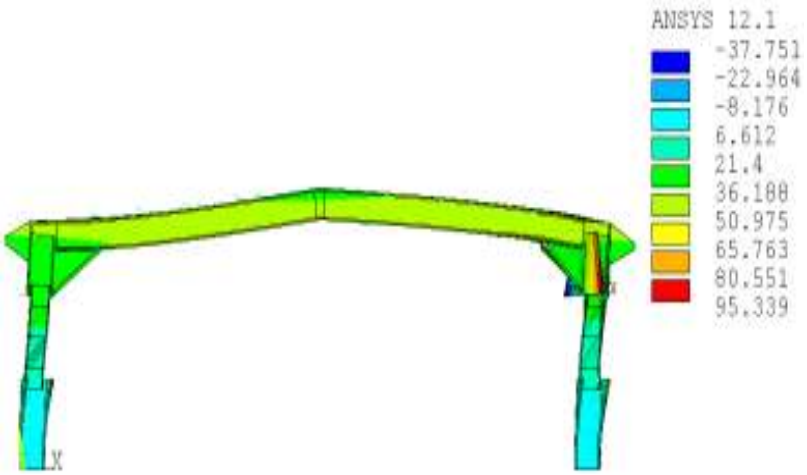

Figure 4.41 Horizontal displacement (mm)

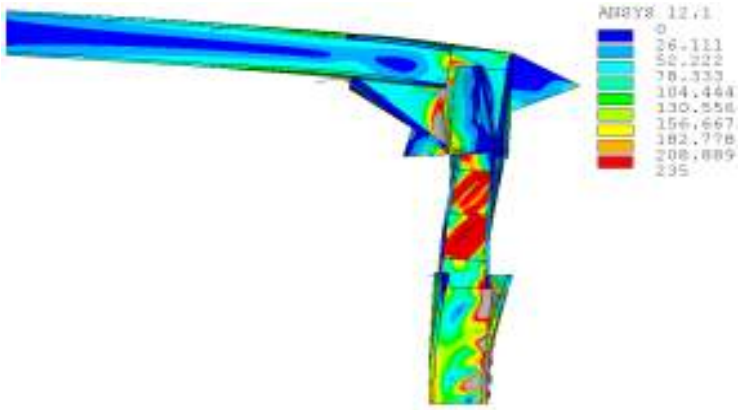

Figure 4.42 Von Mises stress (MPa) with link value (right)

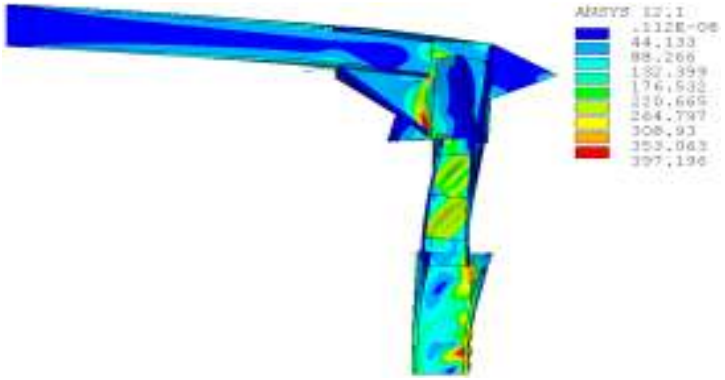

Figure 4.43 Von Mises stress (MPa) with frame value (right)

(6) Results (5) for the channel section with dimension less than the frame column. In this test the link will be the channel link with the same dimension of the frame column as in Table 3.11 (see Figure 3.49). The thickness for the flange 6mm and the web 3mm with stiffeners at the middle and at distance 250mm from the connection on one side of the link. The results for this new link are shown in Figure 4.44 to Figure 4.49, for the force displacement diagram, the horizontal displacement, the von Mises stress for the right side of the frame with the value of link's yield strength and frame's yield strength and finally the von Mises stress for the left sides of the frame for the two values of yield strength respectively. Figure 4.44 and Figure 4.45 show good

resistance for buckling for both link and frame members and good ductility behaviour was observed from the force displacement diagram and the horizontal displacement when compared with that one for the frame without link in Figure 3.40. The frame failed at 5600N with 34 mm displacement. Also no buckling was observed for both the frame profiles and link (see Figure 4.46 to Figure 4.49), and the link achieved yielding. However there is yielding in the column at the base due to the buckling of the web and the flange of the column at the base.

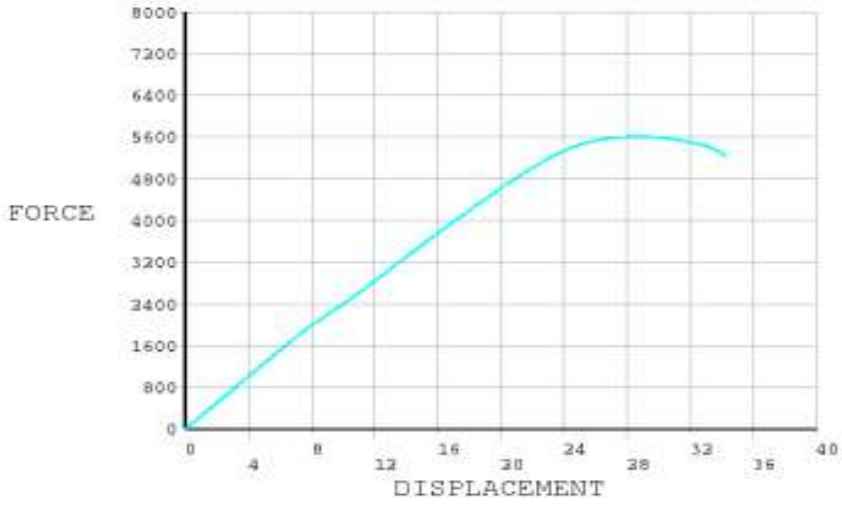

Figure 4.44 Force (N) vs. displacement (mm) diagram

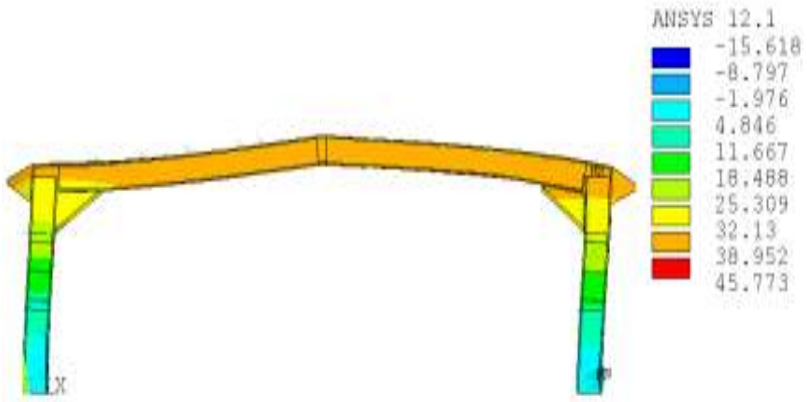

Figure 4.45 Horizontal displacement (mm)

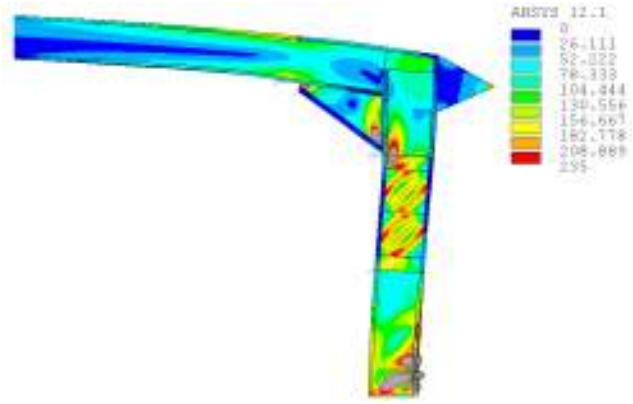

Figure 4.46 Von Mises stress (MPa) with link value (right)

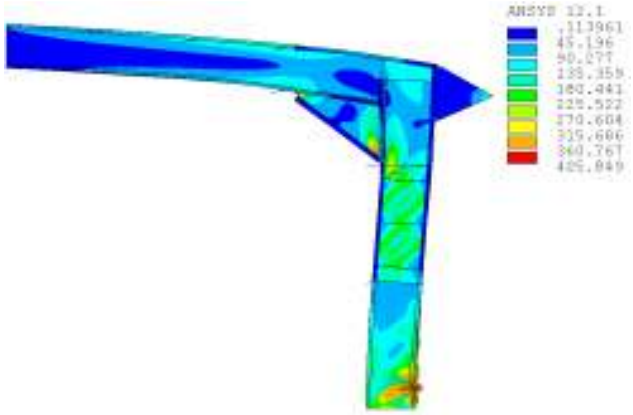

Figure 4.47 Von Mises stress (MPa) with frame value (right)

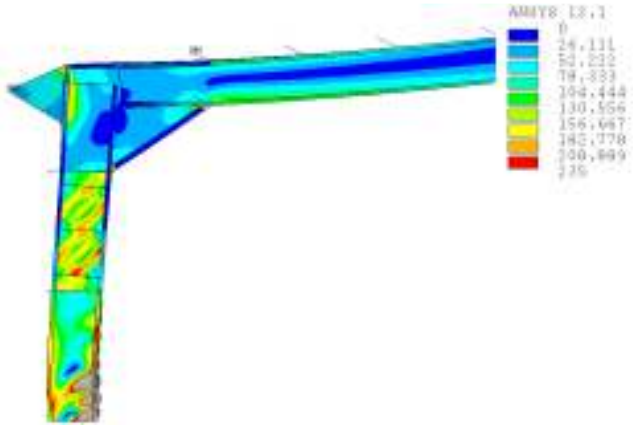

Figure 4.48 Von Mises stress (MPa) with link value (left)

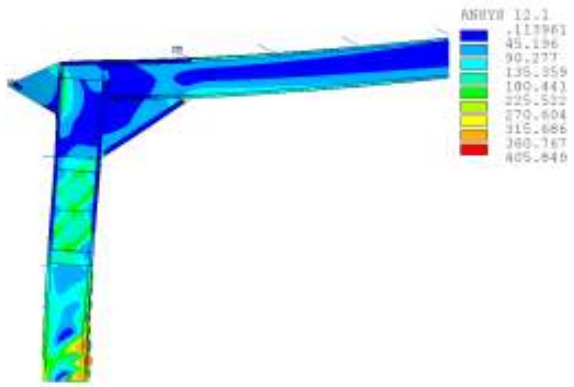

Figure 4.49 Von Mises stress (MPa) with frame value (left)

(7) After the previous result the frame member improved by providing the column under the link with plate of thickness 3mm to have total thickness for the column 6mm to protect the coulmn at the base from the yielding. The results for the link with plates on the coulmns under the link are shown in Figure 4.50 to Figure 4.53 for the force displacement diagram, the von Mises stress for the right side of the frame with the value of link's yield strength and frame's yield strength and finally the von Mises stress for the left side of the frame with the value of link's yield strength. From Figure 4.50 the force displacement diagram, the structure performance has not improved as the displacement is 30 mm and the reaction forces are bigger this time (8500 N), in addition there is the cost of using a splice plate to protect the column base. The link yielded and no buckling for frame and the link (see Figure 4.51, Figure 4.52 and Figure 4.53).

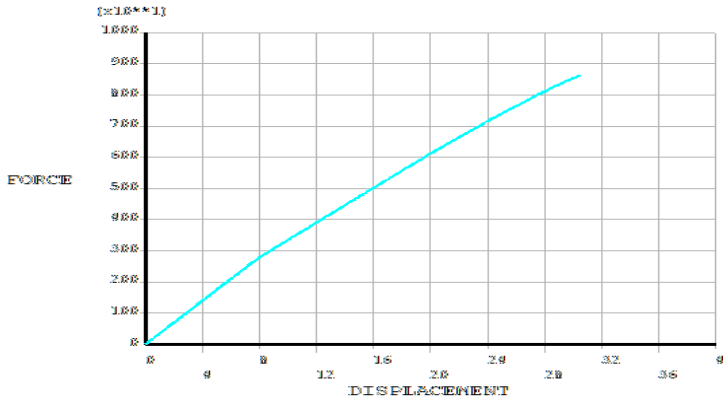

Figure 4.50 Force (N) vs. displacement (mm) diagram

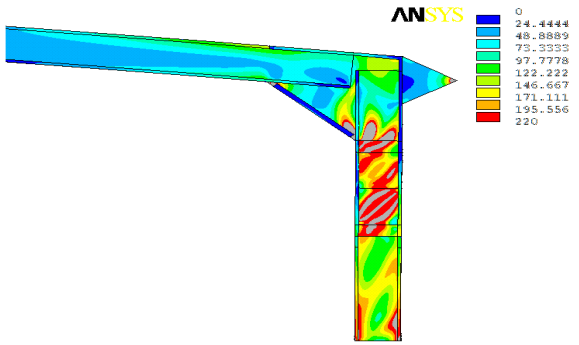

Figure 4.51 Von Mises stress (MPa) with link's value (right)

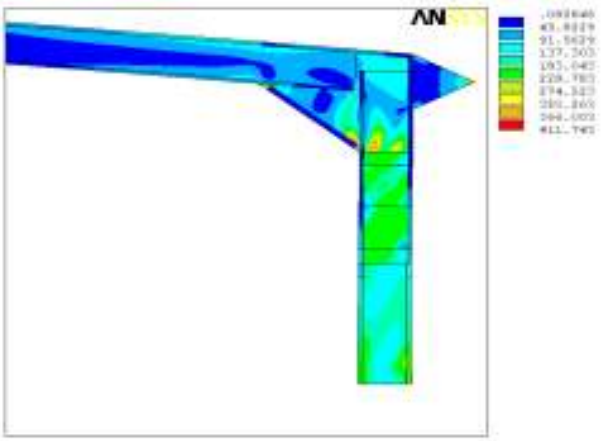

Figure 4.52 Von Mises stress (MPa) with frame's value (right)

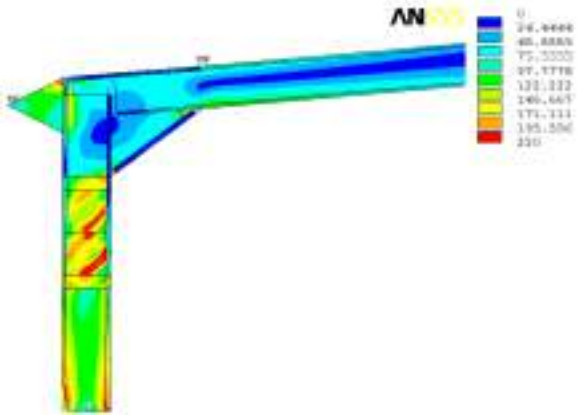

Figure 4.53 Von Mises stress (MPa) with link's value (left)

(8) After results (7) the frame was tested with the same link but with stiffeners at middle and 250 mm distance from connection but on both sides of the link.

The results for the link with stiffeners on both sides are shown in Figure 4.54 to Figure 4.57, for the force displacement diagram, the horizontal displacement, the von Mises stress for the right side of the frame with the value of link's yield strength and frame's yield strength and finally the von Mises stress for the left sides of the frame for the two values of yield strength respectively. In this case no buckling for both the frame members and the link as shown in Figure 4.56 and Figure 4.57. The ductility improved as the horizontal displacement when the structure failed is 35mm but the failure forces value is very small according to the force displacement diagram in Figure 4.54.

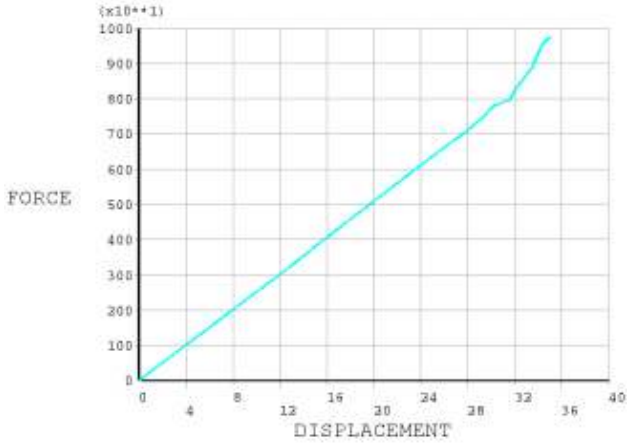

Figure 4.54 Force (N) vs. displacement (mm) diagram

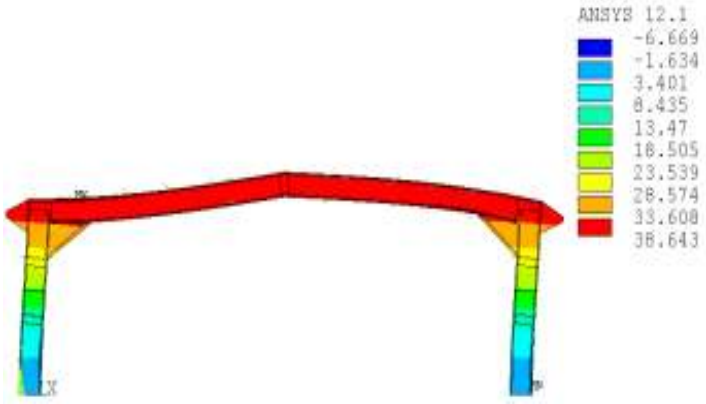

Figure 4.55 Horizontal displacement (mm)

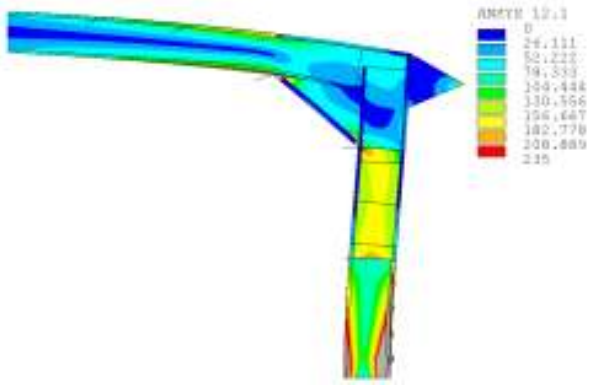

Figure 4.56 Von Mises stress (MPa) with link value (right)

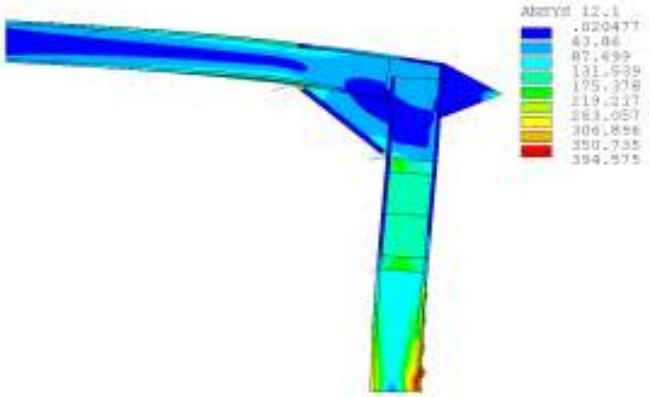

Figure 4.57 Von Mises stress (MPa) with frame value (right)

(9) The next test for the link with the same dimension except the stiffeners at link ends placed at the ends of the link not at distance 250 mm on one side of the link and the area for the connection with the coulmn was provided with thickness for the flange 8mm and for the web 4mm. The results for this new arrangement for the link are shown in Figure 4.58 to Figure 4.61, for the force displacement diagram, the horizontal displacement, the von Mises stress for the right side of the frame with the value of link's yield strength and frame's yield strength respectively. The analysis resulted in a good behaviour for buckling prevention (see Figure 4.60 and Figure 4.61) but the capacity curve did not extend beyond the elastic zone and the displacement when the

structure failed is 27mm less than 34mm for the frame without the link (see Figure 4.58 and Figure 4.59).

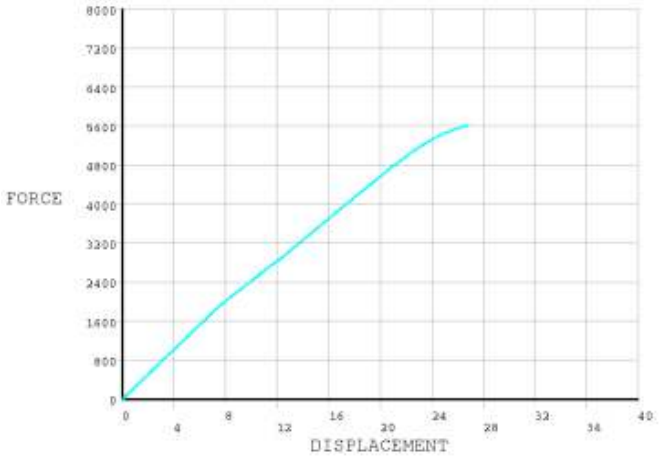

Figure 4.58 Force (N) vs. displacement (mm) diagram

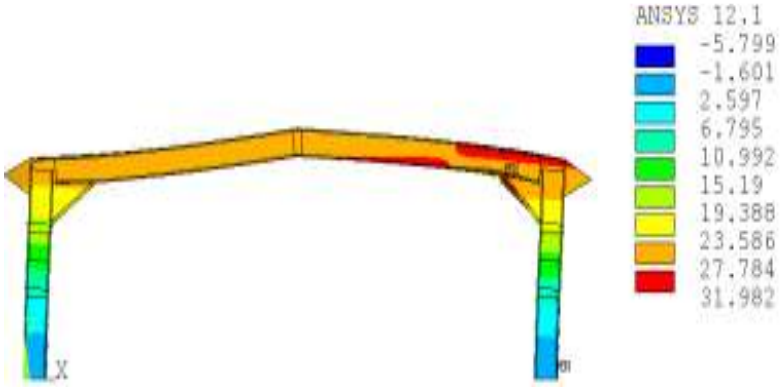

Figure 4.59 Horizontal displacement (mm)

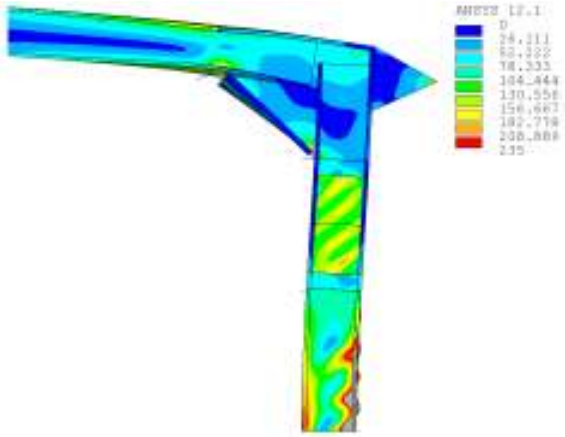

Figure 4.60 Von Mises stress (MPa) with link value (left)

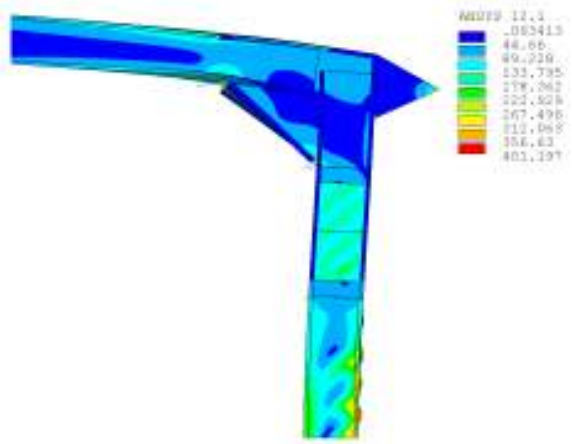

Figure 4.61 Von Mises stress (MPa) with frame value (left)

(10) The link model here is the same arrangment for the previous test except the stiffeners for the link were place at both sides of the link. The results for the link with stiffeners on both sides are shown in Figure 4.62 to Figure 4.65, for the force displacement diagram, the horizontal displacement, the von Mises stress for the right side of the frame with the value of link's yield strength and frame's yield strength and finally the von Mises stress for the left sides of the frame for the two values of yield strength respectively. Figure 4.62 and Figure 4.63 show good ductility with horizontal displacement 34 mm but there is buckling for some parts of the frame members (see Figure 4.64 and Figure 4.65).

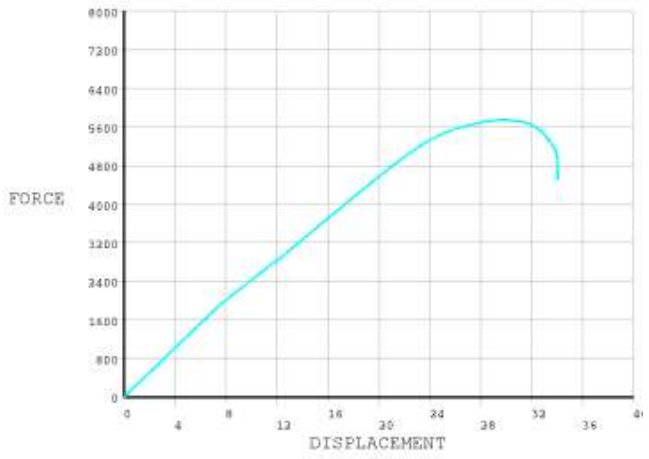

Figure 4.62 Force (N) vs. displacement (mm) diagram

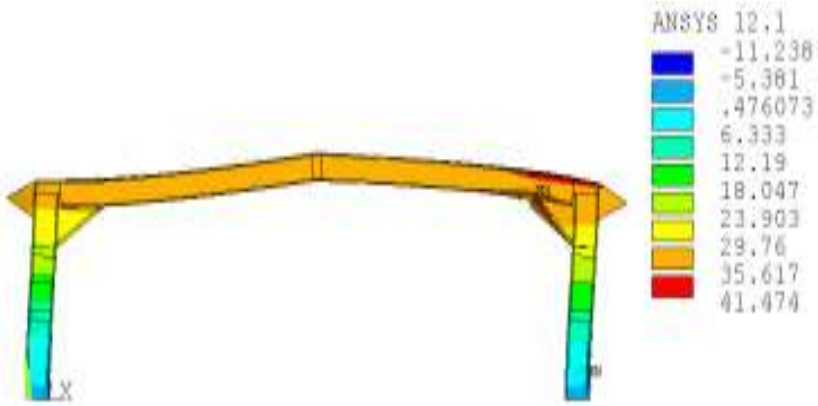

Figure 4.63 Horizontal displacement (mm)

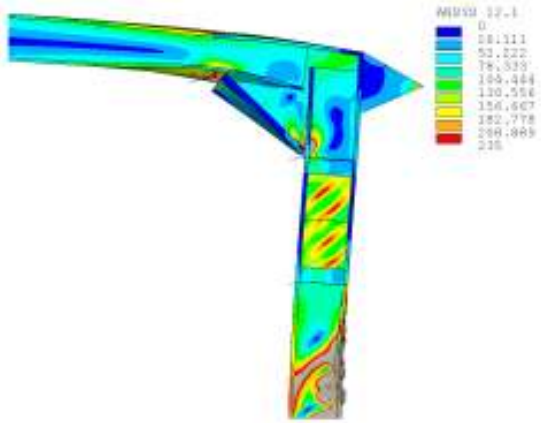

Figure 4.64 Von Mises stress (MPa) with link value (right)

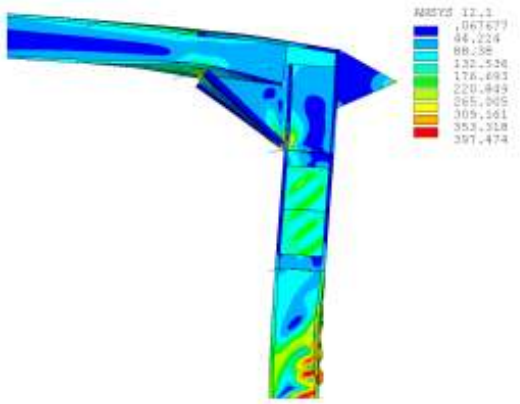

Figure 4.65 Von Mises stress (MPa) with frame value (right)

4.4.2.3 Effect of the yield strength value

(11) The frame was analysed with the same link like result (6) but with changing the yeild strength for the link from 235 MPa to 190 MPa to have weaker link to protect the frame structure and prevent yeilding of column. (Note the same effect would probably be achieved in practice by reducing the section modulus and maintaning the yield stress.) The results are shown in Figure 4.66 to Figure 4.68, for the force displacement diagram, the von Mises stress for the right side of the frame with the value of link's yield strength and frame's yield strength. It is clear that no change in the result compared with the result for yield strength 235 MPa (see Figure 4.44), as the ductility is the same with about 34 mm displacement when the frame structure failed in this test (see Figure 4.44). Also there is yielding for the column at the base but no buckling for the frame and the link sections (see Figure 4.67and Figure 4.68).

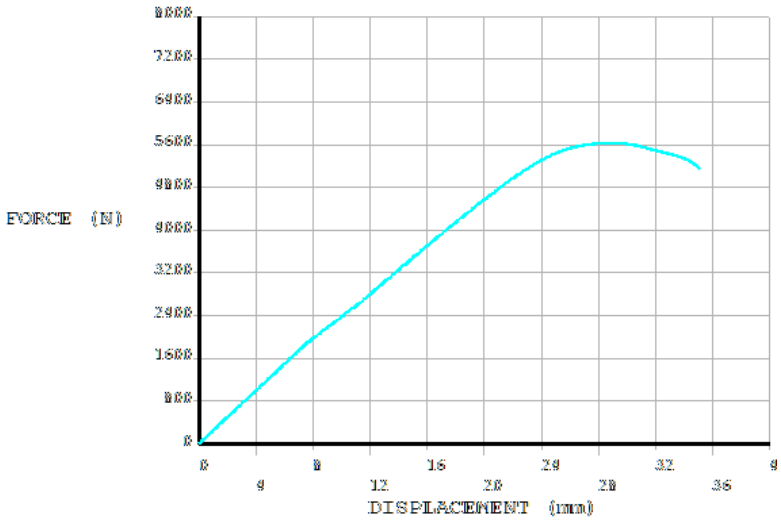

Figure 4.66 Force (N) vs. displacement (mm) diagram

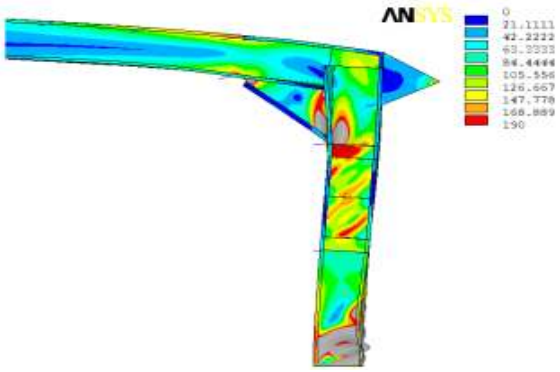

Figure 4.67 Von Mises stress (MPa) with link's value (right)

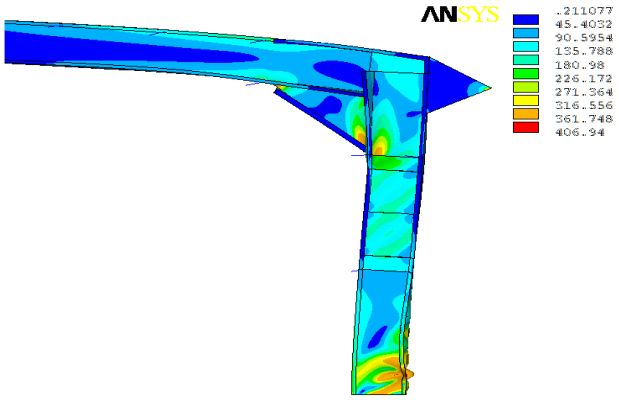

Figure 4.68 Von Mises stress (MPa) with frame's value (right)

4.4.2.4 Effect of the length and postion of the link

(12) The frame was analysed with localized links at each end of the columns to protect the column base, the yeild strength for the link was 235 MPa. The stiffeners were used along the both links to prevent buckling of the links. The results are shown in Figure 4.69 to Figure 4.73, for the force displacement diagram, the von Mises stress for the right side of the frame with the value of frame's yield strength and link's yield strength. The ductility is about 28 mm displacement when the frame structure failed in this test (see Figure 4.74). The links yielded but there was buckling in the web of the links as in Figure 4.71 and Figure 4.73. Localized links at the bottom of the columns was not effective to protect the frame sections as the yielding of the column at the middle was observed (see Figure 4.70 and Figure 4.72).

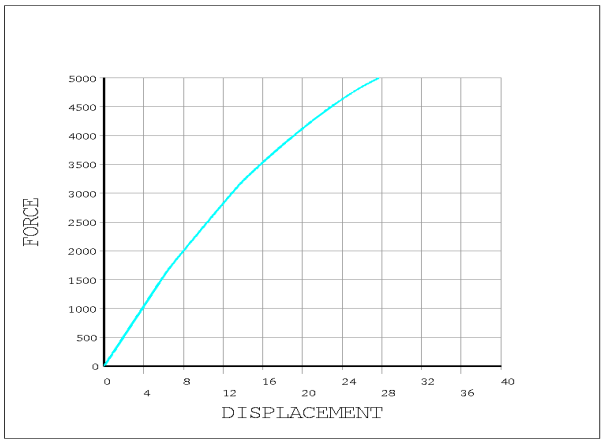

Figure 4.69 Force (N) vs. displacement (mm) diagram

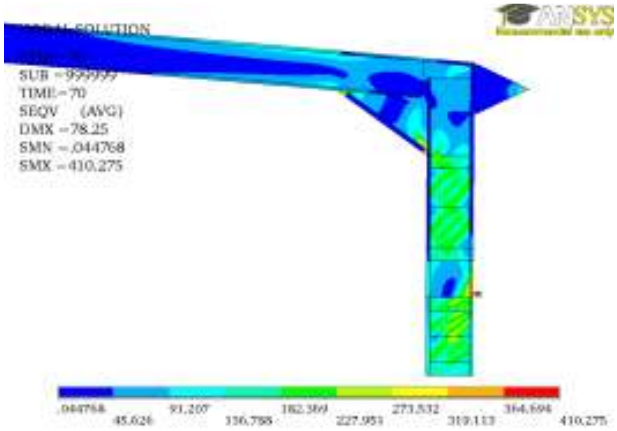

Figure 4.70 Von Mises stress (MPa) with frame's value (right)

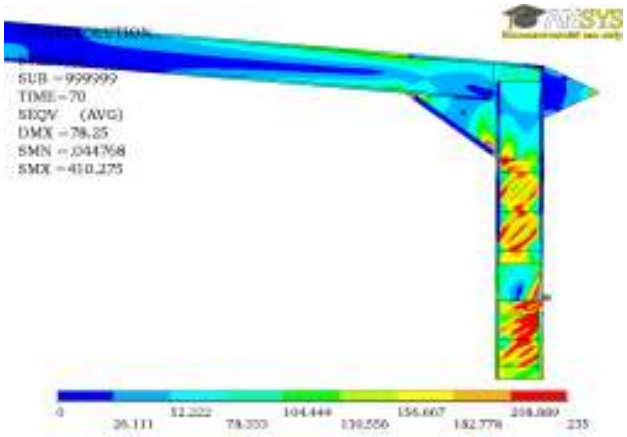

Figure 4.71 Von Mises stress (MPa) with link's value (right)

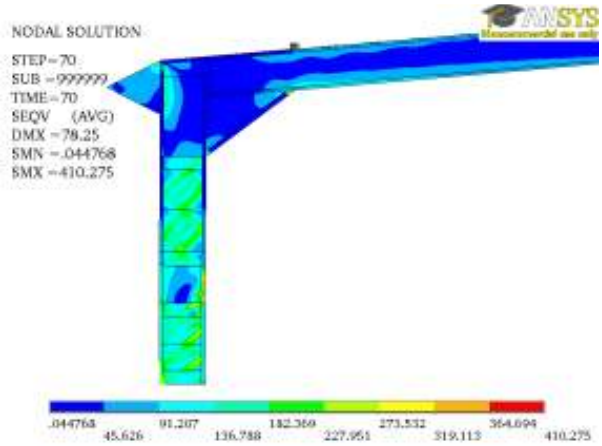

Figure 4.72 Von Mises stress (MPa) with frame's value (left)

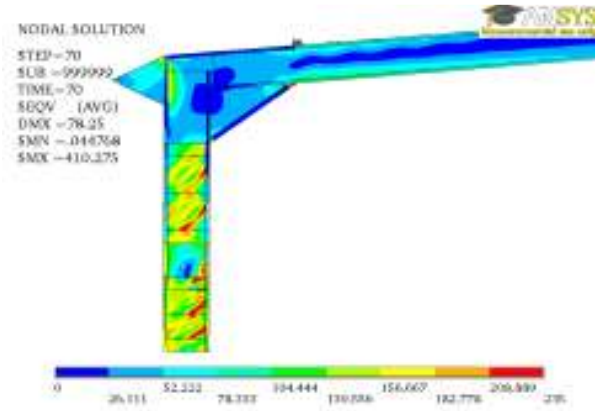

Figure 4.73 Von Mises stress (MPa) with link's value (left)

(13) The frame was analysed with link to cover all the column length, the yeild strength for the link was 235 MPa. This to check the response when the link cover the complete length of the column. The stiffeners were used along the column to prevent buckling of the link. The results are shown in Figure 4.74 to Figure 4.76, for the force displacement diagram, the von Mises stress for the right side of the frame with the value of frame's yield strength and link's yield strength. The ductility is about 31 mm displacement when the frame structure failed in this test (see Figure 4.74). The link yielded but there was buckling in the web of the link (see Figure 4.76). Increasing the numbers of the stiffeners increased the moment resistance of the column without preventing buckling of the web and resulted in the buckling of rafter (see Figure 4.75).

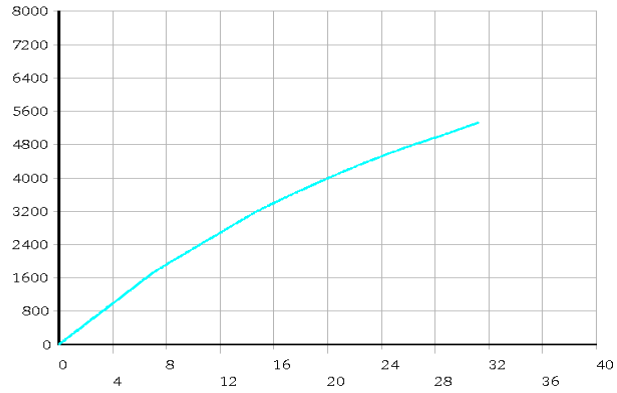

Figure 4.74 Force (N) vs. displacement (mm) diagram

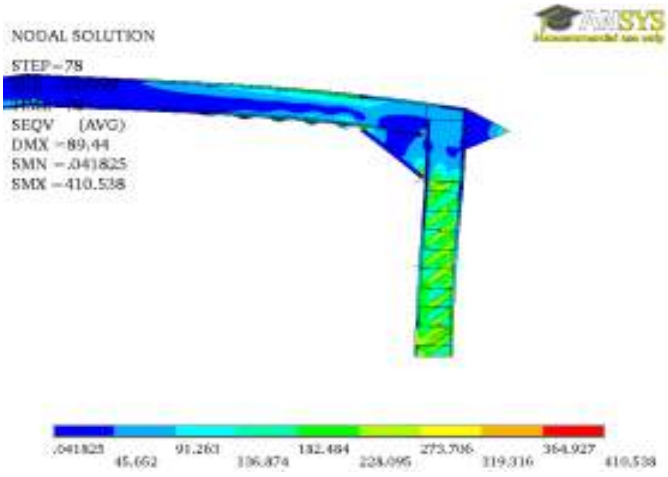

Figure 4.75 Von Mises stress (MPa) with frame's value (right)

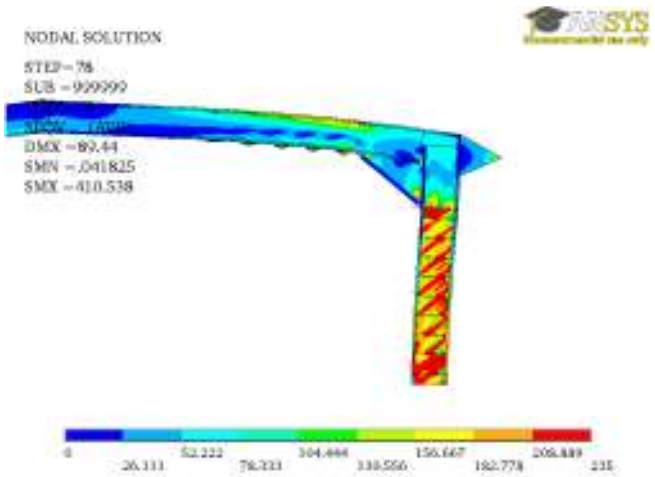

Figure 4.76 Von Mises stress (MPa) with link's value (right)

4.4.3 Summary of the preliminary nonlinear static analysis

A three-dimensional detailed finite element model for the frame with the link attached was developed using ANSYS. The inelastic behaviour of the steel elements was considered. The material is introduced by means of bilinear isotropic elastic-perfectly plastic model. The steel frame elements were modelled using 8-node shell elements. Large-displacement analysis was conducted.

From the result above it is obvious that the back to back lipped channel link with dimensions 850x325 is the effective one of all the type of link (see Figure 3.49).

According to the results of the frame performance with different types of links, the following observations were obtained:

1. Link with lipped section or back to back channel section is more effective more than I section link in prevention of buckling for the frame components.
2. Thinner link's web is not good for the link even with using of stiffeners as this causes the buckling for the web of the link in all cases.
3. Providing stiffeners for the link would be effective for good performance of the link and frame but they are not enough to protect the slender web from buckling.
4. Using of two links at each end of the columns to protect the frame members and achieve the expected plastic hinges at upper and lower of the column is not effective. This caused the buckling of the frame members (rafter).

From these preliminary analyses and assessment for link by nonlinear static analysis, the link will be used for the preliminary dynamic analysis of the frame using real earthquakes records and artificial records, the link with back to back lipped channel section with dimension 850x325 and thickness 6 mm for the flange and 3mm for the web, provided with stiffeners on one side at the middle and at distance 250mm (about 1/8 of the link span) from the connection with the frame members as shown in Figure 4.46. In the next section the frame will be assessed and the effectiveness of link on the performance of the light gauge steel portal frame will be checked under different seismic excitations and ground motion records. The conclusions from the preliminary analyses will be used for the final design of the link in section 4.9 of this thesis.

4.5 Nonlinear Dynamic Analysis

The most sophisticated approach for examining the inelastic response of a structure involves the application of nonlinear dynamic analysis, which determines the time-history of the model's response under the action of an earthquake record. The effects on a structure's response, due to the higher modes of vibration, are automatically accounted for, while the need for examining different distributions of lateral loads is eliminated. With this method high accuracy of response predictions is achieved using either an artificial or an actual earthquake record provided that the hysteretic behaviour of all structural elements is appropriately modelled. Despite the increased accuracy of the nonlinear time-history analysis, the method is usually employed only for very important structures and/or for research purposes. The accelerograms used play a significant role in the structure's response obtained by this method. In order to reduce the scatter in the calculated results, the FEMA 356 committee and Eurocode 8 suggest that the analysis should be carried out based on three or more ground motion records (Konstantinidis, 2001). In this section the nonlinear time analysis for portal frame structure was carried out under scaled real earthquake data (see section 0) and artificial earthquakes (see section 4.7) using the commercially available finite element software ANSYS. Using artificial earthquakes (harmonic excitations) is recommended in this study as the generated accelerograms are highly controlled frequency and good for comparing different structures.

4.5.1 Damping and & Rayleigh damping parameters

Damping is one of the most effective parameters governing the global behaviour of the structural system. The deformation response of a system depends not only on the natural period of the system, but also on its damping ratio ξ. However, damping is governed by changes over time in the plasticity of the member material. Ideally, in dynamic analysis, damping should be changed simultaneously in relation to the elasto-plastic condition of the frame. However, in practice, a constant damping ratio is used as a representative damping value for every condition. Newmark and Hall (1982) recommended some damping ratios to be used in the analysis of different structures. These recommended damping values are given in Table 4.3 for two levels of motion: working stress levels or stress level no more than one half the yield point, and stresses at or just below the yield point. For each stress level, a range of damping values is given; the higher value of damping are to be used for ordinary structures, and the lower value for special structures to be designed more conservatively.

Damping is present in most system and needs to be specified in most dynamic analysis. In ANSYS software there are many forms of damping available, one of them is Rayleigh damping where damping is a function of frequency and is introduced via the Rayleigh Damping Coefficients (a_0) and (a_1) which are used to form the damping matrix [C] as these coefficients are not themselves damping values. To construct a classical damping matrix we consider Rayleigh damping as below:

$$C = a_0 M + a_1 K \qquad \text{Equation 4.1}$$

The damping ratio for the n^{th} mode of such a system is

$$\xi_n = \frac{a_0}{2\omega_n} + \frac{a_1}{2}\omega_n \qquad \text{Equation 4.2}$$

in which ω is the natural frequency of the frame. The first term of equation 4.2 represents mass-proportional damping, and the second represents stiffness proportional damping. The coefficients a_0 and a_1 can be determined for specified ratio values ξ_i and ξ_j for the i^{th} and j^{th} modes respectively. Applying equation 4.2 for two modes (i and j) to have two algebraic equations, this can be solved to determine the coefficients a_0 and a_1. If both modes are assumed to have the same damping ratioξ, then (Chopra, 2001):

$$a_0 = \xi \frac{2\omega_i \omega_j}{\omega_i + \omega_j} \qquad a_1 = \xi \frac{2}{\omega_i + \omega_j} \qquad \text{Equation 4.3}$$

The constants a_0 and a_1, are input parameters for the dynamic analysis within the ANSYS finite element software. The damping matrix is then known from equation 4.1 and the damping ratios for any other mode, given by equation 4.2, varies with the modal natural frequency, (Chopra, 2001).

According to the damping values in Table 4.3, for the frame model in this study critical damping ξ equal 5% was specified for the first mode and for the twentieth mode with ω1 and ω20. By this way the first mode and mode twenty will have exactly the same damping, and all modes in between will have somewhat smaller similar values than ξ and the modes with frequencies larger than ω20 will have somewhat larger damping values than ξ because the damping ratio for modes higher than the twentieth will increase monotonically with frequency and thus eliminating their contribution to response because of their high damping (see Figure 4.77) (Chopra, 2001).

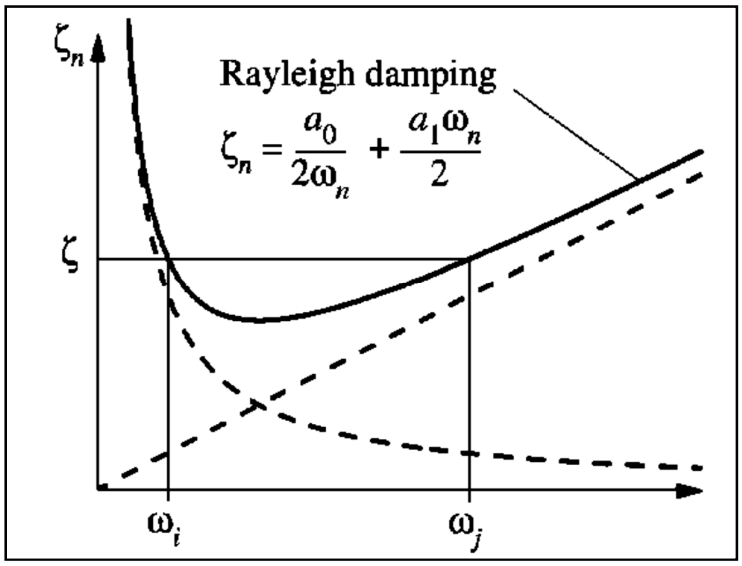

Figure 4.77 Variation of modal damping ratios with natural frequency

Table 4.3 Recommended values for damping ratios for different structures

Stress level	Type and condition of structure	Damping ratio
Working stress, less than ½ yield point	•Welded steel, prestressed concrete, well reinforced concrete (slight cracking).	2-3
	• Reinforced concrete with considerable cracking.	3-5
	• Bolted and/or riveted steel, wood structures with nailed or bolted joints.	5-7
At or just below yield point	• Welded steel, prestressed concrete without complete loss in prestress.	5-7
	• prestressed concrete with no prestress left	7-10
	• Reinforced concrete	7-10
	• Bolted and/or riveted steel, wood structures with nailed or bolted joints.	10-15
	• Wood structures with nailed joints.	15-20

4.5.2 Frame modelling for dynamic analysis and vibration periods

The model used in the time history analysis using ANSYS finite element package is the same as the structural configuration like the model in section 3.11.1. The finite element assemblies for frame members are fundamentally the same as the frame modelling explained in section 3.5.1.2 of this thesis for the frame without a link and in section 4.4 for the frame with the link. The same materials properties, type of element (SHELL 181) and material modelling was used with the finite element software ANSYS software. However it was necessary to change the finite element mesh, as the time history analysis using ground motion records is expensive in terms of analysis time for which increasing the mesh size would be effective in significant saving of time if this achieve good result, without sacrificing the accuracy or effectiveness of the analysis result. The mesh size used for static analysis was mentioned in section 3.5.1.2 of this thesis.

Use of 100 mm mesh was chosen for this analysis after comparison with other types of mesh to the original mesh size 25mm that used for the preliminary analysis of the frame. The comparison was based in finding the dynamic properties of the frame include natural frequencies and vibration periods using different sizes of mesh. Mesh 100mm was found the best one of mesh sizes 50mm, 150mm and 200mm.The dynamic properties of the frame with mesh size 100mm are shown in Table 4.4. When compared these properties with values obtained by 25mm mesh size in Table 3.8, was almost identical. From these results mesh 100mm will be effective for nonlinear dynamic analysis. This was worthwhile because the run times for the analysis were long with small mesh size (25mm). Since the frame structure used in the analysis is provided with lateral restraints (purlins and rails), the dynamic properties obtained using ANSYS with shell element model for the frame with both cases, without links and with the links are shown in Table 4.5 and Table 4.6 respectively.

The frame without restraints is different structure from the frame with restraints in terms of dynamics properties. The restraints affect the vibration periods and modes for that there is different in values in table Table 4.4 compare to Table 4.5. The mode shapes of the frame are between the four modes have been mentioned in section 3.6.3, vertical bound, side sway and torsional in all cases.

Mass per unit area for the shell element is equal to 40 (kg/m^2) was added to the roof members (rafters) in the model to represent the mass of the roof services such as purlins, cladding, sheeting and insulation in the dynamic analysis. For the shell element, uniform thickness is applied for each element in the model and therefore, the thickness of each node in an element is the same.

Table 4.4 Frequencies and periods of the structure using shell element

Mode	Frequency(Fi) cycles/sec	Frequency ω rad/sec	T sec
1	0.68069	4.2747332	1.469098
2	4.2242	26.527976	0.236731
3	5.7546	36.138888	0.173774
4	7.0928	44.542784	0.140988
5	8.664	54.40992	0.11542
6	10.45	65.626	0.095694
7	11.812	74.17936	0.08466
8	12.687	79.67436	0.078821
9	13.307	83.56796	0.075148

Table 4.5 Frequencies and periods of the frame with purlins using shell element

Mode	Frequency(Fi) cycles/sec	Frequency ω rad/sec	T sec
1	12.687	79.67436	0.078821
2	13.981	87.80068	0.071526
3	13.983	87.81324	0.071515
4	14.151	88.86828	0.070666
5	14.166	88.96248	0.070592
6	15.681	98.47668	0.063771
7	16.768	105.30304	0.059637
8	17.162	107.77736	0.058268
9	17.712	111.23136	0.056459

Table 4.6 Frequencies and periods of the frame with purlins and link using shell element

Mode	Frequency(Fi) cycles/sec	Frequency ω rad/sec	T sec
1	12.939	81.25692	0.077286
2	14.158	88.91224	0.070631
3	14.206	89.21368	0.070393
4	15.537	97.57236	0.064362
5	15.953	100.18484	0.062684
6	15.956	100.20368	0.062672
7	17.396	109.24688	0.057484
8	17.507	109.94396	0.05712
9	19.368	121.63104	0.051632

4.6 Selection and Scaling of Input Ground Motions

To evaluate the seismic action of composite frames efficiently with a few earthquake records, it is important to choose records that impart large deformation. The seismic behaviour of the structure is highly affected by the characteristics of the input ground motion. While a natural earthquake record may impose a large energy to the structure, the effective range of the frequencies is generally not broad. It is therefore necessary to investigate the effective frequencies of each record, comparing it with the natural period of the frame in consideration, (Tsujii, 2001).

The selected ground motions have different spectrum intensities from one another. Hence, to compare the seismic response of a structure subjected to different records, all of the time history accelerations should be scaled to the same spectrum intensity or specifically the spectrum intensity of the elastic spectrum in Eurocode 8 (2004) for the design peak ground acceleration as detailed in section 4.6.2 of this thesis. This section explains the procedure for selecting and scaling the ground acceleration records

4.6.1 Selection of real earthquake records

The ratio of the peak ground acceleration to the peak ground velocity, the so-called as a/v ratio, is meaningful and useful to categorise the characteristics of earthquake

records. Zhu, at el (1988) reported the importance of the a/v ratio. They categorised earthquake ground motions into three types along the a/v ratio; (A) 'normal' ground motions possessing large energy over a broad range of frequencies, (B) accelerograms of the records giving many large amplitudes in the high-frequency range, (C) records containing a large response at low frequencies, (Tsujii, 2001).

Peak ground acceleration is normally influenced by the high frequencies of the earthquake records, while peak ground velocity is associated with moderate to low frequencies due to the integration of the ground accelerations. Hence, high a/v ratios mean that the record is categorised as type (B) above; by contrast type (C) has a low a/v ratio, (Tsujii, 2001). The three categories of a/v ratios may be defined in the following ranges:

$$\text{Low } \{ a/v < 0.8g/(m/s) \}$$

$$\text{Normal } \{ 0.8g/(m/s) \le a/v \le 1.2g/(m/s) \} \qquad \text{Equation 4.4}$$

$$\text{High } \{ 1.2g/(m/s) < a/v \}$$

According to these categories, eight earthquake records were selected as candidates for the input ground motion from major and strong earthquake events. A broad range of a/v ratio was considered in the selection of the earthquake records herein. The location and magnitude of each record is shown in Table 4.7. The a/v ratio and the category as calculated by Equation 4.4 above are shown in Table 4.8.

When examining the response of a structure in the inelastic range using a suite of actual strong motion records, it is convenient and more appropriate to refer to the response spectrum of the record, which summarises the peak response of all SDOF systems to a particular component of the ground motion (Chopra, 2001). Hence, for each selected earthquake record the spectral displacement, the pseudo-velocity and pseudo-acceleration response spectra can be constructed for a wide range of natural vibration periods corresponding to a SDOF system. The prefix pseudo-spectrum is used to distinguish the term from the peak values of velocity and acceleration (Konstantinidis, 2001). Figure 4.78 to Figure 4.85 show the raw data for the acceleration time history. Moreover, the acceleration spectrum, velocity and

displacement spectrum were plotted as well for the eight records as representatives of each event. A value of 5% was used as a damping ratio when calculating the pseudo response spectrum using the SeismoMatch software (Seismosoft, 2002).

As shown in Table 4.8 , different a/v ratios were obtained from the same earthquake events for all earthquake data, such as Coalinga, record CO0332 has a high a/v ratio while record CO0346 has a low value for a/v ration. For Loma Prieta, record LP 0732 has a low a/v ratio but record LP 0738 has a normal one. On the other hand Northridge records vary between normal ratio for NR0893 and high ratio for NR0935. Finally Kobe records KB1056 and KB1057 are categorised as having a high and low a/v ratio respectively. The soil conditions and/or the epicentral distance may be the main factors for these differences. It is emphasised that the study of different values of a/v ratios as such is beyond the scope of this thesis.

Considering limitations on the number of dynamic analyses that it was practical to perform, a stricter selection was needed to impose the most effective motion to the portal frame under consideration. It was necessary to choose effective records whose frequency range of peak spectral acceleration matched the natural periods of the structure. As described previously in Table 4.4 to Table 4.6 the natural periods of the structure range from 0.051 to 1.46 sec for the portal frame in both cases with restrained and without restrained. For frame with restrained the natural periods range from 0.051 to 0.078 sec. The effective natural period range should be taken as being approximately 0.051 to 0.5 sec as the fundamental period of vibration of the building is 0.243 sec.

When we examine the earthquake acceleration and response spectra in Figure 4.78 to Figure 4.85, we find that three records are out of the range of selection based on the effective periods of the structure and should have been rejected. As shown in Figure 4.79, Figure 4.80 and Figure 4.84 theses records; CO0346, LP0732 and KB1057 have the peak range of the spectral acceleration in the longest periods (around 1.5 sec) or the lowest frequencies. In addition from Figure 4.80 and Figure 4.84, records LP0732 and KB1057 have a characteristic strong motion which occurs in longer range than the predicted longest period of 0.5 sec for the portal frame structure in this study. On the other hand, the ground motion records with low a/v ratio probably will not impose dangerous impact to the steel structure. Since the

ultimate limit state of the global structure is generally associated with inelastic global displacement. To choose the three suitable and most effective earthquake records from the remaining five candidates records the effective range must be determined with respect to not only the acceleration but also the velocity and displacement, the spectral velocity and displacement were calculated as shown in Figure 4.78 and Figure 4.85.

From the spectral velocity and displacement in Figure 4.82, it is obvious that record NR0893 is not suitable due to its longer range characteristic for acceleration and velocity also its peak response displacement is too long. On the other hand it is clear that record LP0738 is not suitable as input ground motion in this study because its peak distribution of the spectral velocity does not meet the desirable range of 0.051 sec to 0.5 sec, (see Figure 4.81).

Consequently, three earthquake records, CO0332, NR0935 and DU1547 were selected as the input ground motions for portal frame assessment (see Figure 4.78, Figure 4.83 and Figure 4.85). All the three records have spectral acceleration and velocity with strong intensity throughout the period range from 0.051 to 0.5 sec specially record NR0935 and record DU1547. Record CO0332 has a sole intense peak in the shortest periods for all spectra, including acceleration, velocity, and displacement.

Table 4.7 Earthquake records and station

Record No	Earthquake	Date	Station	Record Component	Magnitude (Ms)
CO0332	Coalinga USA	2/05/1983	PC6W	C06000	6.5
CO0346			PFZ14	Z14000	
LP0732	Loma Prieta USA	18/10/1989	HCH	HCH180	7.1
LP0738			GA6	G06000	
NR0893	Northridge USA	17/01/1994	WLC	LOS000	6.7
NR0935			TCH	TAR360	
KB1057	Kobe JAPAN	16/01/1995	TAK	TAK000	6.9
DU154	Duzce TURKEY	12/11/1999	BLU	BOL000 BOL-UP	7.3

Table 4.8 Ground motion details and a/v ratio

Record	PGA (g)	PGV (cm/s)	PGD (cm)	a/v Ratio	Category
CO0332	0.126	11.0	1.34	1.15	High
CO0346	0.282	40.9	8.1	0.69	Low
LP0732	0.247	38.5	17.83	0.64	Low
LP0738	0.126	12.8	4.74	0.98	Normal
NR0893	0.41	43.0	11.75	0.95	Normal
NR0935	0.99	77.6	30.45	1.28	High
KB1057	0.611	127.1	35.77	0.48	Low
DU1547	0.728	56.4	23.07	1.29	High

4.6.2 Scaling of selected ground motions based on Eurocode spectrum

In order to apply nonlinear dynamic analysis and compare the effect of the input motions on structural behaviour, using natural earthquake records consistent with the design spectrum, it is necessary to scale the selected ground accelerograms for the records CO0332, NR0935 and DU1547. Kappos (2000) showed that scaling is also necessary when the assessment of the structure's response to be carried out at a number of different limit states (e. g. life safety, collapse prevention).

Thus, one would like to scale the independent earthquake records so that they exhibit equal velocity spectra. There are different scaling techniques proposed in the literature that are used by earthquake engineers. The most common is defined by Housner (1952), here the scaling factor is taken equal to the ratio of the target spectrum intensity, to the spectrum intensity of the natural record that is to be scaled.

The target spectrum intensity is found from the area under the target velocity response spectrum. The velocity spectrum can be derived from the acceleration design spectrum by dividing with the natural frequency ω.

The spectrum intensity of the record to be scaled is found from the area under the pseudo-velocity response spectrum. The area typically corresponds to the range of periods $0.1 \leq T \leq 2$ .5 sec and is calculated for damping ratios of 0 to 20% as in equation 4.5 below.

Kappos and Kyriakakis (2000) have a similar method but use different periods.

$$SI = \int_{0.1}^{2.5} S_{pv}(T, \xi) dT \qquad \text{Equation 4.5}$$

Where ξ is the fraction of critical damping that takes a value of 0 or 0.2. T is the response period of the structural system.

Kappos and Kyriakakis (2000) suggested the range of periods for which the spectrum intensities are calculated should be between 0.8 and 1.2 of the fundamental period of the structure. Martinez-Rueda in 1997 suggested that the period limits within which the spectrum intensities should be calculated should be the fundamental period of the structure at Yield and in the post hardening range. In the light of the above, and given the fact that it is beyond the scope of the present research to examine a rational scaling method of earthquake records, the method proposed by Kappos and Kyriakakis (2000) was adopted for the purpose of scaling the selected input motions to match the design spectrum to EN 1998-1(2004) specification.

Equation (4.5) seems to work well for scaling earthquake records to the design code spectrum for a wide range of structural periods. Instead of using the period range, $0.8 \leq T \leq 1$ .2 sec, suggested by (Kappos and Kyriakakis, 2000), it may be better to change the period range to take into account the natural periods of the structure under consideration. Considering the periods of the structure for the study, the period range used in equation (4.5) should probably be replaced by 0.04 sec to 0.5 sec, which is suitable with the vibration periods of the structure.

$$SI = \int_{0.04}^{0.5} S_{pv}(T, \xi) dT \qquad \text{Equation 4.6}$$

Following the above equation (4.6), the selected three records CO0332, NR0935 and DU1547 were scaled so that they exhibited the same spectrum intensity or specifically the spectrum intensity of the elastic spectrum in Eurocode 8 (2004) for the design peak ground acceleration of 0.23g for subsoil class (C) with a damping ratio of 5%. Table 4.9 provides the spectrum intensity, the scaling factors of the selected ground motions to the design earthquake for the selected records. In this case, the value of 25.74 cm is the result of the spectrum intensity of the elastic spectrum in Eurocode 8 (2004) for subsoil class (C). For the purpose of scaling the natural records to the seismic level corresponding to collapse prevention, the resulting scaling factors for the design earthquake are doubled as implemented by Kappos (1997) and by Konstantinidis (2001).

Comparisons of response spectra for the three ground motions with the target spectrum before scaling are shown in Figure 4.86. Use was made for the scaled records generated by SeismoMatch software (Seismosoft, 2002). Comparisons of response spectra for the three scaled ground motions with target spectrum are shown in Figure 4.87. SeismoMatch software scaled the earthquake to match the design spectrum using Eurocode method. The method modifies real earthquakes and matches displacement at short periods (< 2 second), velocity at intermediate periods (1- 2 second) and acceleration at long periods (> 0.75 second) to the target spectrum. Real earthquakes even when scaled will not perfectly match a design code spectrum. The three scaled earthquakes will not be precisely equivalent (which is why multiple scaled earthquakes are used for design purposes).

Table 4.9 Scaling of the selected natural records accelerations

Record	PGA (g)	Spectrum intensity SI (cm)	Scaling factor
CO0332	0.126	15.87	1.622
NR0935	0.99	70.03	0.368
DU1547	0.728	62.39	0.413

4.7 Use of Generated Accelerations (Artificial Earthquakes)

Natural records of an earthquake event can help closely induce real behaviour if the structure in consideration is subjected to the event. However, as described above, independent earthquake records generally have narrow frequency ranges with large accelerations. Use of such records for input motion does not always produce intense structural oscillation. For the purpose of testing the survivability of a structure in practice, the seismic response against the design spectra defined in Eurocode 8 (2004) seems to be suitable for evaluation. The generated records constitute artificial ground motions that approximate the elastic spectra in the design code.

From the above discussion, generated record was chosen as the input ground motion for the study of the frame. This record corresponds to the code design spectrum for EC8 spectrum, type 1, ground: C and design PGA = 0.23g in Eurocode 8 (2004). This generated acceleration increases continually until the failure of the structure with the link and without link. It is a harmonic excitation with acceleration of

Maxac t^2 sin ($2\pi t/T$):

Where:

Maxac is the design earthquake (0.23) multiply by 9.81 multiply by 20;

t is the time; and

T is the vibration period of the structure.

The harmonic earthquakes (a modulated sine wave, with increasing amplitude) were generated to the elastic natural frequencies of the different structures so as to have strong effect on the structure response. As the structure without link and with the link are different structures the artificial records was generated for every structure with its own vibration period using the fundamental period for each structure tabulated in Table 3.6 and Table 4.6. The fundamental vibration period for the frame without link was 0.078821, while it is 0.077286 for the frame with the link. The total time for both excitations for every structure was assumed as 1.5 sec with time step 0.005 sec.

Acceleration time history

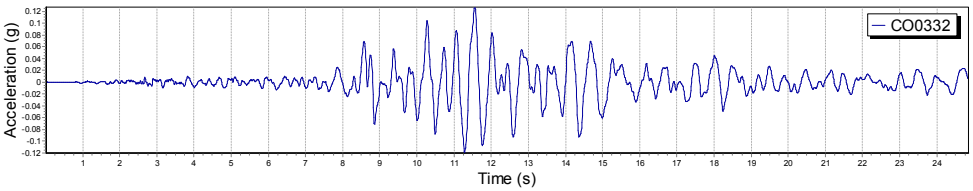

Pseudo aceleration spectrum

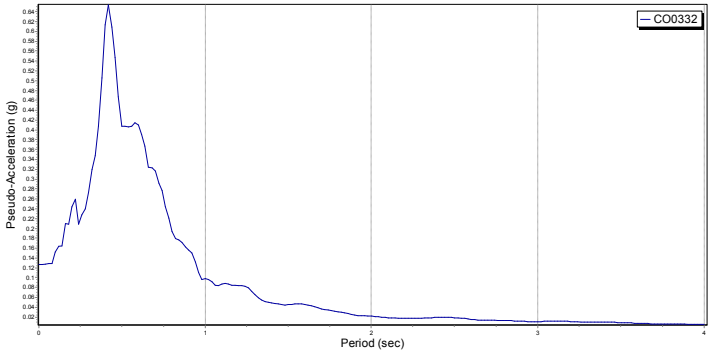

Pseudo velocity spectrum

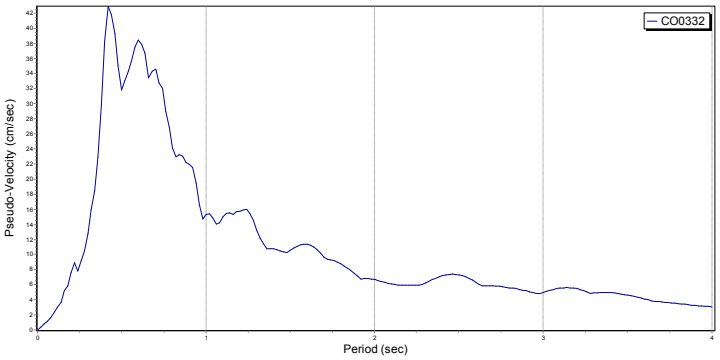

Displacement spectrum

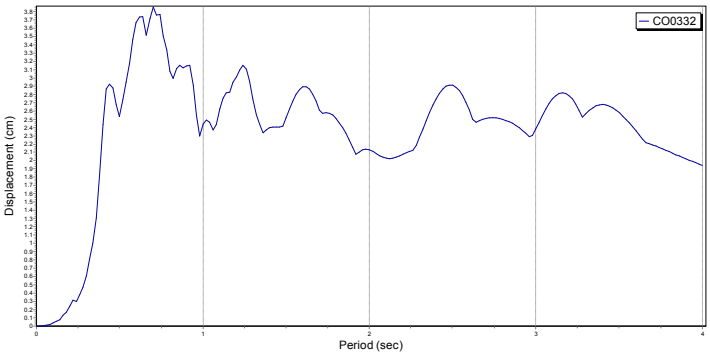

Figure 4.78 Acceleration and response spectrum of record Coalinga 0332(CO0332); Damping 5%.

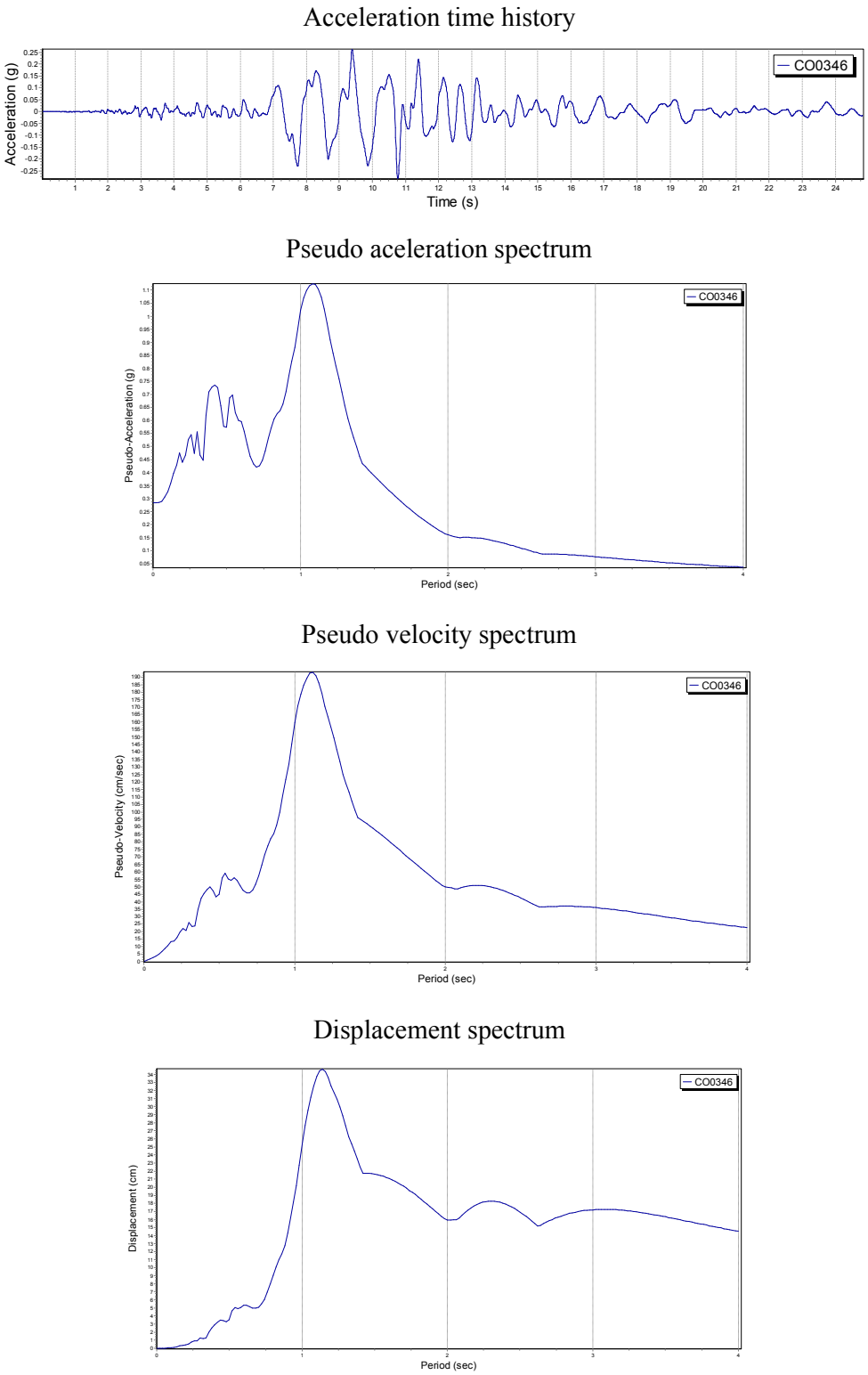

Figure 4.79 Acceleration and response spectrum of record Coalinga 0346 (CO0346); Damping 5%.

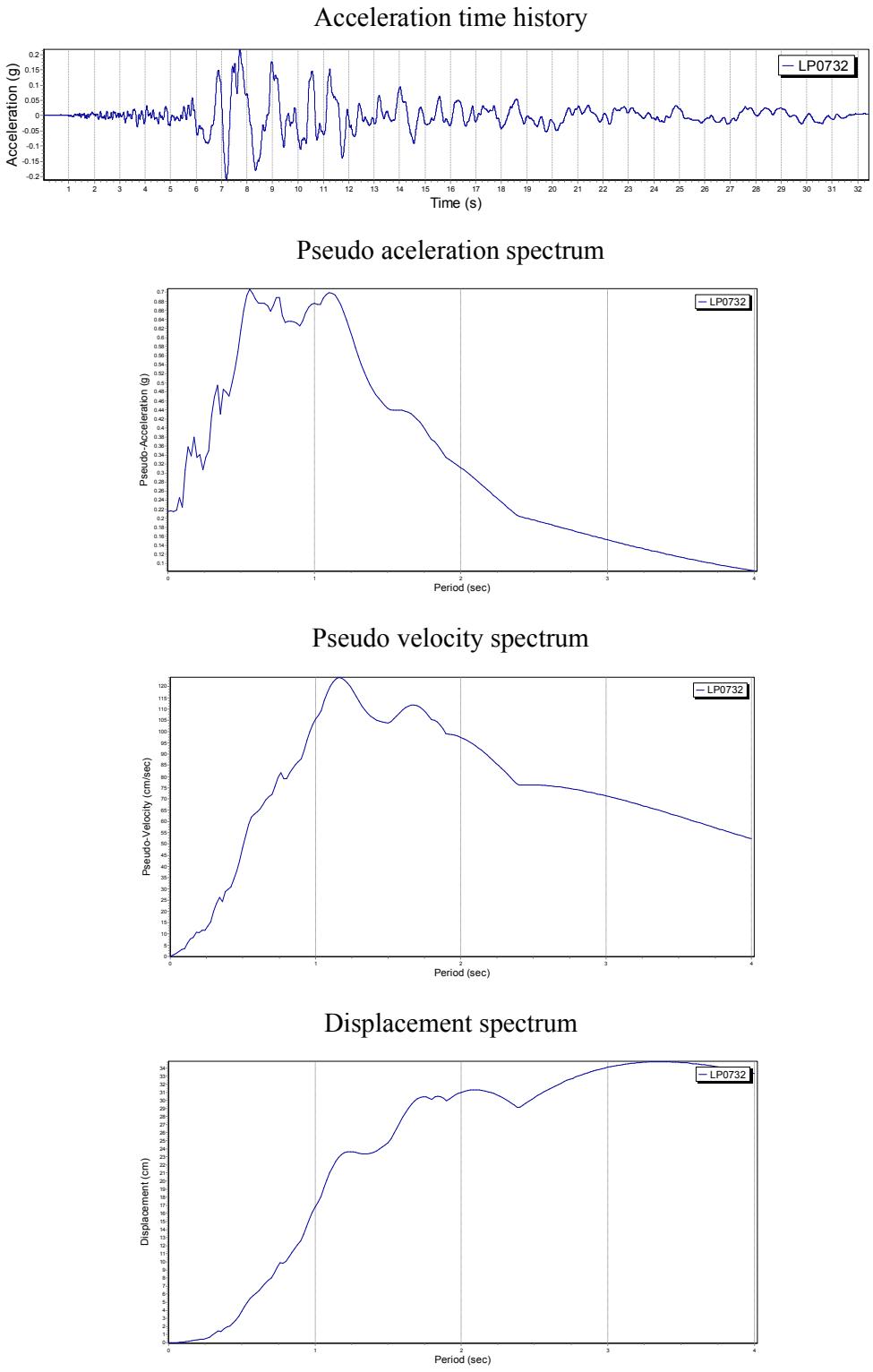

Figure 4.80 Acceleration and response spectrum of record Loma Prieta 0732 (LP0732); Damping 5%.

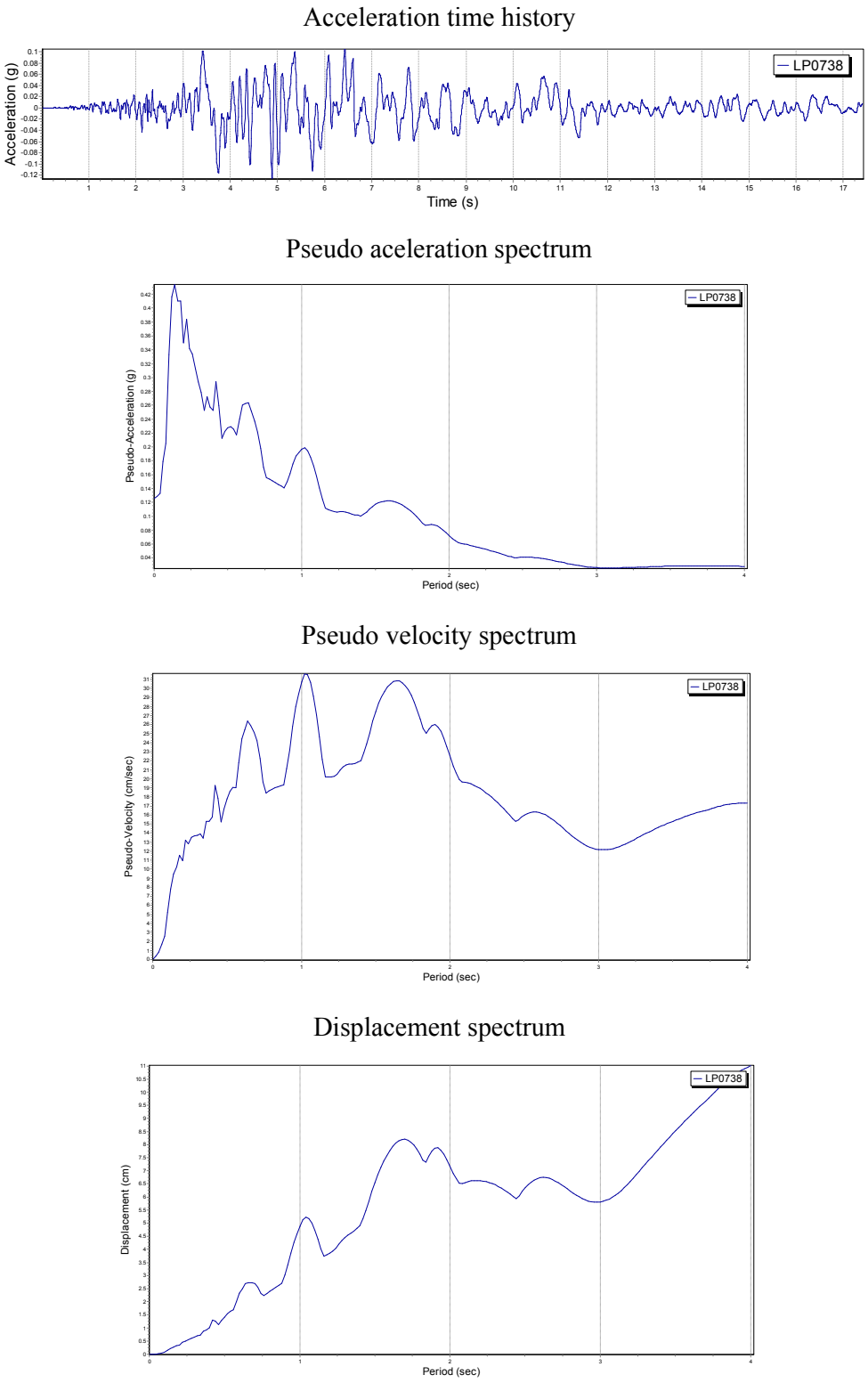

Figure 4.81 Acceleration and response spectrum of record Loma Prieta 0738 (LP0738); Damping 5%.

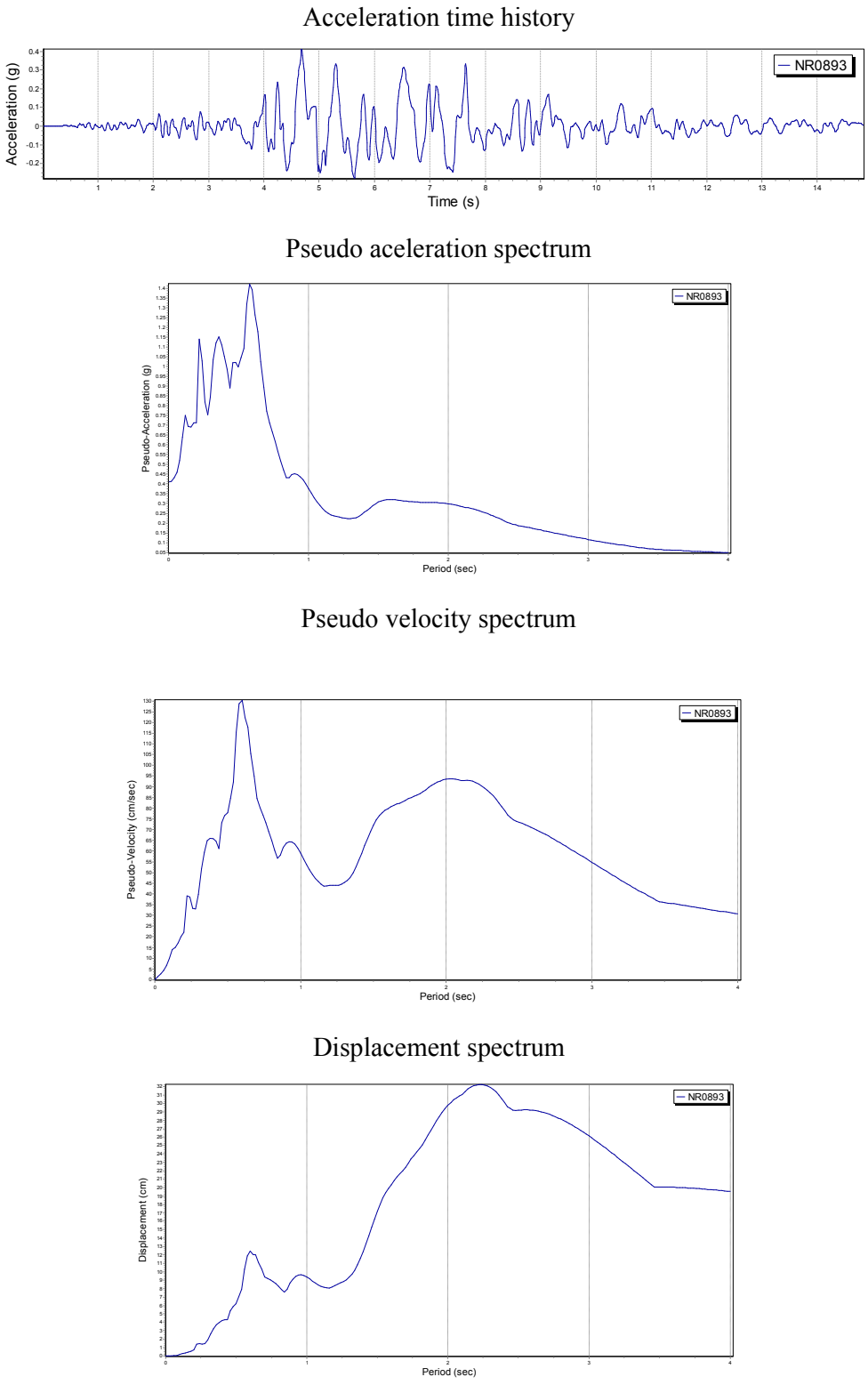

Figure 4.82 Acceleration and response spectrum of record Northridge 0893 (NR0893); Damping 5%.

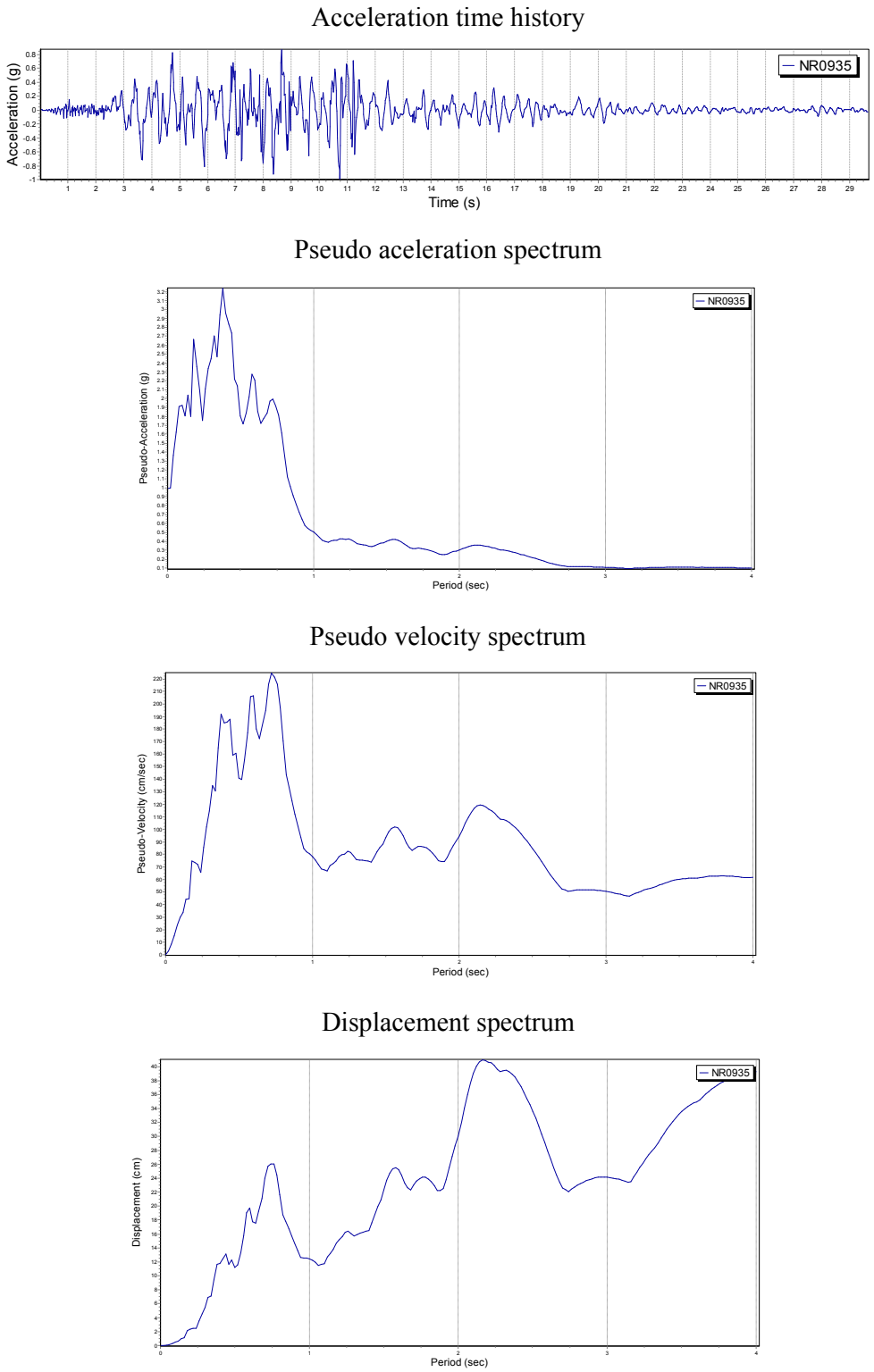

Figure 4.83 Acceleration and response spectrum of record Northridge 0935 (NR0935); damping 5%.

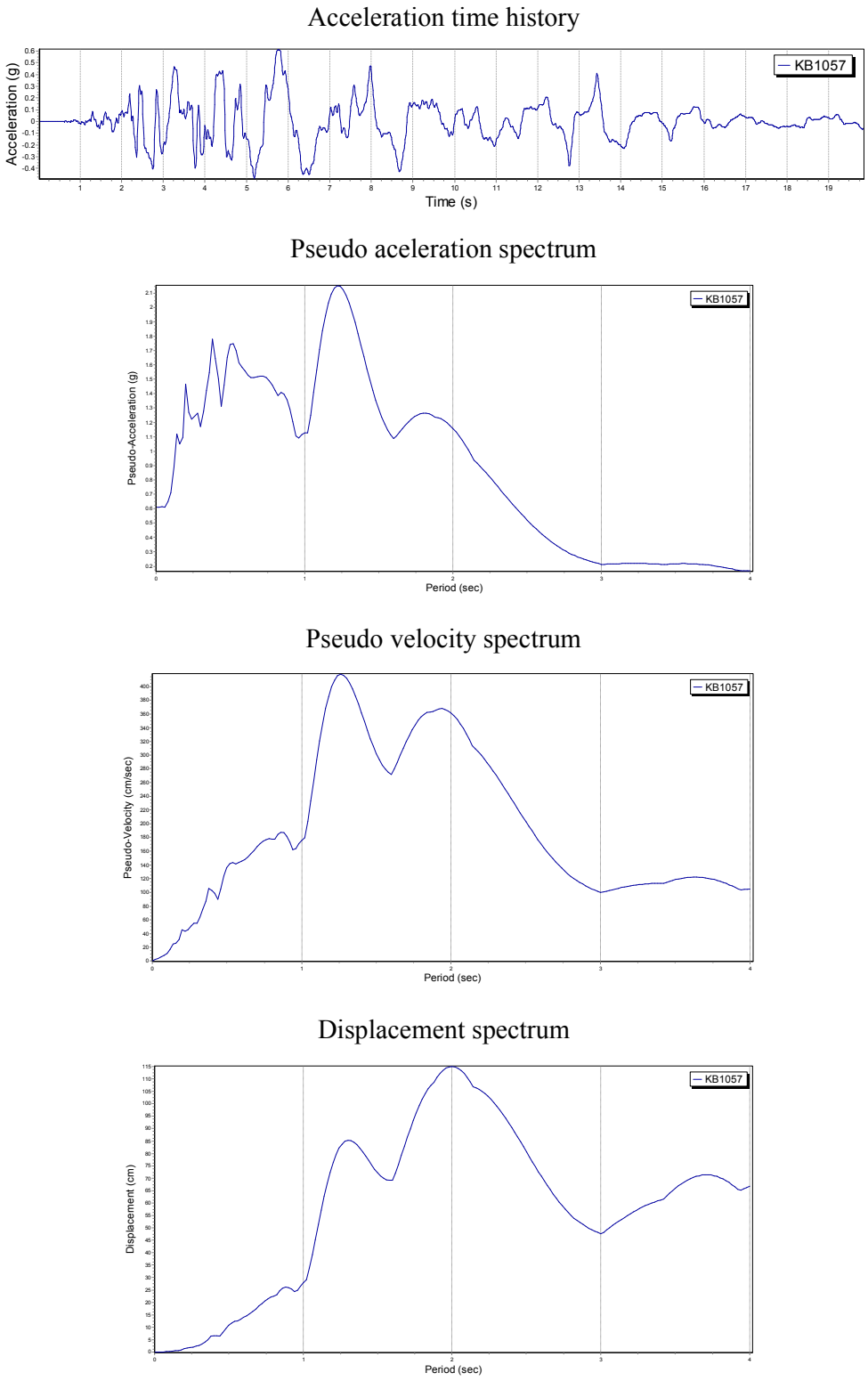

Figure 4.84 Acceleration and response spectrum of record Kobe 1057 (KB1057); damping 5%.

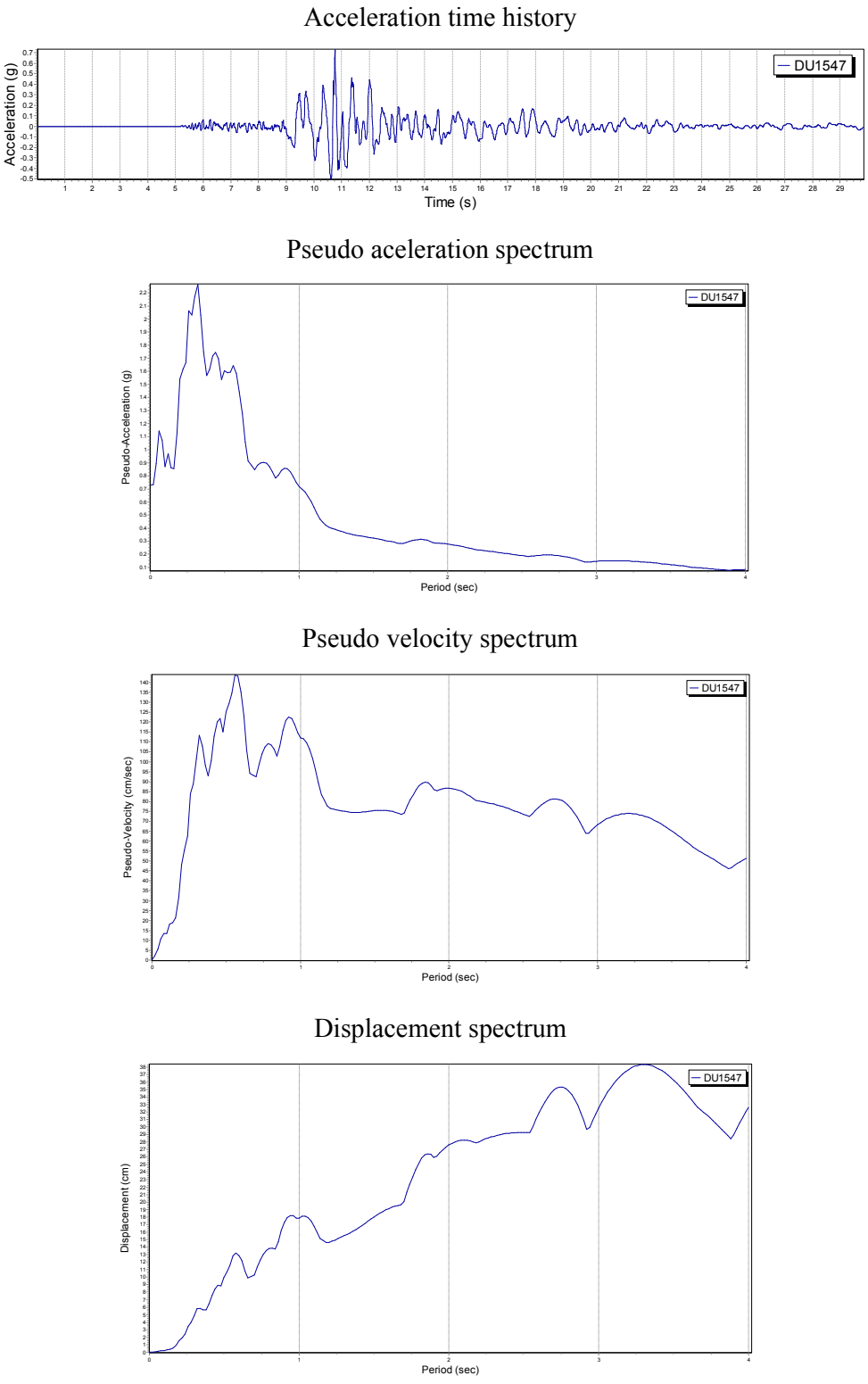

Figure 4.85 Acceleration and response spectrum of record Duzce 1547 (DU 1547); damping 5%.

Pseudo acceleration spectra

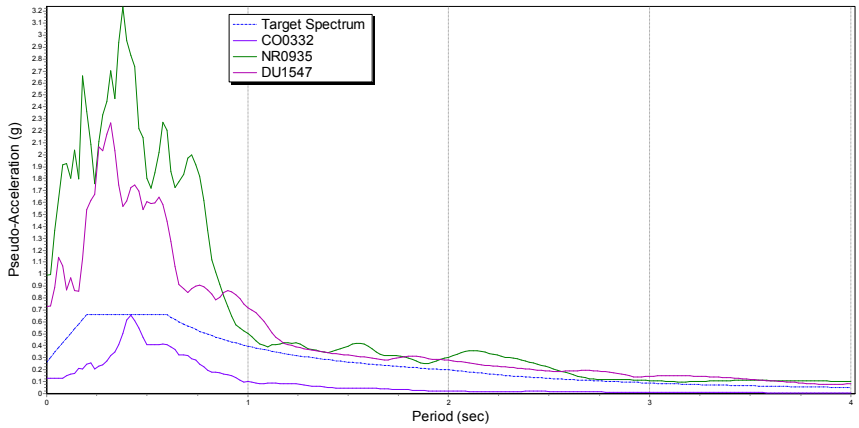

Pseudo velocity spectra

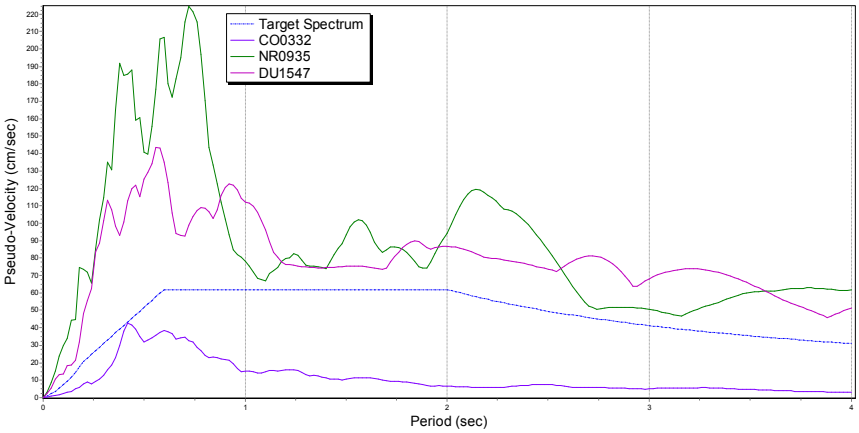

Displacement spectra

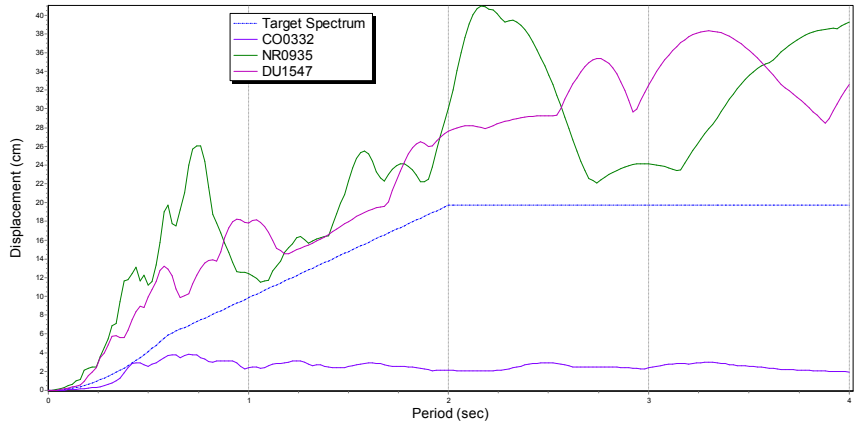

Figure 4.86 Comparison of elastic response spectra of the selected records and EC8 spectrum, type 1, ground: C (design PGA = 0.23g, damping ratio = 5%).

Pseudo acceleration spectra

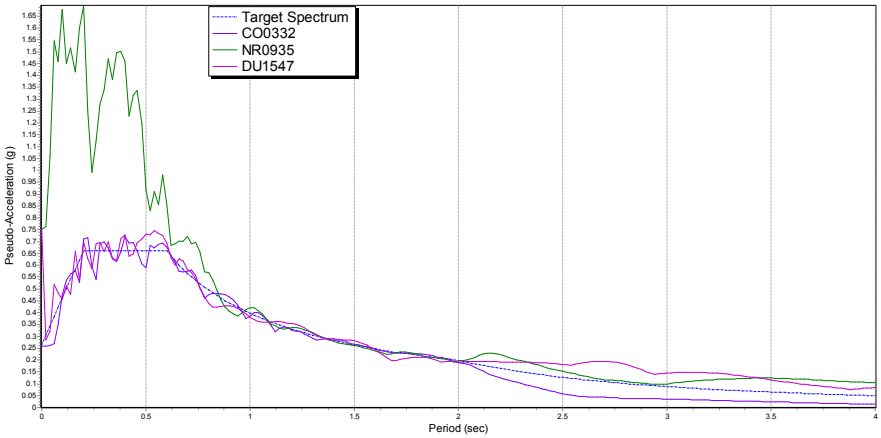

Pseudo velocity spectra

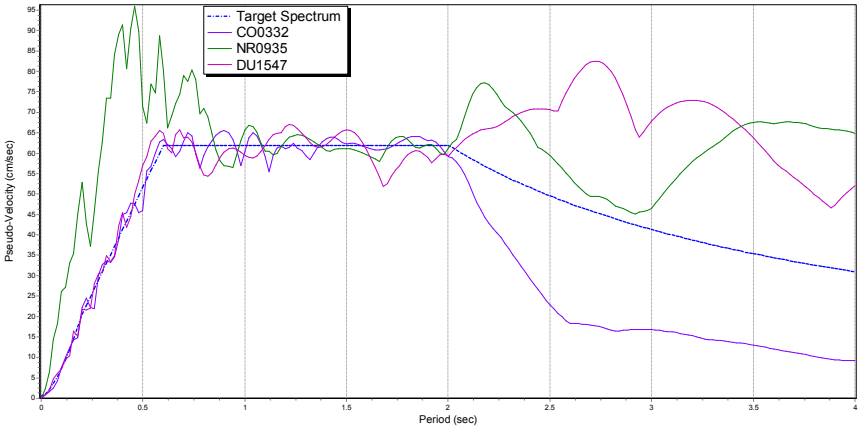

Displacement spectra

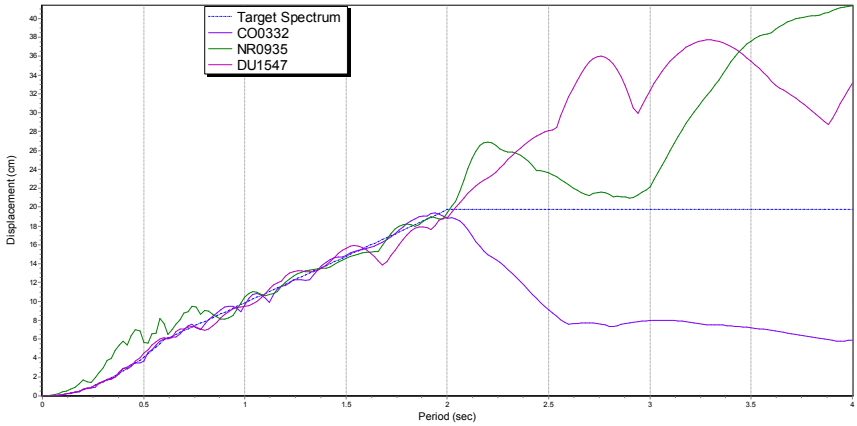

Figure 4.87 Comparison of elastic response spectra of the scaled records and EC8 spectrum, type 1, ground: C (design PGA = 0.23g, damping ratio = 5%).

4.8 Preliminary Assessment of the Performance of the Designed Portal Frame Structure using Nonlinear Dynamic Analysis

The results of six inelastic time-history analyses for the frame with link and without link are presented in Figure 4.88 to Figure 4.121 at the end of this section, which illustrate the base shear time history, the roof displacement time history, the acceleration time history and the von Mises stress using the selected input motions scaled to the design earthquake level. From the base shear time history and roof displacement time history diagrams it is seen that the response of the structure subjected to varying input motions shows different patterns due to the differences in the characteristics of the input accelerograms. The frame was analysed with lateral restraints for both cases without link and with the link using the dynamic properties in Table 4.5 and Table 4.6.

It has to be mentioned that as the damping values for the analysis obtained according to the first mode and the twenty mode of vibration of the frame. The effect of damping appears in the analysis for the forces as the value of damping will increase monotonically with frequency and thus reduce the contribution of the higher modes to response as explained before in Section 4.5.1. This explains why we use modes until twenty modes so as to have the contribution of many modes to response.

4.8.1 Coalinga earthquake results

First the frame with link and without link was analysed under the scaled real records of Coalinga earthquake. The results of the two cases for the base shear and roof displacement obtained from ANSYS results are shown in Figure 4.88 to Figure 4.95. Figure 4.88 and Figure 4.89 show the base shear in case without link and with the link as it is observed that the base shear was smaller in case of the frame with the link as it is 34 N compared with 36 N where there is no link. From the results for roof displacement in Figure 4.90 and Figure 4.91 the maximum horizontal displacement is 0.147E-05 m without link and 0.185E-05 m for the frame with the link which is very small when compared with the value for frame failure which is 0.034 m, for that no failure happened for the frame. Figure 4.92 and Figure 4.93 show the acceleration in the structure with similar value equal 0.110 g for both types of structure. Both of the structures have good earthquake resistant appear in the von

Mises stress in Figure 4.94 and Figure 4.95 as the value is 147E2 MPa for the frame without link and is 144E2 MPa for the frame with the link which is less than the yield strength for the frame (355E9 MPa).

4.8.2 Northridge earthquake results

Figure 4.96 and Figure 4.97 show the base shear for the response of the steel portal frame due to the analyses of the frame without link and with the link under the scaled real ground motion of Northridge earthquake. In both cases the base shear is 1500 N, no different was observed. Figure 4.98 and Figure 4.99 show the horizontal displacement for both structures without link and with the link having similar values as 0.0023m, less than 0.032m the value for failure. The acceleration for the frame without link is 120 m/sec^2, while it is 115 m/sec^2 for the frame with the link less than the frame without link. Both of the structures without link and with the link did not achieve yielding in any part of them as the von Mises stress has value 259E3 MPa for the frame without link and value 225E3 MPa for the frame with the link as shown in Figure 4.102 and Figure 4.103. No failure has been observed in both structures.

4.8.3 Duzce earthquake results

Finally, the light gauge steel portal frame without link and with the link was analysed under the scaled real ground motion of Duzce earthquake with horizontal and vertical excitation. The results are shown in Figure 4.104 to Figure 4.111 for the base shear, roof displacement and acceleration for the two cases with the link and without link. Figure 4.104 and Figure 4.105show the base shear for the frame without link with value 58N greater than the value for the frame with the link 48 N. Also the frame without link has value of roof displacement 0.000085 m while it is 0.000082 m for the frame with the link as shown in Figure 4.106 and Figure 4.107. Figure 4.108 and Figure 4.109 show the acceleration in the structure after the excitation with value 0.575 g for the frame without link and 0.43 g for the frame with the link which is less than the case without link. Both types of structure have good performance under real earthquake records and no yielding in any part of them according to Figure 4.110 and Figure 4.111, as the value for von Mises stress is 135E2 MPa for the frame without link and it is 325E2 MPa for the frame with the link, both less than the yield strength of the frame (355E9 MPa).

4.8.4 Artificial earthquake results

As all the results for real earthquake records no failure was recorded for the structure, use was made for generated accelerations. The analysis was performed for the structure without link and with link.

The harmonic accelerations (artificial earthquake) was generated according to the frequency of every structure as the frame without link and with the link are independent structures with different values of frequencies and vibration periods as in Table 4.5 and Table 4.6.

The results for frame without link and with the link are shown in Figure 4.112 to Figure 4.121. From the results for the harmonic excitation the frame with the link seems to have good resistance and good strength compared with frame without link, as was observed from the results starting with base shear result, the base shear is 1400 N in case of frame without link while it is 1200 N for the frame with the link as shown in Figure 4.112 and Figure 4.113. In the other hand the roof displacement was found about 24 mm for frame without link while it was 20 mm for the frame with the link as shown in Figure 4.114 and Figure 4.115. Also the acceleration for frame with the link was about 135 m/sec^2, while it was 110 m/sec^2 for the frame with the link. The frame without link failed with maximum horizontal displacement about 28 mm, while the frame in case with the link failed with maximum horizontal displacement about 27 mm. The frame seems to be more stable in case of the frame with link comparison with frame without link as in Figure 4.118 and Figure 4.119. However both the frame without link and the link failed without achieving yielding in any part of them as the von Mises stress for the frame without link is 295E9 MPa and is 270E9 MPa for the frame with the link which is less than the yield strength for the frame which is 355E9 MPa (see Figure 4.120and Figure 4.121). Also no yielding for the link member was observed and the failure criterion in both cases was failure of the column at the base due to the buckling of the cold formed members. The buckling prevented the frame from achieving nonlinear behaviour or a plastic mechanism.

Result for Coalinga Earthquake

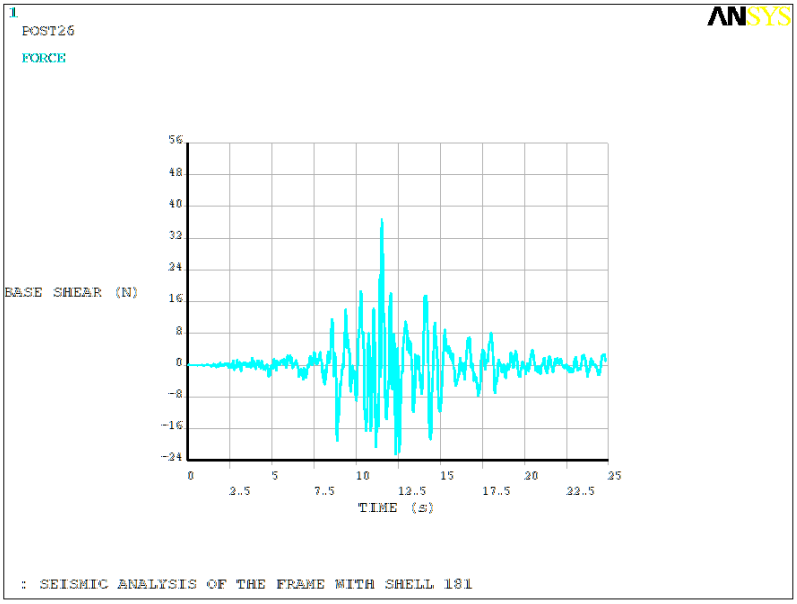

Figure 4.88 Base shear for frame without link

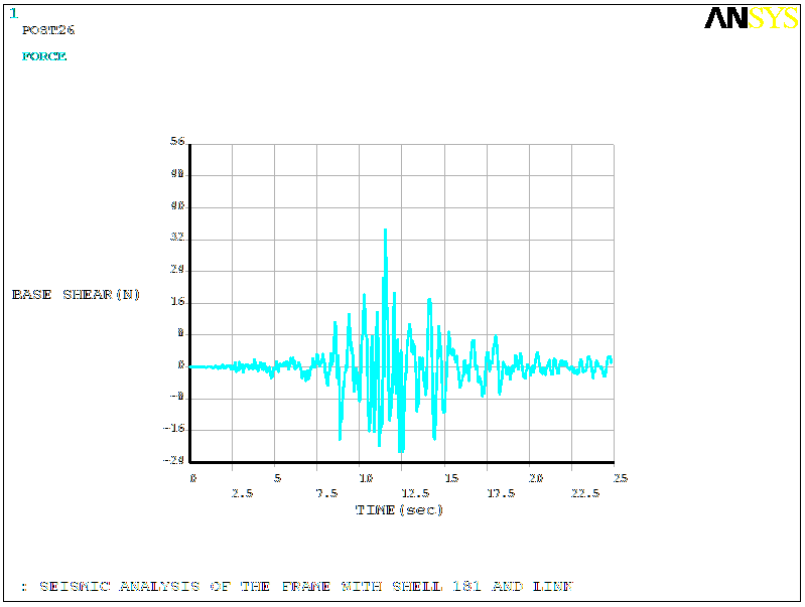

Figure 4.89 Base shear for frame with link

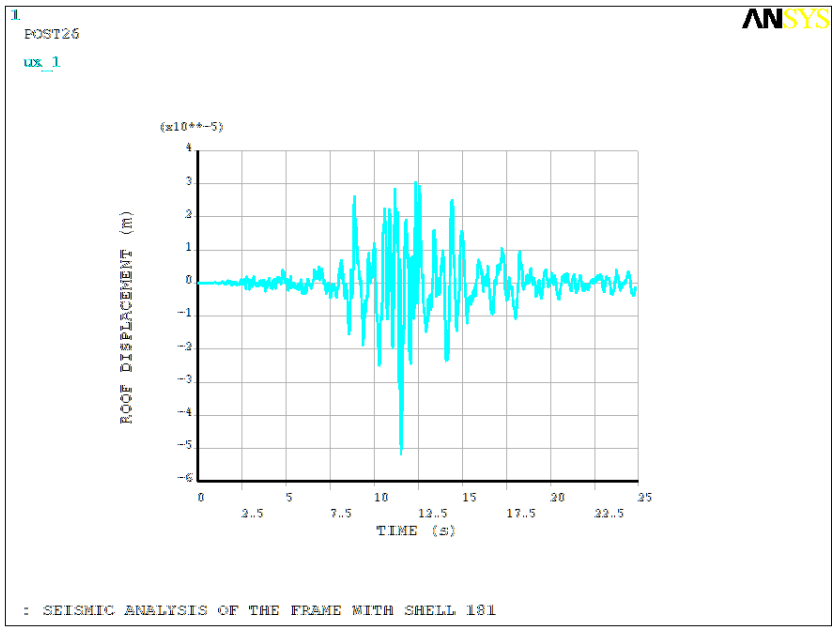

Figure 4.90 Roof displacement for frame without link

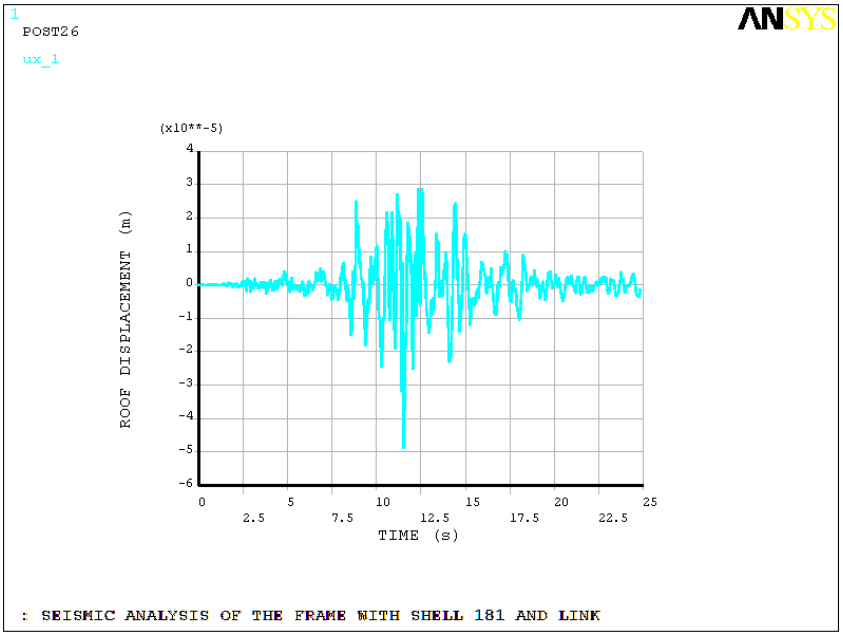

Figure 4.91 Roof displacement for frame with link

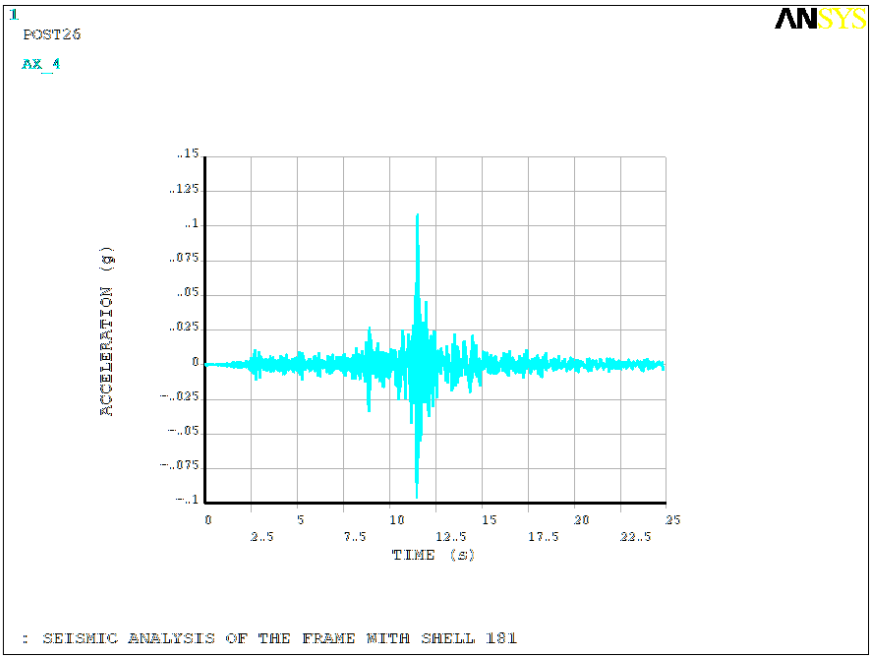

Figure 4.92 Acceleration time history for frame without link

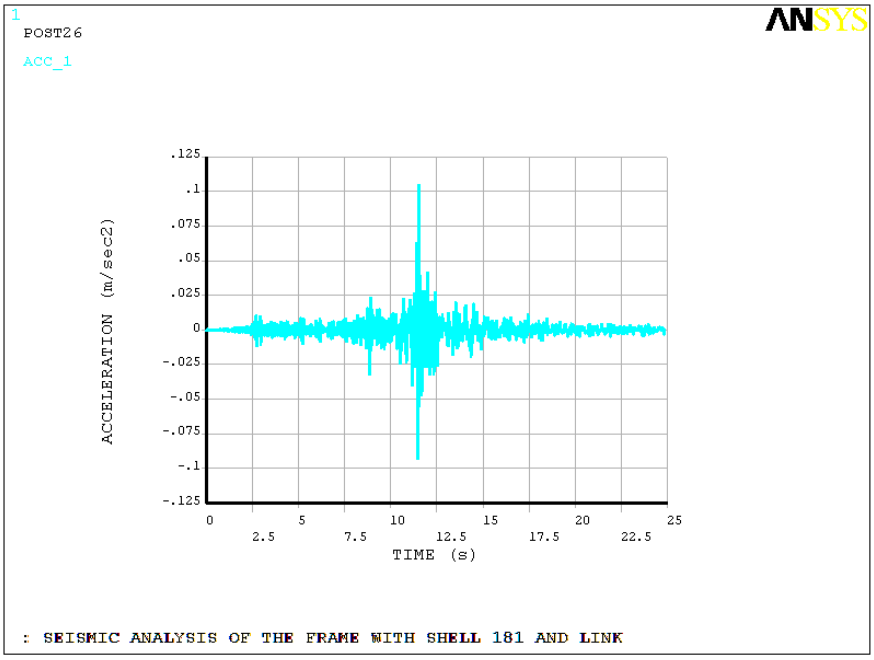

Figure 4.93 Acceleration time history for frame with link

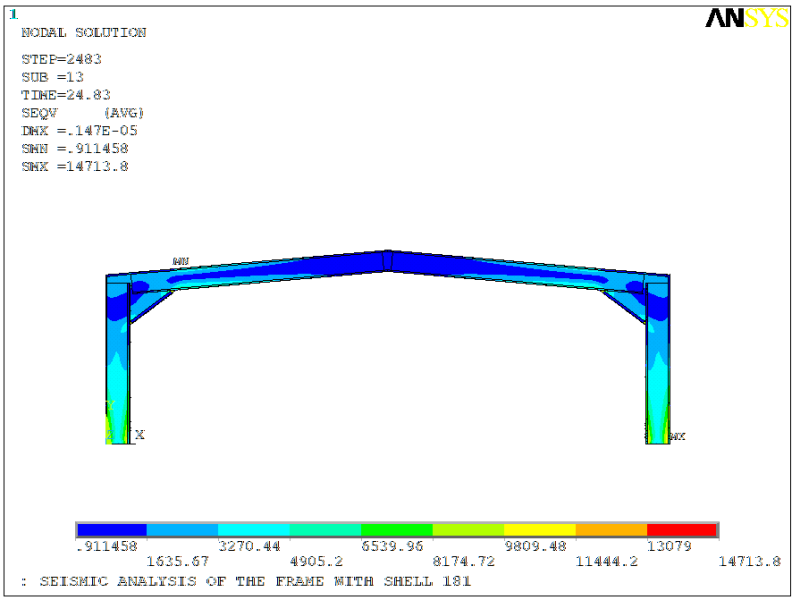

Figure 4.94 Von Mises stress (MPa) for frame without link

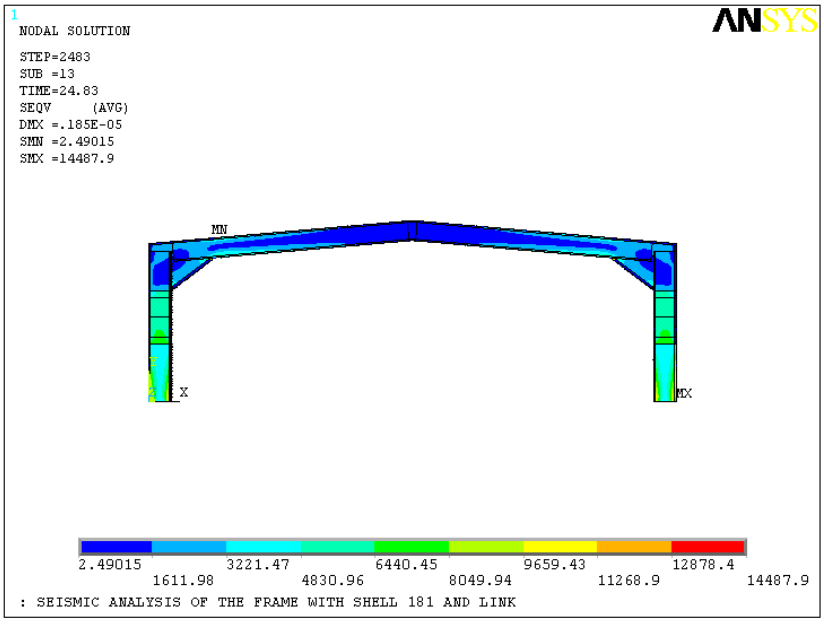

Figure 4.95 Von Mises stress (MPa) for frame with link

Result for Northridge Earthquake

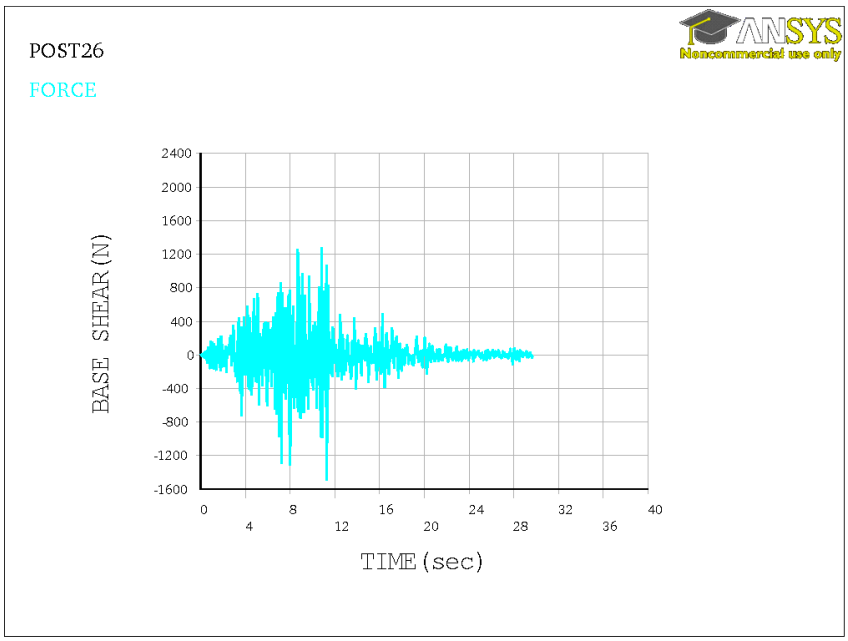

Figure 4.96 Base shear for frame without link

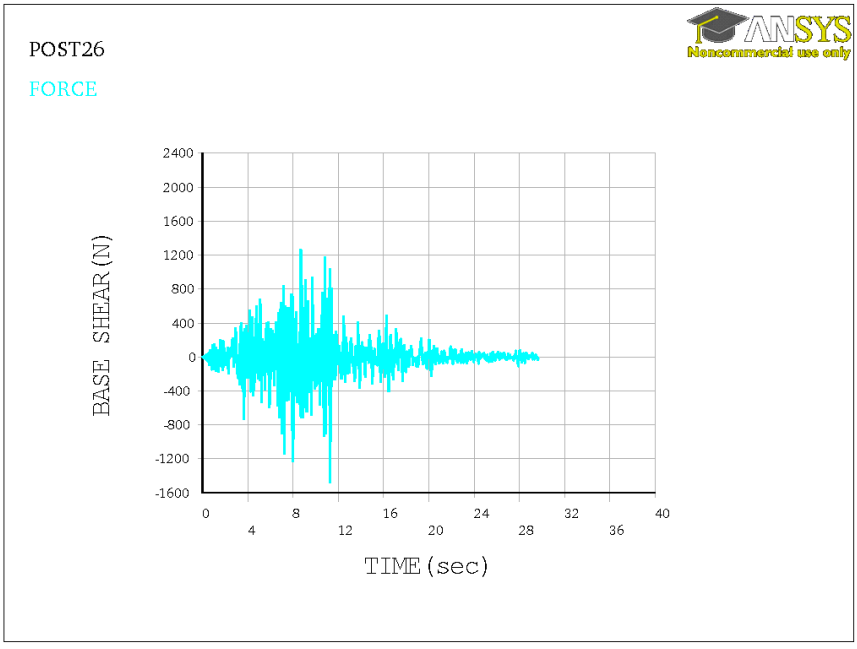

Figure 4.97 Base shear for frame with link

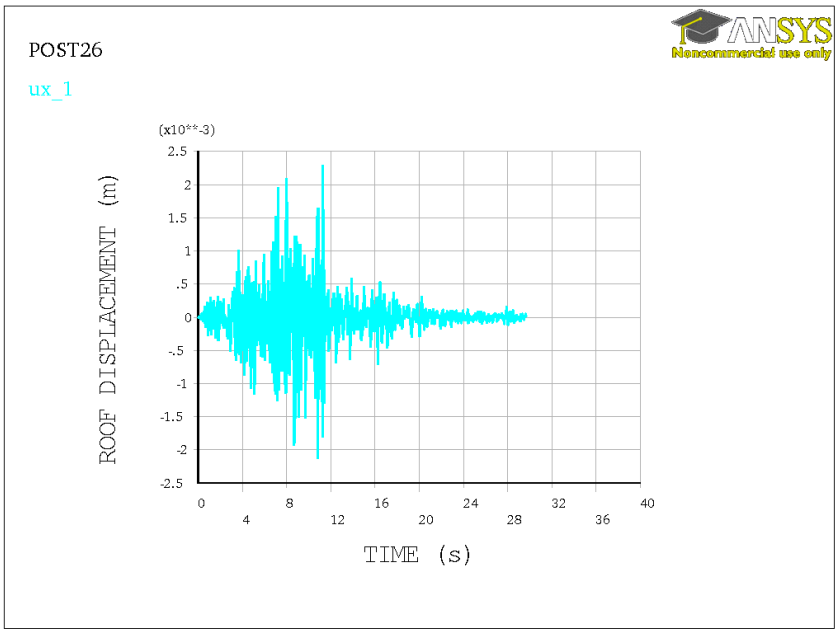

Figure 4.98 Roof displacement for frame without link

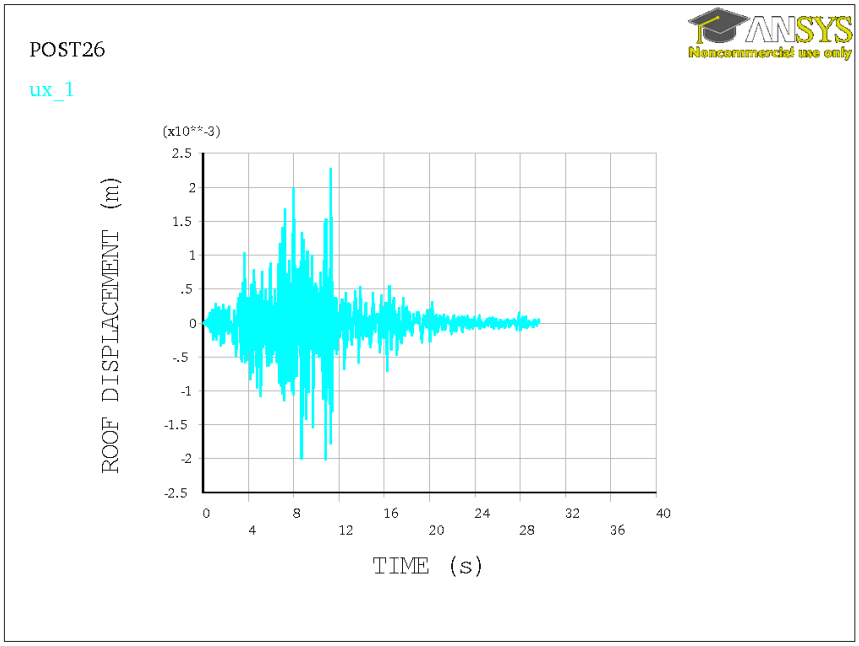

Figure 4.99 Roof displacement for frame with link

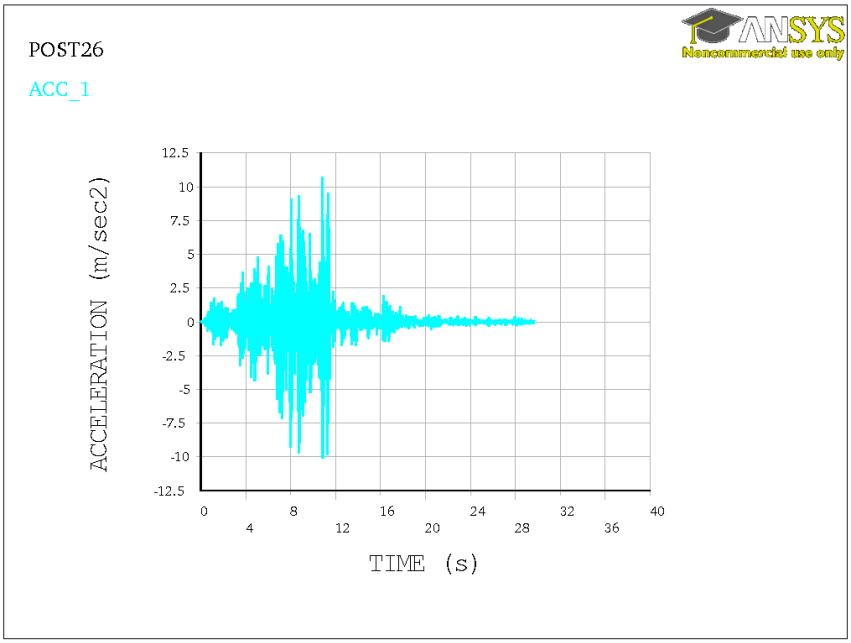

Figure 4.100 Acceleration time history for the frame without link

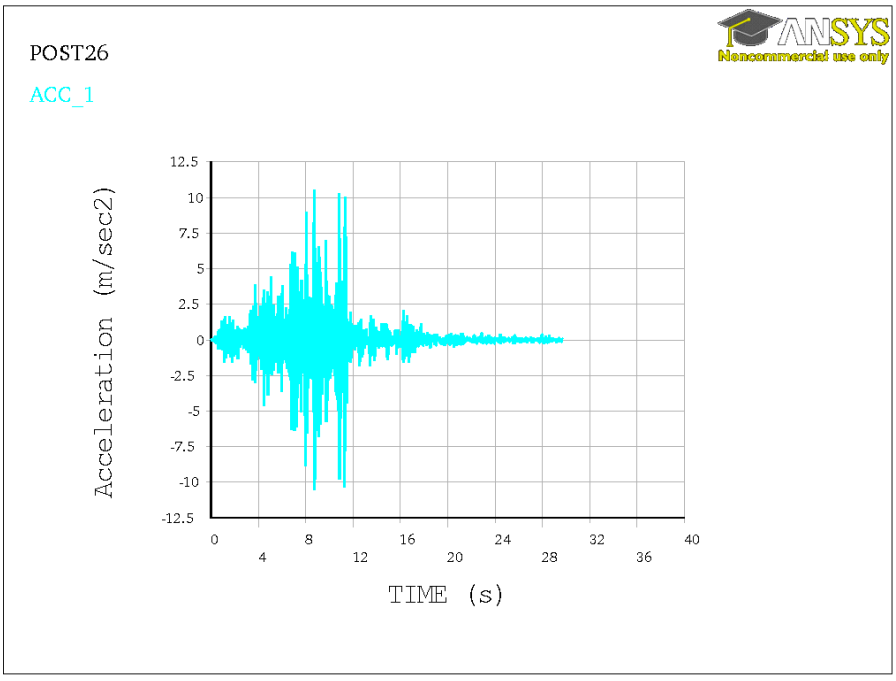

Figure 4.101 Acceleration time history for the frame with link

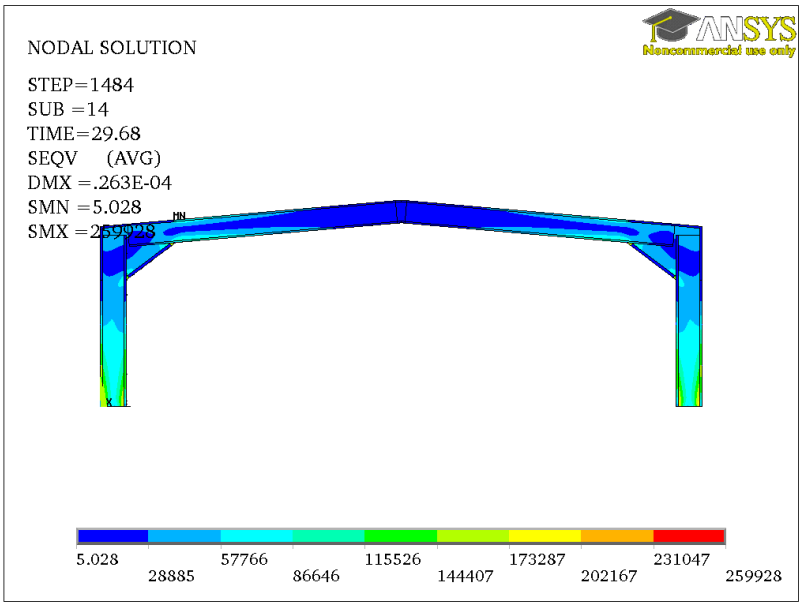

Figure 4.102 Von Mises stress (MPa) for frame without link

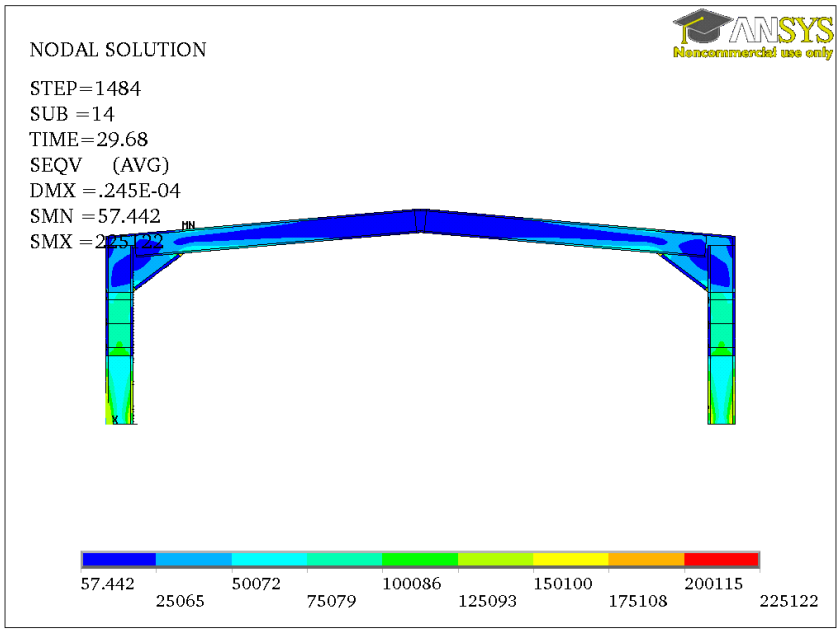

Figure 4.103 Von Mises stress (MPa) for frame with link

Result for Duzce Earthquake

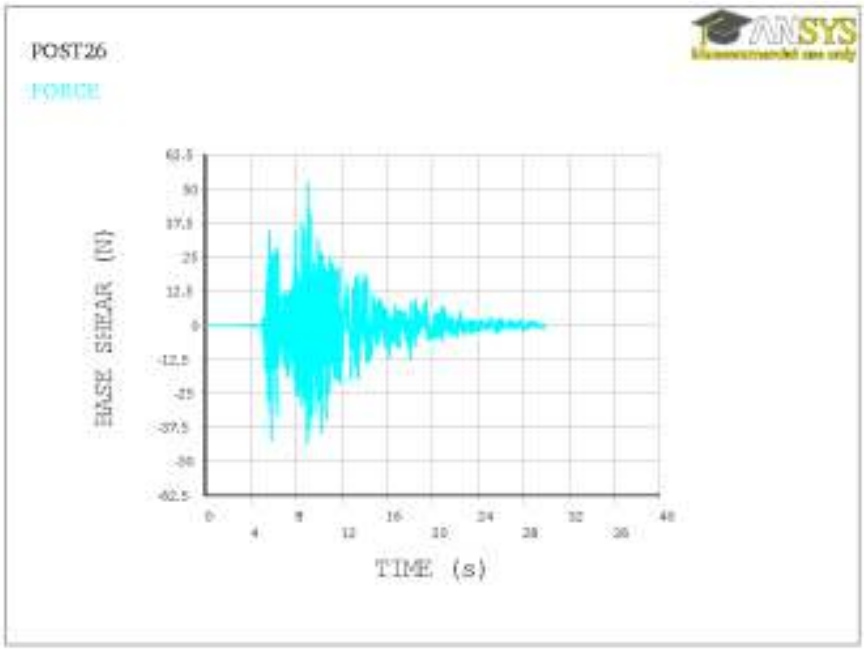

Figure 4.104 Base shear for frame without link

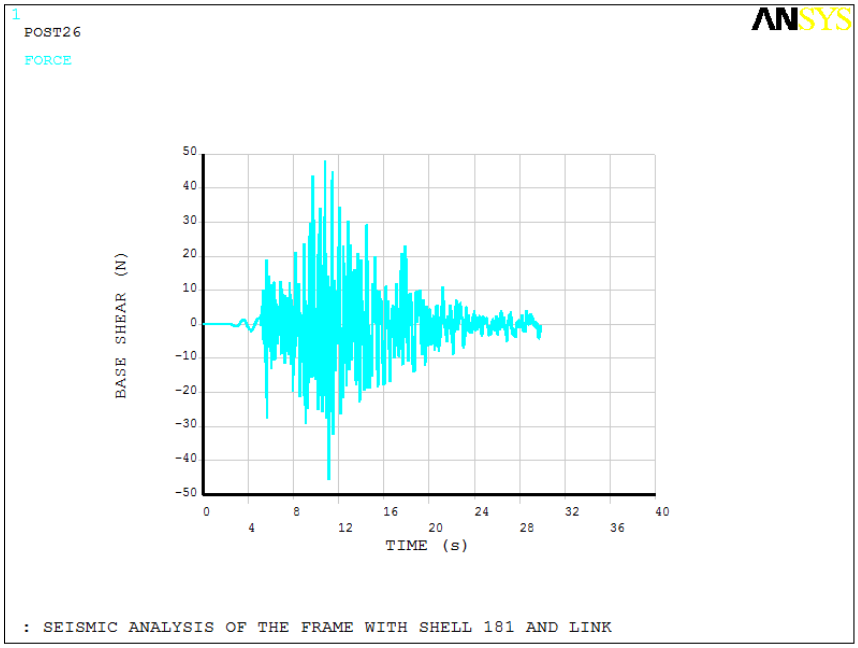

Figure 4.105 Base shear for frame with link

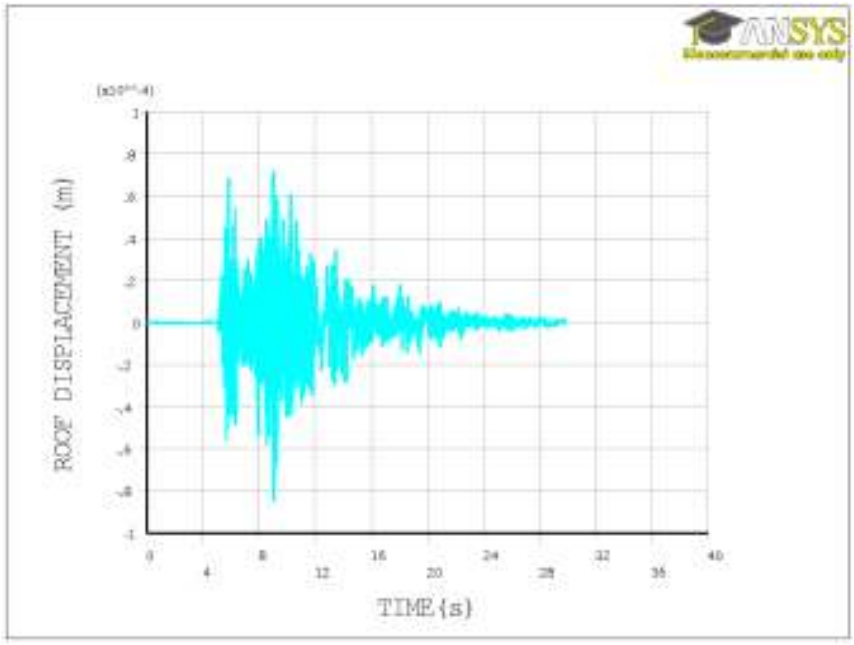

Figure 4.106 Roof displacement for frame without link

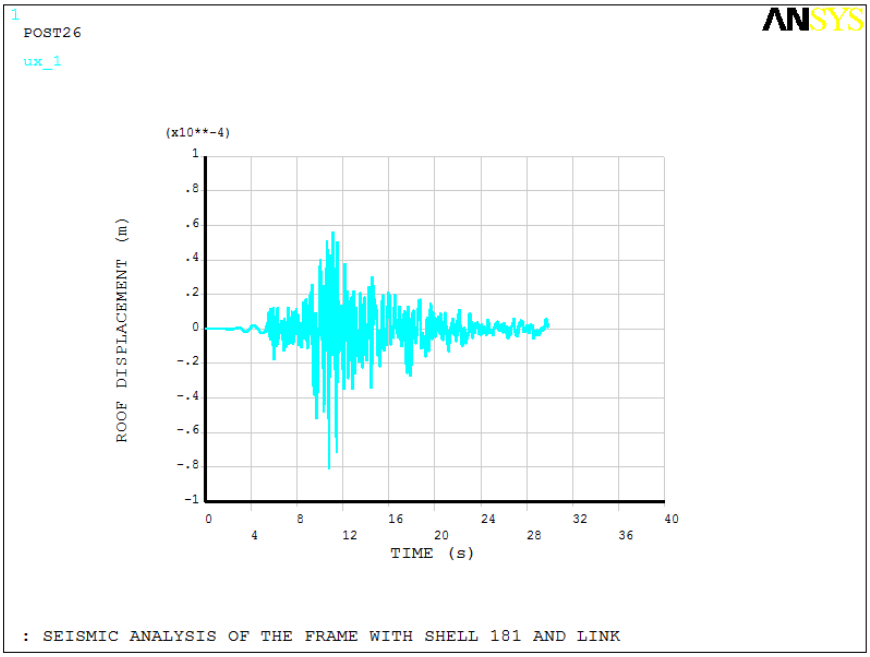

Figure 4.107 Roof displacement for frame with link

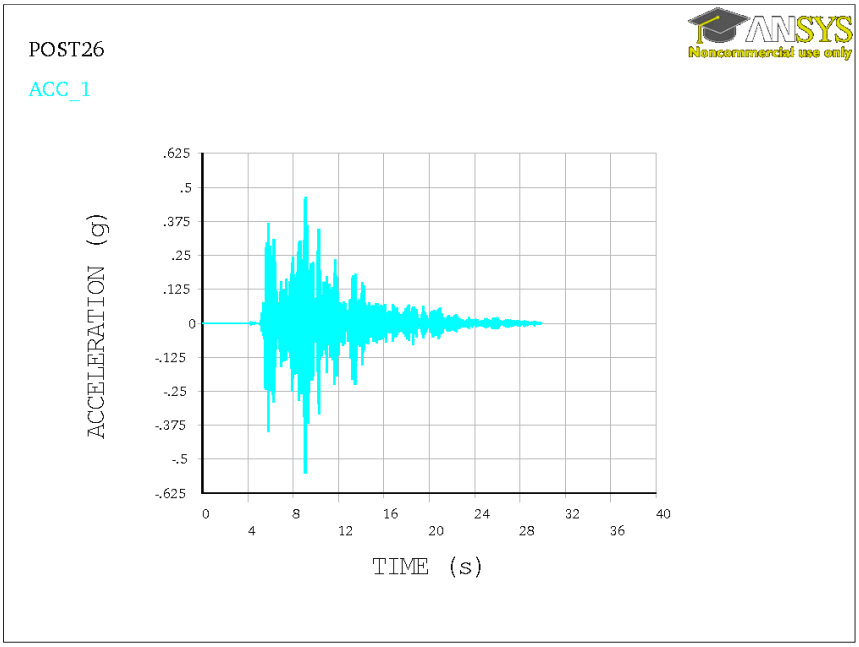

Figure 4.108 Acceleration time history for frame without link

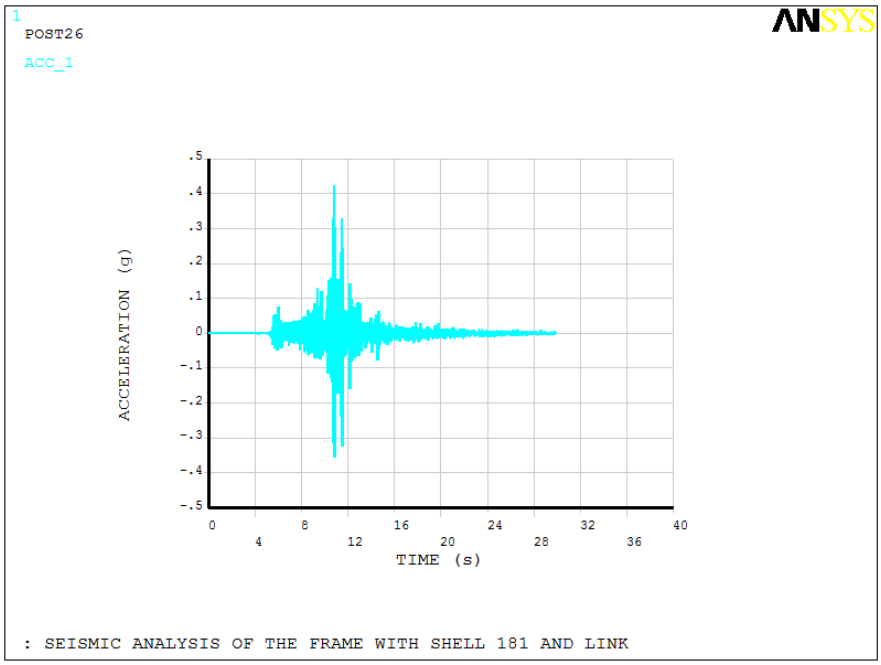

Figure 4.109 Acceleration time history for frame with link

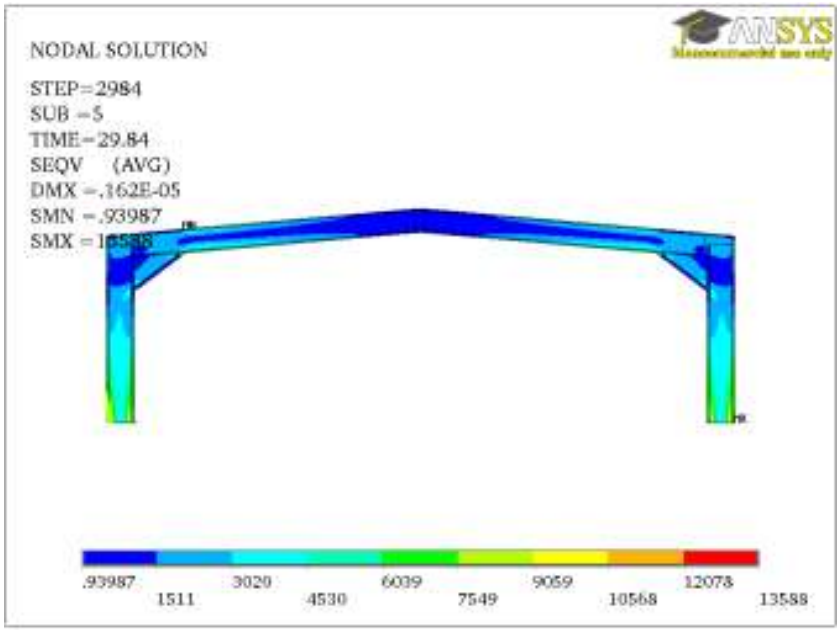

Figure 4.110 Von Mises stress (MPa) for frame without link

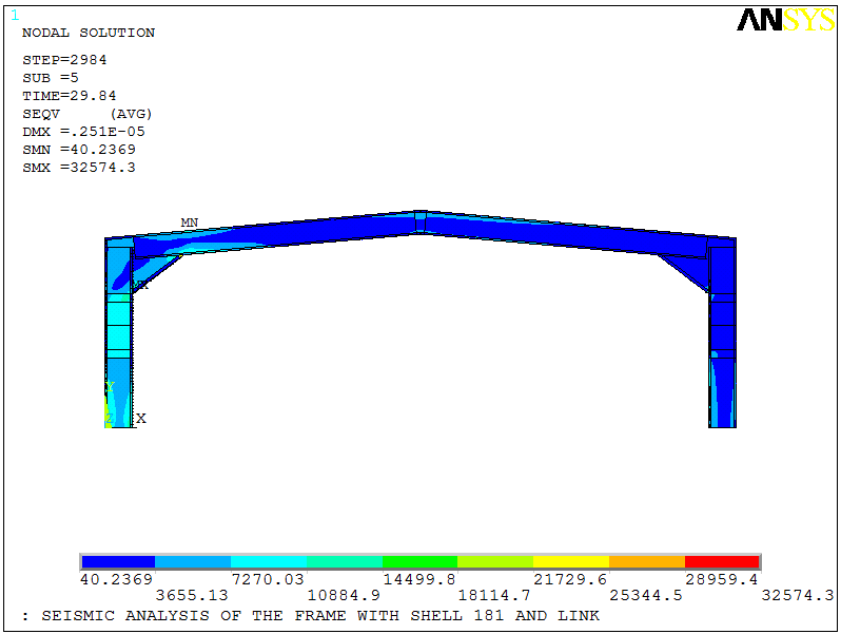

Figure 4.111 Von Mises stress (MPa) for frame with link

Result for Harmonic Excitation

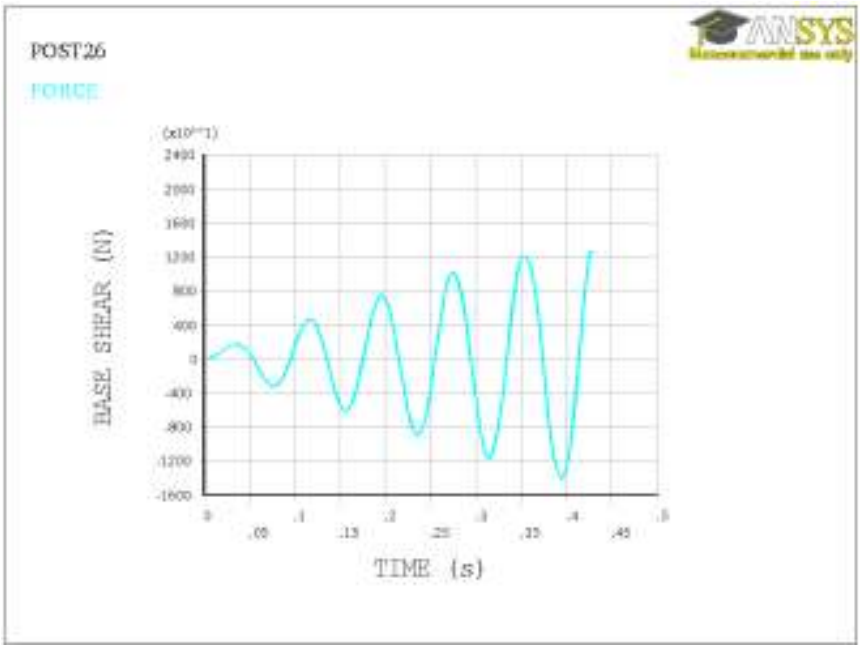

Figure 4.112 Base shear for frame without link

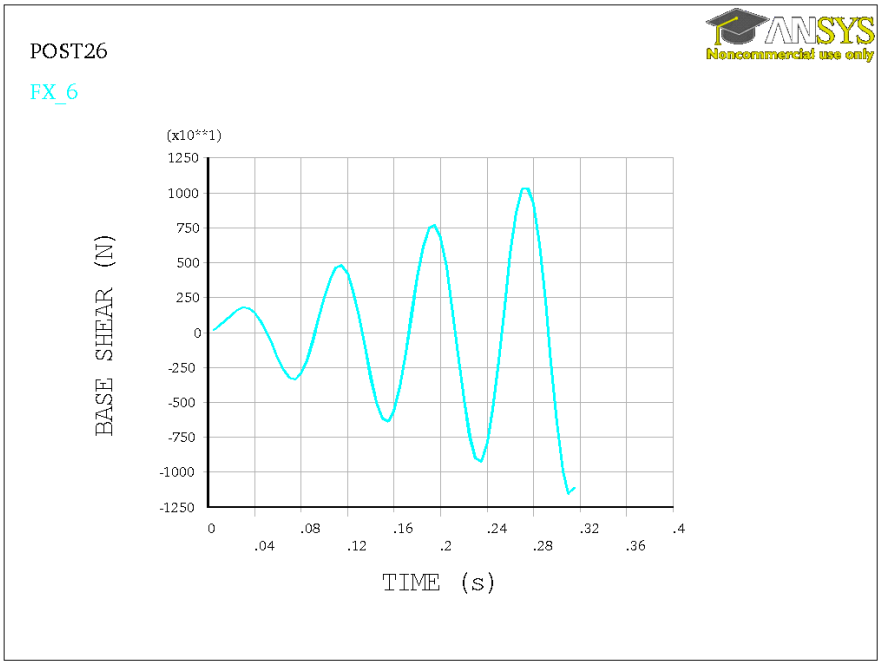

Figure 4.113 Base shear for frame with link

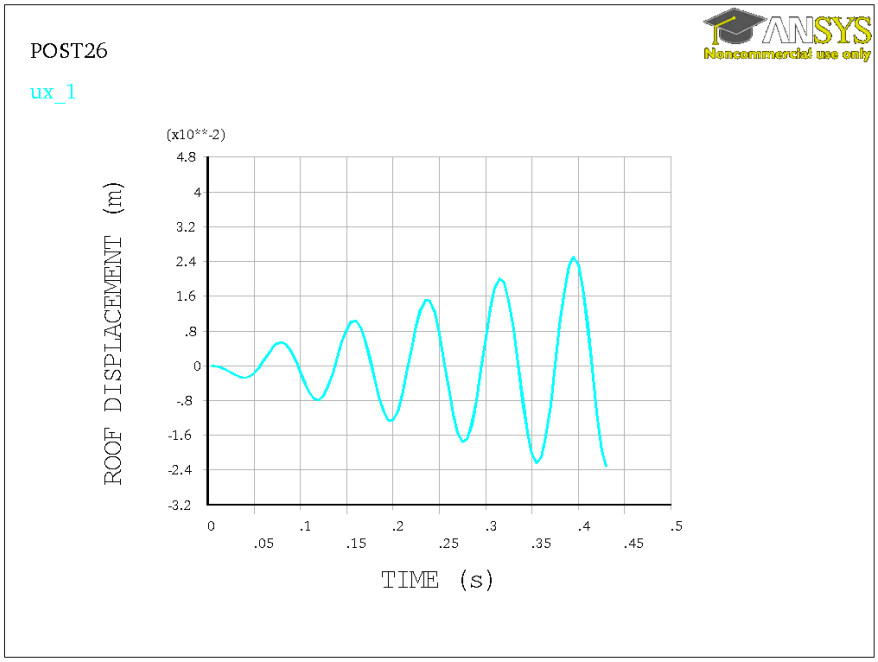

Figure 4.114 Roof displacement for frame without link

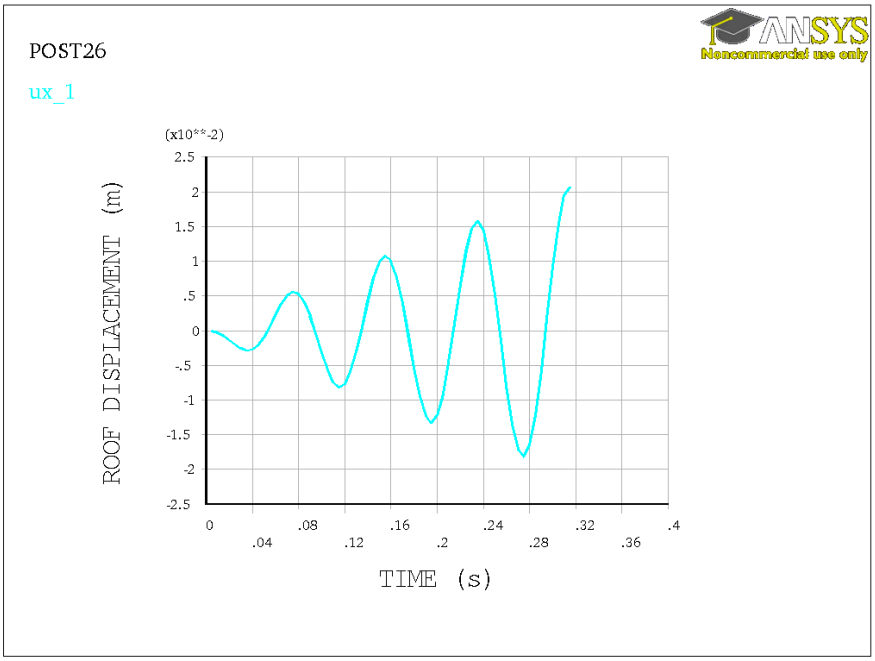

Figure 4.115 Roof displacement for frame with link

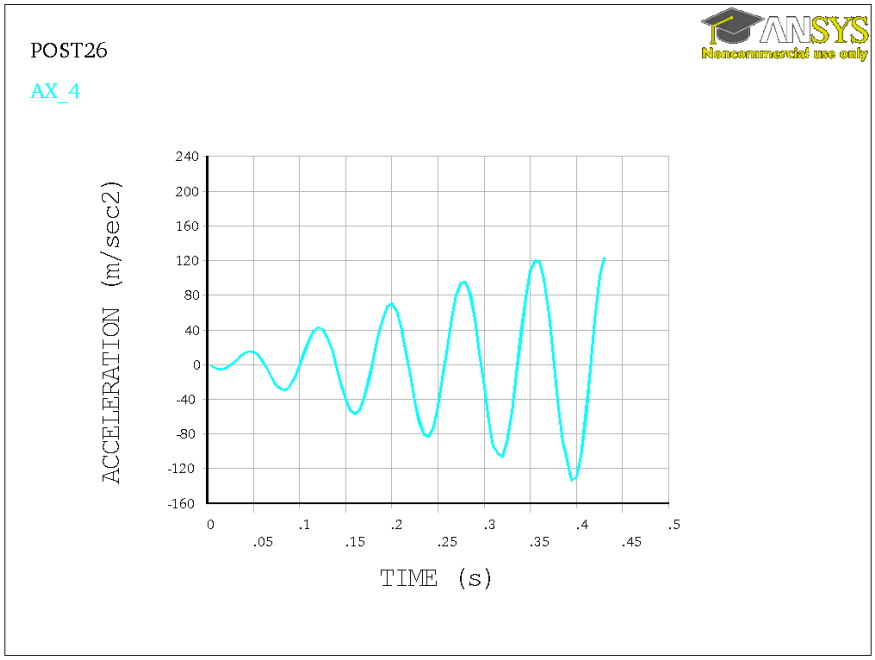

Figure 4.116 Acceleration time history for frame without link

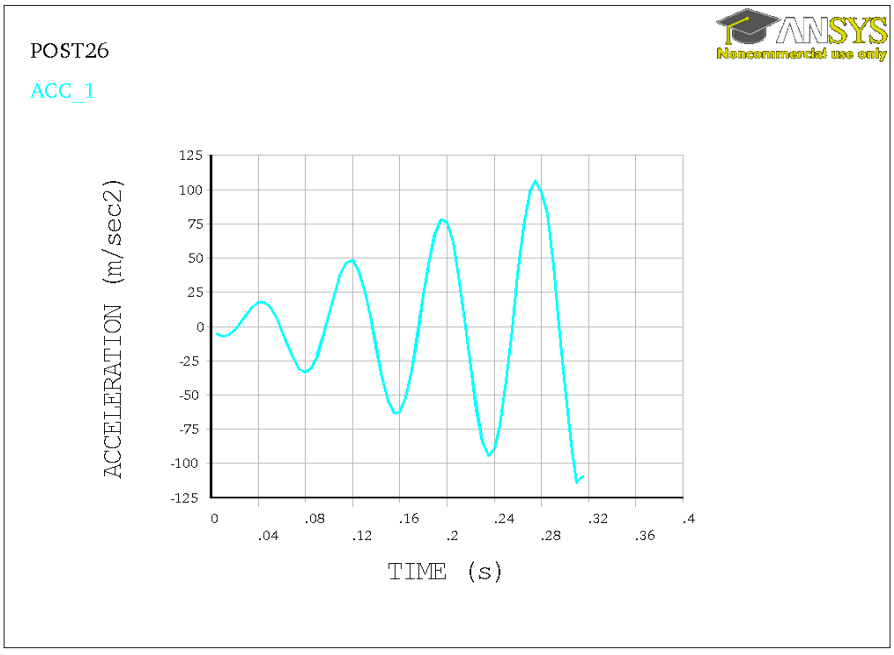

Figure 4.117 Acceleration time history for frame with link

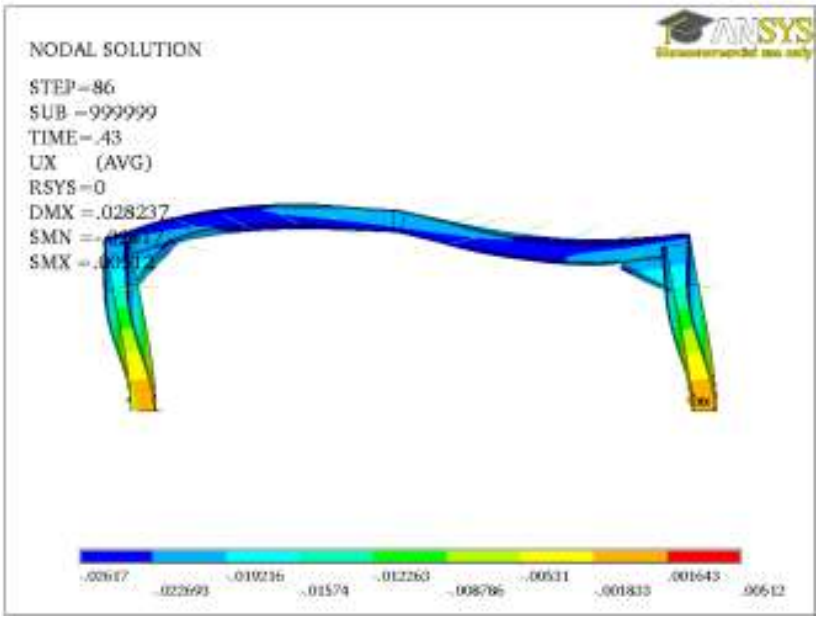

Figure 4.118 Horizontal displacement (m) for frame without link

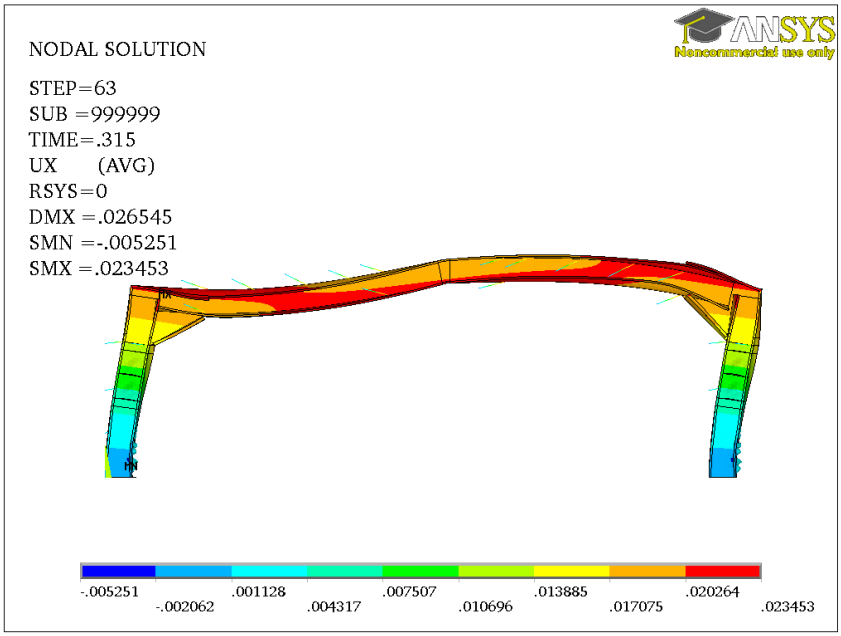

Figure 4.119 Horizontal displacement (m) for frame with link

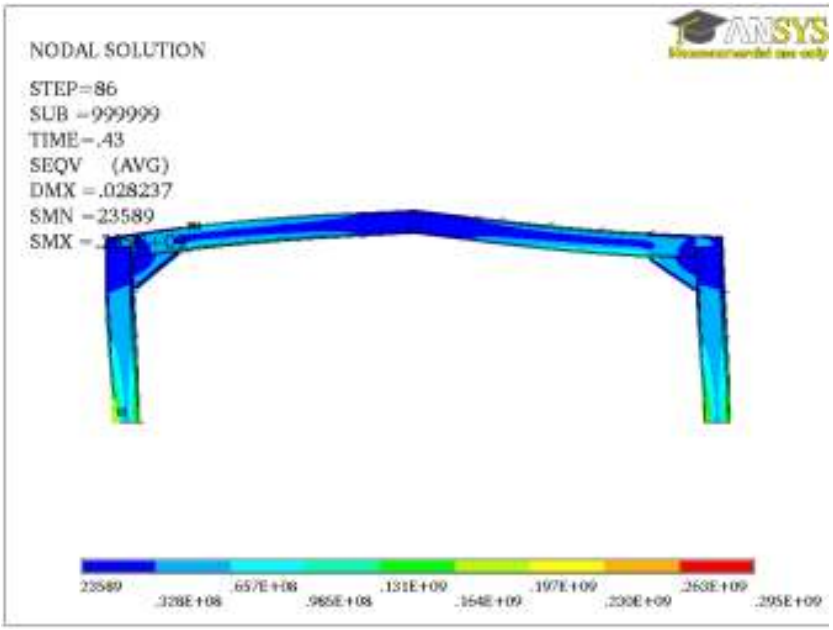

Figure 4.120 Von Mises stress (MPa) for frame without link

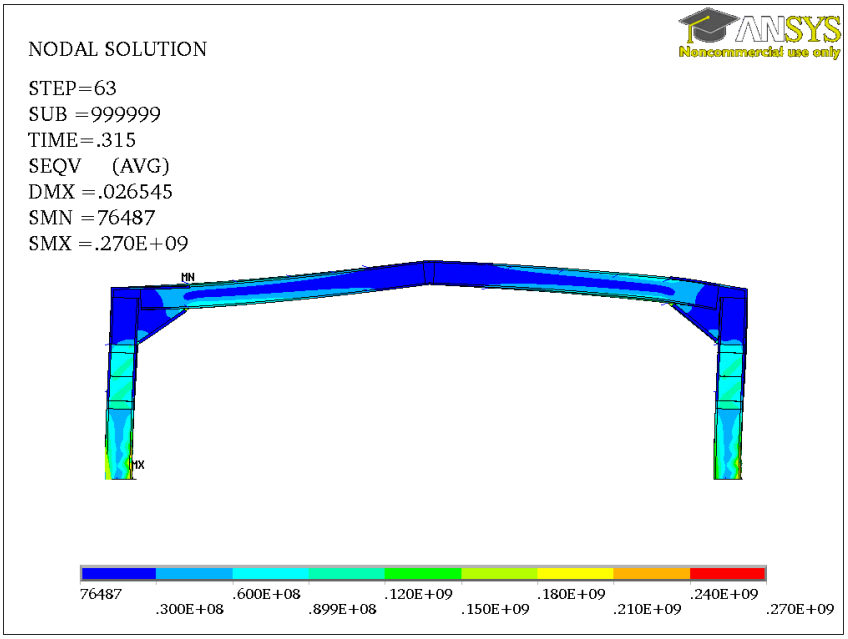

Figure 4.121 Von Mises stress (MPa) for frame with link

4.9 Optimisation of the Seismic Link for a Light Gauge Steel Portal Frame

4.9.1 Introduction

The preliminary nonlinear static analysis of the frame with link for different types of links, and nonlinear dynamic analysis for the frame with the best link resulted in some observations according to parameters that control the efficiency of the link. These observations could be used for the final design of the link for light gauge steel portal frame structure. The observations obtained by the preliminary analysis are summarized as:

a) Link with lipped section or back to back channel section is more effective more than I section link in prevention the buckling of the frame components.
b) Link with flange thickness stockier than flange of the frame members gives good stability for both the link and frame members sections.
c) Thinner link's web is not good for the link even with using stiffeners as this causes the buckling of the link's web in all cases.
d) Providing stiffeners for the link would be effective for good performance of the link and frame but they are not enough to protect the slender web from buckling.
e) Increasing of the stiffeners to protect the link web from buckling caused the buckling of the rafter. This is not desirable with the objectives of the research to have undamaged structure members and limiting the failure to the link.
f) Using flexural link with length 2500 mm is not effective to improve the seismic performance of the structure as there is significant yielding at the bottom of the column and this span should be increased.
g) Using of two links at each end of the columns to protect the frame members and achieve the expected plastic hinges at upper and lower of the column is not working. And would be effective to have the link to cover the complete column to protect the structure. As flexural link or long link, the link span controlled by equation (3.42).
h) The best link was better in the preliminary static analysis but not in the dynamic analysis.

i) An artificial earthquake (increasing harmonic excitation) is effective for the purpose of testing the survivability of the structure in this work. This was tuned to the elastic natural period of each different structural concept and was considered a better basis for the comparison of different concepts than using specific earthquakes. Use of such records (real records) for input motion does not always produce intense structural oscillation, where independent earthquake records generally have differences in the energy content at different frequencies.

4.9.2 Design approach

The design method followed for the structural design of the slender portal frame is:

1) The frame rafters would be "low dissipative structure", as classified according to EN 1998-1 (2004) but the dissipative column zone component parts will play the role of seismic protection devices for these portal frame rafter members. The frame rafter design will remain elastic and not buckle during the earthquake, because the applied moments is limited by the capacity of the column links.
2) The column dissipative zones have the capability to resist earthquake actions through inelastic behaviour (see Figure 4.122). These column zones are designed to yield before the frame rafter members buckle and to protect the frame components from buckling which is potentially a problem with the use of light gauge steel material.

4.9.3 Final design of the link

From the observations and assessment of the frame with the link, the link is very controllable since it has many design parameters that should be considered in order to optimize the use of this link in dissipating energy in thin gauge steel portal frame structures.

According to these observations obtained by the preliminary analysis of the structure with link above and according to section 3.12 which outlined the topics for the ductile link design, this section covers the design rules and the final design for the

link that will be effective for light gauge steel portal frame structure. The design rules for the link are detailed as following:

a) The link will be used for the frame structure as seismic performance improvement device, is the link with back to back lipped channel section as it was shown its effectiveness against buckling to be a link section.
b) Both the flange and the web thickness for the link must be stockier than the thickness for the flange and web of the frame members.
c) The length of the link has to have length as flexural link according to section 3.12.5 and equation (3.42).
d) The link should protect the bottom and top of the column, in order to achieve the plastic mechanism and hinges in the column whilst keeping the frame members undamaged. It is simplest to use the link section for the whole column length.
e) The limitation of width/thickness ratio and height/thickness ratio must be applied according to section 3.12.4 of this thesis for cold formed sections.
f) The section used for the link should be section with moment resistance less than 2/3 0r (0.7) the buckling moment resistance of the rafter section to prevent the buckling of the rafter before the yielding (or before the maximum post yielding moment) in the column link.

4.9.3.1 Design procedure and detailed description of the link:

According to the above rules the link was designed. The design procedure was carried out for the link as:

1) The section was chosen as back to back channel cold formed steel section.
2) The buckling moment resistance of the rafter was found 189 KN m. The section for the link was chosen with moment resistance about 0.7 the buckling moment resistance of the rafter.
3) The slenderness limiting was applied according to section 3.12.4 of this thesis with some modification as recommended by Wilkinson and Hancock (1997) to use a straight line interaction formula for classification of sections in

bending for both web and flange. The section was chosen to be compact section to prevent buckling and to achieve the yielding of the link whilst protecting the slender components of the structure. Accordingly these values were used for slenderness limiting: b/t= 15 and d/t= 30 for flange and web thickness for the link section.

4) The link length is taken as long link according to section 3.12.5 to dissipate energy though flexural strains. Also it was found from the preliminary analysis that the link should cover the complete column to have plastic hinges at upper and lower of the column when the link yields and the structure fails (see Figure 4.122). This resulted in length equal 4220 mm for the link in this study as it is equal to the whole column length under the knee connection.
5) The yield strength value for the link was chosen according to section 3.12.6, resulted in link with yield strength equal to 190 MPa to have moment resistance about 0.7 the buckling resistance of the rafter.
6) No stiffeners were used as the thickness of the flange and the web for the link was limited to slenderness limit.

The final link for the frame structure is back to back channel lipped section with depth 350mm and width 90mm, yield strength equal to 190 MPa and moment resistance equal to 149 KN m about 0.78 the buckling resistance of the rafter (see Figure 4.123).

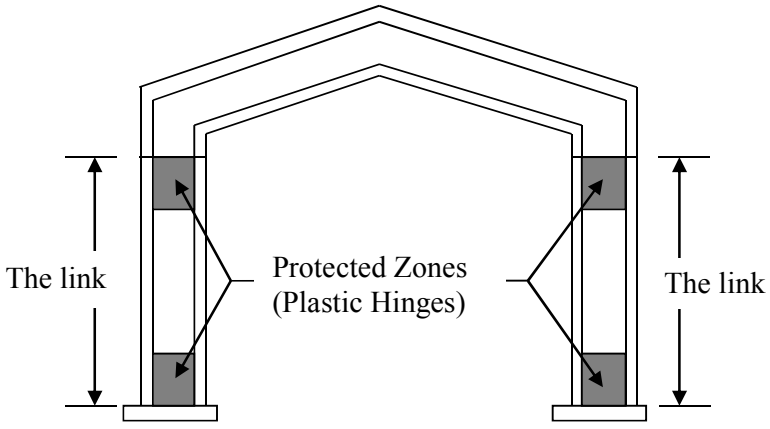

Figure 4.122 The frame with the links

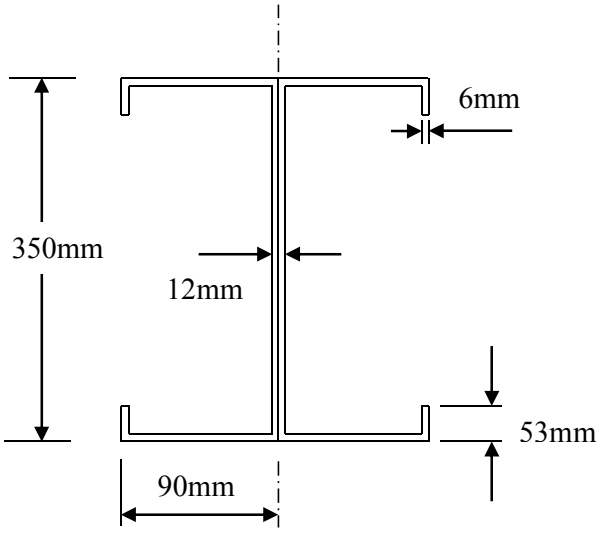

Figure 4.123 The final seismic link section

4.9.3.2 Link connection to the frame members (knee connection)

In this section the connection between the link and the frame members is presented. The proposed connections are bolted connections. The link (column) connects to the frame member as part of the knee connection through cold formed steel end plate using welded bracket elements (S355: Fy = 355 N/mm2) and M20 grade 8.8 bolts (see Figure 4.124). For simplicity and according to Dubina et al (2010) work which detailed in section 2.5.3.3, this connection was modelled in the finite element model as rigid. The finite models in Dubina et al (2010) had showed a good agreement with experimental tests. But to verify that the link connection will perform well in the extreme earthquake conditions, hand calculations were carried out. The moment resistance of the connection is determined and compared with the moment resistance of the frame section to show that the connection has moment resistance greater than the frame section and the connection will perform well during earthquakes.

The connecting bolts are subjected to shear and their design was carried out according to EN 1993 part 1-8 (2005) assuming the rotation of the joint around the centroid of the bolt group and a linear distribution of forces in each bolt, proportional to their distance from the centre of rotation.

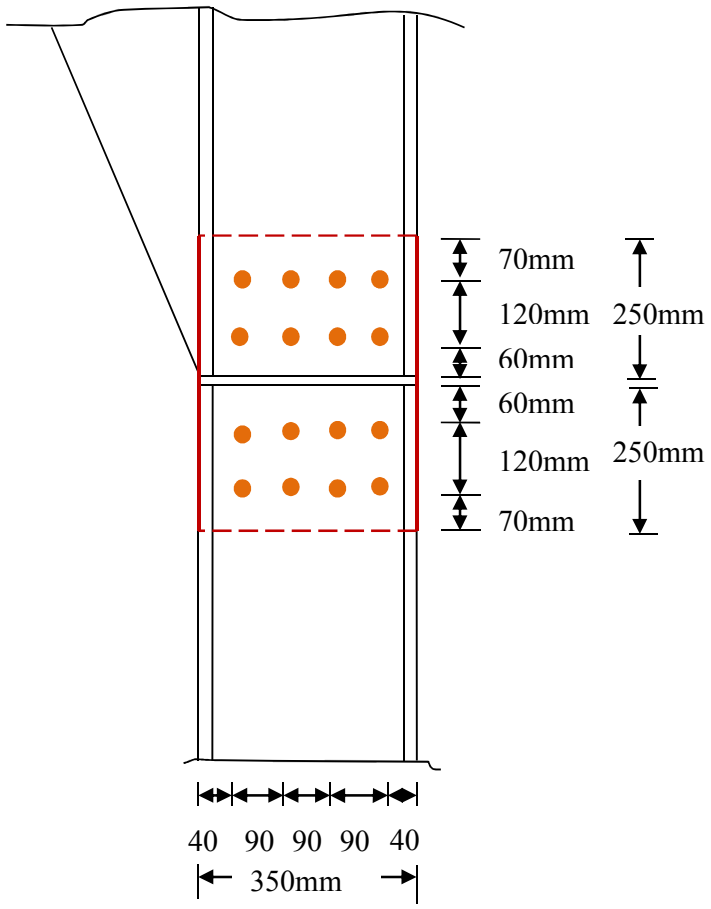

Figure 4.124 Details of the link connection with the frame member

The moment resistance of the bolted connection was determined using the component method. The component method is a general procedure for design of strength and stiffness of joints in building frames, and is implemented in EN1993-1-8 (2005) as was explained in section 2.5.5.2 of this thesis. Always determination of the moment resistance of bolted connection is done using a two-steps procedure. In the first step, only components related to bolt resistance are included in order to determine the moment resistance of the bolted connection $M^{b}_{C;Rd}$. In a second step, the connection moment resistance is obtained as the minimum of the moment of resistance of the bolted connection $M^{b}_{C;Rd}$ and the resistance of the connected cold-formed member $M^{column}_{,Rd}$ as:

$$M_{c,Rd} = \min\left(M^{b}{}_{C,Rd}, M^{column}{}_{,Rd}\right) \qquad \text{Equation 4.7}$$

But here in this case we need to determine the moment resistance of the connection and compare it with the moment resistance of the connected member to show that no failure will happen to the link connection before the yielding of the link (the column).

Moment resistance of the bolted connection was determined as EN 1993 part1-8 (2005):

$$M^{b}{}_{C,Rd} = \sum_{r} F_{tr,Rd} h_r \qquad \text{Equation 4.8}$$

Where $F_{tr,Rd}$ is the effective tension resistance of bolt row r (minimum value of components related to bolt row r); hr is the distance between bolt row r and the centre of compression.

Moment resistance of the cold-formed member $M^{column}{}_{,Rd}$ was determined using measured geometrical and mechanical characteristics, and effective cross-section modulus. Table 4.10 presents resistance of bolt rows. The weakest component of bolts is bearing on bracket. Moment resistance of the bolted connection $M^{b}{}_{C;Rd}$ determined by the component method amounted to 196 kNm, which was larger than the moment resistance of the cold-formed member $M^{column}{}_{,Rd}$, amounting 149 kNm. Therefore, this type of connection is a full strength one and will perform well during earthquakes.

Table 4.10 Resistance of connection components

Bolt row	Component			Bolt-row resistance, $F_{tr\text{-}Rd}$ (KN)
	Bolts in shear (KN)	Bolts in bearing on cold formed member (KN)	Bolts in bearing on the bracket (KN)	
1	482.3	480	280	280
2	482.3	480	280	280
3	482.3	480	280	280
4	482.3	480	280	280

4.9.4 Detailed finite element analysis of the frame with the optimised link

4.9.4.1 Introduction

In the previous sections, the portal frame with link was preliminarily tested using the finite element software ANSYS. The steel elements for steel cold formed section were modelled using shell elements and the material is introduced by means of bilinear isotropic elastic-perfectly plastic model during the whole preliminary analyses. Large-displacement analysis was conducted.

In this section, a detailed finite element analysis was conducted to determine the actual behaviour of the optimised link. The steel elements were modelled using quadrilateral shell elements. The inelastic behaviour of these elements was considered using the von Mises yield criterion. The large displacement and p-delta effects were considered.

4.9.4.2 Steel elements material modelling

4.9.4.2.1 Stress-Strain Curve for Steel Elements

Typical stress-strain curve for steel under tension is shown in Figure 4.125. The same curve is obtained under compression if support is provided to prevent buckling. The stress is defined as the load per original cross-sectional area of the steel specimen. This stress is known as the engineering stress or the nominal stress. Similarly, the strain is obtained by dividing the total elongation (or contraction in compression test) over the original length. This strain is known as the nominal strain. The relationship between the stress and strain is proportional up to a point, known as the yielding point, before which the steel behaves linearly elastic. The ratio between the stress and strain in the elastic part is known as the modulus of elasticity or Young's modulus, E, which equals approximately 210E03 MPa for structural steels. After yielding, the strain increases up to 15-20 times the maximum elastic strain while the stress remains constant. This part of the curve is known as the plastic range or yield plateau. For larger strains, the stress increases with the increase in strains but with a much smaller rate than the original elastic one. The increase in stress is known as strain hardening. This stress increase continues up to the maximum stress, after

which the stress falls off with the increase in the strain until the failure occurs (Ibrahim, 2005).

4.9.4.2.2 The von Mises yield criterion

The von Mises yield surface allows isotropic yielding. The uniaxial yield stress can be obtained in terms of the three principal stresses as:

$$\sigma_y^{\,2} = \frac{1}{2}\left[(\sigma_1 - \sigma_2)^2 + (\sigma_2 - \sigma_3)^2 + (\sigma_3 - \sigma_1)^2\right] \qquad \text{Equation 4.9}$$

Where σ_1, σ_2 and σ_3 are the tensile or compressive stresses that act in the three principal directions and σ_y is the yield stress. The principal stresses act in the three mutually perpendicular planes that have zero shear stress. The von Mises yield surface assumes that the yielding is independent of the equivalent stress (Ibrahim, 2005).

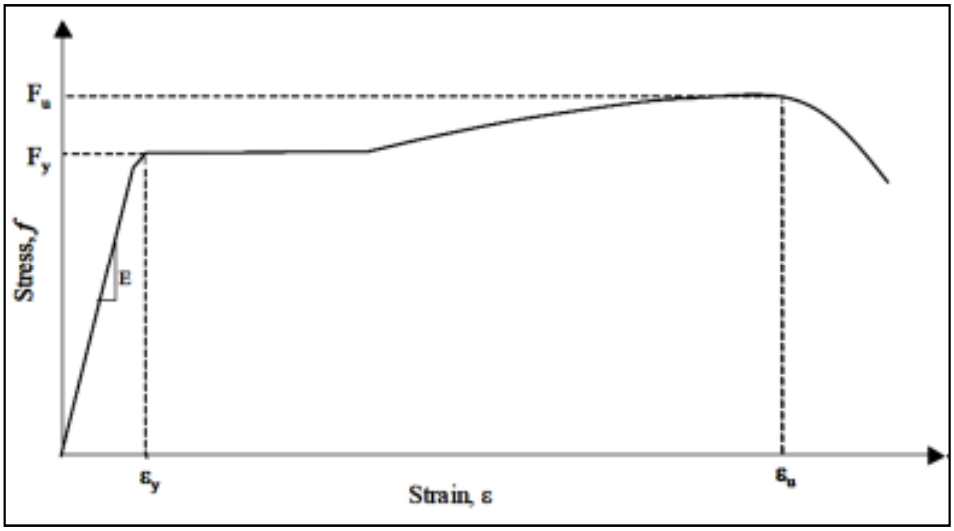

Figure 4.125 Typical stress-strain curve for the steel (Ibrahim, 2005)

4.9.4.2.3 Modelling the inelastic behaviour of the steel

One of the advantages of modelling the link in ANSYS is the availability of considering the inelastic behaviour of the steel elements. In order to do so, the elastic-plastic behaviour of steel was considered. For many engineering applications, the use of engineering stress and strain values (the nominal stress and strain) for material stress-strain curves will be sufficient for obtaining correct answers in a plasticity analysis. Engineering stress and strain are commonly represented by these equations (DRD, 2010):

$$\varepsilon = \frac{\Delta l}{l_0} \qquad \sigma = \frac{F}{A} \qquad \text{Equation 4.10}$$

However, engineering strain is a small strain measure which is invalid once the strain in the model is no longer 'small' (approximately 5%). True strain, which is a nonlinear strain measure that is dependent upon the final length of the model, is used for large strain simulations. True stress and strain are commonly represented by these equations (DRD, 2010):

$$\varepsilon = \ln\frac{l}{l_0} \qquad \tau = \frac{F}{A} \qquad \text{Equation 4.11}$$

To model the plasticity in ANSYS, true stress and true strain (also called log strain) must be used instead of the nominal stress and strain.
The engineering strain is defined as (Ibrahim, 2005):

$$\varepsilon_{Eng} = \frac{l - l_0}{l_0} = \frac{l}{l_0} - 1 \qquad \text{Equation 4.12}$$

Accordingly, true strain, ε, can be obtained from (Ibrahim, 2005):

$$\varepsilon = \ln\frac{l}{l_0} = \ln\left(1 + \varepsilon_{Eng}\right) \qquad \text{Equation 4.13}$$

Assuming the incompressibility of the material, its volume remains constant (Ibrahim, 2005).

$$l_0 A_0 = lA \qquad \text{Equation 4.14}$$

So, the actual area, A, is calculated from (Ibrahim, 2005):

$$A = \frac{A_0 l_0}{l} \qquad \text{Equation 4.15}$$

Now, the relation between the true stress and nominal stress is defined as (Ibrahim, 2005)

$$\sigma = \frac{F}{A} = \frac{Fl}{A_0 l_0} = \sigma_{Eng} \frac{l}{l_0} \qquad \text{Equation 4.16}$$

$$\sigma = \sigma_{Eng}\left(1 + \varepsilon_{Eng}\right) \qquad \text{Equation 4.17}$$

The true strain calculated from the aforementioned equations is a combination of elastic strain and plastic strain. According the plastic strain can be obtained from the following equation (Ibrahim, 2005):

$$\varepsilon_{pl} = \varepsilon_t - \varepsilon_{el} = \varepsilon_t - \frac{\sigma}{E} \qquad \text{Equation 4.18}$$

Where ε_{pl} is the true plastic strain, ε_t is the true total strain, σ is the true stress, and E is the modulus of elasticity (Ibrahim, 2005).

As there is no material test data available for the cold formed section used in this model and as was explained in section 3.12.6, use was made for bilinear model in ANSYS with two variables, the elastic modulus and the tangent modulus. To model the steel hardening, an isotropic hardening model was used. This model assumes that the centre of the yield surface remains stationary in the stress space however the size of the yield surface changes uniformly in all directions such that the yield stress varies according to the plastic strains. This model is suitable for dynamic problems with large deformations.

4.9.4.2.4 Geometric modelling of the link

Reduced-integration elements use one fewer integration point in each direction than the fully integration elements. For linear elements, using the reduced integration causes a numerical problem called hourglassing. To explain this problem, consider a

linear reduced-integration element is subjected to bending moment, M (Ibrahim, 2005). An expected deformation mode is shown in Figure 4.126. The dotted lines remain unchanged in the length after deformation. The angle between these lines is unchanged as well (Ibrahim, 2005). Accordingly, no stress is developed at the single integration point. This means that no stiffness in the element can resist such type of deformations. For coarse meshes with these element types, this deformation mode can propagate through the entire mesh causing poor results (Ibrahim, 2005). ANSYS uses an artificial hourglass stiffness to prevent the propagation of these modes. However this affects the accuracy of the results, accordingly, very fine mesh of linear-reduced integration elements is recommended (Sun, 2006). Although quadratic reduced-integration elements also have hourglass modes, it is almost impossible for these modes to propagate in a normal mesh and it is rare problem for sufficiently fine mesh (Ibrahim, 2005). Accordingly, this type of elements is used in the model. The steel elements were modelled as shell 181 elements, which are eight-node quadrilateral reduced integration shell elements. This supports to use fine mesh in the finite element model.

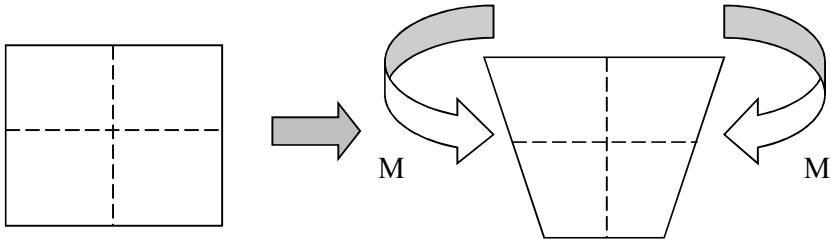

Figure 4.126 Shape change of the reduced integration element after bending

4.9.4.3 Finite elements analysis of the frame with the link

In order to determine the effect of the link on the response of light gauge portal frame structures when subjected to earthquakes action, the frame was examined with the optimised link (see Figure 4.123) was attached to the frame. As first stage the frame structure was analyzed by nonlinear static analysis, applying monotonic lateral displacements until failure, similar to the preliminary analysis of the frame in

section 4.3. After that, a dynamic analysis was carried out using artificial generated records.

The frame was modelled with three-dimensional finite element model using ANSYS software. The frame has the same structural configuration as the model in section 3.11.1. The finite element assemblies for frame members are fundamentally the same as the frame modelling explained in section 3.5.1.2 of this thesis. With the exception for the link materials properties, the model was defined with the same materials properties, type of element, material modelling and finite element idealisation as the last models. The link was modelled with the same element type (SHELL 181) but with different material properties to enhance the development of yielding in the link to absorb the earthquake and protect the slender components of the frame structure. The material properties considered for the link were in section 3.12 and the pervious sections. The finite elements model of the steel frame with the link is shown in Figure 4.127.

In the all-aforementioned analyses, the nonlinear geometry, large displacement and P-δ effects were considered in the nonlinear analyses.

4.9.4.3.1 Nonlinear static analysis results

The frame with the link was analysed applying horizontal displacement until failure. The displacements were applied in the structure on both the knee joints in order to avoid the failure of the node where the displacement was applied. Also the displacements applied at five nodes in the triangular area as explained in section 3.5.1.3. The results are shown in Figure 4.128 to Figure 4.132. From these results for the frame with the link when compared with the results for the frame without link (Figure 3.38, Figure 3.39 and Figure 3.40) the ductility has improved, when the frame failed the total displacement after the elastic zone was about 88 mm with displacement at global yield equal to about 47 mm (see Figure 4.128) while the total displacement after failure for the frame without link was 34mm (Figure 3.40). The structure failed due to the yielding of the links and the plastic hinges occurred at the lower and the upper of the both links. This could be observed by the yielding of the links in Figure 4.130 and Figure 4.132 where the picture was took with the yield strength value of the link (190 MPa). Figure 4.129 and Figure 4.131 show the von

Mises stress for the frame when the picture was took with the value for the von Mises stress with the yield strength value of the frame members. No yielding was observed for the main frame members (the upper part of the column and the rafter). From these results the frame members (excluding the link) did not yield, and they kept undamaged.

Figure 4.127 The finite element model of the frame with the link

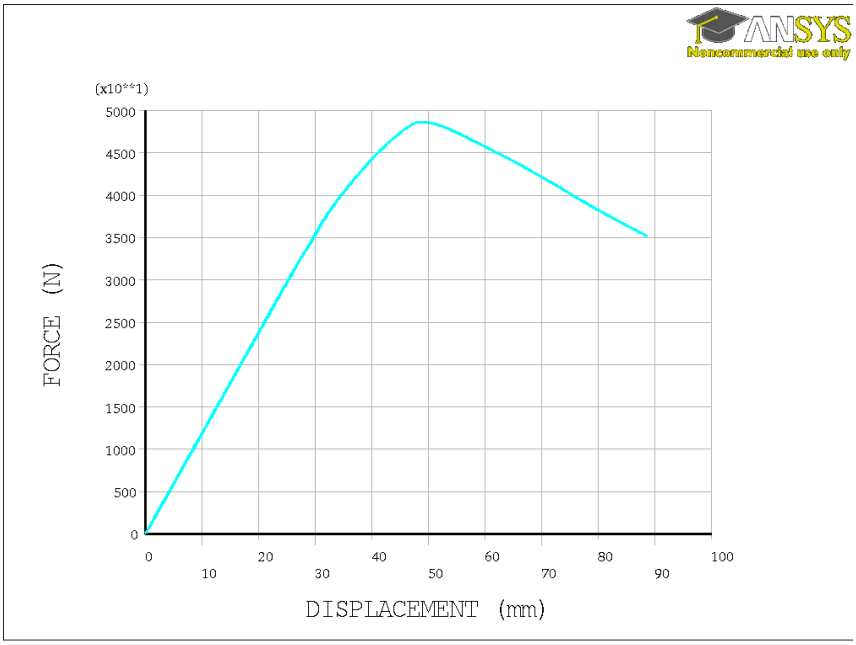

Figure 4.128 Force vs. displacement diagram

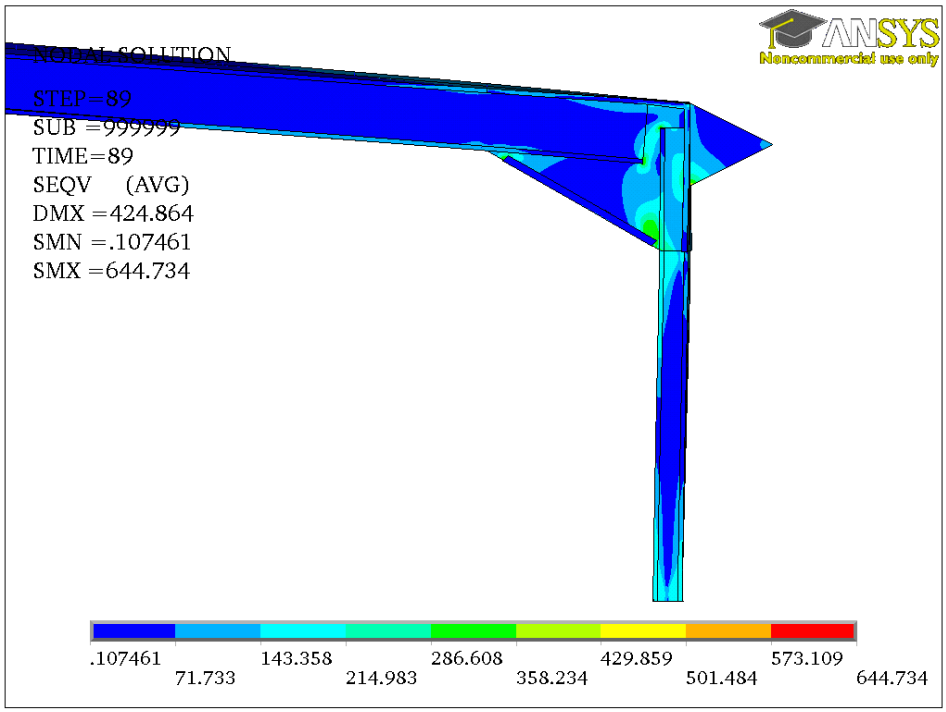

Figure 4.129 Von Mises stress in MPa (yield stress is frame value)

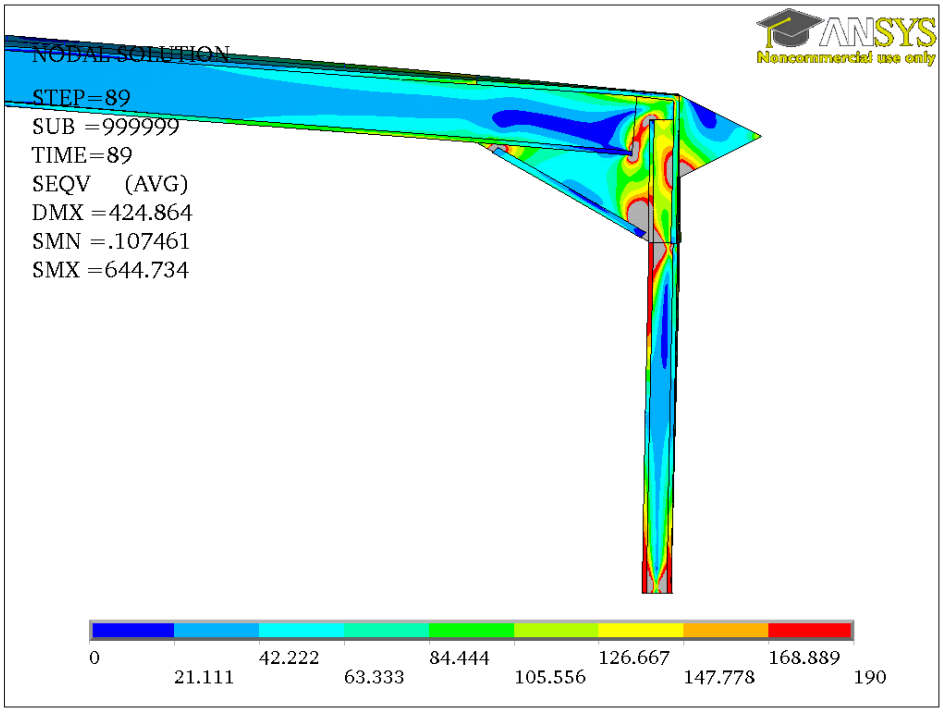

Figure 4.130 Von Mises stress in MPa (yield stress is link value)

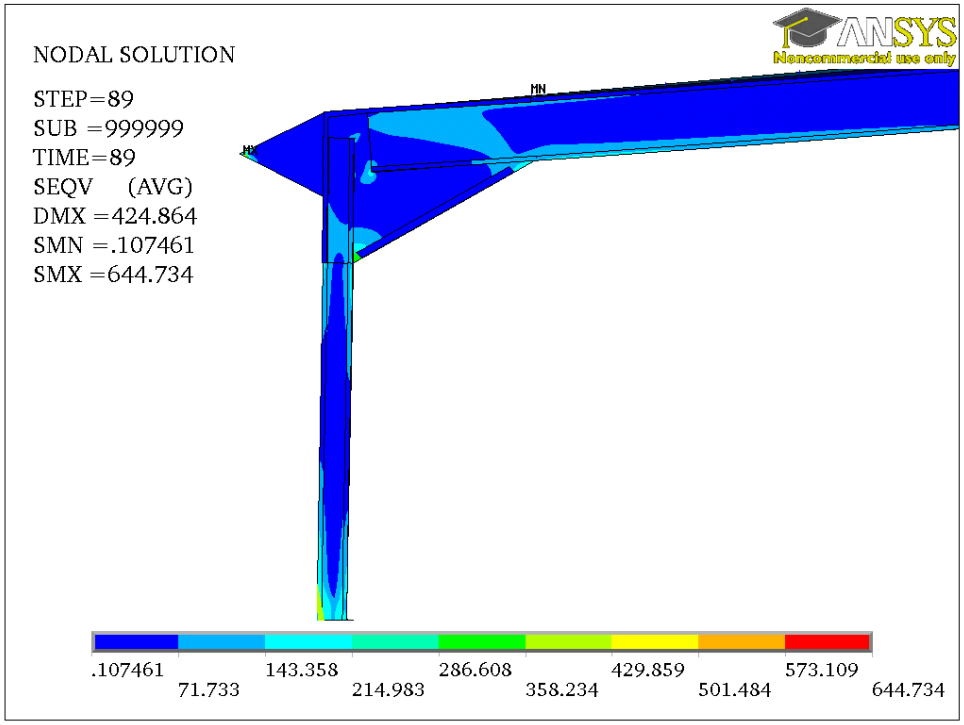

Figure 4.131 Von Mises stress in MPa (yield stress is frame value)

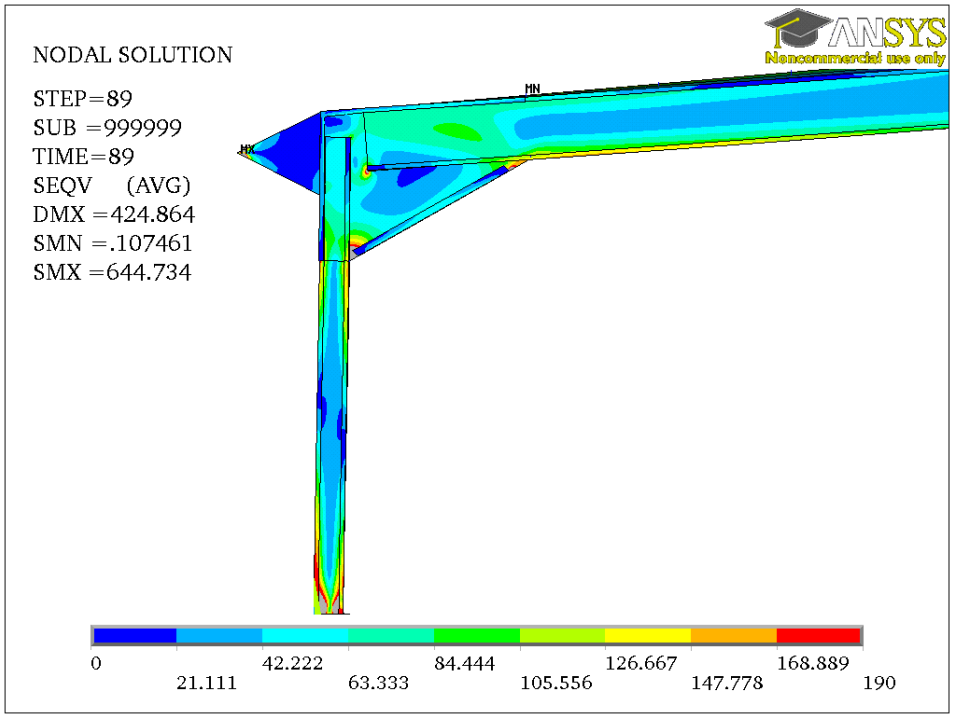

Figure 4.132 Von Mises stress in MPa (yield stress is link value)

4.9.4.3.2 Nonlinear dynamic analysis results

The dynamic analysis was performed by base excitation using artificial records (a modulated sine wave, with increasing amplitude). The harmonic excitation (artificial earthquake) was generated according to the frequency of every structure as the frame without link and with the link are independent structures with different values of frequencies and vibration periods as in Table 4.5 and Table 4.11. The mesh size use in both structures, the frame without link and with the link was 25 mm to have accurate results according to section 4.9.4.2.4 and the validation of the finite element model in appendix A of this thesis.

The results of the frame without link are shown in Figure 4.133 to Figure 4.137 and with the link are shown in Figure 4.138 to Figure 4.145. The frame without link failed due to the failure of the column at the base without achieving yielding in any part of it. The maximum value for the von Mises obtained is 501E4 MPa which is less than the yield strength for the structure members equal to 355E6 MPa (see Figure 4.133 for the right side of the frame and Figure 4.134 for the left side of the frame). The maximum horizontal displacement when the frame structure failed is about 2.2E-4 m, and the base shear is 135 N (see Figure 4.135 and Figure 4.136), these results showed that the frame with the link performs well compared to the frame without link when subjected to earthquake motion.

On the other hand the frame with the link failed after achieved the yielding of the links and the plastic hinges occurred at the lower and the upper of the both links similar to the results of the static analysis for the frame with the link in the previous section. This could be observed by the yielding of the links in Figure 4.139 and Figure 4.141 where the picture was took with the yield strength value of the link (190E6 MPa). Figure 4.138 and Figure 4.140 show the von Mises stress for the frame when the picture for the von Mises stress was took with the value of the frame members. The frame members (excluding the link) did not yield, and they kept undamaged, as no yielding was observed for the main frame members (the upper part of the column and the rafter). The hysteresis curves of the link member for the total strain which include the elastic strain and the plastic strain are shown in Figure 4.142 and Figure 4.143 for strain in the horizontal direction, and vertical direction. These hysteresis curves show the yielding of the links in the protected zone where the

plastic hinges occurred. Also the frame with link achieved good ductility as the total horizontal displacement for the frame when failed is about 60mm after yielding, this was observed from the roof displacement time history diagram in Figure 4.144. Finally the acceleration for the frame with the link was about 110 m/sec^2 (see Figure 4.145) which is greater than the value of the frame without link (8.6 m/sec^2) as the structure with the link resisted the excitation for longer period up to the failure than the frame without link which failed before completing one cycle of amplitude (see Figure 4.136). The structure without link failed at 0.01 sec, about two steps as the time step for the applied generated records is 0.005 sec, for that no sine wave for the time history plots in Figure 4.135, Figure 4.136 and Figure 4.137.

From the results of the analyses under the harmonic excitation, the frame with the link has a good resistance and a good strength compared with the frame without link. From the results it was observed that the frame with the link achieved full yielding for the links resulted in ductile structure with roof displacement 60 mm compared with 0.22 mm for the frame without link. The yielding of the links followed by plastic hinges at the upper and the lower of the columns but the frame whole slender components were undamaged. From these results the objectives of the research were achieved by having ductile light gauge steel portal frame structure and earthquake tolerant structure.

The values of base shear and the roof displacement have been obtained by the dynamic analysis for the frame without link is very small and this could be explained by that the applied acceleration is very big so as to have the failure mode of both of the structures for comparison and this caused the failure by buckling of the base before yielding.

Table 4.11 Frequencies and periods of the frame with purlins and the optimised link using shell element

Mode	Frequency(Fi) cycles/sec	Frequency ω rad/sec	T sec
1	7.7083	48.408124	0.12973
2	10.382	65.19896	0.096321
3	16.967	106.55276	0.058938
4	17.084	107.28752	0.058534
5	18.465	115.9602	0.054157
6	18.532	116.38096	0.053961
7	20.252	127.18256	0.049378
8	20.894	131.21432	0.047861
9	23.193	145.65204	0.043116
10	23.813	149.54564	0.041994
11	24.704	155.14112	0.040479
12	24.753	155.44884	0.040399
13	25.009	157.05652	0.039986
14	25.67	161.2076	0.038956
15	25.78	161.8984	0.03879
16	26.073	163.73844	0.038354
17	27.346	171.73288	0.036568
18	28.683	180.12924	0.034864
19	28.826	181.02728	0.034691
20	29.438	184.87064	0.03397

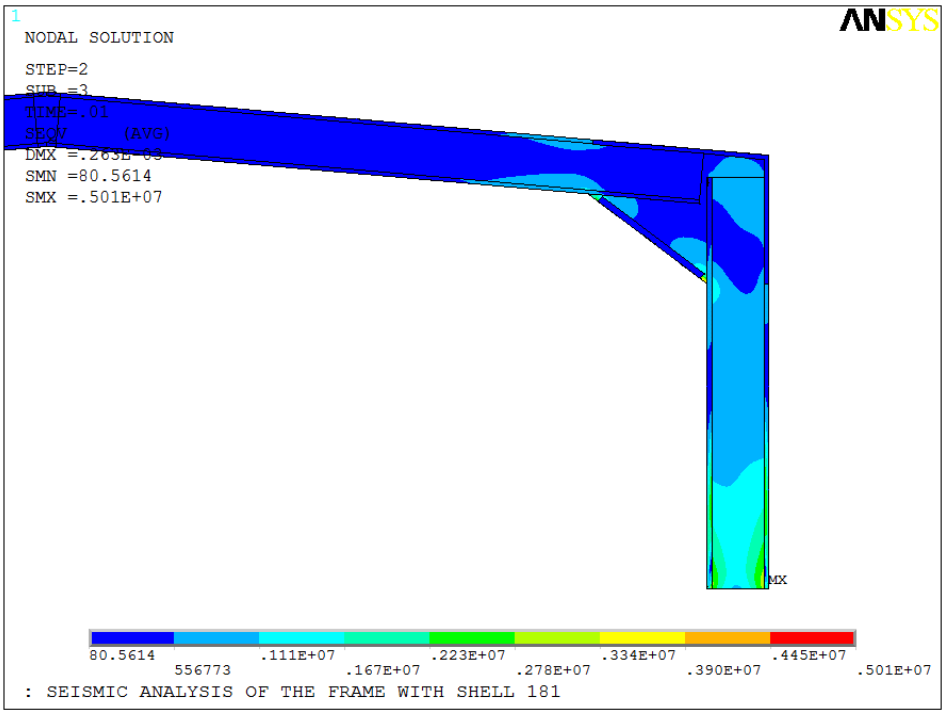

Figure 4.133 Von Mises stress in MPa right

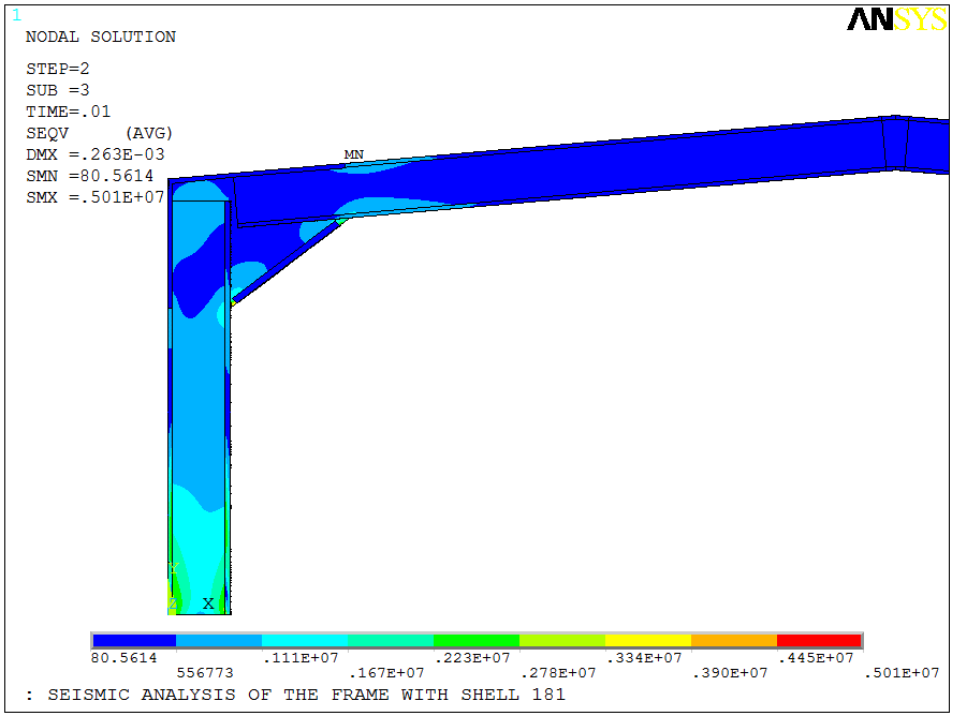

Figure 4.134 Von Mises stress in MPa left

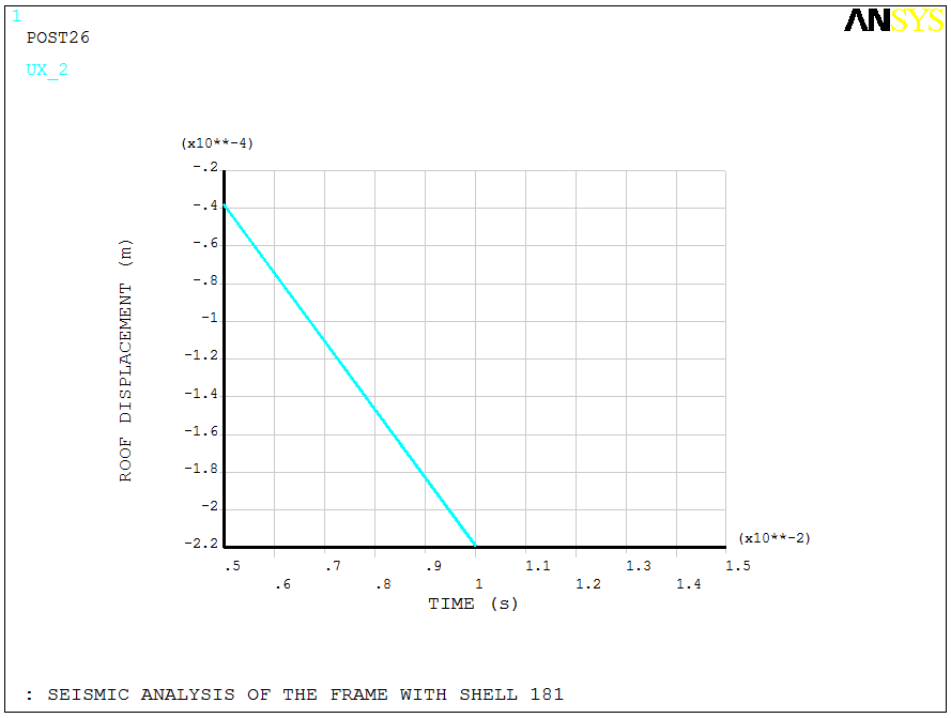

Figure 4.135 Roof displacement time history

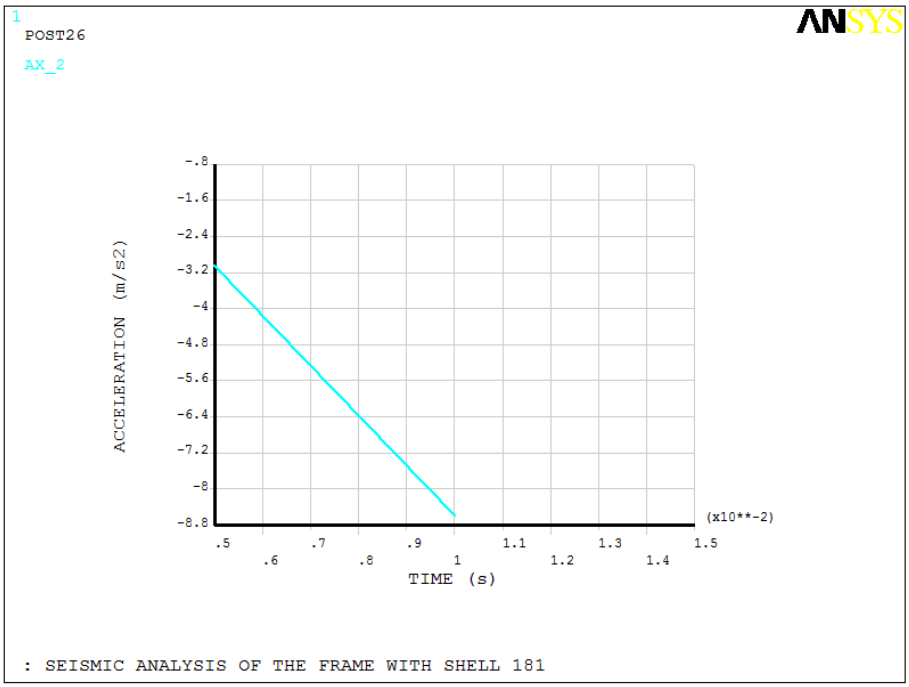

Figure 4.136 Acceleration time history

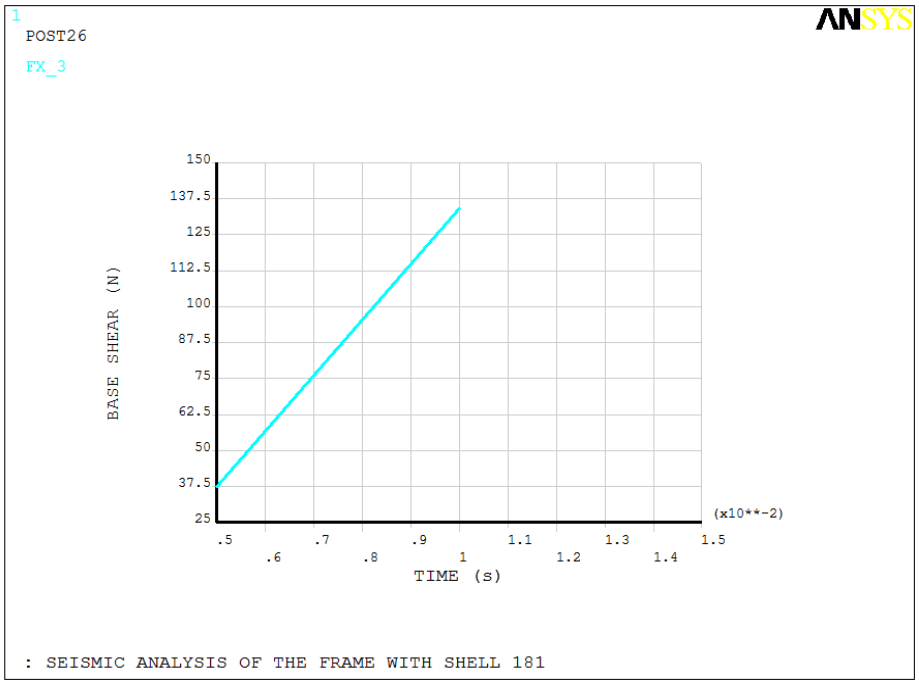

Figure 4.137 Base shear time history

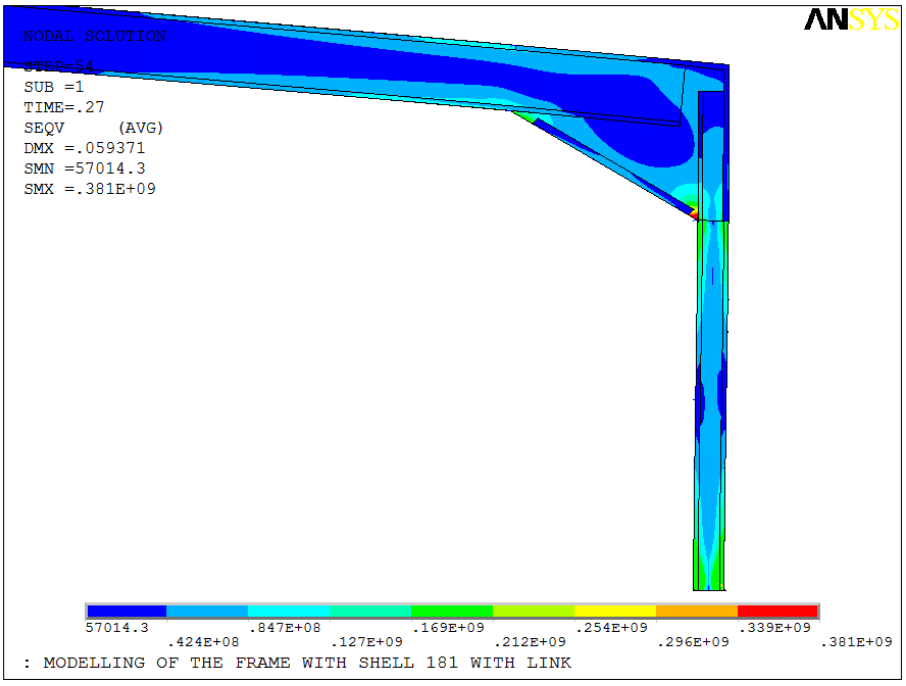

Figure 4.138 Von Mises stress (MPa) right (frame value)

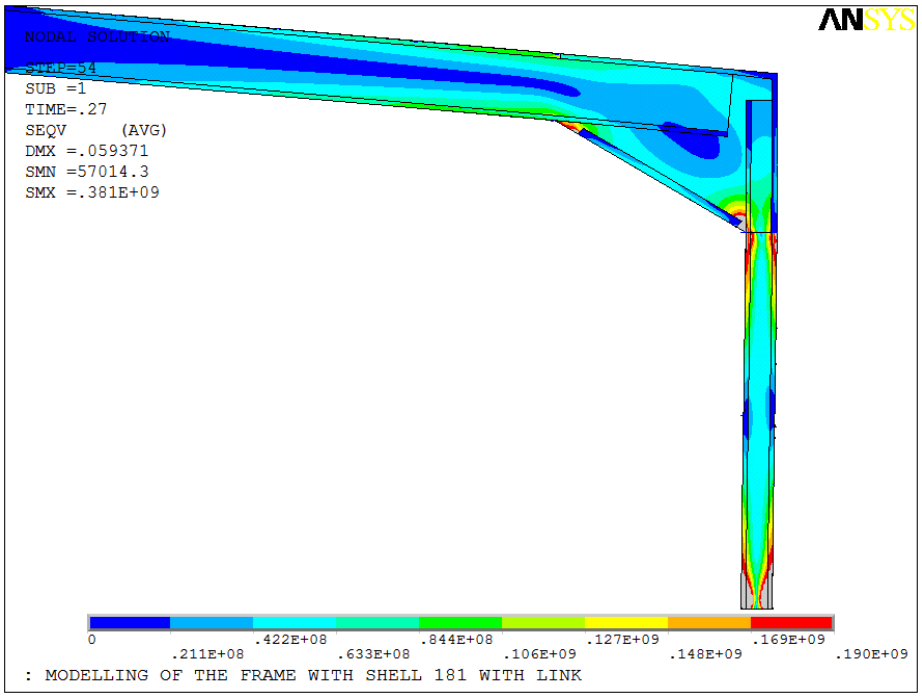

Figure 4.139 Von Mises stress (MPa) right (link value)

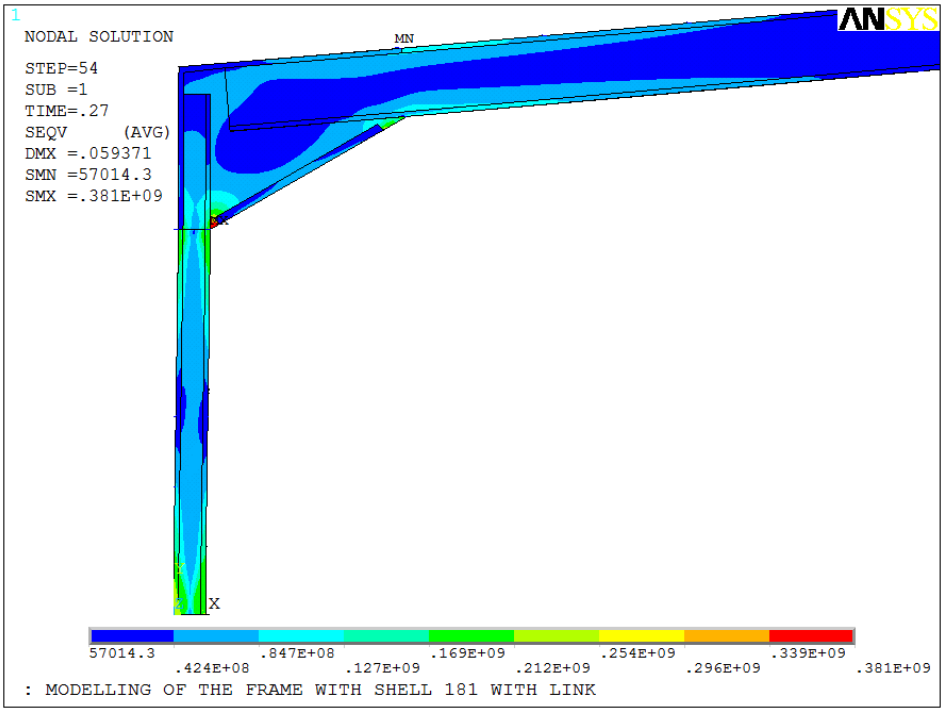

Figure 4.140 Von Mises stress (MPa) left (frame value)

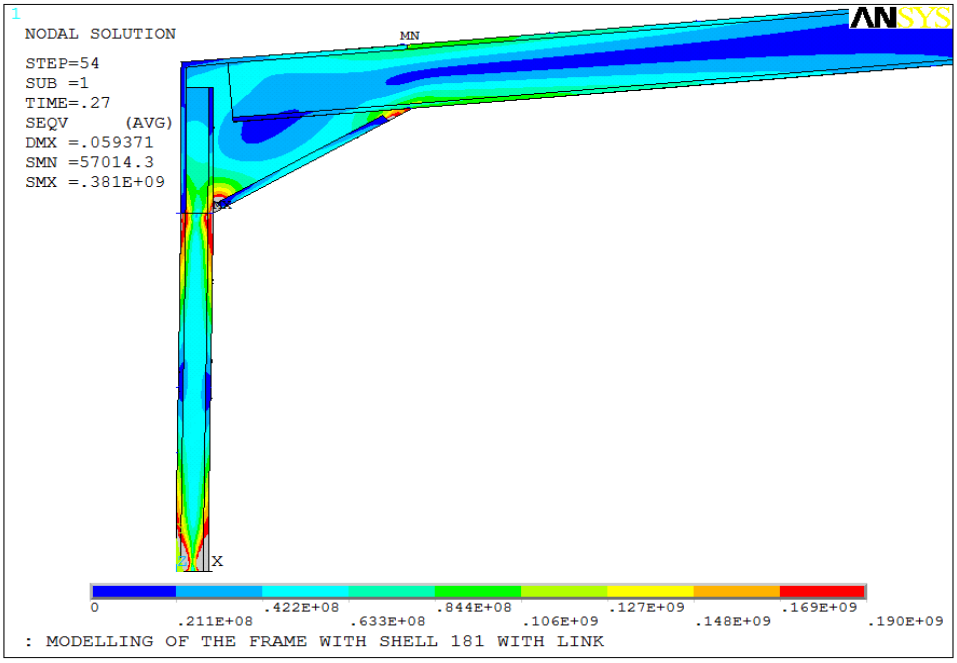

Figure 4.141 von Mises stress (MPa) left (link value)

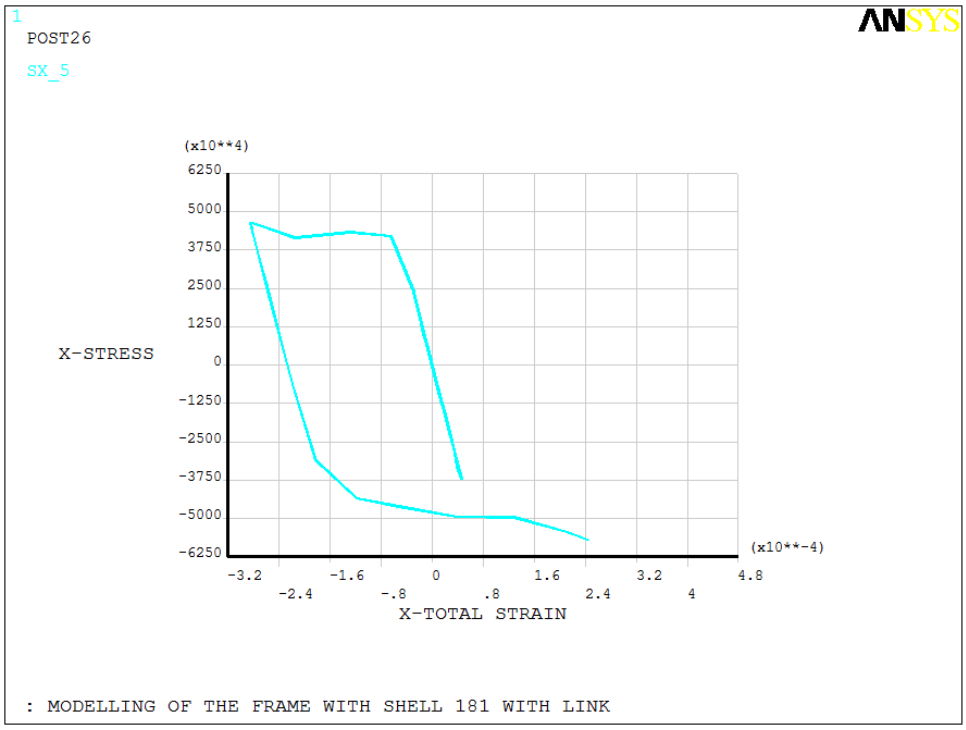

Figure 4.142 Hysteresis curve for the horizontal total strain

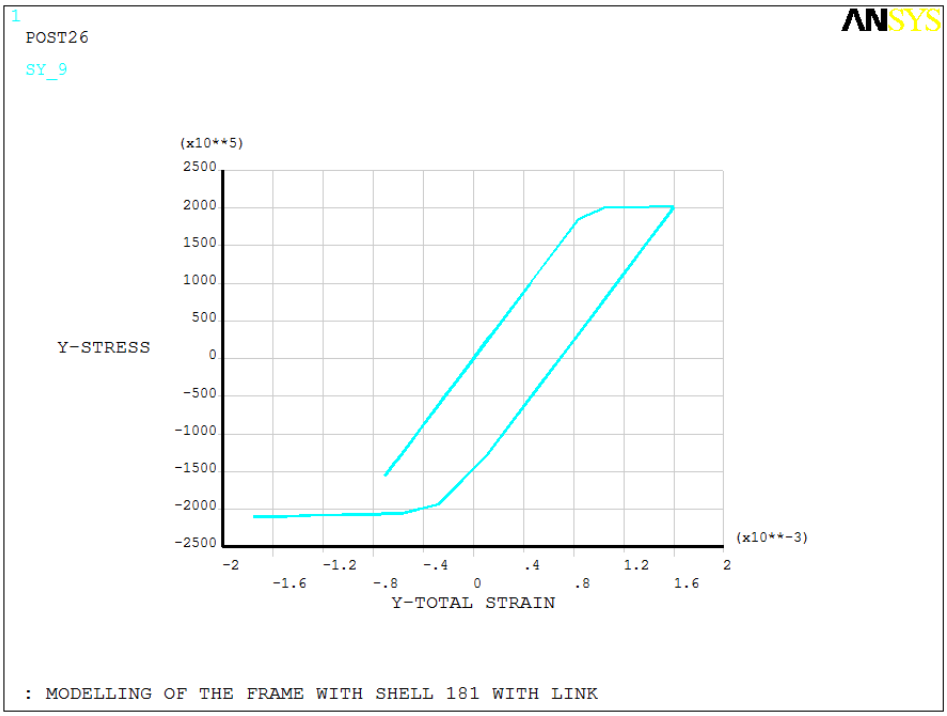

Figure 4.143 Hysteresis curve for the vertical total strain

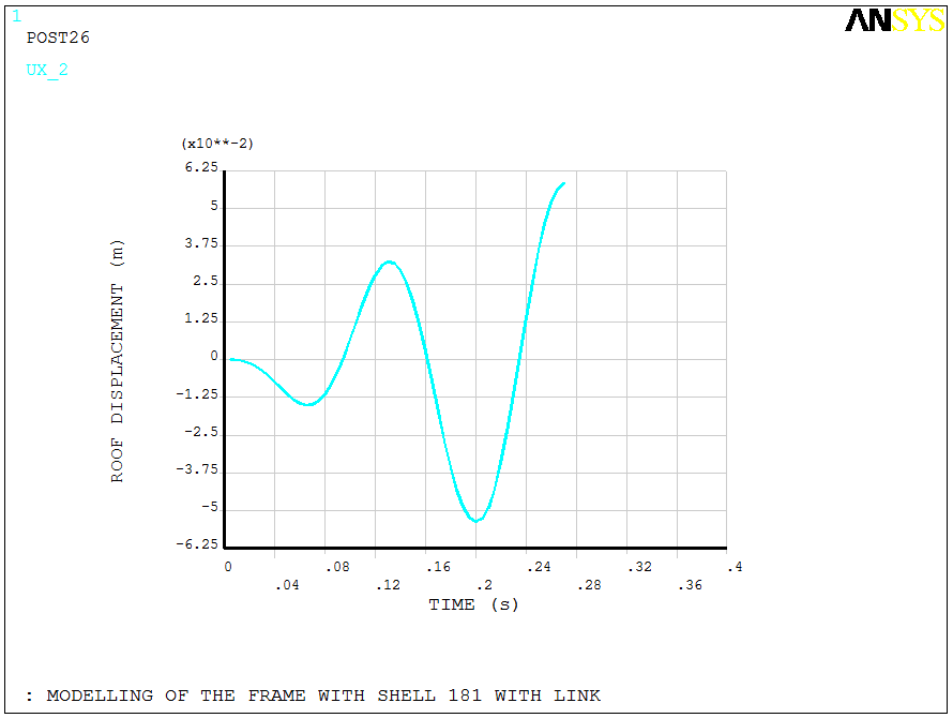

Figure 4.144 Roof displacement time history

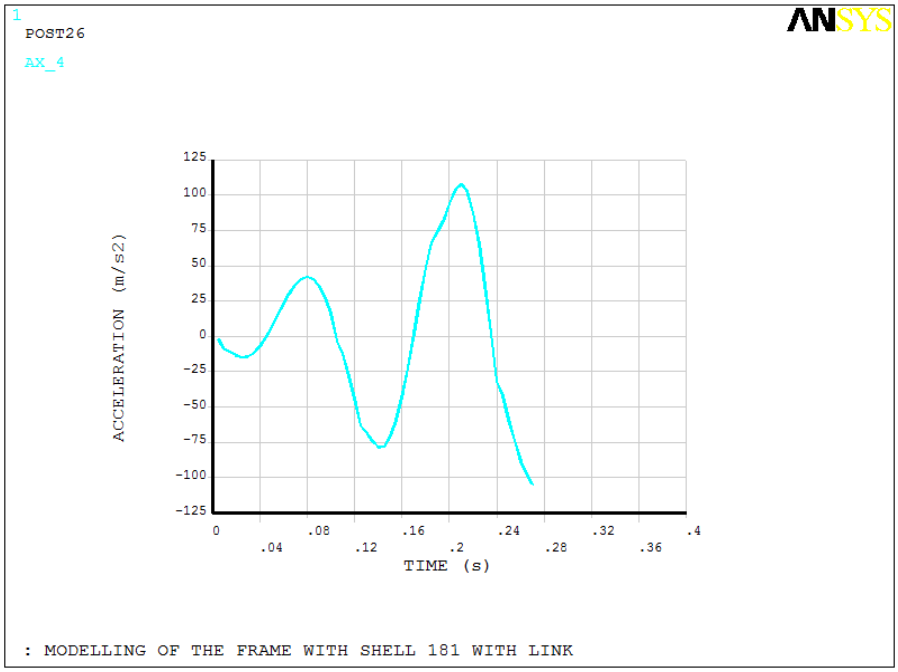

Figure 4.145 Acceleration time history

4.10 Practicalities of Removal and Reuse of the Structure after Earthquake Event

After an earthquake the link may be damaged and the whole building may have a permanent side- sway "set". It would be practical to replace the links (or probably the whole columns) one by one. Whilst temporary supports between rafters and ground were provided. The structure would not be in an offset position so the columns would require new bolt hole to be drilled into the foundation. The bolt would be secured with a grout or resin. The foundation should originally be constructed oversize to allow for the possibility of the new position that results from the earthquake-induced permanent set.

4.11 Concluding Remarks

In order to investigate the effect of the link on the response of designed light gauge steel portal frame structures, different types of links were examined using nonlinear static analysis as preliminary analysis for the link. The link was attached to the frame in the columns and the analysis carried out by changing the parameters to find the best link result (these parameters were explained in 3.12.6 which affect in the link response). A three dimensional finite element analysis carried out for the frame using finite element software ANSYS under horizontal displacements. The preliminary analysis then carried out for the frame with the best link using dynamic analysis by base excitation using scaled real records of Coalinga, Northridge and Duzce earthquake and finally at last stage a base excitation using artificial earthquake was carried out. The results of these analyses resulted in some observations according to parameters that control the efficiency of the link. These observations used for the final design of the link for light gauge steel portal frame structure.

Initial attempts to improve the structural response in an earthquake were based on using the link to cover the complete column and stiffening the columns whilst making the rafters (roof) sufficiently strong so that the column reached their moment capacity and then protected the rafters from being overloaded. Unfortunately none of the stiffening arrangements investigated resulted prevented buckling at large strain. Whilst stiffening could have been investigated further, the design was becoming complicated and so the decision was made to use an unstiffened compact section instead.

Then the optimised link tested using nonlinear static and dynamic analyses. Both analyses showed a significant improvement of the structural response using the link. The buckling of the frame components was considerably reduced as in the result of the frame with the link. First under the horizontal displacement the frame with the link failed at a total displacement of 88mm compared with value of 34 mm for the frame without link.

At the final stage of the research an assessment was carried out for the frame with link and without the link using nonlinear dynamic time history analyses, in an artificial earthquake (increasing harmonic excitation). This was tuned to the elastic natural period of each different structural concept and was considered a better basis

for the comparison of different concepts than using specific earthquakes, where differences in the energy content at different frequencies may make a particular concept perform better, but only in that particular earthquake. Under ground acceleration the frame without link failed at an applied acceleration of 12.05 m/sec^2 while the frame with the link failed at an applied acceleration of 38.62 m/sec^2. From the results it was observed that the frame with the link achieved full yielding of the links and the plastic hinges occurred at the upper and the lower of the columns (the link). The yielding was limited to the links members but the frame whole slender components were undamaged. These resulted in having ductile portal frame structure made of light gauge steel with component parts to yield and protect the structure.

Chapter 5

5 Conclusions and Recommendations for Further Study

5.1 Summary

In this research, the performance of a light weight portal frame structure made of thin gauge steel in earthquake prone areas is evaluated, firstly at the material and member level, to optimise the design of the structure using numerical investigation and hand calculations and then through the analytical assessment of the building using a finite element approach. The static equivalent method and the dynamic method were used for the evaluation of the initial forces for the design purpose. Two analytical techniques (i.e. static displacement pushover and dynamic time-history), at the forefront of current research, were employed to assess the behaviour of the light gauge steel portal frame structure designed in accordance with Eurocode 3 (2006) and Eurocode 8 (2004).

A new cyclic link dissipation device is introduced to protect the structure under seismic loads. The link is constructed from the same frame members section with light gauge steel that can be assembled at the same time as the frame sections at any structural steel fabrication plant.

In order to accomplish the research objectives, first a model of the frame with cold formed steel was investigated numerically using the commercially available finite element software ANSYS. The non-linear material model used was bilinear, isotropic elastic-perfectly plastic, and used the von Mises yield criterion. Non-linear geometric behaviour was considered and this included large displacement and P-δ effects in the analyses. The analysis resulted in a general understanding of the response of this type of light gauge steel structure in earthquake areas to help in the design of the structure. This is beneficial because, in the seismic design of structures

to Eurocode 3 and Eurocode 8, there are limited recommendations and provisions for this type of structure.

From the first investigation the importance of lateral restraints for this types of structure, when subject to horizontal forces or earthquake action, was noticeable: lateral torsional buckling is the main cause of failure for this type of structure, if it is not well restrained. Therefore the design utilized lateral restraints directly or indirectly to the purlins.

The potential benefits of utilising light gauge steel or slender steel for the construction of portal frame buildings in earthquake prone areas were examined. The modes of failure of the designed frame structure were investigated with a three-dimensional detailed finite element model. This demonstrated that, as was expected, premature failure of the frame is due to buckling of the slender frame section profiles. Such a mode of failure is not desirable in an earthquake resistant structure as the capacity drops very suddenly when the structure is overloaded. In contrast a structure with more ductility has the capability to absorb energy and can better survive the shaking from the ground accelerations.

A long link was investigated with different sections and dimensions to act as seismic protection and improve the response of the frame. The section properties and yield strength of the column link was chosen to allow for yielding of the link so that it would work as a dissipative zone. The moment resistance of the link was chosen to be about 2/3 of the moment resistance of the frame members.

Preliminary analyses of the frame without and with the link were performed using the commercially available finite element software ANSYS. These analyses resulted in observation used for the final design of the link.

The assessment of the designed light gauge steel building was carried out by means of two analytical procedures, the nonlinear static (pushover) analysis as first step for assessment of link and frame and the nonlinear dynamic analysis. The assessment using the former nonlinear static procedure was carried out by applying horizontal

displacements which helps to model the resistance of the frame after the yield point, while the latter procedure involved either the use of accelerograms of three of the most damaging earthquakes recorded in the world or with a simplified increasing harmonic excitation. The simplified, increasing harmonic excitation was preferred for this research work as:

1. It allowed the excitation frequency to be that of the natural frequency of each of the different structural concepts,
2. The analyses were quick to perform, and
3. Each analysis would eventually result in structural failure.

The dynamic analyses carried out by base excitation with different real ground motion records used the horizontal components for the Coalinga and Northridge earthquake and both the horizontal components and the vertical components for the Duzce earthquake to check the response of the frame, despite the fact that the structure is always well behaved for vertical accelerations as a result of the design requirements to carry the gravity loads. However more extreme vertical accelerations are also accounted for in design. This will require further research as there are options of designing for:

- Ductile vertical behaviour by providing an additional link at the apex of the rafters.
- Elastic vertical behavior of the frame rafters by providing sufficient strength to resist the vertical component of the earthquake without the benefit of ductile behavior.

A long compact column link was chosen to act as seismic protection and to improve the response of the frame. It did not seem sensible to change from compact section to slender section within the column, although this could be economic if the columns were long. The structure performance with the optimised link was investigated by the nonlinear static (pushover) analysis and later by nonlinear dynamic analysis with a simplified increasing harmonic excitation (artificial earthquake). The mode of failure

of the designed frame structure with the link was investigated as a last stage of the assessment of the frame structure performance during earthquakes.

5.2 Conclusions

Based on the results of both the pushover and the nonlinear dynamic analyses, the seismic performance of the designed building with the energy dissipating column links was judged to be very satisfactory. According to the results of the study, the following observations and conclusion were drawn:

1. Slender steel (cold formed or thin walled steel) could be used effectively for framing of portal frame buildings earthquake resistant without using shear walls. Lateral buckling must be prevented, most easily by utilizing the purlins. The buckling or premature failure by buckling of the slender rafter sections can be prevented by using a column link with stockier "compact" section.
2. A link was attached in the column with special specifications that allow for dissipating energy, by the formation of plastic hinges; the inelastic action under strong earthquake motion is restricted primarily to these links which will yield in flexural manner.
3. The link is attached to the both columns below the knee connection and has a moment capacity that is about 2/3rds that of the roof rafters. This effectively improved frame performance by protecting frame members profiles from buckling.
4. The link should be long enough to act as a dissipative zone and to yield in cyclic bending. In this work the link is over the whole column length (because localized links at each end caused the yielding of the middle part of the column).
5. The link should have yield strength (Fy) to be selected as the rules for the dissipative zones in Eurocode 8 (2004), that the nominal value of the yield strength (Fy) of the steel specified for the component of the frame (non

dissipative zones) exceeds the upper value of the yield strength ($Fy_{,max}$) of the link (dissipative zone). This leads to the use of steels with yield strength 355 MPa for frame members and the use of steel with yield strength 190 MPa for the link where the upper yield strength ($Fy_{,max}$) of the link is limited to 355 MPa.

6. Links have different responses and effects due to their section type, dimensions, arrangement and web and outstand slenderness. The I section link was observed with less protection for buckling even with stiffeners attached. The compact link with back to back lipped channel section was observed as an effective link for energy dissipation and buckling preventing.
7. The link should be used with a stocky, compact section to prevent the whole of the frame from instability and buckling due to the slender walls of the frame sections. From this work it appears preferable to use a compact section for the column link than to stiffen a slender section. No need for using stiffeners with stocky section for the link (column).
8. The design method obtained from this research could be used for another structure as the design is based on calculation but needs to be verified for different sizes of buildings before applying it by the practise engineer.
9. This work encourages the use of suitably designed slender steel for earthquake prone areas and it is verified by numerical analyses with the well known finite element package ANSYS. It could be the basis of a design methodology for earthquake-resistant, portable and slender steel structures.

5.3 Recommendations for Future Work

Research on slender structures, including cold formed steel structure has been continuous since the late 80's. Despite great research efforts there are still issues that have not been addressed or require further verification based on experimental investigations. They include:

1. Frame should be designed and checked for earthquake resistance with different dimensions, different roof angles and different types of column base

connections, such as pinned and semi rigid, with the link attached and without the link.

2. Despite the earthquake resistant structure full strength connections, a study could consider the possibility of using semi rigid connections for slender structure.
3. The effects of vertical earthquake accelerations should be studied in more detail and the possible advantages of a further, energy dissipating, link at the apex of the roof rafters investigated.
4. The option of using a higher strength steel for the links, with less stockier plate and outstand b/t ratios should be investigated.
5. Full-scale links should be constructed and the required cyclic displacement loading applied, to both check the finite element analysis and to ensure that the link has the required capacity to resist buckling and fracture.

References

AISC. (1989). "Specification for Structural Steel Buildings-Allowable Stress Design and Plastic Design", AISC, American Institute of Steel Construction, Chicago, IL.

AISC. (1994). "Executive summary-Interim observations and recommendations of AISC Special Task Committee on the Northridge Earthquake", Proceedings of AISC Special Task Committee on the Northridge Earthquake Meeting, American Institute of Steel Construction, Chicago, Ill.

AISC. (2005). "Seismic Provisions for Structural Steel Buildings", AISC, American Institute of Steel Construction, 341-05, Washington, D. C.

AISC. (2005). "Prequalified Connections for Special and Intermediate Steel Moment Frames for Seismic Applications", AISC American Institute of Steel Construction 358-05, Washington, D.C.

AISI. (2001). "North American Specification for the Design of Cold-Formed Steel Structural Members with Commentary", AISI American Iron and Steel Institute Washington, D.C.

Al Nageim, H. and MacGinley, T. (2005). "Steel Structures: Practical Design Studies", 3rd edition, Taylor and Francis, London.

ArcelorMittal. (1996). "Earthquake Resistant Steel Structures", Forest Stewardship Council, Luxembourg.

ArcelorMittal. (2012). "Steel Buildings in Europe, 2, Single storey buildings Part 2: Concept design", [Online], available from website http://www.arcelormittal.com/sections/index.php?id=167 , Accessed 28 March 2012.

ArcelorMittal. (2012). "Design Manual: Steel Buildings in Europe, 2, Single storey buildings Part 4: Detailed design of portal frames", [Online], available from website http://www.arcelormittal.com/sections/index.php?id=167 , Accessed 28 March 2012.

Ashtiani, F. A .D (1996)**.** "Seismic Behaviour of Steel Frames with Semi-rigid Connections", PhD thesis, Imperial College of Science, Technology and Medicine Univ. of London.

ANSYS, Inc. (2009a). Documentation 12.1.

ANSYS, Inc. (2009b). "Structural Analysis Guide", Release 12.1.

Barltrop, N. D. P. and Adam, A. S. (1991). "Dynamics of Fixed Marine Structures", 3rd edition, Butterworth Heinemann, London.

Bayan, A, Sariffuddin, S. and Hanim O. (2011). "Cold Formed Steel Joints and Structures -A review", J International Journal of Civil and Structural Engineering, Vol. 2(2): pp. 612–625.

Berman, J. W. and Bruneau, M. (2007). "Experimental and Analytical Investigation of Tubular Links for Eccentrically Braced Frames", J Engineering Structures 29: pp. 1929–1938.

Berman, J. W. and Bruneau, M. (2008). "Tubular Links for Eccentrically Braced Frames I: Finite Element Parametric Study", J Structural Engineering, ASCE, Vol. 134(5): pp. 692–701.

Berman, J. W, Okazak, T. and Hauksdottir, H. O. (2010). "Reduced Link Sections for Improving the Ductility of Eccentrically Braced Frame Link-to-Column Connections", J Structural Engineering, Vol. 136(5): pp. 543–553.

Bose, S. K, McNeice G.M and Sherbourne A. N. (1972). "Column Webs in Steel Beam to Column Connexions", Part I: Formulation and Verification, J Computers & Structures, Vol.2: pp. 253–72.

Bruneau, M. et. al. (2011). "Steel Building Damage from the Christchurch Earthquake of February 22, 2011, NZST" J of the Structural Engineering Society New Zealand (SESOC), Vol.24 (2): pp.27 - 42.

BS 5950-5 (1998). "Structural use of Steel Work in Building. Part 5: Code of practice for design of cold formed thin gauge sections", British Standards Institution.

BS 4-1 (2005). "Structural Steel Sections. Part 1: Specifications for Hot- rolled Sections", British Standards Institution.

Calderoni, B., De Martino, A., Landolfo, R. And Ghersi, A. (1994)." On the Seismic Resistance of Light Gauge Steel Frames", Behaviour of Steel Structures in Seismic Area- STESSA 94.Ed by F.M Mazzolani and V Gioncu,E and F N Spon, London.

Chao, S. H. et. al. (2006). "Ductile Web Fracture Initiation in Steel Shear Links", J Structural Engineering, Vol. 132(8): pp. 192–1200

Chen, W. F. and Lui, E.M. (2006). "Earthquake Engineering for Structural Design", CRC press, Taylor and Francis, USA.

Chopra, A. and K. (2001). "Dynamics of Structures, Theory and Applications in Earthquake Engineering", Prentice-Hall, New Jersey, U.S.A.

Chung, K. F. and Lau, L.(1999). "Experimental Investigation on Bolted Moment Connections among Cold formed Steel Members", J Engineering Structures, Vol. 21: pp. 898-911.

Clifton, C. et. al. (2011). "Steel Structures Damage from the Christchurch Earthquake Series of 2010/2011", Bulletin of the New Zealand Society for Earthquake Engineering, Vol. 44 (4): pp.297-318.

Clough, R. W. and Penzien, J. (1993). "Dynamics of Structure", 2nd Edition, McGraw-Hill.

Devos, G. P. and Rensburgt, B.W.(1997)." Lightweight Cold-formed Portal Frames for Developing Countries", J Buildmg and Environment, Vol. 32(5): pp. 417-425.

Díaz, C. et. al. (2011). "Review on the Modelling of Joint Behaviour in Steel Frames", J Constr. Steel Res, 67(5): pp. 741-758.

DRD Technology (2010). "Engineering Strain vs. True Strain", Advanced Technology Through Computer Aided Engineering, [Online], available from http://www.drd.com/techsupport/eng_true_strain.htm, Accessed 3rd November 2013.

Dubina, D. et. al. (2004a). "Strength, Stiffness and Ductility of Cold-formed Steel Bolted Connections", The Fifth International Workshop on Connections in Steel Structures, Amsterdam, the Netherlands.

Dubina, D. (2004b). "Ductility and Seismic Performance of Thin Walled Cold-Formed Steel Structures", J Steel Structures, 4: pp. 209–222.

Dubina, D. (2008). "Structural Analysis and Design Assisted by Testing of Cold-Formed Steel Structures", J Thin-Walled Structures, 46: pp. 741–764.

Dubina, D. et. al. (2010). "Imperfections Sensitivity Analysis of Pitched Roof Cold-formed steel Portal Frames", SDSS'Rio 2010, Stability and Ductility of Steel Structures, Rio de Janeiro, Brazil.

Dundu, M. and Kemp, A. R. (2006). "Plastic and Lateral-torsional Buckling Behaviour of Single Cold-Formed Channels Connected Back-to-Back", J Structural Engineering, ASCE, Vol. 132(8): pp. 1223-1233.

Dundu, M. and Kemp, A. R. (2006). "Strength Requirements of Single Cold-Formed Channels Connected", J Constr. Steel Res, 62:pp. 250–261.

Dundu, M. (2011). "Design Approach of Cold-formed Steel Portal Frames", J Steel Structures, Vol 11(3): pp. 259-273.

ECCS - European Convention for Constructional Steelwork (1985). "Recommended Testing Procedures for Assessing the Behaviour of structural Elements under Cyclic Loads", Technical Committee 1, TWG 1.3 – Seismic Design, No.45.

Elghazouli, A. Y. (2009). "Seismic Design of Buildings to Eurocode 8", First edition, Spon press, New York, USA.

Elnashai, A. S. and Izzuddin, B. A. (1993). "Modelling of Material Nonlinearities in Steel Subjected to Transient Dynamic Loading", J Earthquake Engineering and Structural Dynamic, Vol. 22: pp. 509-532.

EN1993-1-8, (2005). "Eurocode 3: Design of Steel Structures. Part 1-8: Design of Joints", CEN-European Committee for Standardisation.

EN 1998-1 (2004). "Eurocode 8: Design of Structures for Earthquake Resistance. Part 1: General rules, Seismic Actions and Rules for Buildings", CEN - European Committee for Standardization.

EN 1993-1-1. (2005). "Eurocode 3: Design of Steel Structures. Part 1-1: General Rules and Rules for Buildings", CEN- European Committee for Standardization.

EN 1993-1-3. (2006). "Eurocode 3: Design of Steel Structures. Part 1-3: General Rules. Supplementary Rules for Cold-Formed Thin Gauge Members and Sheeting", CEN- European Committee for Standardization.

Feng, X. (1994). "The Influence of Semi-rigid Connections on the Behaviour of Slender Structures", PhD thesis, Oxford Brookes University.

FEMA. (2000). "Prestandard and Commentary for the Seismic Rehabilitation of Buildings", FEMA 356, Federal Emergency Management Agency, Washington D. C.

FEMA. (2009). "Concept of Seismic Resistant Design", Instructional Material Complementing, FEMA 451B Topic 7 Notes. Federal Emergency Management Agency, Washington, D.C.

FEMA. (2009). "Seismic Load Analysis 9", Instructional Material Complementing, FEMA 451, Federal Emergency Management Agency, Washington, D.C.

Ghosh, S. K. (2003). "Seismic Design using Structural Dynamics (2000 IBC)", International Code Council, Inc, USA.

Hancock, G. J. (2003). "Review Article, Cold-Formed Steel Structures", J Constructional Steel Research 59: pp. 473–487.

IBC. (2000). "International Building Code", International Code Council, Inc, USA.

Ibrahim, Y.E. (2005). "A Visco-plastic Device for Seismic Protection of Structures", Ph.D. thesis, Virginia Polytechnic Institute and State University.

Ibrahim, Y.E., Marshall, J. and Charney, F.A.(2007). "A Visco-plastic Device for Seismic Protection of Structures", J Constr. Steel Res, 63: pp. 1515–1528.

ISDG. (2011). "Cold-formed steel sections-I", Institute for Steel Development and Growth, [Online]. Available from http://www.steel-insdag.org/TeachingMaterial/Chapter19.pdf, [Accessed 17th October 2013].

IPL, Image from Project Link (2011). "Project Link Design & Construction Ltd", [Online]. Available from http://www.projectlinkuk.com/project-services.htm, [Accessed 2nd April 2013].

Issa, H. K. and Mohammad, F.A. (2009). "Weight and Displacement Optimizations of Steel Portal Frames to Eurocode 3 using", 8th World Congress on Structural and Multidisciplinary Optimization.

Itani, A. M., Lanaud, C., Dusicka, P. (2001). "Non Linear Finite Element Analysis of Built-Up Shear Links", Report No.CCEER 01-03, Centre for Civil Engineering Earthquake Research, Univ. of Nevada.

Itani, A. M., Lanaud, C., Dusicka, P. (2003). "Analytical Evaluation of Built-up Shear Links Under Large Deformations", J Computers and Structures 81: pp. 681–696.

Jor, F. et. al. (2002). "Finite Element Analyses of Seismic Responses of the Berkeley Town House" Lawrence Berkeley National Laboratory.USA.

Kappos, A. J. (1997). "Influence of Capacity Design Method on The Seismic Response of RC Columns", J Earthquake Engineering, 1(2): pp. 341-99.

Kappos, A. J. and Kyriakakis, P. (2000). "A re-evaluation of Scaling Techniques for Natural Records", J Soil Dynamics and Earthquake Engineering, 20: pp. 111-123.

Kennedy, D.J.R. and Hafez M. (1984) "A study of End-plate Connections for Steel Beams", Canadian Journal of Civil Engineering, Vol.11 (2): pp.139–49.

Kirk, P. (1986). "Design of A Cold-formed Section Portal Frame Building System", Proc. 8th International Speciality Conference on Cold-formed Steel Structures, St. Louis, University of Missouri-Rolla, pp. 295-310.

Knight, J. and Kutyn, K. (2010). "Seismic Time History Analysis Examples and Verification in S-FRAME", S-FRAME Software Inc, USA & Canada.

Konstantinidis, D. (2001). ''Seismic Design and Performance Assessment of RC Building Made of High Strength Materials" PhD thesis, Univ. of London.

Krishnamurthy, N. And Graddy D. E. (1976) "Correlation Between 2- and 3-Dimensional Finite Element Analysis of Steel Bolted End-plate Connections", J Computers & Structures, Vol.6 (4–5): pp.381-400.

Kumar, S.R and Kumar, A.R. (2012). "Design of Steel Structures II", (Web Course), Department of Civil Engineering, Indian Institute of Technology Madras, available from http://www.slashdocs.com/zzhks/design-of-steel-structures-ii-prof-s-r-satish-kumar-prof-a-r-santha-kumar-1.html, Accessed 14th April 2010.

Kwon, Y. B, Chung, H.S. and Kim, G. (2006). "Experiments of cold-formed steel connections and portal frames", J of Structural Engineering, Vol. 132(4): pp.600-607.

Lam, D., Ang, T. C. and Chiew, S. P. (2008). "Structural Steel Work: Design to Limit State Theory", 3rd edition, Elsevier Ltd, Oxford.

Lemonis, M. E. and Gantes, C.J. (2009). "Mechanical Modelling of the Nonlinear Response of Beam-to-Column Joints", J of Constructional Steel Research, Vol.65: pp. 879–90.

Lim, J. B. P. (2001). "Joint Effects in Cold-Formed Steel Portal Frames", PhD thesis, Univ. of Nottingham.

Lim, J. B. P., and Nethercot, D. A (2002). "Design and Development of a General Cold-formed Steel Portal Framing System", J The Structural Engineer; 80 (21): pp.31-40

Lim, J. B. P., and Nethercot, D. A (2003). "Ultimate Strength of Bolted Moment-Connections between Cold-Formed Steel Members", J Thin-Walled Structures, 41(11): pp.1019–1039.

Lim, J. B. P and Nethercot, D. A (2004a). "Stiffness Prediction for Bolted Moment—Connections between Cold-Formed Steel Members", J Constr. Steel Res, 60(1): pp. 85–107.

Lim, J. B .P and Nethercot, D. A. (2004b). "Finite Element Idealization of a Cold-Formed Steel Portal Frame", J of Structural Engineering, ASCE, Vol. 130(1): pp. 78–94.

Logan, D. L. (2007). "A first Course in the Finite Element Method", 4th Edition, Nelson, Thomson Canada Limited, Canada.

Madenci, E. and Guven, I. (2006). "The Finite Element Method and Applications in Engineering using ANSYS", Springer Science+Business Media, LLC, USA.

Maguire, J. R. and Wyatt, T. A. (2002). "Dynamics: An Introduction for Civil and Structural Engineers", 2nd edition, Institute of Civil Engineers, London.

Mäkeläinen, P. and Kankaanpää, J. (1996). "Structural Design Study on A Light-Gauge Steel Portal Frame with Cold-formed Sigma Sections", Proc. 13th International Specialty Conference on Cold-Formed Steel Structures, St. Louis, University of Missouri-Rolla, pp. 349-371.

Martinez-Rueda, J. E. (1997). "Energy dissipation devices for seismic upgrading of RC structures", PhD. Thesis, ESEE Section, Imperial College, London.

Midorikawa, M. et. al. (2012). "Earthquake and Tsunami Damage on Steel Buildings Caused by the 2011 Tohoku Japan Earthquake", Proc. of the International Symposium on Engineering Lessons Learned from the 2011 Great East Japan Earthquake, Tokyo, Japan.

Mills, J. and LaBoube, R. (2004). "Self-Drilling Screw Joints for Cold-Formed Channel Portal Frames", Journal of Structural Engineering, ASCE, Vol. 130(11): pp. 1799-1806.

Moaveni, S. (1999). "Finite Element Analysis Theory and Application with ANSYS", Prentice-Hall, Inc, USA.

Nelson, T. and Wang, E. (2004). "Reliable FE-Modelling with ANSYS", Proc. 11th International ANSYS'2004 Users Conference & Exhibition, Pittsburgh, PA, USA.

Nethercot, D. A. (2001). "Limit States Design of Structural Steelwork", 3rd edition, Health Press, London.

Newmark, N. M. and Hall, W. J. (1982). "Earthquake Spectra and Design", Earthquake Engineering Research Institute, Berkley, California, pp. 53-54.

Okazaki, T. And Engelhardt, M. D. (2007). "Cyclic Loading Behaviour of EBF Links Constructed of ASTM A992 Steel", J Constr. Steel Res, 63: pp. 751–765.

Ono, T., Suzuki, T. (1986). "Inelastic Behaviour and Earthquake-Resistance Design Method for Thin-Walled Metal Structures". Proceedings on IABSE Coll. on Thin-Walled Metal Structures in Building, Stockholm, pp. 115-122.

Peer Strong Motion Database, (2000). "Real Earthquake Records Data", Regents of the University of California, [Online], available from http://peer.berkeley.edu/smcat/search.html, Accessed 2nd March 2013.

Philpot, T. A. (2011). "Mechanics of Materials, An Integrated Learning System", John Wiley & Sons, Inc, USA.

Rai, D. C. and Wallace, B. J. (1998). "Aluminium Shear –Links for Enhanced Seismic Resistance", J Earthquake Engng. Struct. Dyn., Vol. 27: pp. 315-342.

Ramadan,T. and Ghobarah, A.(1995). "Analytical Model for Shear –Link", J of Structural Engineering, ASCE, Vol. 121(11): pp. 15741580.

Ramberg, W. and Osgood, WR. (1943). "Description of Stress–Strain Curves by Three Parameters", National Advisory Committee for Aeronautics, Technical report 902.

Rhodes, J. and Burns, R. (2006). " Development of a Portal Frame System on the Basis of Component Testing", Proc. 18th International Specialty Conference on Cold-Formed Steel Structures, St. Louis, University of Missouri-Rolla, pp. 367-385.

Richards, P.W. and Uang, C. M. (2005). "Effect of Flange Width-Thickness Ratio on Eccentrically Braced Frames Link Cyclic Rotation Capacity", J of Structural Engineering, ASCE, Vol. 131(10): pp. 1546–1552.

Richards, P.W. and Uang, C. M. (2006). "Testing Protocol for Short Links in Eccentrically Braced Frames", J of Structural Engineering, ASCE, Vol. 132(8): 1183–1191.

Seismosoft. (2002). "SeismoMatch Software", Seismosoft Company, [Online], available from http://www.seismosoft.com/en/HomePage.aspx , Accessed 15th March 2013.

Standard Australia (1990). "AS 4100 Steel Structures", Standard Australia, Sydney.

Sun, E. Q. (2006). "Shear Locking and Hourglassing in MSC Nastran, ABAQUS, and ANSYS", Msc Software Event, [Online], available from http://web.mscsoftware.com/events/vpd2006/na/presentations/tech_papers/27.pdf, Accessed 3rd November 2013.

Szakats, G. A. (2006). "Improving Earthquake Resistance of Small Buildings, Houses and Community Infrastructure", AC Consulting Group Ltd, New Zealand.

Tazarv, M. (2011). "Linear Time History Analysis of MDOF Structure by Mode Superposition Method", Version 1.1, Carleton University.

Tremblay, R. et. al. (1995). "Performance of Steel Structures During the 1994 Northridge Earthquake", Can. J. Civ. Eng. 22: pp.338-360.

Tsujii, M. (2001). "Response and Design of Steel Concrete Composite Frames Subjected to Earthquake Motion", PhD thesis, Imperial College of Science, Technology and Medicine, Univ. of London.

Utexas, Ce. (2013a). "Design of Seismic-Resistant Steel Building Structures: Part 1 Introduction and Basic Principles", Civil Architectural and Environmental Engineering, University of Texas, [Online], available from http://www.ce.utexas.edu/prof/wood/ce384r/ReadingAssignments/Seismic-Resistant%20Steel%20Design%20-%20Intro.pdf, Accessed 19 March 2013.

Utexas, Ce. (2013b). "Design of Seismic-Resistant Steel Building Structures: Part 4 Eccentrically Braced Frames (EBFs)", Civil Architectural and Environmental Engineering, University of Texas, [Online], available from http://www.ce.utexas.edu/prof/wood/ce384r/ReadingAssignments/Seismic-Resistant%20Steel%20Design%20-%20 EBFs.pdf, Accessed 19 March 2013.

Vrany, T. (2006). "Effect of Loading on the Rotational Restraint of Cold-formed Purlins", J Thin-Walled Structures 44: pp. 1287–1292.

Wales, M.W. and Rossow, E.C. (1983). "Coupled Moment-axial Force Behaviour in Bolted Joint", J Structural Engineering, Vol.109 (5): pp.1250–66.

Wilkinson, T. and Hancock, G. J. (1997). "Tests to Investigate the Web Slenderness Limits for Cold-formed RHS in Bending", Proc. 15th Australian Conference on the Mechanics of structures and Materials, Melbourne, Australia, pp. 559-564.

Williams, A. (2000). "Seismic Design of Building and Bridges for Civil and Structural Engineers", 3rd edition, Engineering press, Texas.

Wong, M. F. and Chung, K.F. (2002). "Structural Behaviour of Bolted Moment Connections in Cold-formed Steel Beam-Column Sub-frames", J. Constr. Steel Res., Vol 58(2): pp.253.

Wrzesien, A. M. and Lim, J.B.P. (2008). "Cold-formed Steel Portal Frame Joints: A Review", 19th Specialty Conference on Cold-formed Steel Structures, St. Louis, Missouri, USA.

Yanvec, P.I., Gillengerten, J.D., and Hamburger, R.O. (1991). "The Performance of Steel Buildings in Past Earthquakes", American Iron and Steel Institute and EQE Engineering, Inc., Washington, D.C.

Yu, W. W. (1999). "Cold-Formed Steel Structures", Structural Engineering Handbook, Ed. Chen Wai-Fah, CRC Press LLC, USA.

Appendix (A) Validation of Shell Model

(1) Plate Buckling Analysis

To verify the accuracy of the finite element shell model, a steel thin plate of 200mm length, 100 mm wide, 1 mm thick with Young's modulus, E = 210GPa and poison ratio 0.3 was modelled using thin shell elements. The analysis carried out to predict the buckling load for this plate using eigenvalue and nonlinear buckling analysis. Thin plate buckling theory predicts that it will buckle when the applied load is 75.9KN/m. A finite element model of the plate was set-up, consisting of a uniform mesh of 128 SHELL181 shell elements, with element mesh size about 12.5 mm as shown in Figure A-1.

In the first part of this verification the critical load for buckling of a thin flat plate has been found by eigenvalue buckling analysis. The second part of this verification shows nonlinear buckling analysis, the more accurate type of buckling analysis.

i. Eigenvalue buckling analysis

Eigen value buckling analysis predicts the theoretical buckling strength of an ideal linear elastic structure. The method corresponds to the textbook approach to elastic analysis. However, imperfections and nonlinearities prevent real-world structures from achieving their theoretical elastic buckling strength. The eigenvalue buckling analysis was performed by loading the vertical edges of the plate by unit force in both sides. The result is shown in table A-1.

ii. Nonlinear buckling analysis

Nonlinear buckling analysis is simply a nonlinear static in which the load is increased until the solution fails to converge, indicating that the structure cannot support the applied load (or that numerical difficulties prevent solution). In this case the large displacement and p-delta effects are considered without counting for nonlinear materials (nonlinear plastic).

The loading conditions were simulated and carried out in two steps; a load step is simply a configuration of loads for which a solution is obtained. Each load step is

divided into one or more substeps, where solutions are calculated. In a nonlinear static analysis, multiple substeps are used to apply the load gradually so that a more accurate solution can be obtained. In the first step, the plate vertical edges were loaded up to 70KN/m, note that all the nodes at the four edges of the plate were constrained to translate in the z-direction (out-of-pane translation), while the others degrees of freedom are free. Then in the second step the load was increased slowly from 70KN/m to 80KN/m, past the expected buckling load. Also a small out-of-plane load was applied to the middle of the plate, to generate the initial out-of-plane displacement to get buckling started.

Table A-1 compares the expected buckling load of the plate by thin plate buckling theory and ANSYS results. It can be seen that the ANSYS model accurately predicts the buckling load of the plate. The smaller value for the expected buckling load obtained by nonlinear buckling analysis compared with eigenvalue buckling analysis is explained by that the nonlinear method predicts the buckling load when the plate starts to buckle results in the fact that it is the more accurate type of buckling analysis.

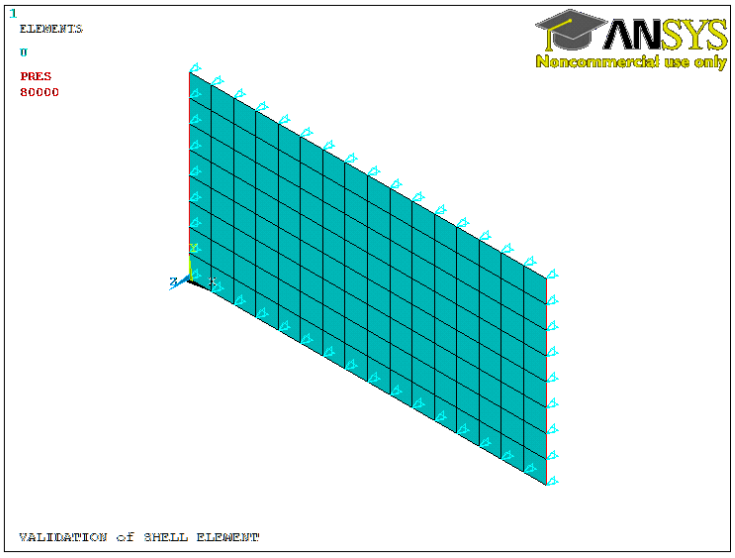

Figure A-1 Plate model with shell elements (SHELL181)

Table A-1 Comparison of the buckling load of the plate

The plate buckling load	Plate theory (KN/m)	ANSYS (KN/m)
Eigenvalue method	75.9	75.127
Nonlinear method	75.9	71.0

(2) Failure Load of Plate and Maximum Displacement

It was shown in the first analysis check, in the previous section, that the buckling analysis using thin shell elements is capable of reproducing fairly accurately the buckling load expected by the plate theory. In this second check, the aim was to validate maximum displacement and failure load of a plate using thin shell elements with mesh size 25mm and bilinear isotropic elastic-perfectly plastic model. The validation compares results for the failure load and maximum displacement by ANSYS using different mesh sizes to find the value which the solution converges close to each others.

The analysis was carried for a steel thin plate of 350mm length, 350 mm wide, 6 mm thick with Young's modulus, E = 205MPa and poison ratio 0.3. The plate was assumed to be made of cold formed steel and modelled with type 181 shell elements. The material was modelled as bilinear isotropic elastic-perfectly plastic. The inelastic behaviour of the steel elements was considered using the von Mises yield criterion as von Mises yield surface allows isotropic yielding. Geometric nonlinearities, large displacement and P-δ effects were considered in the analyses.

The plate was loaded at up and down edges with increasing load until failure. The boundary conditions for the right and the left sides of the plate were constrained in the out-of-plane translation (z-direction), and the vertical translation (y-direction). And the up and down edges of the plate were constrained in the out-of-plane translation (z-direction) and the horizontal translation (x-direction). While all the rotational degrees of freedom at the four edges of the plate were constrained in the simulations.

A non-linear static analysis was carried out with applying forces up to failure using different finite elements size (mesh size). The mesh sizes used for the validation in mm were 15, 18, 20, 22.5, 25, 27.5, 30, 35, 40 and 45.

Figures A-2 and A-3 show the resultsof the anlsyses of the plate in termsof maximum displacement values and failure load obtained by differnt mesh sizes.from the figures it can be seen that the mesh size 25 mm is part of where the solution converges close to each other's. This makes the use of shell element model with mesh size 25mm and bilinear isotropic elastic-perfectly plastic model sensible. The mesh size less than 25 mm may be gives good results but is computationally expensive in terms of time, for that shell elements with mesh size 25mm are ideal for the model in this reaearch.

Considering the results in Table A.1 and Figures A-2 and A-3, we can conclude that the ANSYS finite element model is in a good agreement with the theoretical results, implying good prediction of the behaviour of a plate bending.

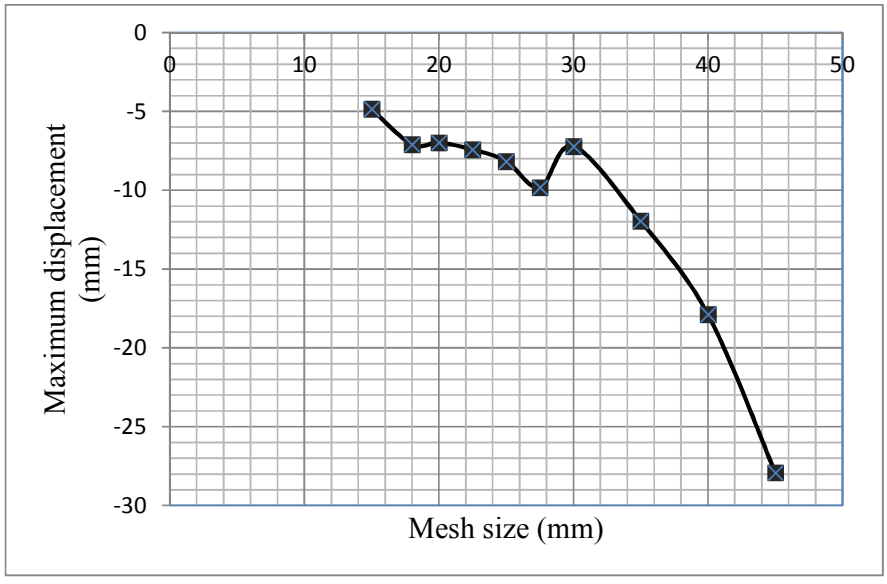

Figure A-2 Maximum displacement with different mesh sizes

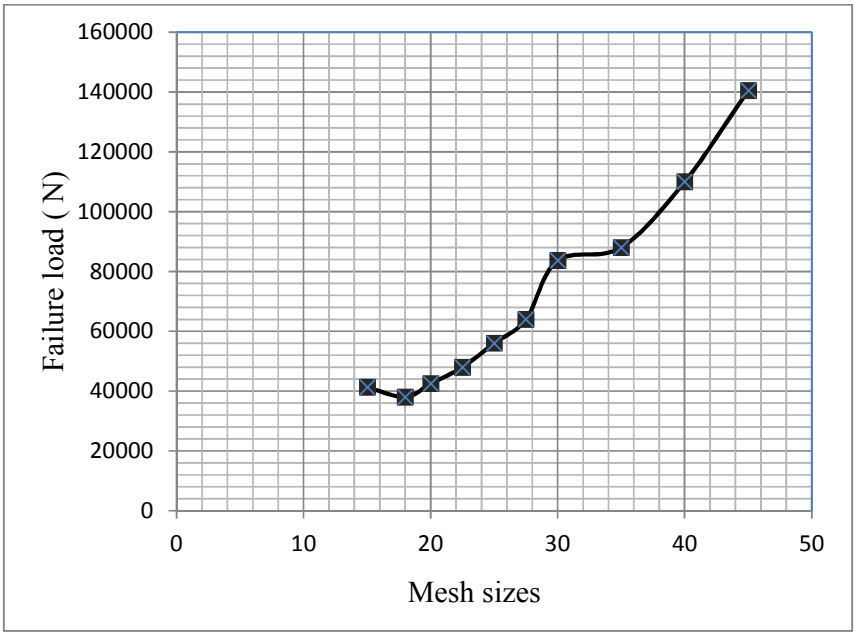

Figure A-3 Failure load with different mesh sizes

Appendix (B) Earthquake Analysis

Response Spectrum Analysis

1. General:

The portal frame is designed following the requirement of Eurocode 8 (2004) and the 2000 IBC. The building

is located in site class D. Dynamic analysis is used here.

2. Design Data:

The member sizes for the structure are chosen as follows:

Columns: Cold formed steel back to back lip channel section 850x650x63x3 mm

Rafters: Cold formed steel back to back lip channel section 750x500x53x3 mm

3. Material Properties:

$Fy := 355$ $E := 205 \cdot 10^9$

Steel Density $Dens := 785($

Poisson ratio $\upsilon := 0.3$

4. Service Load:

Total weight $Wt := 29000$

5.1 Seismic Design Data; Eurocode 8 (2004):

The design spectrum proposed for the elastic analysis of the structures by Eurocode 8 shall be determined in accordance with the procedure of section 3.2.2.5 in EC8 using the equations below.

The structure will be for a school or hospital, assume buildings whose integrity during earthquakes is of vital importance for civil protection: Use Group =IV,γ_1=1.4

$\gamma 1 := 1.4$

- Effective peak ground acceleration normalised by the acceleration of gravity: a_{gR}=0.163 g, the design ground acceleration on type A ground a_g is equal to a_{gR} times the importance factor γ_I, $a_g = \gamma_I a_{gR}$=0.23(medium-to-high seismicity)

  agr := 0.23

- Subsoil class: C (referring to Deep deposits of dense or medium dense sand, gravel or stiff clay with thickness from several tens to many hundreds of metres)

- Type 1 response spectrum (for earthquake magnitude greater than 5.5)

Break points periods:

Tb := 0.2 Tc := 0.6 Td := 2.0

Soil parameter: Sp := 1.15

Behaviour factor for low dissipative structure: q := 1.5

Design Basis

Using of the equivalent lateral- force procedure is allowed by Eurocode 8 for regular structures which respond essentially in one single mode of vibration.
Otherwise, the Dynamic analysis Procedure must be used.
In this structure the Equivalent Lateral force procedure could be used because it is regular in plan and elevation. But the need for the response of the structure for translation and axial forces as well makes using the modal spectra analysis more accurate. (4.3.3.2 through 4.3.3.3) has been used.

5.2 Seismic Design Data; International Building Code 2000 (2000 IBC):

Ground motion accelerations, represented by response spectra and coefficients derived from these spectra, shall be determined in accordance with the general procedure of section 1615.1 in 2000 IBC.

The mapped maximum considered earthquake spectral response acceleration at short periods:

$Ss := 1.5 \cdot g$ Section 1615.2.2

$S1 := 0.6 \cdot g$ 2000 IBC

The structure will be for school or hospital, assume essential facilities or Seismic Use Group =III Table 1604.5

And seismic importance factor, $IE := 1.5$ 2000 IBC

Site Class = D Section 1615.1.1

Table 1615.1.1

2000 IBC

Site coefficient, Fa $Fa := 1.0$ Table 1615.1.2(1)

Site coefficient, Fv $Fv := 1.5$ Table 1615.1.2(2)

The maximum considered earthquake spectral response acceleration for short periods, S_{MS}, and at 1 second period , S_{M1}, adjusted for site class effects, shall be determined by Equation 16-16 and 16-17, respectively in section 1615.1.2 2000 IBC.

Adjusted Ss= $SMS := Fa \cdot Ss = 14.71 \frac{m}{s^2}$ Eq. 16-16

Adjusted S1= $SM1 := Fv \cdot S1 = 8.826 \frac{m}{s^2}$ Eq. 16-17

The design spectrum

Five- percent damped design spectral response acceleration at short periods, S_{DS}, and at 1 second period S_{D1}, shall be determined from Equations 16-18 and 16-19 in section 1615.1.3 in 2000 IBC

At short periods: $SDS := \frac{2}{3} \cdot \left(\frac{SMS}{g} \right) = 1$ Eq. 16-18

At 1 second period: $SD1 := \frac{2}{3} \cdot \left(\frac{SM1}{g} \right) = 0.6$ Eq. 16-19

Ordinary moment - resisting frame (OMRF) system gives $Ra := 4$ Table 1617.6

200IBC

Seismic Design Category (SDC): based on both S_{DS} [Table 1616.3(1)] and S_{D1} [Table 1616.3(2)] in IBC, the **SDC** for this structure is D

Design Basis

Using of the equivalent lateral- force procedure is not allowed by the International Building code for building exceeding 240 feet in height in **SDC** D and above. In these cases, the Dynamic analysis Procedure must be used.

In this structure the Equivalent Lateral force procedure could be used because the height of the building is 6m (19.6850 feet) in **SDC** D (less than 240 feet). But for accurate design, modal Spectra analysis (1618.1 through 1618.9) has been used.

6. The Modal analysis by solving the Eigen value problem

Give:

$hs := 6$

$Icol := 112881078810^{-12}$

Member stiffness matrix

Member 1: $A1 := 9756 \cdot 10^{-6}$ $E1 := 205 \cdot 10^{9}$

$Ixx1 := 112881078810^{-12}$ $L := 6$

$$k1 := \begin{pmatrix} \frac{E1 \cdot A1}{L} & 0 & 0 & \frac{-E1 \cdot A1}{L} & 0 & 0 \\ 0 & \frac{12 \cdot E1 \cdot Ixx1}{L^3} & \frac{6 \cdot E1 \cdot Ixx1}{L^2} & 0 & \frac{-12 \cdot E1 \cdot Ixx1}{L^3} & \frac{6 \cdot E1 \cdot Ixx1}{L^2} \\ 0 & \frac{6 \cdot E1 \cdot Ixx1}{L^2} & \frac{4 \cdot E1 \cdot Ixx1}{L} & 0 & \frac{-6 \cdot E1 \cdot Ixx1}{L^2} & \frac{2 \cdot E1 \cdot Ixx1}{L} \\ \frac{-E1 \cdot A1}{L} & 0 & 0 & \frac{E1 \cdot A1}{L} & 0 & 0 \\ 0 & \frac{-12 \cdot E1 \cdot Ixx1}{L^3} & \frac{-6 \cdot E1 \cdot Ixx1}{L} & 0 & \frac{12 \cdot E1 \cdot Ixx1}{L^3} & \frac{-6 \cdot E1 \cdot Ixx1}{L^2} \\ 0 & \frac{6 \cdot E1 \cdot Ixx1}{L^2} & \frac{2 \cdot E1 \cdot Ixx1}{L} & 0 & \frac{-6 \cdot E1 \cdot Ixx1}{L^2} & \frac{4 \cdot E1 \cdot Ixx1}{L} \end{pmatrix}$$

For member 1 the local and the global frames of reference are aligned in the same therefore, the stiffness matrix for element (1) can be computed from the equation above directly

$$k1 = \begin{pmatrix} 3.333\times 10^{8} & 0 & 0 & -3.333\times 10^{8} & 0 & 0 \\ 0 & 1.286\times 10^{7} & 3.857\times 10^{7} & 0 & -1.286\times 10^{7} & 3.857\times 10^{7} \\ 0 & 3.857\times 10^{7} & 1.543\times 10^{8} & 0 & -3.857\times 10^{7} & 7.714\times 10^{7} \\ -3.333\times 10^{8} & 0 & 0 & 3.333\times 10^{8} & 0 & 0 \\ 0 & -1.286\times 10^{7} & -2.314\times 10^{8} & 0 & 1.286\times 10^{7} & -3.857\times 10^{7} \\ 0 & 3.857\times 10^{7} & 7.714\times 10^{7} & 0 & -3.857\times 10^{7} & 1.543\times 10^{8} \end{pmatrix}$$

Member 2:

$A2 := 8136 \cdot 10^{-6}$ $E2 := 205 \cdot 10^{9}$

Ixx2:= 71020500810^{-12} L2 := 10.038

For element (2), the stiffness matrix represented with respect to the local coordinate system

$$k2xy := \begin{pmatrix} \frac{E2\cdot A2}{L2} & 0 & 0 & \frac{-E2\cdot A2}{L2} & 0 & 0 \\ 0 & \frac{12\cdot E2\cdot Ixx2}{L2^{3}} & \frac{6\cdot E2\cdot Ixx2}{L2^{2}} & 0 & \frac{-12\cdot E2\cdot Ixx2}{L2^{3}} & \frac{6\cdot E2\cdot Ixx2}{L2^{2}} \\ 0 & \frac{6\cdot E2\cdot Ixx2}{L2^{2}} & \frac{4\cdot E2\cdot Ixx2}{L2} & 0 & \frac{-6\cdot E2\cdot Ixx2}{L2^{2}} & \frac{2\cdot E2\cdot Ixx2}{L2} \\ \frac{-E2\cdot A2}{L2} & 0 & 0 & \frac{E2\cdot A2}{L2} & 0 & 0 \\ 0 & \frac{-12\cdot E2\cdot Ixx2}{L2^{3}} & \frac{-6\cdot E2\cdot Ixx2}{L2^{2}} & 0 & \frac{12\cdot E2\cdot Ixx2}{L2^{3}} & \frac{-6\cdot E2\cdot Ixx2}{L2^{2}} \\ 0 & \frac{6\cdot E2\cdot Ixx2}{L2^{2}} & \frac{2\cdot E2\cdot Ixx2}{L2} & 0 & \frac{-6\cdot E2\cdot Ixx2}{L2^{2}} & \frac{4\cdot E2\cdot Ixx2}{L2} \end{pmatrix}$$

$$k2xy = \begin{pmatrix} 1.662\times 10^{8} & 0 & 0 & -1.662\times 10^{8} & 0 & 0 \\ 0 & 1.727\times 10^{6} & 8.67\times 10^{6} & 0 & -1.727\times 10^{6} & 8.67\times 10^{6} \\ 0 & 8.67\times 10^{6} & 5.802\times 10^{7} & 0 & -8.67\times 10^{6} & 2.901\times 10^{7} \\ -1.662\times 10^{8} & 0 & 0 & 1.662\times 10^{8} & 0 & 0 \\ 0 & -1.727\times 10^{6} & -8.67\times 10^{6} & 0 & 1.727\times 10^{6} & -8.67\times 10^{6} \\ 0 & 8.67\times 10^{6} & 2.901\times 10^{7} & 0 & -8.67\times 10^{6} & 5.802\times 10^{7} \end{pmatrix}$$

For element (2), the transformation matrix is

$$T2 := \begin{pmatrix} \cos(275\text{deg}) & \sin(275\text{deg}) & 0 & 0 & 0 & 0 \\ -\sin(275\text{deg}) & \cos(275\text{deg}) & 0 & 0 & 0 & 0 \\ 0 & 0 & 1 & 0 & 0 & 0 \\ 0 & 0 & 0 & \cos(275\text{deg}) & \sin(275\text{deg}) & 0 \\ 0 & 0 & 0 & -\sin(275\text{deg}) & \cos(275\text{deg}) & 0 \\ 0 & 0 & 0 & 0 & 0 & 1 \end{pmatrix}$$

$$T2 = \begin{pmatrix} 0.087 & -0.996 & 0 & 0 & 0 & 0 \\ 0.996 & 0.087 & 0 & 0 & 0 & 0 \\ 0 & 0 & 1 & 0 & 0 & 0 \\ 0 & 0 & 0 & 0.087 & -0.996 & 0 \\ 0 & 0 & 0 & 0.996 & 0.087 & 0 \\ 0 & 0 & 0 & 0 & 0 & 1 \end{pmatrix}$$

$$T2^{T} = \begin{pmatrix} 0.087 & 0.996 & 0 & 0 & 0 & 0 \\ -0.996 & 0.087 & 0 & 0 & 0 & 0 \\ 0 & 0 & 1 & 0 & 0 & 0 \\ 0 & 0 & 0 & 0.087 & 0.996 & 0 \\ 0 & 0 & 0 & -0.996 & 0.087 & 0 \\ 0 & 0 & 0 & 0 & 0 & 1 \end{pmatrix}$$

Substituting for T^T*Kxy* T to have K_{member}

$k2 := T2^T \cdot k2xy \cdot T2$

$$k2 = \begin{pmatrix} 2.976\times 10^6 & -1.428\times 10^7 & 8.637\times 10^6 & -2.976\times 10^6 & 1.428\times 10^7 & 8.637\times 10^6 \\ -1.428\times 10^7 & 1.649\times 10^8 & 7.556\times 10^5 & 1.428\times 10^7 & -1.649\times 10^8 & 7.556\times 10^5 \\ 8.637\times 10^6 & 7.556\times 10^5 & 5.802\times 10^7 & -8.637\times 10^6 & -7.556\times 10^5 & 2.901\times 10^7 \\ -2.976\times 10^6 & 1.428\times 10^7 & -8.637\times 10^6 & 2.976\times 10^6 & -1.428\times 10^7 & -8.637\times 10^6 \\ 1.428\times 10^7 & -1.649\times 10^8 & -7.556\times 10^5 & -1.428\times 10^7 & 1.649\times 10^8 & -7.556\times 10^5 \\ 8.637\times 10^6 & 7.556\times 10^5 & 2.901\times 10^7 & -8.637\times 10^6 & -7.556\times 10^5 & 5.802\times 10^7 \end{pmatrix}$$

$$k3xy := k2xy = \begin{pmatrix} 1.662\times 10^8 & 0 & 0 & -1.662\times 10^8 & 0 & 0 \\ 0 & 1.727\times 10^6 & 8.67\times 10^6 & 0 & -1.727\times 10^6 & 8.67\times 10^6 \\ 0 & 8.67\times 10^6 & 5.802\times 10^7 & 0 & -8.67\times 10^6 & 2.901\times 10^7 \\ -1.662\times 10^8 & 0 & 0 & 1.662\times 10^8 & 0 & 0 \\ 0 & -1.727\times 10^6 & -8.67\times 10^6 & 0 & 1.727\times 10^6 & -8.67\times 10^6 \\ 0 & 8.67\times 10^6 & 2.901\times 10^7 & 0 & -8.67\times 10^6 & 5.802\times 10^7 \end{pmatrix}$$

For element (3), the transformation matrix is

$$T3 := \begin{pmatrix} \cos(265\text{deg}) & \sin(265\text{deg}) & 0 & 0 & 0 & 0 \\ -\sin(265\text{deg}) & \cos(265\text{deg}) & 0 & 0 & 0 & 0 \\ 0 & 0 & 1 & 0 & 0 & 0 \\ 0 & 0 & 0 & \cos(265\text{deg}) & \sin(265\text{deg}) & 0 \\ 0 & 0 & 0 & -\sin(265\text{deg}) & \cos(265\text{deg}) & 0 \\ 0 & 0 & 0 & 0 & 0 & 1 \end{pmatrix}$$

$$T3 = \begin{pmatrix} -0.087 & -0.996 & 0 & 0 & 0 & 0 \\ 0.996 & -0.087 & 0 & 0 & 0 & 0 \\ 0 & 0 & 1 & 0 & 0 & 0 \\ 0 & 0 & 0 & -0.087 & -0.996 & 0 \\ 0 & 0 & 0 & 0.996 & -0.087 & 0 \\ 0 & 0 & 0 & 0 & 0 & 1 \end{pmatrix}$$

$$T3^{T} = \begin{pmatrix} -0.087 & 0.996 & 0 & 0 & 0 & 0 \\ -0.996 & -0.087 & 0 & 0 & 0 & 0 \\ 0 & 0 & 1 & 0 & 0 & 0 \\ 0 & 0 & 0 & -0.087 & 0.996 & 0 \\ 0 & 0 & 0 & -0.996 & -0.087 & 0 \\ 0 & 0 & 0 & 0 & 0 & 1 \end{pmatrix}$$

Substituting for T^{T}*Kxy* T to have K_{member}

$k3 := T3^{T} \cdot k3xy \cdot T3$

$$k3 = \begin{pmatrix} 2.976\times 10^{6} & 1.428\times 10^{7} & 8.637\times 10^{6} & -2.976\times 10^{6} & -1.428\times 10^{7} & 8.637\times 10^{6} \\ 1.428\times 10^{7} & 1.649\times 10^{8} & -7.556\times 10^{5} & -1.428\times 10^{7} & -1.649\times 10^{8} & -7.556\times 10^{5} \\ 8.637\times 10^{6} & -7.556\times 10^{5} & 5.802\times 10^{7} & -8.637\times 10^{6} & 7.556\times 10^{5} & 2.901\times 10^{7} \\ -2.976\times 10^{6} & -1.428\times 10^{7} & -8.637\times 10^{6} & 2.976\times 10^{6} & 1.428\times 10^{7} & -8.637\times 10^{6} \\ -1.428\times 10^{7} & -1.649\times 10^{8} & 7.556\times 10^{5} & 1.428\times 10^{7} & 1.649\times 10^{8} & 7.556\times 10^{5} \\ 8.637\times 10^{6} & -7.556\times 10^{5} & 2.901\times 10^{7} & -8.637\times 10^{6} & 7.556\times 10^{5} & 5.802\times 10^{7} \end{pmatrix}$$

For member 4 the local and the global frames of reference are aligned in the same therefore, the stiffness matrix for element (4) can be computed from the general equation above directly.

Since member (4) is typical in the properties to member (1), therefore:

$$k4 := k1$$

$$k4 = \begin{pmatrix} 3.333\times 10^{8} & 0 & 0 & -3.333\times 10^{8} & 0 & 0 \\ 0 & 1.286\times 10^{7} & 3.857\times 10^{7} & 0 & -1.286\times 10^{7} & 3.857\times 10^{7} \\ 0 & 3.857\times 10^{7} & 1.543\times 10^{8} & 0 & -3.857\times 10^{7} & 7.714\times 10^{7} \\ -3.333\times 10^{8} & 0 & 0 & 3.333\times 10^{8} & 0 & 0 \\ 0 & -1.286\times 10^{7} & -2.314\times 10^{8} & 0 & 1.286\times 10^{7} & -3.857\times 10^{7} \\ 0 & 3.857\times 10^{7} & 7.714\times 10^{7} & 0 & -3.857\times 10^{7} & 1.543\times 10^{8} \end{pmatrix}$$

Formation global stiffness matrix

K global for the whole structure

$$KG1 := \begin{pmatrix} ka11 & ka12 & 0 & 0 & 0 \\ ka21 & ka22 + kb11 & kb12 & 0 & 0 \\ 0 & kb21 & kb22 + kc11 & kc12 & 0 \\ 0 & 0 & kc21 & kc22 + kd11 & kd12 \\ 0 & 0 & 0 & kd21 & kd22 \end{pmatrix}$$

Appling the boundary conditions for nodes 1&5 as fixed with x, y and $\theta = 0$

The global matrix will be:

$$KG := \begin{pmatrix} ka22 + kb11 & kb12 & 0 \\ kb21 & kb22 + kc11 & kc12 \\ 0 & kc21 & kc22 + kd11 \end{pmatrix}$$

$$ka22 := \begin{pmatrix} \frac{E1\cdot A1}{L} & 0 & 0 \\ 0 & \frac{12\cdot E1\cdot Ixx1}{L^{3}} & \frac{-6\cdot E1\cdot Ixx1}{L^{2}} \\ 0 & \frac{-6\cdot E1\cdot Ixx1}{L^{2}} & \frac{4\cdot E1\cdot Ixx1}{L} \end{pmatrix}$$

$$ka22 = \begin{pmatrix} 3.333\times 10^{8} & 0 & 0 \\ 0 & 1.286\times 10^{7} & -3.857\times 10^{7} \\ 0 & -3.857\times 10^{7} & 1.543\times 10^{8} \end{pmatrix}$$

$$kb11 := \begin{pmatrix} 2.975\times 10^{6} & -1.428\times 10^{7} & 8.637\times 10^{6} \\ -1.428\times 10^{7} & 1.649\times 10^{8} & 7.556\times 10^{5} \\ 8.637\times 10^{6} & 7.556\times 10^{5} & 5.802\times 10^{7} \end{pmatrix}$$

$$ka22 + kb11 = \begin{pmatrix} 3.363\times 10^{8} & -1.428\times 10^{7} & 8.637\times 10^{6} \\ -1.428\times 10^{7} & 1.778\times 10^{8} & -3.781\times 10^{7} \\ 8.637\times 10^{6} & -3.781\times 10^{7} & 2.123\times 10^{8} \end{pmatrix}$$

$$kb12 := \begin{pmatrix} -2.975\times 10^{6} & 1.428\times 10^{7} & 8.637\times 10^{6} \\ 1.428\times 10^{7} & -1.649\times 10^{8} & 7.556\times 10^{5} \\ -8.637\times 10^{6} & -7.556\times 10^{5} & 2.901\times 10^{7} \end{pmatrix}$$

$$kb21 := \begin{pmatrix} -2.976\times 10^{6} & 1.428\times 10^{7} & -8.637\times 10^{6} \\ 1.428\times 10^{7} & -1.649\times 10^{8} & -7.556\times 10^{5} \\ 8.637\times 10^{6} & 7.556\times 10^{5} & 2.901\times 10^{7} \end{pmatrix}$$

$$kb22 := \begin{pmatrix} 2.976\times 10^{6} & -1.428\times 10^{7} & -8.637\times 10^{6} \\ -1.428\times 10^{7} & 1.649\times 10^{8} & -7.556\times 10^{5} \\ -8.637\times 10^{6} & -7.556\times 10^{5} & 5.802\times 10^{7} \end{pmatrix}$$

$$kc11 := \begin{pmatrix} 2.976\times 10^{6} & 1.428\times 10^{7} & 8.637\times 10^{6} \\ 1.428\times 10^{7} & 1.649\times 10^{8} & -7.556\times 10^{5} \\ 8.637\times 10^{6} & -7.556\times 10^{5} & 5.802\times 10^{7} \end{pmatrix}$$

$$kb22 + kc11 = \begin{pmatrix} 5.952\times 10^{6} & 0 & 0 \\ 0 & 3.298\times 10^{8} & -1.511\times 10^{6} \\ 0 & -1.511\times 10^{6} & 1.16\times 10^{8} \end{pmatrix}$$

$$kc12 := \begin{pmatrix} -2.976\times 10^{6} & -1.428\times 10^{7} & 8.637\times 10^{6} \\ -1.428\times 10^{7} & -1.649\times 10^{8} & -7.556\times 10^{5} \\ -8.637\times 10^{6} & 7.556\times 10^{5} & 2.901\times 10^{7} \end{pmatrix}$$

$$kc21 := \begin{pmatrix} -2.976\times 10^{6} & -1.428\times 10^{7} & -8.637\times 10^{6} \\ -1.428\times 10^{7} & -1.649\times 10^{8} & 7.556\times 10^{5} \\ 8.637\times 10^{6} & -7.556\times 10^{5} & 2.901\times 10^{7} \end{pmatrix}$$

$$kc22 := \begin{pmatrix} 2.976\times 10^{6} & 1.428\times 10^{7} & -8.637\times 10^{6} \\ 1.428\times 10^{7} & 1.649\times 10^{8} & 7.556\times 10^{5} \\ -8.637\times 10^{6} & 7.556\times 10^{5} & 5.802\times 10^{7} \end{pmatrix}$$

$$kd11 := \begin{pmatrix} 3.333\times 10^{8} & 0 & 0 \\ 0 & 1.286\times 10^{7} & 3.857\times 10^{7} \\ 0 & 3.857\times 10^{7} & 1.543\times 10^{8} \end{pmatrix}$$

$$kc22 + kd11 = \begin{pmatrix} 3.363\times 10^{8} & 1.428\times 10^{7} & -8.637\times 10^{6} \\ 1.428\times 10^{7} & 1.778\times 10^{8} & 3.933\times 10^{7} \\ -8.637\times 10^{6} & 3.933\times 10^{7} & 2.123\times 10^{8} \end{pmatrix}$$

$$KG := \begin{pmatrix} ka22 + kb11 & kb12 & 0 \\ kb21 & kb22 + kc11 & kc12 \\ 0 & kc21 & kc22 + kd11 \end{pmatrix}$$

$$KG := \begin{pmatrix} 3.363\times 10^{6} & -1.428\times 10^{7} & 8.637\times 10^{6} & -2.975\times 10^{6} & 1.428\times 10^{7} & 8.637\times 10^{6} & 0 & 0 & 0 \\ -1.428\times 10^{7} & 1.778\times 10^{8} & -3.781\times 10^{7} & 1.428\times 10^{7} & -1.649\times 10^{8} & 7.556\times 10^{5} & 0 & 0 & 0 \\ 8.637\times 10^{6} & -3.781\times 10^{7} & 2.123\times 10^{8} & -8.637\times 10^{6} & -7.556\times 10^{5} & 2.901\times 10^{7} & 0 & 0 & 0 \\ -2.975\times 10^{6} & 1.428\times 10^{7} & -8.637\times 10^{6} & 5.95\times 10^{6} & 0 & 0 & -2.976\times 10^{6} & -1.428\times 10^{7} & 8.637\times 10^{6} \\ 1.428\times 10^{7} & -1.649\times 10^{8} & -7.556\times 10^{5} & 0 & 3.298\times 10^{8} & -1.511\times 10^{6} & -1.428\times 10^{7} & -1.649\times 10^{8} & -7.556\times 10^{5} \\ 8.637\times 10^{6} & 7.556\times 10^{5} & 2.901\times 10^{7} & 0 & -1.511\times 10^{6} & 1.16\times 10^{8} & -8.637\times 10^{6} & 7.556\times 10^{5} & 2.901\times 10^{7} \\ 0 & 0 & 0 & -2.976\times 10^{6} & -1.428\times 10^{7} & -8.637\times 10^{6} & 3.363\times 10^{8} & 1.428\times 10^{7} & -8.637\times 10^{6} \\ 0 & 0 & 0 & -1.428\times 10^{7} & -1.649\times 10^{8} & 7.556\times 10^{5} & 1.428\times 10^{7} & 1.778\times 10^{8} & 3.933\times 10^{7} \\ 0 & 0 & 0 & 8.637\times 10^{6} & -7.556\times 10^{5} & 2.901\times 10^{7} & -8.637\times 10^{6} & 3.933\times 10^{7} & 2.123\times 10^{8} \end{pmatrix}$$

$$KG - KG^{T} = \begin{pmatrix} 0&0&0&0&0&0&0&0&0 \\ 0&0&0&0&0&0&0&0&0 \\ 0&0&0&0&0&0&0&0&0 \\ 0&0&0&0&0&0&0&0&0 \\ 0&0&0&0&0&0&0&0&0 \\ 0&0&0&0&0&0&0&0&0 \\ 0&0&0&0&0&0&0&0&0 \\ 0&0&0&0&0&0&0&0&0 \\ 0&0&0&0&0&0&0&0&0 \end{pmatrix}$$

The global lumped mass is:

$$M := \begin{pmatrix} M1 + M2 & 0 & 0 \\ 0 & M2 + M3 & 0 \\ 0 & 0 & M3 + M4 \end{pmatrix}$$

The lumped mass matrix for one node

Mass Matrix

$$M1 := \begin{pmatrix} Mx & 0 & 0 \\ 0 & My & 0 \\ 0 & 0 & M\theta \end{pmatrix}$$

For rafter:

$Mr := 681 \cdot kg$

$Ir := 56 \cdot kg \cdot m^2$

For column

$Mc := 460 \cdot kg$

$Ic := 52 \cdot kg \cdot m^2$

Values for Mass will be applied

$0.5 \cdot Mr = 340.5kg$

$0.5 \cdot Ir = 28 m^2 \cdot kg$

$0.5 \cdot Mc = 230kg$

$0.5 \cdot Ic = 26 m^2 \cdot kg$

$$M1 := \begin{pmatrix} 230 & 0 & 0 \\ 0 & 230 & 0 \\ 0 & 0 & 26 \end{pmatrix} \qquad M2 := \begin{pmatrix} 340 & 0 & 0 \\ 0 & 340 & 0 \\ 0 & 0 & 28 \end{pmatrix}$$

$$M3 := \begin{pmatrix} 340 & 0 & 0 \\ 0 & 340 & 0 \\ 0 & 0 & 28 \end{pmatrix} \qquad M4 := \begin{pmatrix} 230 & 0 & 0 \\ 0 & 230 & 0 \\ 0 & 0 & 26 \end{pmatrix}$$

The global mass matrix is:

$$MG := \begin{pmatrix} 570 & 0 & 0 & 0 & 0 & 0 & 0 & 0 & 0 \\ 0 & 570 & 0 & 0 & 0 & 0 & 0 & 0 & 0 \\ 0 & 0 & 54 & 0 & 0 & 0 & 0 & 0 & 0 \\ 0 & 0 & 0 & 680 & 0 & 0 & 0 & 0 & 0 \\ 0 & 0 & 0 & 0 & 680 & 0 & 0 & 0 & 0 \\ 0 & 0 & 0 & 0 & 0 & 56 & 0 & 0 & 0 \\ 0 & 0 & 0 & 0 & 0 & 0 & 570 & 0 & 0 \\ 0 & 0 & 0 & 0 & 0 & 0 & 0 & 570 & 0 \\ 0 & 0 & 0 & 0 & 0 & 0 & 0 & 0 & 54 \end{pmatrix}$$

Determine determinant for Matrix -ω 2M+K is: Mω

The natural frequencies are given by the solutions of the determinant for matrix [k]-ω 2[m] or by solving the eigenvalue problem.

$$A := MG^{-1} \cdot KC$$

$$\text{eigenvals}(A) = \begin{pmatrix} 4.206 \times 10^{6} \\ 3.947 \times 10^{6} \\ 1.814 \times 10^{6} \\ 7.828 \times 10^{5} \\ 5.845 \times 10^{5} \\ 3.006 \times 10^{5} \\ 9.426 \times 10^{3} \\ 666.78 \\ 2.848 \times 10^{3} \end{pmatrix}$$

$$\text{eigenvecs}(A) = \begin{pmatrix} 3.642\times 10^{-3} & 2.829\times 10^{-3} & -5.746\times 10^{-3} & 0.036 & 0.012 & -0.055 & -0.388 & 0.814 & -0.496 \\ -0.011 & -0.013 & -0.011 & -0.444 & -0.111 & 0.68 & -0.495 & 0.032 & 0.313 \\ 0.667 & 0.709 & 0.236 & -0.097 & -0.041 & 0.149 & -0.057 & 3.481\times 10^{-3} & 0.093 \\ -1.057\times 10^{-4} & -4.565\times 10^{-3} & -2.514\times 10^{-4} & 4.109\times 10^{-3} & -9.209\times 10^{-3} & 0.098 & 0.529 & 0.573 & 0.525 \\ -6.005\times 10^{-4} & 1.861\times 10^{-3} & 1.211\times 10^{-3} & 0.743 & 0.113 & 5.247\times 10^{-3} & -0.425 & 0.013 & 0.402 \\ 0.325 & 7.153\times 10^{-4} & -0.942 & 3.429\times 10^{-4} & 0.106 & -0.076 & 0.033 & -0.055 & 0.041 \\ -4.083\times 10^{-3} & 3.073\times 10^{-3} & 8.918\times 10^{-3} & -0.163 & 0.98 & 0.065 & 4.457\times 10^{-3} & 7.628\times 10^{-4} & 1.221\times 10^{-3} \\ 0.012 & -0.013 & 9.946\times 10^{-3} & -0.451 & -0.02 & -0.687 & -0.372 & 0.064 & 0.443 \\ 0.67 & -0.705 & 0.236 & 0.099 & 0.035 & 0.148 & 0.042 & -0.028 & -0.108 \end{pmatrix}$$

Mode	Frequency F_i (cycles/sec)	Natural Frequency ω_i (rad/sec)	T(sec)
1	4.111796747	25.82208357	0.243
2	8.4978752	53.4	0.118
3	15.45980722	9.71E+01	0.064684
4	87.30414116	5.48E+02	0.011454
5	121.7398084	7.65E+02	8.21E-03
6	140.8853271	8.85E+02	7.10E-03
7	214.4662695	1.35E+03	4.66E-03
8	316.3544293	1.99E+03	3.16E-03
9	326.5690256	2.05E+03	3.06E-03

$Fi = \omega i / 2\pi$

$Ti = 1/Fi$

ϕ the matrix of mode shapes (in columns) is:

$$\phi := \text{eigenvecs}(A) = \begin{pmatrix} 3.642\times 10^{-3} & 2.829\times 10^{-3} & -5.746\times 10^{-3} & 0.036 & 0.012 & -0.055 & -0.388 & 0.814 & -0.496 \\ -0.011 & -0.013 & -0.011 & -0.444 & -0.111 & 0.68 & -0.495 & 0.032 & 0.313 \\ 0.667 & 0.709 & 0.236 & -0.097 & -0.041 & 0.149 & -0.057 & 3.481\times 10^{-3} & 0.093 \\ -1.057\times 10^{-4} & -4.565\times 10^{-3} & -2.514\times 10^{-4} & 4.109\times 10^{-3} & -9.209\times 10^{-3} & 0.098 & 0.529 & 0.573 & 0.525 \\ -6.005\times 10^{-4} & 1.861\times 10^{-3} & 1.211\times 10^{-3} & 0.743 & 0.113 & 5.247\times 10^{-3} & -0.425 & 0.013 & 0.402 \\ 0.325 & 7.153\times 10^{-4} & -0.942 & 3.429\times 10^{-4} & 0.106 & -0.076 & 0.033 & -0.055 & 0.041 \\ -4.083\times 10^{-3} & 3.073\times 10^{-3} & 8.918\times 10^{-3} & -0.163 & 0.98 & 0.065 & 4.457\times 10^{-3} & 7.628\times 10^{-4} & 1.221\times 10^{-3} \\ 0.012 & -0.013 & 9.946\times 10^{-3} & -0.451 & -0.02 & -0.687 & -0.372 & 0.064 & 0.443 \\ 0.67 & -0.705 & 0.236 & 0.099 & 0.035 & 0.148 & 0.042 & -0.028 & -0.108 \end{pmatrix}$$

7. Determination Earthquake participation factors and modal mass for each mode

$$L = n\Sigma\, i=1\ Mi\ \phi\ i1$$

$$Lm1 := 570\cdot\left(\phi_{0,0}\right) + 570\cdot\left(\phi_{1,0}\right) + 680\cdot\phi_{3,0} + 680\cdot\phi_{4,0} + 570\cdot\phi_{6,0} + 570\cdot\phi_{7,0}$$

$$Lm1 = -0.289$$

$$M1 := 570\cdot\left(\phi_{0,0}\right)^2 + 570\cdot\left(\phi_{1,0}\right)^2 + 680\cdot\left(\phi_{3,0}\right)^2 + 680\cdot\left(\phi_{4,0}\right)^2 + 570\cdot\left(\phi_{6,0}\right)^2 + 570\cdot\left(\phi_{7,0}\right)^2$$

$$M1 = 0.171$$

$$Lm2 := 570\cdot\phi_{0,1} + 570\cdot\phi_{1,1} + 680\cdot\phi_{3,1} + 680\cdot\phi_{4,1} + 570\cdot\phi_{6,1} + 570\cdot\phi_{7,1}$$

$$Lm2 = -13.645$$

$$M2 := 570\cdot\left(\phi_{0,1}\right)^2 + 570\cdot\left(\phi_{1,1}\right)^2 + 680\cdot\left(\phi_{3,1}\right)^2 + 680\cdot\left(\phi_{4,1}\right)^2 + 570\cdot\left(\phi_{6,1}\right)^2 + 570\cdot\left(\phi_{7,1}\right)^2$$

$$M2 = 0.228$$

$$Lm3 := 570\cdot\phi_{0,2} + 570\cdot\phi_{1,2} + 680\cdot\phi_{3,2} + 680\cdot\phi_{4,2} + 570\cdot\phi_{6,2} + 570\cdot\phi_{7,2}$$

$$Lm3 = 1.641$$

$$M3 := 570\cdot\left(\phi_{0,2}\right)^2 + 570\cdot\left(\phi_{1,2}\right)^2 + 680\cdot\left(\phi_{3,2}\right)^2 + 680\cdot\left(\phi_{4,2}\right)^2 + 570\cdot\left(\phi_{6,2}\right)^2 + 570\cdot\left(\phi_{7,2}\right)^2$$

$$M3 = 0.195$$

$$Lm4 := 570\cdot\phi_{0,3} + 570\cdot\phi_{1,3} + 680\cdot\phi_{3,3} + 680\cdot\phi_{4,3} + 570\cdot\phi_{6,3} + 570\cdot\phi_{7,3}$$

$$Lm4 = -74.474$$

$$M4 := 570\cdot\left(\phi_{0,3}\right)^2 + 570\cdot\left(\phi_{1,3}\right)^2 + 680\cdot\left(\phi_{3,3}\right)^2 + 680\cdot\left(\phi_{4,3}\right)^2 + 570\cdot\left(\phi_{6,3}\right)^2 + 570\cdot\left(\phi_{7,3}\right)^2$$

$$M4 = 619.745$$

$$Lm5 := 570\cdot\phi_{0,4} + 570\cdot\phi_{1,4} + 680\cdot\phi_{3,4} + 680\cdot\phi_{4,4} + 570\cdot\phi_{6,4} + 570\cdot\phi_{7,4}$$

$$Lm5 = 560.925$$

$$M5 := 570\cdot\left(\phi_{0,4}\right)^2 + 570\cdot\left(\phi_{1,4}\right)^2 + 680\cdot\left(\phi_{3,4}\right)^2 + 680\cdot\left(\phi_{4,4}\right)^2 + 570\cdot\left(\phi_{6,4}\right)^2 + 570\cdot\left(\phi_{7,4}\right)^2$$

$$M5 = 563.4$$

$$Lm6 := 570\cdot\phi_{0,5} + 570\cdot\phi_{1,5} + 680\cdot\phi_{3,5} + 680\cdot\phi_{4,5} + 570\cdot\phi_{6,5} + 570\cdot\phi_{7,5}$$

$$Lm6 = 71.96$$

$$M6 := 570\cdot\left(\phi_{0,5}\right)^2 + 570\cdot\left(\phi_{1,5}\right)^2 + 680\cdot\left(\phi_{3,5}\right)^2 + 680\cdot\left(\phi_{4,5}\right)^2 + 570\cdot\left(\phi_{6,5}\right)^2 + 570\cdot\left(\phi_{7,5}\right)^2$$

$$M6 = 542.672$$

$$Lm7 := 570\cdot\phi_{0,6} + 570\cdot\phi_{1,6} + 680\cdot\phi_{3,6} + 680\cdot\phi_{4,6} + 570\cdot\phi_{6,6} + 570\cdot\phi_{7,6}$$

$$Lm7 = -641.142$$

$$M7 := 570\cdot\left(\phi_{0,6}\right)^2 + 570\cdot\left(\phi_{1,6}\right)^2 + 680\cdot\left(\phi_{3,6}\right)^2 + 680\cdot\left(\phi_{4,6}\right)^2 + 570\cdot\left(\phi_{6,6}\right)^2 + 570\cdot\left(\phi_{7,6}\right)^2$$

$$M7 = 617.186$$

$$Lm8 := 570\cdot\phi_{0,7} + 570\cdot\phi_{1,7} + 680\cdot\phi_{3,7} + 680\cdot\phi_{4,7} + 570\cdot\phi_{6,7} + 570\cdot\phi_{7,7}$$

$$Lm8 = 917.545$$

$$M8 := 570\cdot\left(\phi_{0,7}\right)^2 + 570\cdot\left(\phi_{1,7}\right)^2 + 680\cdot\left(\phi_{3,7}\right)^2 + 680\cdot\left(\phi_{4,7}\right)^2 + 570\cdot\left(\phi_{6,7}\right)^2 + 570\cdot\left(\phi_{7,7}\right)^2$$

$$M8 = 603.982$$

$$Lm9 := 570\cdot\phi_{0,8} + 570\cdot\phi_{1,8} + 680\cdot\phi_{3,8} + 680\cdot\phi_{4,8} + 570\cdot\phi_{6,8} + 570\cdot\phi_{7,8}$$

$$Lm9 = 779.501$$

$$M9 := 570\cdot\left(\phi_{0,8}\right)^2 + 570\cdot\left(\phi_{1,8}\right)^2 + 680\cdot\left(\phi_{3,8}\right)^2 + 680\cdot\left(\phi_{4,8}\right)^2 + 570\cdot\left(\phi_{6,8}\right)^2 + 570\cdot\left(\phi_{7,8}\right)^2$$

$$M9 = 605.634$$

8. Determine effective weight and participating mass for each mode:

$Wm = (Lm^2/Mm) \times g$

$$W1 := \frac{Lm1^2}{M1}\cdot 9.81$$

$$W1 = 4.775$$

$$W2 := \frac{Lm2^2}{M2}\cdot 9.81$$

$$W2 = 7.997\times 10^3$$

$$W3 := \frac{Lm3^2}{M3}\cdot 9.81$$

$$W3 = 135.188$$

$$W4 := \frac{Lm4^2}{M4}\cdot 9.81$$

$$W4 = 87.793$$

$$W5 := \frac{Lm5^2}{M5}\cdot 9.81$$

$$W5 = 5.479\times 10^3$$

$$W6 := \frac{Lm6^2}{M6}\cdot 9.81$$

$$W6 = 93.609$$

$$W7 := \frac{Lm7^2}{M7}\cdot 9.81$$

$$W7 = 6.534\times 10^3$$

$$W8 := \frac{Lm8^2}{M8}\cdot 9.81$$

$$W8 = 1.367\times 10^4$$

$$W9 := \frac{Lm9^2}{M9} \cdot 9.81 \qquad W9 = 9.842 \times 10^3$$

9. Participating mass:

$$PM = Wm/W$$

$$PM1 := \frac{W1}{Wt} = 1.646 \times 10^{-4}$$

$$PM2 := \frac{W2}{Wt} = 0.276$$

$$PM3 := \frac{W3}{Wt} = 4.662 \times 10^{-3}$$

$$PM4 := \frac{W4}{Wt} = 3.027 \times 10^{-3}$$

$$PM5 := \frac{W5}{Wt} = 0.189$$

$$PM6 := \frac{W6}{Wt} = 3.228 \times 10^{-3}$$

$$PM7 := \frac{W7}{Wt} = 0.225$$

$$PM8 := \frac{W8}{Wt} = 0.472$$

$$PM9 := \frac{W9}{Wt} = 0.339$$

We will use only first three mode shapes and natural frequencies, since stability condition for numerical solution will not meet in modes above three (higher modes have very small periods in this structure.

$$\Sigma PM := PM7 + PM8 + PM9$$

$$\Sigma PM = 1.036$$

10. Determination (spectral acceleration) and seismic design coefficient, Csm for each mode using International building code (IBC)

The modal seismic response coefficient for this structure:

$$Sam1 := SDS$$

Equation 16-53

1618.4 2000 IBC

$$Csm1 := \frac{Sam1 \cdot IE}{Ra \cdot T}$$

$$Csm1 = 0.375\frac{1}{T}$$

Less than or equal to Csm2

$$Sam2 := SD1 \qquad T2 := 1$$

$$Csm2 := \frac{Sam2 \cdot IE}{Ra \cdot T2} \qquad Csm2 = 0.225$$

Mode 1: T=3.06E-03 sec

$$Cs1 := \frac{0.15}{3.06E\text{-}03} \cdot g = 480.718\frac{m}{s^2}$$

Should be less than 0.15 g Use 0.15 g

Mode 2: T=3.16E-03 sec

$$Cs2 := \frac{0.15}{3.16E\text{-}03} \cdot g = 465.506\frac{m}{s^2}$$

Should be less than 0.15 g Use 0.15 g

Mode 3: T=4.66E-03 sec

$$Cs3 := \frac{0.15}{4.66E\text{-}03} \cdot g = 315.665\frac{m}{s^2}$$

Should be less than 0.15 g Use 0.15 g

Mode 4: T=7.10E-03 sec

$$Cs4 := \frac{0.15}{7.10E\text{-}03} \cdot g = 207.183\frac{m}{s^2}$$

Should be less than 0.15 g Use 0.15 g

Mode 5: T=8.21E-03 sec

$$Cs5 := \frac{0.15}{8.21E\text{-}03} \cdot g = 179.171\frac{m}{s^2}$$

Should be less than 0.15 g Use 0.15 g

Mode 6: T=1.15E-02 sec

$$Cs6 := \frac{0.15}{1.15E\text{-}02} \cdot g = 127.913 \frac{m}{s^2}$$

Should be less than 0.15 g Use 0.15 g

Mode 7: T=6.47E-02 sec

$$Cs7 := \frac{0.15}{6.47E\text{-}02} \cdot g = 22.736 \frac{m}{s^2}$$

Should be less than 0.15 g Use 0.15 g

Mode 8: T=2.43E-01 sec

$$Cs8 := \frac{0.15}{2.43E\text{-}01} \cdot g = 6.053 \frac{m}{s^2}$$

Should be Less than 0.15 g Use 0.15 g

Mode 9: T=1.18E-01 sec

$$Cs9 := \frac{0.15}{1.18E\text{-}01} \cdot g = 12.466 \frac{m}{s^2}$$

Should be less than 0.15 g Use 0.15 g

12. Determination of modal base shears

Vm = Csm*Wm/g

Equation 16-51
1618.4 (2000 IBC)

Mode 1: $V1 := 0.15 \cdot W1 = 0.716$

Mode 2: $V2 := 0.15 \cdot W2 = 1.2 \times 10^3$

Mode 3: $V3 := 0.15 \cdot W3 = 20.278$

Mode 4: $V4 := 0.15 \cdot W4 = 13.169$

Mode 5: $V5 := 0.15 \cdot W5 = 821.777$

Mode 6: $V6 := 0.15 \cdot W6 = 14.041$

Mode 7: $V7 := 0.15 \cdot W7 = 980.059$

Mode 8: $V8 := 0.15 \cdot W8 = 2.051 \times 10^3$

Mode 9: $V9 := 0.15 \cdot W9 = 1.476 \times 10^3$

$$Vd := (V7 + V8 + V9) = 4.508 \times 10^3$$

11. Determination of design base shear from static - force procedure to compare with base shear from dynamic analysis using Eurocode 8.

The design spectrum for elastic analysis Sd:

The design spectrum for the period of the structure:

For Ta greater than Tb and less than Tc the design spectrum Sd; Sd= a g * Sp*2.5/q Equation 3.14 (EC8)

Period using Approximate Fundamental Period Formula:

$$Ta = CT\,(hn)^{3/4}$$

$CT := 0.085$

$hn := 6.875$

$$Ta := CT\cdot(hn)^{\frac{3}{4}} = 0.361$$

$\beta := 0.2$

$$Sdsa := agr\cdot Sp\cdot\left(\frac{2.5}{q}\right)$$

$Sdsa = 0.441$

The seismic design shear (Fb)= λ *M*SD

M, the mass of the structure

$\lambda := 0.85$

$mt := 9.66 \quad tonne$

$$Fb1 := \lambda\cdot mt\cdot Sdsa$$

$Fb1 = 3.62 \quad KN$

14. Determination of design base shear from static - force procedure to compare with base shear from dynamic analysis using the international building code

V = SD1*IE *W/R*T

Greater than or equal 0.044SDS*IE*W 1617.4.1.1

2000 IBC

Less than or equal SDS*IE*W/R

Less than or equal 0.5*S1*IE/R

Period using Approximate Fundamental Period 1617.4.2

Formula: 2000 IBC

$Ta = CT\,(hn)^{3/4}$

$Ta = 0.361$

$VS := \frac{SDS \cdot IE \cdot W}{Ra} = 0.375W$ **This governs**

Less than $\frac{SD1 \cdot IE \cdot W}{Ra \cdot Ta} = 0.623W$

Greater than $0.044\,SDS \cdot IE \cdot W = 0.066W$

Greater than $\frac{0.5 \cdot S1 \cdot IE \cdot W}{Ra \cdot g} = 0.113W$

Use V= 0.375W

$Vs := 0.375 \cdot Wt = 1.087 \times 10^4$

The base shear V using modal analysis should not be less than that using the static procedure based on a period = 1.2Cu Ta according to IBC

10.87 KN > 5.508 KN

$Vs > Vd$

So, the modal forces must be scaled up.

Scale factor= $\frac{Vs}{Vd}$

$Sf := \frac{Vs}{Vd}$

$Sf = 2.413$

Scale up modal results

$Vd1 := Sf \cdot V7$ $Vd1 = 2.365 \times 10^3$

$Vd2 := Sf \cdot V8$ $Vd2 = 4.949 \times 10^3$

$Vd3 := Sf \cdot V9$ $Vd3 = 3.562 \times 10^3$

$$Vds := \left(Vd1^2 + Vd2^2 + Vd3^2\right)^{0.5}$$

$$Vds = 6.54 \times 10^3$$

15. Distribution of base shear for each mode over height of the structure

Lateral force at level i for mode m, Fim= (wi ϕ im/ Σ wi ϕ im)* Vm 1618.5

2000 IBC

Mode 1:

Node	Weight Wi	ϕi	Wi φ i	Fi
2	$wi1 := 28$	$\phi 1 := \phi_{0,0}$	$wi1 \cdot \phi 1 = 0.102$	$\frac{wi1 \cdot \phi 1}{wi1 \cdot \phi 1} \cdot Vds \cdot 10^{-3} = 6.54$

Mode 2:

Node	Weight Wi	ϕi	Wi φ i	Fi
2	$wi2 := 28$	$\phi 2 := \phi_{0,1}$	$wi2 \cdot \phi 2 = 0.079$	$\frac{wi2 \cdot \phi 2}{wi2 \cdot \phi 2} \cdot Vds \cdot 10^{-3} = 6.54$

Mode 3:

Node	Weight Wi	ϕi	Wi φ i	Fi
2	$wi3 := 28$	$\phi 3 := \phi_{0,2}$	$wi3 \cdot \phi 3 = -0.161$	$\frac{wi3 \cdot \phi 3}{wi3 \cdot \phi 3} \cdot Vds \cdot 10^{-3} = 6.54$

Mode 4:

Node	Weight Wi	ϕi	Wi φ i	Fi
2	$wi4 := 28$	$\phi 4 := \phi_{0,3}$	$wi4 \cdot \phi 4 = 1.018$	$\frac{wi4 \cdot \phi 4}{wi4 \cdot \phi 4} \cdot Vds \cdot 10^{-3} = 6.54$

Mode 5:

Node	Weight Wi	ϕi	Wi φ i	Fi
2	$wi5 := 28$	$\phi 5 := \phi_{0,4}$	$wi5 \cdot \phi 5 = 0.322$	$\frac{wi5 \cdot \phi 5}{wi5 \cdot \phi 5} \cdot Vds \cdot 10^{-3} = 6.54$

Mode 6:

Node	Weight Wi	ϕi	Wi φ i	Fi
2	$wi6 := 28$	$\phi 6 := \phi_{0,5}$	$wi6 \cdot \phi 6 = -1.548$	$\frac{wi6 \cdot \phi 6}{wi6 \cdot \phi 6} \cdot Vds \cdot 10^{-3} = 6.54$

Mode 7:

Node	Weight Wi	ϕi	Wi φ i	Fi
2	$wi7 := 28$	$\phi 7 := \phi_{0,6}$	$wi7 \cdot \phi 7 = -10.854$	$\frac{wi7 \cdot \phi 7}{wi7 \cdot \phi 7} \cdot Vds \cdot 10^{-3} = 6.54$

Mode 8:

Node	Weight Wi	ϕi	Wi φ i	Fi
2	$wi8 := 28$	$\phi 8 := \phi_{0,7}$	$wi8 \cdot \phi 8 = 22.789$	$\frac{wi8 \cdot \phi 8}{wi8 \cdot \phi 8} \cdot Vds \cdot 10^{-3} = 6.54$

Mode 9:

Node	Weight Wi	ϕi	Wi φ i	Fi
2	$wi9 := 28$	$\phi 9 := \phi_{0,8}$	$wi9 \cdot \phi 9 = -13.893$	$\frac{wi9 \cdot \phi 9}{wi9 \cdot \phi 9} \cdot Vds \cdot 10^{-3} = 6.54$

It is constant because it is single storey building.

Appendix (C) Design of portal frame with EC3

1. Basic Data

Total length $b := 40$

Spacing $s := 5$ Rafter length D $D := 10.04$

Bay width $L := 20$ $f := 0.875$

Height $h := 6$

Roof angle $\alpha := 5$ $E := 205 \cdot 10^3$

$\upsilon := 0.3$ $Gsh := \frac{E}{2(1 + \upsilon)}$

2. Loads

2.1 Permanent loads (KN/m)

Self -weight of the beam $Gs := 0.13$ EN 1991-1-1

Purlins, cladding, sheeting and insulation= Gr $Gr := 0.364$

On slope $g1 := Gs + Gr = 0.494$

On plan $g2 := (Gs + Gr) \cdot \frac{10.04}{10}$ $g2 = 0.496$

for an internal frame $Gk := g2 \cdot s$ $Gk = 2.48 \ \frac{KN}{m}$

$Gf := Gk \cdot 10 \ KN$

Self weight of columns= $Gc := 4.53 \ KN$

$Gt := Gf + Gc = 29.329$

Total dead load for seismic action Gsm

$Gsm := Gt \cdot 2 = 58.658$

2.2 Snow loads (KN/m)

Characteristic values for snow loading on the roof in [kN/m]

EN 1991-1-3

$Sn := 0.8 \cdot 1.0 \cdot 1.0 \cdot 0.772$

$Sn = 0.618$

for an internal frame $Qsn := Sn \cdot s$

For this case where, the structure will be in place with no snow

$Qs := 0$

2.3 Imposed load on roof (KN)

Characteristic values for loading on the roof (type H: not accessible)

$qk := 0.6$

NA to BS EN 1991-1-1 Table NA.7

On plan $qk1 := qk \cdot \frac{10.04}{10}$

$Qk := qk1 \cdot s$ $Qk = 3.012 \ \frac{KN}{m}$

for an internal frame

$Q := Qk \cdot 10$

$Q = 30.12 \ KN$

Total imposed load for seismic action Gsm

$Qsm := Q \cdot 2 = 60.24$

2.4 Earthquake load (KN/m)

Characteristic values for loading for earthquake loading in kN/m for an internal frame

$QeH := 4.71 \ KN$

2.5 Seismic mass

$M = G + \psi_{Ei} Q$

$\varphi := 1$

$\psi_{2i} := 0.6$

$\psi Ei := \varphi \cdot \psi 2i$

$\psi Ei = 0.6$

Seismic mass $Ms := Gsm + \psi Ei \cdot Qsm = 94.802$

Seismic mass

$$Msm := \frac{Ms}{9.81} = 9.664 \quad \text{Tonne}$$

Total mass=Msm

3. Load combinations

3.1 Partial safety factor

EN 1990

$\gamma_{Gmax} = 1.35$ (permanent loads)

EN 1990

Table A1.1

$\gamma_Q = 1.50$ (variable loads)

$\psi_{2i} = 0.6$ (imposed)

3.2 ULS Combinations

Combination 1: $\gamma_{Gmax} G + \gamma_Q Q_s$

Combination 2: $G + \psi_{2i} Q + E$ EN 1990

Q=3.012 kN/m for imposed load

$\gamma 1 := 1.35$ $\gamma q := 1.5$ $\psi 2i = 0.6$

$Comb1 := \gamma 1 \cdot Gk + \gamma q \cdot Qk$

$Comb2 := Gk + \psi 2i \cdot Qk$

Combination Values

Comb1 = 7.866

Comb2 = 4.287 Plus the horizontal forces for earthquake effect

4 Sections

4.1 Column

Try 850x650x63x3 - back to back lip channel section - steel grade S 355

Depth hc := 0.850 Lip depth Ld := 0.06

Web Depth hw := 0.84 Lip thickness Lt := 0.00

Width b := 0.650 fy := 35

Web thickness tw := 0.006

Flange thickness tf := 0.00 Rxx:= 340.153293

Mass mc := 76.5 $\frac{Kg}{m}$ Ryy := 123.378681

Section area Ac := 0.009756

Second moment of area /xx Ixx:= 0.00112881078

Second moment of area /yy Iyy := 0.000148508750

Torsion constant It := 0.000677736

Elastic modulus/xx Zx := 0.00265602538

Plastic modulus/xx Sx := 0.00612503

Elastic modulus/yy Zy := 0.000456950

4.2 Rafter

Try 750x500x53x3 - back to back lip channel section - steel grade S 355

Depth hr := 0.750 Lip depth Ldr := 0.053

Web Depth hwr := 0.744 Lip thickness Ltr := 0.003

Width br := 0.500

Web thickness twr := 0.006

Flange thickness tfr := 0.003

Mass mr := 64.12 $\frac{Kg}{m}$

Section area Ar := 0.00813

Second moment of area /xx Ixxr := 0.000710205008

Second moment of area /yy Iyyr := 0.000071000000

Torsion constant Itr := 0.000588636

Elastic modulus/xx Zxr := 0.00189388002

Plastic modulus/xx Sxr := 0.00441444

Elastic modulus/yy Zyr := 0.000284000

5. Buckling amplification factor α cr EN 1993-1-1 :5.2.1(3)

In order to evaluate the sensitivity of the frame to 2 nd order effects, a buckling analysis

is performed to calculate the buckling amplification factor α_{cr} for the load combination given the highest vertical load: Combination 1: $\gamma_{Gmax} G + \gamma_Q Q_s$

This calculation requires the deflections of the frame to be known under this load combination.

$C1 = 7.866$ $C1 := 1.35 \cdot Gk + 1.5 \cdot Qk$

5.1 Analysis using the coefficient in the steel manual for fixed bases

Constants

$h := 6$ $D := 10.0$

$k := \frac{h}{D}$ $k = 0.598$

$f := 0.87$

$\phi := \frac{f}{h}$ $\phi = 0.146$

$m := 1 + \phi$ $B := 3 \cdot k + 2$ $B = 3.793$

$m = 1.146$

$C := 1 + 2 \cdot m$

$C = 3.292$

$k1 := 2\left(k + 1 + m + m^2\right)$ $k1 =$ ∎

$k2 := \left(k + \phi^2\right)$ $k2 = 0.619$

$R := \phi \cdot C - k$ $R = -0.118$

$N1 := k1 \cdot k2 - R^2$ $N1 = 5.007$

$N2 := 3 \cdot k + B$ $N2 = 5.586$

Note. Ma= Me Note. Mb= Md Note. Va=Ve Note. Ha=He

I. Design load $\omega := 1.35 \cdot Gk + 1.5 \cdot Qk$

$\omega = 7.866$

$Ma := \frac{\omega \cdot L^2}{16} \cdot \frac{k \cdot (8 + 15 \cdot \phi) + \phi^2}{N1}$ $Me := Ma$

$Ma = 239.944$ $Me = 239.944$

$$Mb := \frac{\omega \cdot L^2}{8} \cdot \frac{k \cdot (16 + 15 \cdot \phi) + \phi^2}{N1} \qquad Md := Mb$$

$$Mb = 855.42 \qquad Md = 855.42$$

$$Mc := \frac{\omega \cdot L^2}{8} - \phi \cdot Ma + m \cdot Mb \qquad Mc = 1.338 \times 10^3$$

$$Va := \frac{\omega \cdot L}{2} \qquad Va = 78.658 \qquad Ve := Va$$

$$Ve = 78.658$$

$$Ha := \frac{Ma - Mb}{h} \qquad Ha = -102.579 \qquad He := Ha$$

$$He = -102.579$$

Design load =7.866

The maximum axial force in the rafters $N_{R,ED}$

$$Nrd1 := 10 \cdot C1$$

$$Nrd1 = 78.658$$

The vertical reaction at each base: Ved $Ved := Va$

$Ved = 78.658$

The horizontal reaction at each base: Hed $Hed := Ha$

$Hed = -102.579$

The maximum axial force in the rafters: Nrd

$Nrd1 = 78.658$

5.2 Axial compression in the rafter EN 1993-1-1 5.2.1(4)

According to the code, if the axial compression in the rafter is significant then α_{cr} is not applicable. In such situations, Appendix B of this document recommends the use of $\alpha_{cr,est}$ instead.

The axial compression is significant if

$$\lambda > 0.3\sqrt{\frac{Afy}{Ned}}$$

or if Ned>= 0.09 Ncr

Ncr is the elastic critical buckling load for the complete span of the rafter

Ned is the design axial load at ULS in the rafter, noted Nrd1 here

L_{cr} is the developed length of the rafter pair from column to column.

$$\cos(5deg) = 0.996 \qquad Lcr := \frac{20}{\cos(5deg)}$$

$$Lcr = 20.076$$

$$Ncr := \frac{\pi^2 \cdot E \cdot 71000000}{\left(Lcr \cdot 10^3\right)^2} \cdot 10^{-3}$$

$$Ncr = 356.402$$

$$0.09 \cdot Ncr = 32.076$$

$$Nrd1 = 78.658$$

$$Nrd > 32.076$$

Therefore axial compression in the rafter is significant and α_{cr} from 1993-1-1 is not applicable.

Stability is assessed based on $\alpha_{cr,est}$

Steel building in Europe part: 4

3.4

5.3 Calculation of α cr, est

An alternative expression, accounting for the axial force in the rafter, has been developed by J. Lim and C. King and is detailed below.

For frames with pitched rafters:

α cr,est=min(α cr,s,est;α cr,r,est)

α cr, r, est only needs to be checked when there are three or more spans, or if the rafter is horizontal, or when the columns are not vertical.

To calculate α_{cr} a notional horizontal force is applied to the frame and the horizontal deflection of the top of the columns is determined under this load.

The notional horizontal force is:

$$Hnhf := \frac{1}{200} \cdot Va$$

$$Hnhf = 0.393$$

The horizontal deflection of the top of the column under this force is obtained $\delta nhf := 0.75$
from the elastic analysis as 0.75 mm
α_{cr} is calculated as follows:

$$\alpha cr := \frac{1}{200} \cdot \frac{h \cdot 10^3}{\delta nhf}$$

$$\alpha cr = 40$$

$$\alpha crest := 0.8 \cdot \left[1 - \left(\frac{Nrd1}{Ncr}\right)\right] \cdot \alpha cr$$

$\left(\frac{Nrd1}{Ncr}\right)$ is the maximum ratio i any rafter

Steel building in Europe part:4
Appendix B

Nrd is the axial force in rafter at ULS

is the Euler load of the rafter for the full span of the rafter pair (assumed pinned)

$\alpha crest = 24.938$

$(\alpha crest > 10)$

EN 1993-1-1 5.2.1(3)

First order elastic analysis may be used and second order effects do not need to be allowed for.

6. Global analysis

EN 1993-1-1:5.2

The joints are assumed to be :

Fixed for column bases

Rigid for beam to column.

6.2 Frame imperfections

EN 1993-1-1: 5.3.2(3)

The global initial sway imperfection may be determined from

$\phi 0 := \frac{1}{200}$ $\alpha h := \frac{2}{\sqrt{h}}$ $mc := 2$ $\alpha m := \sqrt{0.5 \cdot \left(1 + \frac{1}{mc}\right)}$

ϕ 0 is the basic value: ϕ 0 = 1/200

$\phi m := \phi 0 \cdot \alpha h \cdot \alpha m$

$\phi m = 3.536 \times 10^{-3}$

Initial sway imperfections may be considered in two ways:

I. By modelling the frame out of plumb

II. By applying equivalent horizontal forces (EHF).

Applying equivalent horizontal forces is the preferred option and the method that is used in this worked example. The equivalent horizontal forces are calculated as:

$H_{EHF} = \phi_m V_{Ed}$

However sway imperfections may be disregarded where HEd >= 0.15 VEd

EN 1993-1-1: 5.3.2(4)

Table 1 shows the total reactions for the structure to determine HEd and VEd

Table 1 Vertical and horizontal reactions

Left column 1		Right column 2		Total		
HEd,1	VEd,1	HEd,2	VEd,2	HEd	VEd	
KN	KN	KN	KN	KN	KN	0.15 VEd
-64.106	-78.66	64.106	-78.66	0	-157.32	-23.598
-40.39	-43.63	29.49	-42.12	-10.9	-85.75	-12.8625

The sway imperfection has to be taken into for the combinations where HEd<0.15 VEd

The effects of initial sway imperfection may be replaced by equivalent horizontal forces: Heq= ϕ m VEd in the combination where HEd < o.15 VEd

Since in combinations 2 there is horizontal load included as earthquake load the sway imperfection has only to be into for combination 1

$Heq := \phi m \cdot 78.66$ $Heq = 0.278$ KN

6.3 Results of the elastic analysis

6.3.1 Ultimate limit states

Moment diagram in Nmm

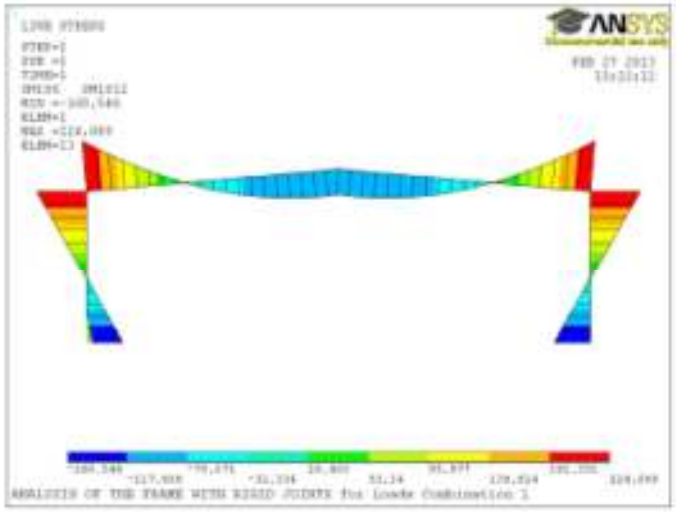

Combination 1

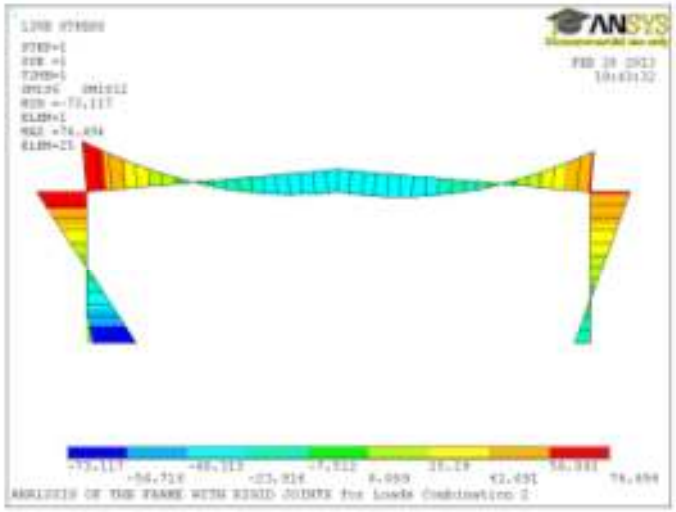

Combination 2

7. Column verification

850x650x63x3 - back to back lip channel section - cold formed steel grade S 355

The verification of the member is carried out for the combination 1:

NEd := 72.78 (Assumed to be constant along the column)

VEd := 78.66 (The vertical reaction, assumed to be constant along the column)

MEd := 224 (At the top of the column)

HEd := 64.106 The horizontal reaction

7.1 Classification of the cross section

7.1.1 The web

The web slenderness is: $\frac{C}{tw}$

EN 1993-1-1

5.5

$$Cw := \frac{hw}{tw}$$

$$\varepsilon := \sqrt{\left(\frac{235}{fy}\right)}$$

Cw = 140.667

ε = 0.814

EN 1993-1-1

Table 5.2 (sheet 1)

The limit for class 3 is:

$$Lw1 := 124 \cdot \varepsilon$$

Lw1 = 100.888

$$Lw2 := 42 \cdot \varepsilon$$

Lw2 = 34.172

Cw is greater than Lw1 and Lw2

The section is section class 4 (slender)

7.1.2 The flange

The flange slenderness is: $\frac{C}{tf}$ bf := 322

$$Cf := \frac{bf}{tf \cdot 1000}$$

Cf = 107.333

EN 1993-1-1

Table 5.2 (sheet2)

The limit for class 3 is:

$$Lf := 14 \cdot \varepsilon$$

Lf = 11.391

Cf is greater than Lf

The section is section class 4 (slender)

Therefore, the section is class 4.the verification of the member will be based on the elastic resistance of the cross-section.

7.2 Resistance of cross section

7.2.1 Shear resistance

The design shear resistance $V_{b,Rd}$ should be determined from:

$\gamma m0 := 1.0$ $\theta := 90$ EN 1993-1-3 2006 6.1.5

$$Vbr := \frac{\frac{hw}{\sin(90deg)} \cdot tw \cdot fbv}{\gamma m0}$$

$sw := hw$

$$\lambda w := 0.346 \frac{sw \cdot 1000}{tw \cdot 1000} \cdot \sqrt{\frac{355}{E}}$$

$\lambda w = 2.025$

For λ w greater or equal to 1.4 EN 1993-1-3 2006 Table 6.1

$$fbv := \frac{0.67 \cdot fy}{\lambda w^2} \qquad fbv = 57.982$$

$$Vbrd := \frac{\frac{hw \cdot 1000}{1} \cdot tw \cdot 1000 \cdot fbv}{\gamma m0} \cdot 10^{-3}$$

$Vbrd = 293.621$

$VEd = 78.66$ less than $Vbrd = 293.621$ OK

Bending and shear interaction

When shear force, axial force and bending moment act simultaneously on a cross section, the shear force can be ignored if it is smaller than 50% of the plastic shear resistance.

EN 1993-1-3 2006 6.1.10

$$\frac{VEd}{Vbrd} = 0.268 \qquad < 0.50$$

No need for more check

The effect of the shear force on the moment resistance may be neglected.

7.2.2 Compression resistance

$$Aeff := Ac$$

$$Nrd := \frac{Aeff \cdot 10^{6} \cdot fy}{\gamma m0} \cdot 10^{-3}$$

EN 1993-1-3 2006 6.1.3

$$Nrd = 3.463 \times 10^{3}$$

$$NEd = 72.78$$

NEd less than Nrd OK

Bending and axial force interaction

$$Mrd := \frac{Zx \cdot 10^{6} \cdot fy}{\gamma m0} \cdot 10^{-3}$$

EN 1993-1-3 2006 6.1.9

$$Mrd = 942.889$$

NEd/Nrd+MEd/Mrd less than 1.0

$$\frac{NEd}{Nrd} + \frac{MEd}{Mrd} = 0.259$$ Less than 1.0 OK

7.2.3 Bending moment resistance

EN 1993-1-3 2006 6.1.4

$$Mrd = 942.889$$

$$MEd = 224$$

MEd less than Mrd OK

7.3 Out of plane buckling resistance

The out-of-plane buckling interaction is verified with expression (6.62) in EN 1993–1-1.

$$\frac{N_{Ed}}{\frac{\chi_y N_{Rk}}{\gamma_{M1}}} + k_{zy}\frac{M_{y.Ed}}{\chi_{LT}\frac{M_{y.Rk}}{\gamma_{M1}}} \le 1$$

The Kyy and Kzy factors will be calculated using the Annex B of EN 1993-1-1

7.3.1 Verification of spacing between intermediate restraints

In this case the restraint to tension flange is provided by the side rails.

These side rails are spaced at 1400 mm

The limiting spacing as given by Annex BB of EN 1993-1-1 is: EN 1993-1-1 Annex BB

$$L_m = \frac{38 i_z}{\sqrt{\frac{1}{57,4}\left(\frac{N_{Ed}}{A}\right) + \frac{1}{756 C_1^2}\frac{W_{pl.y}^2}{A I_t}\left(\frac{f_y}{235}\right)^2}}$$

C1 is a factor that accounts for the shape of the bending moment diagram.

For a linear bending moment diagram, C1 (Cψ here) depends on the ratio of the minimum and the maximum bending moments in the segment being considered. Steel building in Europe part: 4 Appendix C

The ratios of bending moments for the middle and bottom segments of the column (without considering the haunch) are as follows:

$\psi c1 := \frac{0}{154} = 0$ → $C\psi 1 := 1.77$

$\psi c2 := \frac{0}{112} = 0$ → $C\psi 2 := 1.77$

$\psi c3 := \frac{154}{271} = 0.568$ → $C\psi 3 := 1.31$

C1 = 1, 31 is the most onerous case and therefore this is the case that will be analysed.

iz is the minimum value of the radius of gyration in the segment

$$Lm := \frac{38 \cdot 123}{\sqrt{\frac{1}{57.4}\left(\frac{NEd \cdot 10^3}{9756}\right) + \frac{1}{756 \cdot 1.31^2} \cdot \frac{(6125034)^2}{9756 \cdot 67773.6} \cdot \left(\frac{fy}{235}\right)^2}}$$

$Lm = 467.558$

Side rail spacing is 1400 mm > 467.47 mm

Therefore the normal design procedure must be adopted and advantage may not be taken of the restraints to the tension flange.

7.3.2 Whole column (4220 mm)

Firstly the whole column is verified. If the flexural buckling, lateral tensional buckling and interaction checks are satisfied for the length of the whole column, no further restraints are required. Otherwise, intermediate tensional restraints will be introduced to the column, or the column size increased.

The frame is not sensitive to second order effects (α cr, est= 27.993 > 10). Then the buckling length for in -plane buckling may be taken equal to the system length.

EN 1993-1-1 5.2.2(7)

Flexural buckling resistance about minor axis-zz (here yy), Nbrdz

EN 1993-1-3 6.2.3

$Lcry := 4.22($

Buckling curve: b for back to back lip channel section

Table 6.3

$\alpha z := 0.34$

EN 1993-1-1 2005 6.3.1.2(2) Table 6.1

$Iz := 14850875($

$$Ncrz := \frac{\pi^2 \cdot E \cdot Iz}{\left(Lcry \cdot 10^3\right)^2} \cdot 10^{-3}$$

EN 1993-1-1
6.3.1.3

$$Ncrz = 1.687 \times 10^4$$

$$\bar{\lambda} = \sqrt{\frac{A_{eff} f_y}{N_{cr}}} = \frac{L_{cr}}{i} \frac{\sqrt{\frac{A_{eff}}{A}}}{\lambda_1}$$

EN 1993-1-1
6.3.1.3(1)

$$\lambda z := \sqrt{\frac{Ac \cdot 10^6 \cdot fy}{Ncrz \cdot 10^3}}$$

$$\lambda z = 0.453$$

$$\chi = \frac{1}{\Phi + \sqrt{\Phi^2 - \bar{\lambda}^2}} \quad \text{but } \chi \le 1.0$$

$$\Phi = 0.5\left[1 + \alpha\left(\bar{\lambda} - 0.2\right) + \bar{\lambda}^2\right]$$

$$\phi z := 0.5\left[1 + \alpha z \cdot (\lambda z - 0.2) + \lambda z^2\right]$$

$$\phi z = 0.646$$

EN 1993-1-1
6.3.1.2

$$\chi z := \frac{1}{\phi z + \sqrt{\phi z^2 - \lambda z^2}}$$

$$\chi z = 0.904$$

Lateral torsional buckling resistance, Mbrd $Lcrlt := 422($

The lateral-torsional buckling resistance of a member is calculated as a reduction factor, χ LT, multiplied by the section modulus and the yield strength of the section. The reduction factor is calculated as a function of the slenderness, λ LT, which depends on the critical moment of the member. The expression for the critical moment, Mcr, is given below. The factor C1 accounts for the shape of bending moment diagram of the member. Appendix C of Steel building in Europe part: 4 provides values of C1 for different shapes of bending moment diagrams. For the case of a linear bending moment diagram, C1 depends on the ratio of the bending moments at the ends of the member, given as ψ

Buckling curve: c for back to back lip channel section $\alpha lt := 0.4($ En 1993-1-1 Table 6.2

$$\psi c := \frac{-207}{271} = -0.764 \quad \rightarrow \quad C\psi := 2.5($$

$Iw := 4.24304E+1$

EN 1993-1-1 6.3.2.2 Table 6.5

$$Mcr := C\psi \cdot \frac{\pi^2 \cdot E \cdot Iz}{(Lcrlt)^2} \cdot \sqrt{\frac{Iw}{Iz} + \frac{Lcrlt^2 \cdot Gk \cdot It \cdot 10^8}{\pi^2 \cdot E \cdot Iz}} \cdot 10^{-6}$$

$$Mcr = 7.13 \times 10^3$$

$$\chi_{LT} = \frac{1}{\Phi_{LT} + \sqrt{\Phi_{LT}^2 - \beta \bar{\lambda}_{LT}^2}} \quad \text{but} \quad \begin{cases} \chi_{LT} \le 1,0 \\ \chi_{LT} \le \dfrac{1}{\bar{\lambda}_{LT}^2} \end{cases}$$

$$\Phi_{LT} = 0.5\left[1 + \alpha_{LT}\left(\bar{\lambda}_{LT} - \bar{\lambda}_{LT,0}\right) + \beta \bar{\lambda}_{LT}^2\right]$$

$$\bar{\lambda}_{LT} = \sqrt{\frac{W_y f_y}{M_{cr}}}$$

$Wy := 2656025.38$

$$\lambda lt := \sqrt{\frac{Wy \cdot fy}{Mcr} \cdot 10^{-6}}$$

$\lambda lt = 0.364$ $\lambda lt0 := 0.2$ $\beta := 1.0$

NA to BS EN 1993-1-1:2005 NA.2.17

$$\phi lt := 0.5 \cdot \left[1 + \alpha lt \cdot (\lambda lt - \lambda lt0) + \beta \cdot \lambda lt^2\right]$$

$\phi lt = 0.606$

$$\chi lt := \frac{1}{\phi lt + \sqrt{\phi lt^2 - \beta \cdot \lambda lt^2}} = 0.916$$

$\chi lt = 0.916$

$$Kc := \frac{1}{1.33 - 0.33 \cdot \psi c} = 0.632$$

$$ft := 1 - 0.5 \cdot (1 - Kc) \cdot \left[1 - 2 \cdot (\lambda lt - 0.8)^2\right] = 0.886$$

less than 1

$$\chi_{LT,mod} = \frac{\chi_{LT}}{f} \text{ (AC}_2\text{) but } \begin{cases} \chi_{LT,mod} \leq 1 \\ \chi_{LT,mod} \leq \dfrac{1}{\overline{\lambda}_{LT}^2} \text{ (AC}_1\text{)} \end{cases}$$

$\chi ltm := \frac{\chi lt}{ft} = 1.034$ not greater than $\frac{1}{\lambda lt^2} = 7.562$

χ lt cannot be greater than 1.0: therefore

$\chi ltm := 1.0$ $\gamma m1 := 1.0$

$$Mbrd := \frac{\chi ltm \cdot Wy \cdot fy}{\gamma m1} \cdot 10^{-6} = 942.889$$

$MbEd := 224$ Less than $Mbrd = 942.889$ OK

Interaction of axial force and bending moment-out of plane buckling

Out-of-plane buckling due to the interaction of axial force and bending moment is verified by satisfying the following expression: EN 1993-1-1 6.3.3(4)

$$\frac{N_{Ed}}{\frac{\chi_y N_{Rk}}{\gamma_{M1}}} + k_{zy}\frac{M_{y.Ed}}{\chi_{LT}\frac{M_{y.Rk}}{\gamma_{M1}}} \le 1$$

EN 1993-1-1 Annex B Table B.2

$$\left[1-\frac{0.05\bar{\lambda}_z}{(C_{mLT}-0.25)}\frac{N_{Ed}}{\chi_z N_{Rk}/\gamma_{M1}}\right] \ge \left[1-\frac{0.05}{(C_{mLT}-0.25)}\frac{N_{Ed}}{\chi_z N_{Rk}/\gamma_{M1}}\right]$$

EN 1993-1-1 Annex B Table B.3

$Cmlt := 0.6 + 0.4\cdot\psi c = 0.294$ Less than 0.4

$Cmlt := 0.4$ $Nbrdz := \frac{\chi z\cdot Ac\cdot 10^6\cdot fy}{\gamma m1}\cdot 10^{-3}$

$$Kzy := 1 - \frac{0.05\cdot\lambda z}{(Cmlt - 0.25)}\cdot\frac{NEd}{Nbrdz} = 0.996$$

$$Kzy1 := 1 - \frac{0.05}{(Cmlt - 0.25)}\cdot\frac{NEd}{Nbrdz} = 0.992$$

Maximum value= 0.995

$$\frac{NEd}{Nbrdz} + 0.995\frac{MEd}{Mbrd} = 0.26$$ Less than 1.0 OK

7.4 In plane buckling

The in-plane buckling interaction is verified with expression (6.61) in EN 1993-1-1.

$$\frac{N_{Ed}}{\frac{\chi_y N_{Rk}}{\gamma_{M1}}} + k_{yy}\frac{M_{y,Ed}}{\chi_{LT}\frac{M_{y,Rk}}{\gamma_{M1}}} \le 1$$

Flexural buckling resistance about the mayor axis yy (here xx), Nbrdy

Buckling curve: a

EN 1993-1-3 6.2.3 Table 6.3

$\alpha y := 0.21$ $Lcry := 4.22($

$Iy := 112881078$

EN 1993-1-1 2005 6.3.1.2(2) Table 6.1

$$Ncry := \frac{\pi^2 \cdot E \cdot Iy}{\left(Lcry \cdot 10^3\right)^2} \cdot 10^{-3}$$

EN 1993-1-1 6.3.1.3

$Ncry = 1.282 \times 10^5$

$$\bar{\lambda} = \sqrt{\frac{A_{eff} f_y}{N_{cr}}} = \frac{L_{cr}}{i}\frac{\sqrt{\frac{A_{eff}}{A}}}{\lambda_1}$$

$$\lambda y := \sqrt{\frac{Ac \cdot 10^6 \cdot fy}{Ncry \cdot 10^3}} \qquad \lambda y = 0.164$$

$$\phi y := 0.5\left[1 + \alpha y \cdot (\lambda y - 0.2) + \lambda y^2\right]$$

EN 1993-1-1 6.3.1.2

$\phi y = 0.51$

$$\chi y := \frac{1}{\phi y + \sqrt{\phi y^2 - \lambda y^2}}$$

$\chi y = 1.008$

$$Nbrdy := \frac{\chi y \cdot Ac \cdot 10^6 \cdot fy}{\gamma m1} \cdot 10^{-3} = 3.49 \times 10^3$$

$NEd = 72.78$ Less than $Nbrdy = 3.49 \times 10^3$ OK

Lateral torsional buckling resistance, Mbrd

Mbrd is the least buckling moment resistance of the calculated one.

Mbrd = 942.889

Interaction of axial force and bending moment-in of plane buckling

In-plane buckling due to the interaction of axial force and bending moment is verified by satisfying the following expression:

$$\frac{N_{Ed}}{\frac{\chi_y N_{Rk}}{\gamma_{M1}}} + k_{yy}\frac{M_{y,Ed}}{\chi_{LT}\frac{M_{y,Rk}}{\gamma_{M1}}} \le 1$$

For Cmy, the relevant braced points are the torsional restraints at the end of the member.

Th

$$C_{my}\left(1+0{,}6\bar{\lambda}_y\frac{N_{Ed}}{\chi_y N_{Rk}/\gamma_{M1}}\right) \le C_{my}\left(1+0{,}6\frac{N_{Ed}}{\chi_y N_{Rk}/\gamma_{M1}}\right)$$

$$Nbrdy := \frac{\chi y \cdot Ac \cdot 10^6 \cdot fy}{\gamma m1}\cdot 10^{-3} = 3.49\times 10^3$$

$$Cmy := 0.6 + 0.4\cdot \psi c = 0.294$$ Less than 0.4

$$Cmy := 0.4$$

$$Kyy := Cmy\cdot\left(1 + 0.6\cdot\lambda y\cdot\frac{NEd}{Nbrdy}\right) = 0.401$$

$$Kyy1 := Cmy\cdot\left(1 + 0.6\cdot\frac{NEd}{Nbrdy}\right) = 0.405$$

The minimum value:0.401

$$\frac{NEd}{Nbrdy} + 0.401\cdot\frac{MEd}{Mbrd} = 0.116$$ Less than 1.0 OK

Validity of column section

In Section 7.2 it has been demonstrated that the cross-sectional resistance of the section is greater than the applied forces.
The out-of-plane and in-plane buckling checks have been verified in Sections 7.3 and 7.4 for the appropriate choice of restraints along the column.

Therefore it is concluded that the **850x650x63x3-back to back lip channel section cold formed steel S355 steel** is appropriate for use as columns in this portal frame.

8. Rafter verification

750x500x53x3 - back to back lip channel section - cold formed steel grade S 355

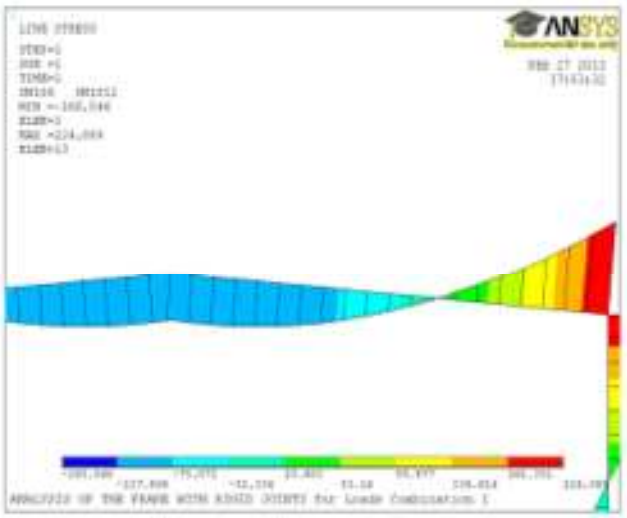

The verification of the member is carried out for the combination 1 :

$$NEdr := \frac{72.78 \cdot 0.875}{10.04} + \frac{78.66 \cdot 10}{10.04} = 84.689$$

NEdr = 84.689 (The maximum value)

VEdr := 72.78 (The maximum value)

MEdr := 181 (The maximum value)

8.1 Classification of the cross section

8.1.1 The web

The web slenderness is: $\frac{C}{tw}$

EN 1993-1-1

5.5

$$Cwr := \frac{hwr}{twr}$$

$$\varepsilon := \sqrt{\left(\frac{235}{fy}\right)}$$

$Cwr = 124$

EN 1993-1-1

Table 5.2 (sheet 1)

$\varepsilon = 0.814$

The limit for class 3 is:

$$Lwr1 := 124 \cdot \varepsilon$$

$$Lwr2 := 42 \cdot \varepsilon$$

$Lw1 = 100.888$

$Lwr2 = 34.172$

Cwr is greater than Lw1 and Lw2

The section is section class 4 (slender)

8.1.2 The flange

The flange slenderness is: $\frac{Cr}{tfr}$ $bfr := 247$

$$Cfr := \frac{bfr}{tfr \cdot 1000}$$

$Cfr = 82.333$

EN 1993-1-1

Table 5.2 (sheet2)

The limit for class 3 is:

$$Lfr := 14 \cdot \varepsilon$$

$Lfr = 11.391$

Cfr is greater than Lfr

The section is section class 4 (slender)

Therefore, the section is class 4.the verification of the member will be based on the elastic resistance of the cross-section.

8.2 Resistance of cross section

8.2.1 Shear resistance

The design shear resistance $V_{b,Rd}$ should be determined from:

$\gamma m0 := 1.0$ $\theta := 90$ EN 1993-1-3 2006 6.1.5

$$Vbrr := \frac{\frac{hwr}{\sin(90deg)} \cdot twr \cdot fbvr}{\gamma m0}$$

$swr := hwr$

$$\lambda wr := 0.346 \frac{swr \cdot 1000}{twr \cdot 1000} \cdot \sqrt{\frac{355}{E}}$$

$\lambda wr = 1.785$

For λ w greater or equal to 1.4 EN 1993-1-3 2006 Table 6.1

$$fbvr := \frac{0.67 \cdot fy}{\lambda wr^2} \qquad fbvr = 74.616$$

$$Vbrdr := \frac{\frac{hwr \cdot 1000}{1} \cdot twr \cdot 1000 \cdot fbvr}{\gamma m0} \cdot 10^{-3}$$

$Vbrdr = 333.087$

$VEdr = 72.78$ Less than $Vbrdr = 333.087$ OK

Bending and shear interaction

When shear force, axial force and bending moment act simultaneously on a cross section, the shear force can be ignored if it is smaller than 50% of the plastic shear resistance.

$$\frac{VEdr}{Vbrdr} = 0.219 \quad < 0.50$$ EN 1993-1-3 2006 6.1.10

No need for more check

The effect of the shear force on the moment resistance may be neglected.

8.2.2 Compression resistance

$Aeff := Ar$

$$Nrdr := \frac{Aeff \cdot 10^6 \cdot fy}{\gamma m0} \cdot 10^{-3}$$

EN 1993-1-3 2006 6.1.3

$Nrdr = 2.888 \times 10^3$

$NEdr = 84.689$

NEd less than Nrd OK

Bending and axial force interaction

$$Mrdr := \frac{Zxr \, 10^6 \cdot fy}{\gamma m0} \cdot 10^{-3}$$

EN 1993-1-3 2006 6.1.9

$Mrdr = 672.327$

NEd/Nrd + MEd/Mrd less than 1.0

$$\frac{NEdr}{Nrdr} + \frac{MEdr}{Mrdr} = 0.299$$ Less than 1.0 OK

8.2.3 Bending moment resistance

EN 1993-1-3 2006 6.1.4

$Mrdr = 672.327$

$MEdr = 181$

MEd less than Mrd OK

8.3 Out of plane buckling resistance

The out-of-plane buckling interaction is verified with expression (6.62) in EN 1993– 1-1.

The Kyy and Kzy factor will be calculated using the Annex B of EN 1993-1-1

8.3.1 Mid span region

The purlin spacing in this region is 1633 mm

Flexural buckling resistance about minor axis-zz (here yy), Nbrdrz

EN 1993-1-3

Buckling curve: b for back to back lip channel section 6.2.3

$Lcryr := 163$ Table 6.3

$\alpha zr := 0.34$

$Izr := 7100000$

EN 1993-1-12005

6.3.1.2(2) Table 6.1

$$Ncrzr := \frac{\pi^2 \cdot E \cdot Izr}{(Lcryr)^2} \cdot 10^{-3}$$

EN 1993-1-1

6.3.1.3

$Ncrzr = 5.387 \times 10^4$

$$\bar{\lambda} = \sqrt{\frac{A_{eff} f_y}{N_{cr}}} = \frac{L_{cr}}{i} \frac{\sqrt{\frac{A_{eff}}{A}}}{\lambda_1}$$

$$\lambda zr := \sqrt{\frac{Ar \cdot 10^6 \cdot fy}{Ncrzr \cdot 10^3}}$$

EN 1993-1-1

6.3.1.3(1)

$\lambda zr = 0.232$

$$\chi = \frac{1}{\Phi + \sqrt{\Phi^2 - \bar{\lambda}^2}} \quad \text{but } \chi \le 1.0$$

$$\Phi = 0,5\left[1 + \alpha(\bar{\lambda} - 0,2) + \bar{\lambda}^2\right]$$

$$\phi zr := 0.5\left[1 + \alpha zr \cdot (\lambda zr - 0.2) + \lambda zr^2\right]$$

$\phi zr = 0.532$

EN 1993-1-1

6.3.1.2

$$\chi zr := \frac{1}{\phi zr + \sqrt{\phi zr^2 - \lambda zr^2}}$$

$\chi zr = 0.989$

Lateral torsional buckling resistance, Mbrdr

In this zone, lateral-torsional buckling is checked between restraints, which are the purlins. For equally spaced purlins, the critical length is at the point of maximum bending moment.

In order to determine the critical moment of the rafter, the C1 factor takes account of the shape of the bending moment diagram.

In this case the bending moment diagram is nearly constant along the segment in consideration, so ψ =1.0

Lcrltr := 1633

Buckling curve: c for back to back lip channel section $\alpha ltr := 0.49$ En 1993-1-1 Table 6.2

$\psi cr := 1.0 \rightarrow C\psi r := 1.0$

Iwr := 3.26762E+1

EN 1993-1-1 6.3.2.2

$$Mcrr := C\psi r \cdot \frac{\pi^2 \cdot E \cdot Izr}{(Lcrltr)^2} \cdot \sqrt{\frac{Iwr}{Izr} + \frac{Lcrltr^2 \cdot Gr \cdot Itr \cdot 10^8}{\pi^2 \cdot E \cdot Izr}} \cdot 10^{-6}$$

Table 6.5

$Mcrr = 1.156 \times 10^4$

$$\chi_{LT} = \frac{1}{\Phi_{LT} + \sqrt{\Phi_{LT}^2 - \beta\bar{\lambda}_{LT}^2}} \text{ but } \begin{cases} \chi_{LT} \le 1.0 \\ \chi_{LT} \le \frac{1}{\bar{\lambda}_{LT}^2} \end{cases}$$

$$\Phi_{LT} = 0.5\left[1 + \alpha_{LT}\left(\bar{\lambda}_{LT} - \bar{\lambda}_{LT,0}\right) + \beta\bar{\lambda}_{LT}^2\right]$$

$$\bar{\lambda}_{LT} = \sqrt{\frac{W_y f_y}{M_{cr}}}$$

Wyr := 1893880.02

$$\lambda ltr := \sqrt{\frac{Wyr \cdot fy}{Mcrr} \cdot 10^{-6}}$$

$\lambda ltr = 0.241$ $\lambda lt0 := 0.2$ $\beta := 1.0$

NA to BS EN 1993-1-1:2005 NA.2.17

$$\phi ltr := 0.5\cdot\left[1 + \alpha ltr\cdot(\lambda ltr - \lambda lt0) + \beta\cdot\lambda ltr^{2}\right]$$

$\phi ltr = 0.539$

$$\chi ltr := \frac{1}{\phi ltr + \sqrt{\phi ltr^{2} - \beta\cdot\lambda ltr^{2}}} = 0.979$$

$\chi ltr = 0.979$

$$Kcr := \frac{1}{1.33 - 0.33\cdot\psi cr} = 1$$

$$ftr := 1 - 0.5\cdot(1 - Kcr)\cdot\left[1 - 2\cdot(\lambda ltr - 0.8)^{2}\right] = 1$$

$$\chi_{LT,mod} = \frac{\chi_{LT}}{f} \text{ (AC}_2\text{) but } \begin{cases} \chi_{LT,mod} \le 1 \\ \chi_{LT,mod} \le \frac{1}{\lambda_{LT}^{2}} \text{ (AC}_2\text{)} \end{cases}$$

$\chi ltmr := \frac{\chi ltr}{ftr} = 0.979$ not greater than $\frac{1}{\lambda ltr^{2}} = 17.189$

$\chi ltmr =$ ▮ $\gamma m1 := 1.0$

$$Mbrdr := \frac{\chi ltmr\cdot Wyr\cdot fy}{\gamma m1}\cdot 10^{-6} = 658.236$$

$MbEdr := 181$ Less than $Mbrdr =$ ▮ OK

Interaction of axial force and bending moment-out of plane buckling

Out-of-plane buckling due to the interaction of axial force and bending moment is verified by satisfying the following expression: EN 1993-1-1 6.3.3(4)

$$\frac{N_{Ed}}{\frac{\chi_y N_{Rk}}{\gamma_{M1}}} + k_{yy}\frac{M_{y,Ed}}{\frac{\chi_{LT} M_{y,Rk}}{\gamma_{M1}}} \le 1$$

EN 1993-1-1 Annex B Table B.2

$$\left[1-\frac{0.05\bar{\lambda}_z}{(C_{mLT}-0.25)}\frac{N_{Ed}}{\chi_z N_{Rk}/\gamma_{M1}}\right] \geq \left[1-\frac{0.05}{(C_{mLT}-0.25)}\frac{N_{Ed}}{\chi_z N_{Rk}/\gamma_{M1}}\right]$$

EN 1993-1-1

Annex B Table B.3

$Cmltr := 0.6 + 0.4 \cdot \psi cr = 1$

$Cmltr = 1$ $\quad Nbrdrz := \frac{\chi zr \cdot Ar \cdot 10^6 \cdot fy}{\gamma m1} \cdot 10^{-3} = 2.856 \times 10^3$

$Kzyr := 1 - \frac{0.05 \cdot \lambda zr}{(Cmltr - 0.25)} \cdot \frac{NEdr}{Nbrdrz} = 1$

$Kzyr1 := 1 - \frac{0.05}{(Cmltr - 0.25)} \cdot \frac{NEdr}{Nbrdrz} = 0.998$

Maximum value= 0.999

$\frac{NEdr}{Nbrdrz} + 0.999\frac{MEdr}{Mbrdr} = 0.304$ Less than 1.0 OK

8.3.1 End of span region

8.3.1.1 Verification of spacing between intermediate restraints

In this case, the restraint to the tension flange is provided by the purlins.

These purlins are spaced at 2445 mm.

The limiting spacing as given by Annex BB of EN 1993-1-1 is:

EN 1993-1-1

Annex BB

BB3.1.1

$$L_m = \frac{38 i_z}{\sqrt{\frac{1}{57,4}\left(\frac{N_{Ed}}{A}\right) + \frac{1}{756 C_1^2}\frac{W_{pl,y}^2}{A I_t}\left(\frac{f_y}{235}\right)^2}}$$

C2 is a factor that accounts for the shape of the bending moment diagram.

For a linear bending moment diagram, C2 (Cψ here) depends on the ratio of the minimum and the maximum bending moments in the segment being considered.

$$Lcryr1 := 95 + 1175 + 1175 = 2.445 \times 10^3$$

$$Lcrltr1 := Lcryr1 = 2.445 \times 10^3$$

Buckling curve: c for back to back lip channel section $\alpha ltr1 := 0.49$ En 1993-1-1table 6.2

Steel building in Europe part: 4 Appendix C EN 1993-1-1 Annex BB BB3.1.1

$\psi cr2 := 0$ → $C\psi r2 := 1.77$

iz is the minimum value of the radius of gyration in the segment

$$Lmr := \frac{38 \cdot 93.4165}{\sqrt{\frac{1}{57.4}\left(\frac{NEdr \cdot 10^3}{8136}\right) + \frac{1}{756 \cdot C\psi r2^2} \cdot \frac{(4414444)^2}{8136 \cdot 58863.6} \cdot \left(\frac{fy}{235}\right)^2}}$$

$$Lmr = 565.629$$

Purlin spacing is 2445 mm > $Lmr = 565.629$ mm

Therefore the normal design procedure must be adopted and advantage may not be taken of the restraints to the tension flange.

Flexural buckling resistance about minor axis-zz (here yy), Nbrdrz EN 1993-1-3 6.2.3

Buckling curve: b for back to back lip channel section Table 6.3

$\alpha zr1 := 0.34$ $Lcryr1 := 95 + 1175 + 1175 = 2.445 \times 10^{3}$

EN 1993-1-1 2005

$Izr := 71000000$

6.3.1.2(2) Table 6.1

$$Ncrzr1 := \frac{\pi^2 \cdot E \cdot Izr}{(Lcryr1)^2} \cdot 10^{-3}$$

EN 1993-1-1

6.3.1.3

$Ncrzr1 = 2.403 \times 10^{4}$

$$\bar{\lambda} = \sqrt{\frac{A_{eff} f_y}{N_{cr}}} = \frac{L_{cr}}{i} \frac{\sqrt{\frac{A_{eff}}{A}}}{\lambda_1}$$

$$\lambda zr1 := \sqrt{\frac{Ar \cdot 10^6 \cdot fy}{Ncrzr1 \cdot 10^3}}$$

EN 1993-1-1

6.3.1.3(1)

$\lambda zr1 = 0.347$

$$\chi = \frac{1}{\Phi + \sqrt{\Phi^2 - \bar{\lambda}^2}} \quad \text{but } \chi \le 1.0$$

$$\Phi = 0.5\left[1 + \alpha(\bar{\lambda} - 0.2) + \bar{\lambda}^2\right]$$

$$\phi zr1 := 0.5\left[1 + \alpha zr1 \cdot (\lambda zr1 - 0.2) + \lambda zr1^2\right]$$

$\phi zr1 = 0.585$ EN 1993-1-1

6.3.1.2

$$\chi zr1 := \frac{1}{\phi zr1 + \sqrt{\phi zr1^2 - \lambda zr1^2}}$$

$\chi zr1 = 0.947$

Lateral torsional buckling resistance, Mbrdr

In this zone, lateral-torsional buckling is checked between restraints, which are the purlins. For equally spaced purlins, the critical length is at the point of maximum bending moment.

In order to determine the critical moment of the rafter, the C1 factor takes account of the shape of the bending moment diagram.

In this case the bending moment diagram is nearly constant along the segment in consideration, so ψ =1.0

$Lcrltr1 := Lcryr1 = 2.445 \times 10^{3}$

Buckling curve: c for back to back lip channel section $\alpha ltr1 := 0.49$ En 1993-1-1 Table 6.2

$\psi cr2 := 0 \rightarrow Cwr2 := 1.77$ Steel building in Europe part: 4 Appendix C

$Iwr := 3.26762E+1$

EN 1993-1-1 6.3.2.2 Table 6.5

$$Mcrr1 := C\psi r2 \cdot \frac{\pi^2 \cdot E \cdot Izr}{(Lcrltr1)^2} \cdot \sqrt{\frac{Iwr}{Izr} + \frac{Lcrltr1^2 \cdot Gk \cdot Itr \cdot 10^8}{\pi^2 \cdot E \cdot Izr}} \cdot 10^{-6}$$

$Mcrr1 = 9.125 \times 10^{3}$

$$\chi_{LT} = \frac{1}{\Phi_{LT} + \sqrt{\Phi_{LT}^2 - \beta\bar{\lambda}_{LT}^2}} \quad \text{but} \quad \begin{cases} \chi_{LT} \le 1.0 \\ \chi_{LT} \le \dfrac{1}{\bar{\lambda}_{LT}^2} \end{cases}$$

$$\Phi_{LT} = 0.5\left[1 + \alpha_{LT}\left(\bar{\lambda}_{LT} - \bar{\lambda}_{LT,0}\right) + \beta\bar{\lambda}_{LT}^2\right]$$

$$\bar{\lambda}_{LT} = \sqrt{\frac{W_y f_y}{M_{cr}}}$$

Wyr := 1893880.02

$$\lambda ltr1 := \sqrt{\frac{Wyr \cdot fy}{Mcrr1} \cdot 10^{-6}}$$

$\lambda ltr1 = 0.271$ $\lambda lt0 := 0.2$ $\beta := 1.0$

NA to BS EN 1993-1-1:2005
NA.2.17

$$\phi ltr1 := 0.5 \cdot \left[1 + \alpha ltr1 \cdot (\lambda ltr1 - \lambda lt0) + \beta \cdot \lambda ltr1^2\right]$$

$\phi ltr1 = 0.554$

$$\chi ltr1 := \frac{1}{\phi ltr1 + \sqrt{\phi ltr1^2 - \beta \cdot \lambda ltr1^2}} = 0.964$$

$\chi ltr1 = 0.964$

$$Kcr1 := \frac{1}{1.33 - 0.33 \cdot \psi cr2} = 0.752$$

$$ftr1 := 1 - 0.5 \cdot (1 - Kcr1) \cdot \left[1 - 2 \cdot (\lambda ltr1 - 0.8)^2\right] = 0.945$$

less than 1

$$\chi_{LT,mod} = \frac{\chi_{LT}}{f} \text{ [AC}_2\text{] but } \begin{cases} \chi_{LT,mod} \le 1 \\ \chi_{LT,mod} \le \dfrac{1}{\bar{\lambda}_{LT}^2} \text{ [AC}_3\text{]} \end{cases}$$

$$\chi ltmr1 := \frac{\chi ltr1}{ftr1} = 1.019 \qquad \text{Not greater than} \qquad \frac{1}{\lambda ltr1^2} = 13.572$$

$\chi ltmr2 := 1$ $\gamma m1 := 1.0$

$$Mbrdr1 := \frac{\chi ltmr2 \cdot Wyr \cdot fy}{\gamma m1} \cdot 10^{-6} = 672.327$$

$MbEdr := 181$ Less than $Mbrdr1 = 672.327$ OK

Interaction of axial force and bending moment-out of plane buckling

Out-of-plane buckling due to the interaction of axial force and bending moment is verified by satisfying the following expression: EN 1993-1-1 6.3.3(4)

$$\frac{\frac{N_{Ed}}{\chi_y N_{Rk}/\gamma_{M1}} + k_{zy}\frac{M_{y,Ed}}{\chi_{LT} M_{y,Rk}/\gamma_{M1}} \le 1}$$

EN 1993-1-1 Annex B Table B.2

$$\left[1 - \frac{0.05\bar{\lambda}_z}{(C_{mLT} - 0.25)} \frac{N_{Ed}}{\chi_z N_{Rk}/\gamma_{M1}}\right] \ge \left[1 - \frac{0.05}{(C_{mLT} - 0.25)} \frac{N_{Ed}}{\chi_z N_{Rk}/\gamma_{M1}}\right]$$

EN 1993-1-1 Annex B Table B.3

$Cmltr1 := 0.6 + 0.4 \cdot \psi cr2 = 0.6$

$Cmltr1 = 0.6$ $Nbrdrz1 := \frac{\chi zr1 \cdot Ar \cdot 10^6 \cdot fy}{\gamma m1} \cdot 10^{-3} = 2.734 \times 10^3$

$$Kzyrr := 1 - \frac{0.05 \cdot \lambda zr1}{(Cmltr1 - 0.25)} \cdot \frac{NEdr}{Nbrdrz1} = 0.998$$

$$Kzyrr1 := 1 - \frac{0.05}{(Cmltr1 - 0.25)} \cdot \frac{NEdr}{Nbrdrz1} = 0.996$$

Maximum value= 0.998

$\frac{NEdr}{Nbrdrz1} + 0.998\frac{MEdr}{Mbrdr1} = 0.3$ Less than 1.0 OK

8.4 In plane buckling

The in-plane buckling interaction is verified with expression (6.61) in EN 1993-1-1.

$$\frac{N_{Ed}}{\frac{\chi_y N_{Rk}}{\gamma_{M1}}} + k_{yy}\frac{M_{y,Ed}}{\chi_{LT}\frac{M_{y,Rk}}{\gamma_{M1}}} \le 1$$

Maximum bending moment and axial force in the rafter, excluding the haunch.

MEdr2 := 117 (The maximum value)

NEdr := 72.78 (The maximum value)

Flexural buckling resistance about the mayor axis yy (here xx), Nbrdy

Buckling curve: a

αyr := 0.21

The buckling length is the system length, which is the distance between the joints (i.e. the length of the rafter, including the haunch),

Lcryr2 := 1004(

.

Iyr2 := 71020500

$$Ncryr := \frac{\pi^2 \cdot E \cdot Iy}{(Lcryr2)^2} \cdot 10^{-3}$$

$Ncryr = 2.266 \times 10^4$

$$\bar{\lambda} = \sqrt{\frac{A_{eff} f_y}{N_{cr}}} = \frac{L_{cr}}{i} \frac{\sqrt{\frac{A_{eff}}{A}}}{\lambda_1}$$

$$\lambda yr := \sqrt{\frac{Ar \cdot 10^6 \cdot fy}{Ncryr \cdot 10^3}} \qquad \lambda yr = 0.357$$

$$\phi yr := 0.5\left[1 + \alpha yr \cdot (\lambda yr - 0.2) + \lambda yr^2\right]$$

$$\phi yr = 0.58$$

$$\chi yr := \frac{1}{\phi yr + \sqrt{\phi yr^2 - \lambda yr^2}}$$

$$\chi yr = 0.964$$

$$Nbrdyr := \frac{\chi yr \cdot Ar \cdot 10^6 \cdot fy}{\gamma m1} \cdot 10^{-3} = 2.784 \times 10^3$$

NEd = 72.78 Less than $Nbrdyr = 2.784 \times 10^3$ OK

Lateral torsional buckling resistance, Mbrd

Mbrd is the least buckling moment resistance of the calculated one.

Min of Mbrdr = 658.236 and Mbrdr1 = 672.327

Mbrdry := Mbrdr = 658.236

Interaction of axial force and bending moment-in of plane buckling

In-plane buckling due to the interaction of axial force and bending moment is verified by satisfying the following expression:

$$\frac{N_{Ed}}{\frac{\chi_y N_{Rk}}{\gamma_{M1}}} + k_{yy}\frac{M_{y,Ed}}{\chi_{LT}\frac{M_{y,Rk}}{\gamma_{M1}}} \le 1$$

For Cmy, the relevant braced points are the torsional restraints at the end of the member.

Th

$$C_{my}\left(1 + 0{,}6\bar{\lambda}_y \frac{N_{Ed}}{\chi_y N_{Rk}/\gamma_{M1}}\right)$$
$$\le C_{my}\left(1 + 0{,}6\frac{N_{Ed}}{\chi_y N_{Rk}/\gamma_{M1}}\right)$$

The expression for Cmy depends on the values of α h and ψ

$\psi cyr := -\frac{132}{230} = -0.574$ Mh := 110 Ms := 117

EN 1993-1-1 Annex B Table B.3

$\alpha hr := \frac{Mh}{Ms} = 0.94$

Therefore Cmy is calculated as:

$Cmyr := 0.95 + 0.05 \cdot \alpha hr$

$Cmyr = 0.997$

$Nbrdyr := \frac{\chi yr \cdot Ar \cdot 10^6 \cdot fy}{\gamma m1} \cdot 10^{-3} = 2.784 \times 10^3$

$Kyyr := Cmyr \cdot \left(1 + 0.6 \cdot \lambda y \cdot \frac{NEdr}{Nbrdyr}\right) = 1$

EN 1993-1-1 Annex B Table B.2

$Kyyr1 := Cmyr \cdot \left(1 + 0.6 \cdot \frac{NEdr}{Nbrdyr}\right) = 1.013$

The minimum value:1

$\frac{NEdr}{Nbrdyr} + 1 \cdot \frac{MEdr}{Mbrdry} = 0.301$ Less than 1.0 OK

The member satisfies the in-plane buckling check.

8.5 Validity of rafter section

In Section 8.2 it has been demonstrated that the cross-sectional resistance of the section is greater than the applied forces.

The out-of-plane and in-plane buckling checks have been verified in Sections 8.3 and 8.4 for the appropriate choice of restraints along the rafter.

Therefore it is concluded that the **750x500x53x3-back to back lip channel section - cold formed steel grade S 355** is appropriate for use as rafter in this portal frame.

9. Haunch verification

The haunch is fabricated from a cutting of a 1400x500x53x3 - back to back lip channel section - cold formed steel grade S 355.

Maximum forces and moments in the haunch

NEdh := 84.6

MEdh := 224

Properties of the whole section:

EN 1993-1-1 does not cover the design of tapered sections (i.e. a haunch), and the verification in this worked example is carried out by checking the forces of an equivalent T-section subject to compression and bending.

The equivalent T-section is taken from a section at mid-length of the hunched member.

The equivalent T-section is made of the bottom flange and 1/3 of the compressed part of the web area, based on 6.3.2.4 of EN 1993-1-1.

The buckling length is 1628 mm (length between the top of column and the first restraint).

Hsh := 1300 Bh := 500 th := 3

Section area Ah := 12876

Second moment of area/yy IY := 3438763108

Second moment of area/zz Iz := 148508750

Elastic modulus/yy Wely := 5020092.128

Elastic modulus/zz Welz := 456950

Properties of the compression part:

$At := 2460$

$Iyt := 593727$

$Izt := 3125288$

Compression in the T section

The total equivalent compression in the T section is calculated by adding the direct axial compression and the compression due to bending.

$$NEdf := \left(NEdh \cdot 10^{3} \cdot \frac{At}{Ah} + \frac{MEdh \cdot 10^{6}}{Wely} \cdot At \right) \cdot 10^{-3} = 125.947$$

Buckling resistance about the minor axis

Buckling curve c is used for welded section $Lcrh := 1628$ EN 1993-1-1 6.3.1.2 Table 6.2

$\alpha zh := 0.49$

$$\lambda 1h := \pi \cdot \sqrt{\frac{E}{fy}} = 75.494$$

$$ifz := \sqrt{\frac{Izt}{At}} = 112.714$$

$$\lambda fz := \frac{Lcrh}{ifz} \cdot \frac{1}{\lambda 1h} = 0.191$$

EN 1993-1-1 6.3.1.2

$$\phi zh := 0.5\left[1 + \alpha zh \cdot (\lambda fz - 0.2) + \lambda fz^{2}\right] = 0.516$$

EN 1993-1-1 6.3.1.2

$$\chi zh := \frac{1}{\phi zh + \sqrt{\phi zh^{2} - \lambda fz^{2}}} = 1.004$$

But χ should be less than 1.0

$\chi zh = 1.004$

$$Nbzrdh := \chi zh \cdot \frac{At \cdot fy}{\gamma m0} \cdot 10^{-3} = 877.172$$

NEdf = 125.947 less than Nbzrdh = 877.172 OK

Verification of buckling resistance of the bottom flange

$\frac{NEdf}{Nbzrdh} = 0.144$ Less than 1.0 OK

10 Purlins and sheeting rails

10.1 Design of purlins

The purlins are simply supported and span 5.0 m between portal frames at a spacing of 1.5 m .The total dead load including purlin weight is 0.43 KN/m2 on the plan and the imposed load is 1.0 KN/m2 and the vertical earthquake load is 0.24KN/m2 and horizontal earthquake load is 7 KN

The design load: Combination 1: $\gamma_{Gmax} G + \gamma_Q Q_s$

Dead load: $D1 := g1 \cdot 5 \cdot 1.5 = 3.705$

Imposed load: $IL := qk \cdot 5 \cdot 1.5 = 4.5$

$D_L := \gamma 1 \cdot D1 + \gamma q \cdot IL = 11.752$

The design load = 17.417 KN

$Moment := \frac{D_L \cdot 5}{8} = 7.345$

Design strength Py

Ppy := 450

Modulus required Zreq $Zreq := \frac{Moment}{Ppy} \cdot 10^3 = 16.322$

Try **Sigma section ASB20012 in Albion section**s ,Zx= 27.34 cm3 ,

Ix= 273.41 cm4 and Z eff, x, c=20.84 cm3

Try **Sigma section M145065200** i**n Kingspan sections**, Zx= 27.40 cm^3,

Ix= 198.62 cm^4

For py= 390n/mm^2 in **Steadman sections**

Modulus required Zreq $Zre := \frac{Moment}{390} \cdot 10^6 = 1.883 \times 10^4$

Try **Zed section 17018 in Steadman sections**, Zx= 24.85 cm3,

Ix= 234.2 cm4 for Py=390N/mm2

Deflection due to imposed load Δ =

$5*W*L^3/384*E*I$

$$\Delta := \frac{5 \cdot IL \cdot 10^3 \cdot 5000^3}{384 \cdot E \cdot 273.41 \cdot 10^4} = 13.068$$

$$\frac{\Delta}{5000} = 2.614 \times 10^{-3}$$

$$\frac{1}{360} = 2.778 \times 10^{-3}$$

Increase section to be **Sigma ASB20023 in Albion section**, Ix=511.51cm4

$$\Delta 1 := \frac{5 \cdot IL \cdot 10^3 \cdot 5000^3}{384 \cdot E \cdot 511.51 \cdot 10^4} = 6.985$$

$$\frac{\Delta 1}{5000} = 1.397 \times 10^{-3}$$ OK

Try **20025 Zed section in Steadman** section .Ix=517.3cm4

Try **M235065170 Sigma in Kingspan**, Ix= 531.67 cm4

Torsional constant for zed section (Tc)= $1/3\ \Sigma\ b*t^3$

bz1 := 16 bz2 := 70 bz3 := 200.14 bz4 := 64 bz5 := 20 tz := 2.35

$$Tc := \frac{1}{3} \cdot \left(bz1 \cdot tz^3 + bz2 \cdot tz^3 + bz3 \cdot tz^3 + bz4 \cdot tz^3 + bz5 \cdot tz^3 \right) = 1.601 \times 10^3$$

Torsional Constant =Tc

10.2 Design of sheeting rails

A simply supported sheeting rail spans 5m. The rails are at 1.5m centres.

The total weight of cladding and self weight of rail is 0.3 KN/mm2

The earthquake horizontal load is 4.71 KN

Use Grade S450 steel for Sigma section. or Grade S390 steel for Zed section.

Vertical load: Vl

$$VL := 0.3 \cdot 5 \cdot 1.5 = 2.25$$

Earthquake load EQL

$$EQL := 4.71$$

The dead load factor acting with wind or earthquake

$$\gamma 1 = 1.35$$

The earthquake load factor acting with dead load

$$\gamma q = 1.5$$

Factored vertical moment, *Mcx*

$$Mx := \frac{\gamma 1 \cdot 2.25 \cdot 5}{8} = 1.898$$

Factored horizontal moment, *Mcy*

$$My := \frac{\gamma q \cdot 4.71}{8} = 0.883$$

Design strength =450N/mm2 **Kingspan sections**

Try M145065220, Zx=29.97 cm4

The moment capacity Mb= Mcy

$$Mbr := 0.8 \cdot 450 \cdot 29.97 \cdot 10^{-3} = 10.789$$

$$Mcyr := Mbr$$

The biaxial bending interaction relationship:

$$\frac{Mx}{Mbr} + \frac{My}{Mcyr} = 0.258$$

Provide M145065220 Sigma section from **Kingspan sections**

Design strength =390N/mm2 **in Steadman sections**

Try 17020, Zx=28.21 cm4

The moment capacity Mb= Mcy

$$Mbr1 := 0.8 \cdot 390 \cdot 28.21 \cdot 10^{-3} = 8.802$$

$$Mcyr1 := Mbr1$$

The biaxial bending interaction relationship:

$$\frac{Mx}{Mbr1} + \frac{My}{Mcyr1} = 0.316$$

Provide 17020 Zed section from **Steadman sections**